Elucidating the role of a novel DNA-binding protein identified in the diatom *Thalassiosira pseudonana* for coping with nutrient and temperature stress

Krisztina Csilla Sárközi

A thesis submitted to the School of Environmental Sciences, at the University of East Anglia, for the degree of Doctor of Philosophy, September 2016

ABSTRACT

Diatoms are associated with nutrient rich waters with high biomass that are commonly found at high latitudes, in coastal waters, in upwelling zones or during seasonal blooms. They display an opportunistic growth described as a 'bloom and bust' life cyce and a remarkable diversity. These caracteristics are considered to be responsible for their success in aquatic environments and the reason why they contribute about 20% of global primary production and allow them to quickly dominate phytoplankton communities when environmental conditions become favourable. The processes that enable this impressive plasticity of diatoms in response to environmental variability are mostly unknown. A novel conserved DNA binding protein (BIG1) was recently identified and found to differentially regulate genes involved in progression through the cell cycle in centric diatoms as well as about 30% of genes found in natural centric diatom blooms. In our study we show that the BIG1 protein is linked to the regulation of initiation of fast growth upon nutrient addition. Overexpression of BIG1 in the model centric diatom *Thalassiosira pseudonana* enabled fast recovery and growth after a period of nitrogen stravation and exposure to low and high temperature as well as fostered growth under suboptimal temperatures. We present evidence that BIG1 has an impact on photosynthesis and suggest its involvement in directing the photosynthetic electron flow around Photosystem I. Our results may provide insights into regulatory processes that govern diatoms' oportunistic growth.

LIST OF CONTENTS

LIST OF FIGURES

LIST OF TABLES

ACKNOWLEDGEMENT

This thesis would not have been possible without the time and support of many patient and gifted people.

First of all I would like to express my deepest gratitude to my supervisor Thomas Mock, whose knowledge and guidance have been invaluable to the completion of my PhD. I would also like to thank my secondary supervisors, Cock Van Oosterhout and Vincent Moulton for their advice and encouragement.

I would like to acknowledge several members of the Mock group. The guidance of Bobbie Lyon, Jan Strauss, Amy Kirkham, Rob Utting and Amanda Hopes was invaluable in the Lab. With patience and persistence they provided practical help and insight. Thanks to Andrew Toseland who guided my first steps through bioinformatics and Bogdan Luca for his advices in statistical programming. Thanks to Katrin Schmidt for sharing her transcriptome data and Irina Grouneva for advice on my thesis.

I would like to thank Erik Buitenhuis for granting me access to the temperature gradient bar, and Leïla Tirichine for her time and training on the ChIP-seq protocol at the École Normale Supérieure in Paris.

Last but certainly not least, I would like to thank my parents and friends for their emotional support. You have supported me through the four year rollercoaster of my PhD - successes and failures both, and for that I am extremely grateful.

CHAPTER 1: INTRODUCTION

1.1 Introduction to phytoplankton

Derived from the Greek words *phyton* (plant) and *planktos* (wanderer or drifter) these free-floating organisms are the drifters of the ocean. Phytoplankton are an extremely diverse, polyphyletic group of microscopic organisms which include cyanobacteria (prokaryotes lacking nuclei) and single-celled protists (eukaryotes possessing nuclei). Protists consist primarily of diatoms, dinoflagellates, coccolithophores, silicoflagellates and green algae (e.g. Prasinophytes). The first phytoplankton (marine cyanobacteria) probably appeared almost 3 billion years ago (Hedges *et al*. 2001). Since then, phytoplankton oxygenated the atmosphere of the Earth, have undergone broad diversification and numerous extinction events, and conquered the freshwater realm (Litchman and Klausmeier 2008). Also, they absorb carbon dioxide (CO_2) from the atmosphere playing an important role in carbon sequestration and climate regulation (Falkowski 1997).

Phytoplankton comes in various forms and feeding strategies. It was commonly accepted that the vast majority belongs to the group of autothrophs. These organisms capture energy from sunlight and transform inorganic matter into organic matter (biomass) by the process known as photosynthesis. Autothrophs are primary producers and account for approximately half of the global primary production although hey make up less than 1% of the plant biomass on earth (Field *et al*. 1998; Katz *et al*. 2004). Due to the requirement of light, they inhabit the upper well-lit surface layer of oceans (euphotic zone) and bodies of fresh water. Their primary production is the basis of marine food webs, providing energy through higher trophic levels, which therefore makes them key players in the global carbon cycle (Field *et al*. 1998; Falkowski *et al*. 2008). Recent studies based on ribosomal DNA (rDNA) analysis from 11,200 species show a strikingly different picture. The study revealed that the most diverse taxa belong to two supergroups which consists mostly of parasitic and phagotrophic (most dinoflagellates and ciliates) taxa, the Alveolata. The other group, the Rhizaria, are a group of amoeboid heterotrophic protists with a broad spectrum of ecological behavior, from phagotrophy to parasitism and symbiosis (de Vargas *et al.* 2015) among the better known are the foraminifera and radiolaria. Intriguingly, according to the same study the most diverse photic-zone plankton are represented by the mixotroph dinoflagellates Dinophyceae (Alveolata). Mixotrophs are able to capture solar energy and ingest prey if photosynthesis cannot occur. Usually they are considered poor competitors for

inorganic nutrients (Smayda 1997; Litchman *et al*. 2007) and follow photoautotrophic diatoms in seasonal successions (Barton *et al*. 2013). However, the second most important eukaryotic group found in the ocean according to de Vargas *et al.* (2015), are diatoms. Diatoms together with other phytoplankton groups play key roles in major elemental cycles in the ocean. Although all major functional groups of phytoplankton are contributors of the carbon cycle, processes such as nitrogen fixation, calcium uptake, and silicon uptake occur almost solely in single groups, such as cyanobacteria, coccolithophores, and diatoms (Egge and Aksnes, 1992; Falkowski *et al.*, 2004; Lessard *et al.*, 2005; Schoemann *et al.*, 2005; Litchman *et al.*, 2012). Phytoplankton are extremely sensitive to global environmental change (Li *et al.*, 2009), changes in composition and size will alter food web structure (Finkel, 2007) and the cycling of carbon (Laws *et al.*, 2000).

1.1.1 The marine carbon cycle

The uptake of CO_2 by phytoplankton in the surface ocean and subsequent sinking of this organic matter to the oceans' interior forms a process termed the biological carbon pump and plays an important role in controlling atmospheric carbon dioxide concentrations (Falkowski *et al.*, 1997, 1998). Most of this sinking organic matter is thought to be carried by large aggregates (Alldredge and Silver, 1988) composed of a mix of material including phytoplankton, detritus, inorganic matter, zooplankton moults, fecal material, and micro-organisms. These rapidly sinking particles aggregate during or after the spring phytoplankton bloom. This 'marine snow' forms via physical coagulation and zooplankton-mediated aggregation (Kiørboe, 2001) predominantly in the upper ocean. Aggregates exported downward are rapidly consumed and reworked by the resident biota, thus forming the base of the mesopelagic food web (Giering *et al.*, 2014; review Buchan *et al.*, 2014). The intensity of carbon fixation and export is strongly dependent on the phytoplankton community composition. In a fourteen years timescale it was found, that globally, diatoms contributed the most to the total phytoplankton production (~50%, the equivalent of ~20 PgC·y−1) followed by coccolithophores, chlorophytes and cyanobacteria, although interannual variations occurred which were associated with climate variability (Rousseaux and Gregg, 2013).

1.1.2 Environmental control on primary production and phytoplankton distribution

About 95% of the living organisms thrive in the euphotic zone and are part of the oceanic food web (Sardet, 2015). The euphotic zone is governed by rapidly changing factors influenced by the temperature, light, salinity and density. Different groups of phytoplankton, as well as individual species, have different temperature optima (Eppley, 1972; Reynolds 1984), hence temperature plays an important role in phytoplankton growth (Eppley, 1972; Raven and Geider, 1988), seasonal succession in both marine and freshwater habitats (Karentz and Smayda 1984; Sommer *et al*. 1986) and productivity (Behrenfeld *et al*. 2006; Finkel *et al*. 2010). Recent studies also suggest that temperature and dissolved oxygen are the strongest correlates of both taxonomic and functional composition in the surface layer (Sunagawa *et al.,* 2015). The limits of species distribution may be determined by physiological tolerance to temperature extremes or by factors such as solar radiation, nutrients or biotic interaction that often co-vary with temperature in aquatic ecosystems (Brown 1995; Chen 2015).

Solar radiation forms the energy responsible for generation of the wind that mixes the ocean. Low latitudes are warmed by the sun more than the poles. This asymmetric heating pattern creates an atmospheric equator-to-pole pressure gradient, which along with the rotation of the Earth, controls the global wind patterns (Falkowski and Oliver, 2007). In addition the continents warm and cool faster than the ocean owing to the latent heat of the water, which results in continent-to-ocean atmospheric pressure gradients and winds along the coast displacing the surface waters (Stomel, 1951; Falkowski and Oliver, 2007). This displacement of surface water away from the coast is replaced by deeper nutrient rich waters. Phytoplankton are able to utilise the available nutrients from the deep water, grow rapidly (Chavez *et al*. 2011) and generate high magnitude spring blooms. In contrast, in the subtropical gyres the euphotic zone is formed from a nutrient limited layer that accounts for most of the primary production, supported mainly by nutrients recycled from organic matter *in situ.* The loss of nutrients by sinking is considered less than 10% (Dore *et al.*, 2008). In this areas phytoplankton thrive in the lower layer of the water column interrupted by occasional rapid blooms in the surface layer over summer (Villareal *et al.*, 2012) see Figure 1.1.

Phytoplankton growth varies seasonally. In temperate coastal waters and high latitudes, blooms peak in spring and summer. During late autumn and winter, convection deepens the mixed layer and therefore dilutes surface phytoplankton populations. Mixed-layer deepening, along with decreasing sunlight, causes phytoplankton division rates to slow down during autumn accompanied by increasing loss rate resulted from zooplankton grazing, viral lysis and sinking out of the mixed layer. Thus, winter time loss rates exceed division rates, therefore phytoplankton concentrations decrease (Behrenfeld and Boss, 2014). The change in concentration, however, has the consequence of decreasing density dependent grazing and viral infection efficiencies making it difficult for zooplankton that feed on phytoplankton to find their prey (Kimmance *et al.*, 2007; Behrenfeld and Boss, 2014). By early winter a tipping point is reached where decreases in loss rates are greater than light driven decreases in phytoplankton division rates. That allows phytoplankton to begin to build up in midwinter, a head start in growth that is a prelude to the massive bloom once the winter's storms cease mixing and conditions for growth improve (Sverdrup 1953; Biello, 2010). Shortly after the outbreak of blooms phytoplankton exhaust the available nutrients and growth decline.

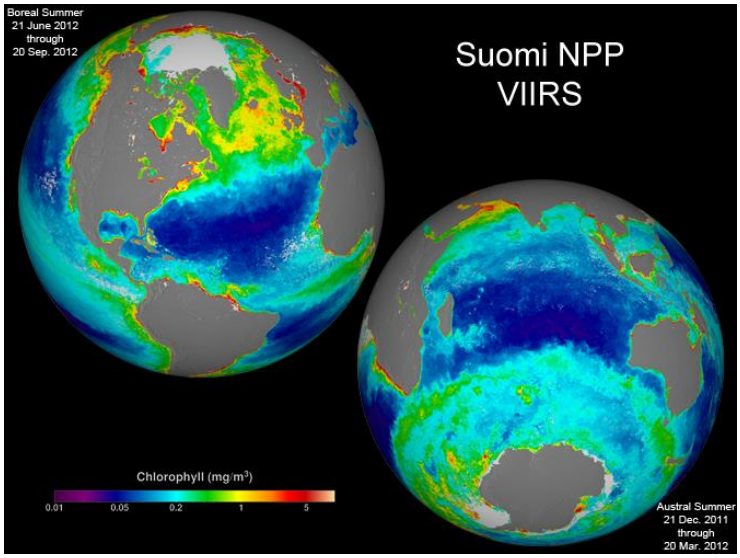

Figure 1.1: *Image of season-long composites of ocean chlorophyll concentrations derived from visible radiometric measurements made by the VIIRS instrument on Suomi NPP in the time period December 2011-Sepetmber 2012. The purple and blue colors represent lower chlorophyll concentrations. The oranges and reds represent higher chlorophyll concentrations. These differences in color indicate areas with lesser or greater phytoplankton biomass. Image credit: NASA/Suomi NPP/Norman Kuring*

Though some oceanic regions concentrate enough nutrients to sustain the phytoplankton community or to generate blooms, often they are scarce in trace elements such as iron. Iron deficiency limits the activity of phytoplankton major photosynthetic pigment therefore is the most limiting trace element to phytoplankton growth and has the greatest effect on algal species diversity (Moore *et al.*, 2002; Sunda, 2012). Iron addition in these areas with high nutrient but low chlorophyll concentration (HNLC) like the Southern Ocean generates phytoplankton blooms dominated by diatoms (Boyd *et al.*, 2004; 2007; de Baar *et al.*, 2005; Smetacek *et al.*, 2012). In addition, different particles can be dumped by wind carried from the land and occasionally this dust is enough to sustain natural phytoplankton blooms in HNLC regions (Cassar *et al.*, 2007; Hamme *et al.*, 2010) dominated by diatoms. These later studies added valuable insights into the resource competitiveness of diatoms underlining their ecological and biogeochemical importance among phytoplankton.

1.1.3 Physiological control on phytoplankton distribution

Cell size in phytoplankton ranges from less than one micron in picocyanobacteria up to several millimeters in oceanic diatoms (Malone, 1980; Chisholm, 1992) and is considered a 'master trait' that places important constraints on many key organismal characteristics and biotic interactions (Barton *et al.*, 2013). Such constraints are imposed on the rate of acquiring (Munk and Riley, 1952; Duysens, 1956) and processing energy and materials from the environment (Brown *et al.*, 2004), to influence evolution (Quigg *et al.*, 2003), food web structure (Laws *et al.*, 2000; Irwin *et al.*, 2006), biogeochemical cycling (Sterner and Elser, 2002; Katz *et al.*, 2004) and ultimately growth rates as reviewed by Finkel *et al.* (2010). Nutrient concentration and supply in the upper layers of the ocean often exert the primary control on the size and taxonomic structure of phytoplankton community (Eppley and Peterson, 1979; Coale *et al.*, 1996). Shifts in cell size towards smaller cells were recorded over geological timescales in relation to the decrease in CO_2 concentration and water column stratification (Finkel *et al.*, 2005; Finkel *et al.*, 2007b) as well as in susceptibility of phorosystem II to photoinactivation and rates of repair (Karentz *et al.*, 1991; Finkel *et al.*, 2009) and in relation to increases in temperature, independent of nutrient concentrations (Hilligsøe *et al.*, 2011). However, it was found that predominantly the larger species are that respond to changes in nutrient concentration (Finkel *et al.*, 2009). In spite of the higher maximum growth rates of smaller cells (Banse, 1976) the

elemental stoichiometry of cells reflected in their C:N:P ratio (Redfield, 1958) may change making them less appealing for their consumers. Consumption of poor-quality prey by zooplankton may result in restricted regeneration of the limiting element and further limit primary production (Mitra and Flynn, 2005). However, larger diatoms are able to store nutrients in their vacuoles to a greater degree than their smaler counterparts allowing them to continue growing and dividing after nutrients become limiting (Raven, 1987). This ability of larger diatoms may be the reason why their blooms occur towards the end of blooms driving higher carbon export (Smayda, 1970). Thus, the size structure and elemental composition of phytoplankton communities can alter both the magnitude of carbon fixed and exported into the deep sea relative to the growth-limiting nutrient (Volk and Hoffert, 1985; Falkowski *et al.*, 2000).

1.2 Evolution of marine phytoplankton

Phytoplankton starting from their early appearance in Paleozoic (approximately 500 million years ago) and their expansion in Cretaceous (145 million years ago) displayed a remarkable ability to populate a wide range of marine, freshwater and terrestrial habitats conquering even the most extreme places on Earth such as hot springs, sea ice and salt lakes (reviewed by Rothshild and Mancinelli, 2001). Their expansion was fostered by the development of a stratospheric layer of ozone generated from oxygen released from cyanobacterial photosynthesis. Hence, understanding the processes which has enabled them to adapt to their current environments allows us to predict the effect of global change on their biogeography.

The processes that shaped phytoplankton genomes were driven by major forces of evolution (mutation, selection, genetic drift and gene flow) complemented by additional evolutionary processes such vertical gene transfer (the transmission of DNA from parent to offspring) and horizontal gene transfer (gene transfer between unrelated species). Algal genomes are composed of host, plastid and bacterial genes likely acquired by horizontal gene transfer (Archibald *et al.*, 2003; Bowler *et al.*, 2008). The protein products of the transferred genes are translated in the host cytoplasm and post-translationally targeted back to the organelles. Some species are characterized by high genetic complexity such as the dinoflagellate *Kryptoperidinium foliaceum* which genome is composed of ten individual genetic entities (Keeling, 2009). The plastid

genome has kept encoding only a small fraction of the genes needed for plastid function. In cryptomonads and chlorachniophytes small eukaryotic nucleuses are retained in the chloroplasts with reduced genomes called nucleomorphs. The nucleoomorph genes most are involved in self-perpetuation of the organelle and its ribosomes (Douglas *et al.*, 2001; Parker *et al.*, 2008).

Phytoplankton, as we know them today show an assemblage of genes derived from photosynthetic organisms, heterotrophic eukaryotes and bacteria as a result of sequential endosymbiotic events summarised by Hopes and Mock (2015) seen in Figure 1.2.

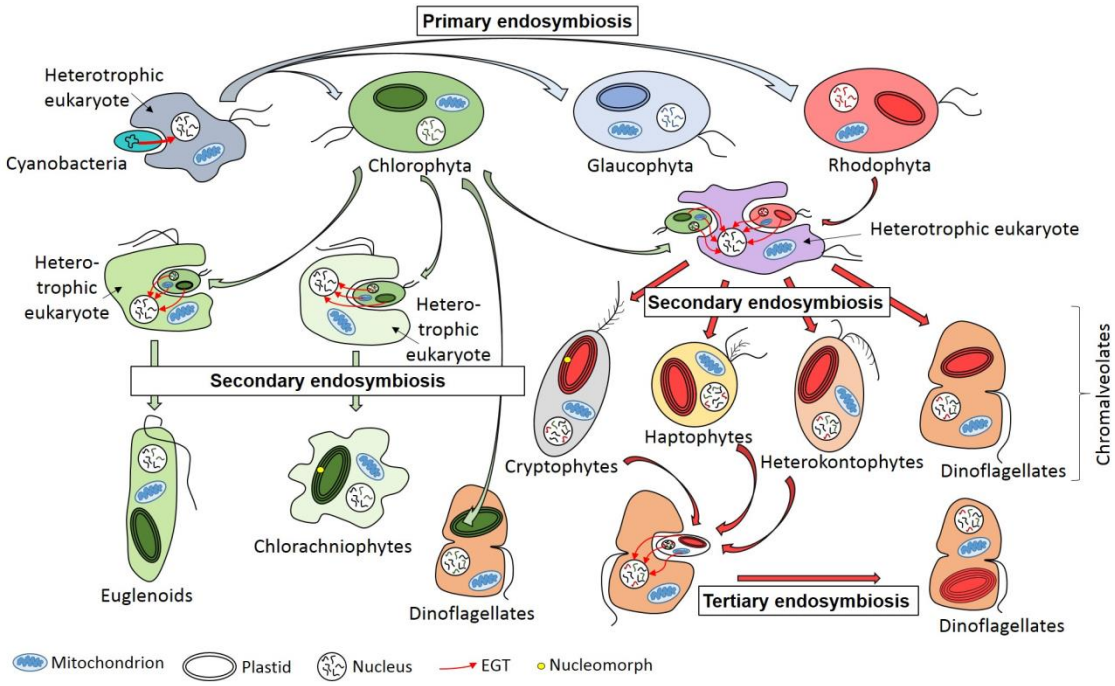

***Figure 1.2**: Phytoplankton evolution according to primary, secondary and tertiary endosymbitic events. Image credit: Amanda Hopes*

The process by which eukaryotic phytoplankton cells and their components arose is supported by recent phylogenetic studies using nuclear and plastid gene sequences. From these studies it infers that chlorophytes, glaucophytes and rhodophytes arose from separate endosymbiotic events in which heterotrophic, single-celled, eukaryotic hosts engulfed a cyanobacteria. The cyanobacteria was integrated into double membrane-bound organelles known as plastids (McFadden, 2001; Falkowski *et al.*, 2004). In contrast to terrestrial plants, a major schism occurred in the evolution of the eukaryotic

phytoplankton that gave rise to two major plastid lineages (Delwiche, 1999; Palmer, 2003). The green lineage appropriated besides chlorophyll *a* chlorophyll *b*, whereas the red lineage uses chlorophyll *c* and phycobilins as accessory photosynthetic pigments (Falkowski and Raven, 1997). The glaucophytes retain a peptidoglycan plastid membrane that differentiates them from the red lineage (Parker *et al.*, 2008). Unlike mitochondria, which arose through single endosymbiosis between a α-proteobacterium and a common ancestor of all extant eukaryotes (Gray *et al.*, 1999), plastids underwent successive endosymbiotic events. The primary endosymbiosis is estimated to have occurred around 1558 million years ago, soon after eukaryotic origin, followed by secondary endosymbiosis 1274 million years ago (Yoon *et al*., 2004). Secondary endosymbiosis took place in heterotrophic eukaryotes with green and red algae becoming plastids with additional one or two membranes (Cavalier-Smith, 1999) accompanied by gene transfer from endosymbionts' nucleus, plastid and mitochondria to the host nucleus. This led to the evolution of three groups with green plastids: the euglenoids, chlorarachniophyte and chlorophyll *b* containing dinoflagellates which all appear to be relatively rare in marine environment (Parker *et al.*, 2008); and four groups with red plastids: the cryptophytes, dinoflagellates, haptophytes (including coccolithophores) and heterokontophytes (including diatoms). It is hypothesised that all microalgae with chlorophyll *c* had acquired their plastids through secondary endosymbiosis (McFadden, 2001). Also, there is consensus that these plastids originated from a single endosymbiotic event in the common ancestor of these lineages (Keeling, 2009). However, there is evidence of prior secondary endosymbiosis in chromalveolates with a green alga, followed by gene transfer to the nucleus and plastid loss (Moustafa *et al.*, 2009). Some dinoflagellates have undergone a tertiary endosymbiosis, whereby heterotrophic dinoflagellates have engulfed cryptophytes, haptophytes (Tengs *et al.*, 2000) or diatoms (Falkowski *et al.*, 2004). These latest processes have continued to be an important ecological and evolutionary force and led to the appearance of the mosaic genomes characterised by a mix and match of genes from different organisms (Armbrust, 2009).

Genes gained through endosymbiotic and horizontal gene transfer, have shaped metabolic pathways that include lipid (Chan *et al.*, 2013) and amino acid (Jiroutová *et al.*, 2007) biosynthesis. Fatty acid biosynthesis in diatoms is controlled by genes from green and red algal lineages and from the heterotrophic host (Chan *et al.*, 2013).

Although the gene acquisition was fuelled by the same endosymbiotic level contrasting origins of the heme biosynthesis in diatom (Oborník and Green, 2005) and in some dinoflagellates (Hackett *et al.*, 2004) are lightened by phylogenetic analysis. The plastid targeted genes had either red (diatoms) or green (certain dinoflagellates) algal origins. In some cases cyanobacterial hosts may acquire gene clusters transferred by viruses allowing them to adapt to low nutrient conditions (Martiny *et al.*, 2006) as well as to high or low light (Coleman *et al.*, 2006). The *hli* gene that encodes the high-light-inducible protein (HLIP) may move among cyanobacterial cells by means of viruses and return in host cells in altered forms increasing the host genetic diversity (Lindell *et al.*, 2004). A recently identified phytochrome gene (Montsant, 2007) in both sequenced diatoms (*Thalassiosira pseudonana* and *Phaeodactylum tricornutum*) originated from brown macroalgal viruses (EsV and FsV) suggests that horizontal gene transfer mediated by viruses may widely occur in marine phytoplankton (Parker *et al.*, 2008). Genes from the primary endosymbiont and eukaryotic host are also found for heme in *T. pseudonana* (Oborník and Green, 2005). Also, *T. pseudonana* has acquired membrane transporter genes via endosymbiotic-horizontal gene transfer originated from both red and green lineage to adapt them in marine environments (Chan *et al.*, 2011).

Latest results in evolutionary phylogeny suggests that key functions such as photosynthetic efficiency and protection from oxidative damage in microbial eukaryotes was significantly enhanced by the ancient transfer of green algal derived genes involved in carotenoid biosynthesis and as a central component of the light-harvesting complex superfamily. But capture of the red algal secondary endosymbiont, provided the chromalveolate lineages the ability to outcompete other photosynthetic groups such as green algae, in particular prasinophytes (Chan *et al.*, 2011) through greater resource efficiency by wider occurrence with depth.

The acquisition of the red plastid offered an almost uninterrupted evolutionary success to diatoms which seem to be the only photosynthetic eukaryotes from the red lineage that radiated and diversified unabated since present (Sinninghe Damsté *et al.*, 2004). Although they are found to be successful in most habitats where dissolved nutrients and sufficient light are available they are most associated to spring blooms in coastal upwelling zones.

1.3 Phytoplankton blooms

Our ability to monitor phytoplankton distribution at the global scale derives from satellite observations of ocean colour (Behrenfeld and Falkowski, 1997) supplemented by *in situ* measurements (Smetacek *et al.*, 2012; Dore *et al.*, 2008). Satellite observations with 1-5 km spatial and 1-8 day temporal resolution detect spectral and intensity variations in light emerging from the surface ocean and allow assessment of basic ecosystem properties, including phytoplankton biomass and chlorophyll concentrations (Behrenfeld, 2014) while *in situ* sampling gives insight into species distribution and cell concentration observed. Some ocean regions exhibit recurring periods of high phytoplankton biomass concentration defined as blooms as seen in Figure 1.3. Phytoplankton blooms are observed in areas where surface nutrients are at least periodically elevated and strong physical forcing can disturb the balance between phytoplankton division and loss rate such as dilution of phytoplankton populations by mixed layer deepening, deep water upwelling or riverine influx (Behrenfeld, 2014).

Figure 1.3*: Image acquired on June 6, 2015, by the Moderate Resolution Imaging Spectroradiometer (MODIS) on NASA's Terra satellite, shows a mass of phytoplankton blooming between Denmark, the United Kingdom, and Germany. The milky, light-colored surface waters are likely filled with coccolithophores, whereas the greener areas are probably rich with diatoms or perhaps dinoflagellates. Image Credit: Jeff Schmaltz, MODIS Land Rapid Response Team, NASA GSFC*

Most phytoplankton blooms develop in the spring months. Spring blooms are key annual events in the phenology of pelagic ecosystems (review Behrenfeld and Boss, 2014), where a rapid increase in phytoplankton biomass has a significant influence on upper ocean biogeochemistry (Lochte *et al.*, 1993, Martin *et al.*, 2011) and food availability for higher trophic levels (Townsend *et al.*, 1994; Platt *et al.*, 2003; Mackas *et al.*, 2007). Spring blooms are particularly prevalent in coastal and high-latitude waters. The high levels of phytoplankton biomass and primary production that occur during these blooms, and its subsequent export out of the surface ocean result in a significant contribution to the biological carbon pump (Townsend *et al.*, 1994; Sanders *et al.*, 2014). Climate-driven surface warming and reduced winter mixing appear to allow blooms to occur earlier (Henson *et al.*, 2009), and alter the frequency of blooms over the annual cycle (Henson *et al.*, 2013). Nevertheless, modelled climate change simulations predict disturbances in the process resulting in a shallower mixed layer which may cause later initiation of the blooming phase, a lower phytoplankton biomass or a shorter blooming period (Behrenfeld, 2014).

Phytoplankton blooms occur when growth rates exceed loss rates in response to higher intensity or longer duration of light exposure, combined with higher sea surface temperature, reduced grazing pressure and higher nutrient levels owing to seasonal mixing events (Sverdrup, 1953; Smith and Nelson, 1985; Geider *et al.*, 1986; Harrison and Cota, 1991; Huysman *et al.*, 1999; Moore *et al.*, 2006; Behrenfeld, 2010; Smyth *et al.*, 2014). Losses can occur through sinking (Smetacek, 1985; Rynearson *et al.*, 2013; Giering *et al.*, 2016), advection or mixing out of euphotic zone (Miller, 2003). Besides physical forces, trophic feedback in plankton ecosystems exerts a dominant control on phytoplankton concentration (Evans and Parslow, 1985). It was recorded that high survival rate of zooplankton following a warm winter can suppress or even delay the emergence of a phytoplankton bloom (Wiltshire and Manly, 2004). Infections by viruses have been shown to cause the collapse of *Phaeocystis* blooms (Jacobsen *et al.*, 2007) underlying even more the sensitive role that ecological interactions play in the initiation and decay of phytoplankton blooms. Nitrogen, phosphorus, iron and silicate are among the most common nutrients that influence both the initiation and termination of blooms, and the balance of these elements often drives the establishment of specific phytoplankton species (Egge and Aksnes, 1992; Lessard *et al.*, 2005, Schoemann *et al.*, 2005).

Despite their importance there is little consensus whether is there a single, globally dominant factor that triggers the initiation of the recurrent spring phytoplankton blooms (Behrenfeld, 2010; Martin, 2012; Smyth *et al.*, 2014). The rapid increase in growth rates during the spring bloom was suggested to be due to some combination of alleviations on factors constraining growth and those determining losses (Daniels *et al.*, 2015). Since Sverdrup (1953) proposed in the hypothesis seen as the seminal theory of spring bloom initiation that blooms will occur when stratification shoals above a critical depth allowing phytoplankton growth to exceed mortality, blooms were reported in the absence of stratification (Townsend *et al.*, 1992) and earlier than expected (Mahadevan *et al.*, 2012) questioning his longterm hypothesis and rising new theories (review Behrenfeld and Boss, 2014).

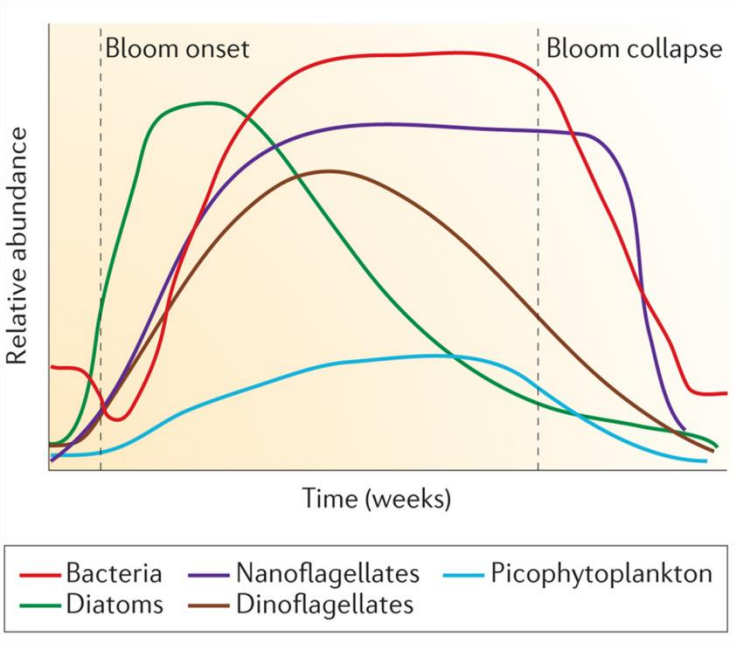

***Figure 1.4**: The succession of the representative phytoplankton species in a bloom in the southern Pacific Ocean from the review of Buchan et al. (2015). Relative abundance of Diatoms (green), Nanoflagellates (dark blue), Dinoflagellates (brown), Picophytoplankton (light blue) and heterotrophic bacteria (red) that feeds on phytoplankton is correlated to the length of the bloom.*

Natural phytoplankton blooms last from weeks to months and are characterized by a succesion of several different phytoplankton species (Chang *et al.*, 2005), although blooms are typically classified according to a dominant species that persists for the

lifetime of the bloom (review Buchan *et al.*, 2014) as seen in Figure 1.4. In the subtropical oceans, by contrast phytoplankton populations bloom occasionally in spring. In these areas phytoplankton typically limited to some genera of large diatoms and cyanobacteria produce rapid surface phytoplankton blooms over summer fuelled by rapid nutrient pulses (Dore *et al.*, 2008; Letelier *et al.*, 2000). In contrast, experimental phytoplankton blooms, which are generated by the controlled use of defined nutrients, usually develop and collapse within one or two weeks (review Behrenfeld and Boss, 2014). Bloom decline may occur in response to 'bottom-up' forces (such as nutrient limitation), 'top-down' forces (such as grazing and viral lysis) or a combination of both (Egge and Aksnes, 1992). During bloom collapse, organic molecules from dying phytoplankton frequently aggregate to form composites of detrital particles which are readily colonized by heterotrophic bacteria (review Buchan *et al.*, 2014) as has been reported for senescent diatom cells (Smith *et al.*, 1992).

In a typical bloom, diatoms dominate the phytoplankton assemblage initially, supressing a pre-bloom pico-phytoplankton-dominated (cells<2 μm) community (Margalef, 1978; Miller, 2004; Barber and Hiscock, 2006). Through either increased predation, nutrient stress, or a changing physical environment (Margalef, 1978), diatoms decline and transition over several weeks onto smaller and motile phytoplankton such as coccolithophores and dinoflagellates (Lochte *et al.*, 1993; Leblanc *et al.*, 2009). Marine diatoms have high maximum growth rates. Under optimal conditions an intriguing 0.54 divisions per hour was recorded in the centric diatom *Chaetoceros salsugineum* (Ichimi *et al.*, 2012). Diatoms like many other planktonic species including dinoflagellates have complex life cycles including resting stages that are formed in unsuitable environmental conditions and sink post-bloom (Smetacek, 1985; Rynearson *et al.*, 2013) to the sediment where can accumulate sometimes over many years (Kraberg *et al.*, 2010). When conditions become favourable again they may act as a seed population for the spring bloom (Backhaus *et al.*, 2003; Genovesi-Giunti *et al.*, 2006). It was also hypothesized based on the observation that diatom blooms generally occur first in coastal waters before progressing to the open ocean (Smetacek, 1985), that coastal diatom populations are horizontally advected into pelagic waters (Daniels *et al.*, 2015).

During summer the biomass of the phytoplankton community in the coastal upwelling zones remains on relatively constant level because of nutrient limitation and is controlled by the number of predators. In autumn remineralisation processes exceed the

nutrient uptake rates of the ambient phytoplankton populations and more nutrients become available due to bacterial activity. This generates a second phytoplankton bloom mostly dominated again by diatoms (Kraberg *et al.*, 2010). Following the breakdown of the autumn bloom caused by light limitation the winter stage is reached again.

Among the blooming phytoplankton groups diatoms are one of the most diverse organisms (Vargas *et al.*, 2015) present in all marine habitats ranging from poles to tropics being able to bloom even under the Arctic sea ice (Arrigo *et al.*, 2012). Diatoms have a greater efficiency of carbon sequestration into the deep ocean, because their heavy silica frustules make them sink faster than other groups of phytoplankton (Smetacek, 1999; Litchman and Klausmeier, 2008). By this biological process diatoms remove carbon from the global carbon cycle over geological time scales (Falkowski, 1997) and exert direct effect on global climate (Falkowski *et al.*, 1998). Some other phytoplankton taxa, such as the dimethyl sulfide-producing coccolithophorid *Emiliana huxleyi* (Brown and Yoder, 1994), are believed to exert regional and possibly global effects (Litchman *et al.*, 2012) functioning as cloud condensation nuclei and affecting solar backscattered radiation (Charlson *et al.*, 1987; Orellana *et al.*, 2011), nonetheless their blooms are major sinks of CO_2 in the global oceans as well (Shutler *et al.*, 2013). In contrast, dinoflagellates exhibit significant ecophysiological differences when compared to diatoms, including greater vulnerability to turbulence, greater dependence on water stratification, mixotrophic tendencies, greater potential use of allelochemicals and motility (Smayda, 1997; Klausmeier and Litchman, 2001).

Phytoplankton blooms can include toxic species that express toxicity to higher trophic levels, largely fish, shellfish, marine mammals, or humans, and include members of the cyanobacteria, dinoflagellates, raphidophytes, haptophytes, and diatoms (Smayda, 1997). Under harmful algal blooms are included human-caused high-biomass outbreaks, that while often comprise non-toxic phytoplankton species, still critically alter ecosystems through hypoxia/anoxia, altered food web efficiencies, stimulation of pathogenic bacteria, or other ecological consequences (Wells *et al.*, 2015).

Although seasonal or occasional phytoplankton blooms occur in regular manner throughout the oceans, as satellite observations and direct sampling proved, diatoms are

the major photoautotroph of spring high magnitude phytoplankton blooms in temperate coastal oceans, their contribution to ocean biogeochemical cycling being undeniable.

1.4 Diatoms in the ocean

Diatoms occur only as single cells or cell aggregations, some 285 genera (Round *et al*., 1990) and 10000-12000 species are recognised (Norton *et al*., 1996) with an estimated 30000-100000 extant species (Mann and Vanormelingen, 2013). They belong to the photosynthetic stramenopiles which include among others radially symmetrical and bilaterally symmetrical diatoms, yellow-green algae (tribophyceans) such as *Vaucheria*, and giant kelps, including *Macrocystis* (Alexopoulos *et al.*, 1996). Fossil and molecular evidence indicates that the earliest diatoms were radially symmetrical, meaning that the arrangement of pores present on them are aligned (striae) and run from the center of the valve to the rim. Such arrangement is found in modern radial centric diatoms as seen in Figure 1.5. Diatoms with valves ornamented with radially arranged pores of a variety of shapes form the bipolar or multipolar centrics (Graham, 2009). A lineage of bipolar centric diatoms gave rise to the pennate diatoms characterised by bilateral symmetry. Such diatoms have elongate shapes with a longitudinal line or sternum from which parallel ribs extend perpendicularly towards the edge. The pennates are subdivided into raphid pennates, which possess a slit-shaped process, called a raphe, and araphid pennates, which lack that feature, but have apical pore fields and apical labiate processes. The raphe slit enables raphid pennates to move actively by means of a cost-effective system of traction over the substratum (Mock and Medlin, 2012). Most raphid pennates are benthic, but some of them such as *Fragilariopsis* and *Pseudo-nitzschia*, have secondarily acquired a planktonic lifestyle. Isoprenoid alkanes characteristic of diatoms found in petroleum of definable age (Sinninghe-Damsté *et al.*, 2004) and fossil records (Suto, 2006) revealed that radial centrics first appeared in the Jurassic, multipolar centrics in the Early Cretaceous, pennates in the Late Cretaceous and the first raphid pennates at 55 million years ago in the Paleogene. Despite being the youngest group of diatoms, raphid pennates are the most diverse (Kooistra *et al.*, 2007).

Diatoms form one of the most abundant group in the oceans (Guiry and Guiry, 2015), thus are important primary producers, responsible for an estimated 20% of global carbon fixation and oxygen production (Smetacek, 1999). They dominate the

phytoplankton of cold nutrient reach waters, such as coastal upwelling areas (Rodrigues *et al.*, 2014) and recently circulated lake waters.

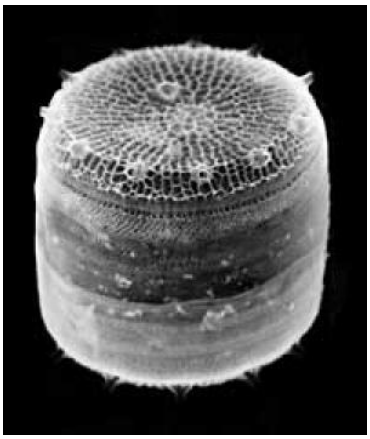

***Figure 1.5**: Scanning electron microscope (SEM) image of the centric diatom Thalassiosira pseudonana. Image credit Nils Kröger, Georgia Institute of Technology, Atlanta (USA).*

Diatoms displays unique features which differentiate them from other photosynthetic stramenopiles. The most distinctive feature is the presence of the frustule or theca which enclose the diatom cells in a structure like a lidded box as seen in Figure 1.6. The frustule is composed of amorphous silica with organic coatings. Silicate represents an energetically inexpensive source of wall material (Falkowski and Raven, 1997). Using silica as cell wall confers several advantages over other cell wall materials such as cellulose. Silica is a relatively heavy material which can ballast diatom cells, allowing them to take advantage of mineral nutrients available in deeper waters (Raven and Waite, 2004). Moreover, silica is inert to enzymatic attack, so the frustule may protect diatoms from attack by microbes or digestion within the guts of grazers (Pickett-Heaps *et al.*, 1990). Some evidence suggests that the silica frustule acts as a pH buffer that increase the activity of diatom carbonic anhydrase facilitating CO_2 uptake (Milligan and Morel, 2002).

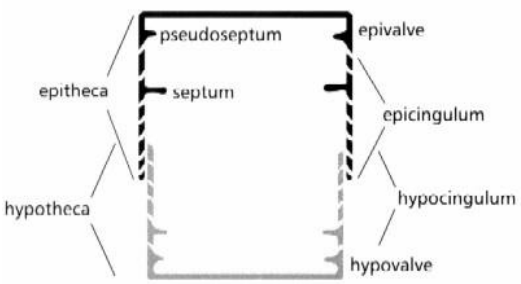

Figure 1.6: *Diagrammatic representation of the diatom frustule viewed in cross-section (After Hasle and Syvertsen, 1997)*

The bottom and the top of the diatom frustule are known as hypotheca and epitheca, respectiviely. The hypotheca is slightly smaller in size because it is overlapped by the epitheca. Each of them are composed of a more or less flattened valve known as hypovalve and epivalve rimed by silica bands that make up the hypocingulum and the epicingulum. This overlapping components make up the frustule cingulum, also known as a girdle. In some cases cingulum rings can be open or closed and may have a protrusion called lingua opposite to the opening formed on the cingulum. Diatoms seen from top or bottom are in valve view, whereas diatoms seen from side view are in girdle view (Graham *et al*., 2009). The diatom frustule is characteristically ornamented with narrow pores known as aerolae, slits or tubes. Such openings aid buoyancy by lightening the heavy frustule, provide increased contact between the cytoplasm and environment facilitating the uptake of nutrients and exudation of metabolites (Mock and Medlin, 2012). Some centric genera such as *Skeletonema* and *Thalassiosira* possess specialized tubes in their valves, called strutted processes or fultoportulae, through which chitin filaments are exuded which may link cells into chains. *Chaetoceros* and *Bacteriastrum* form chains by means of setae (strait silica tubes) likely evolved as a grazer deterrent. Diatom motility is often associated to the ability of raphid diatoms to produce mucilage which can form a stalk what is used to adhere to surfaces (Wustman *et al.*, 1997). The secretion of mucilage can happen from the rimoportula, a tubular process on the valve of some diatoms (Medlin et al., 1986) like in *Odontella* (Pickett-Heaps *et al.*, 1986), from aggregations of polar pores known as ocelli like in *Triceratium* spp. (Graham *et al.*, 2009) or from tubular processes. Mucilage stalks are thought to confer the ability to overcome shading and possibly allow greater access to water column nutrients (Cohn and Weitzell, 1996).

Furthermore, diatoms share several features with other photosynthetic stramenopiles, such as the accessory pigments fucoxanthin and chlorophyll *c* besides chlorophyll *a* the major photosynthetic pigment. Diatoms golden-brown or brown colour comes from the presence of the xanthophyll fucoxanthin. Fucoxanthin is part of the light-harvesting peripheral antennae of the diatom photosynthetic apparatus which is composed from fucoxanthin chlorophyll *a/c* binding proteins (FCPs) that form large complexes. These complexes possess a large number of carotenoids only found within photosynthetic heterokonts and haptophytes, such as fucoxanthin (Fx), as well as diadinoxanthin (Ddx) and diatoxanthin (Dtx) pigments that are involved in their unique xanthophyll cycle (Lepetit *et al.*, 2011). Xanthophylls are known also for their role in protecting cells photosystem from the deleterious effects of high-intensity light. Cells possess one or more plastids located within the periplastidal endoplasmic reticulum also known as the chloroplast endoplasmic reticulum. As a result plastids have four enclosing membranes. In most photosynthetic stramenopiles plastids display a girdle lamellae, a thylakoid that runs around the periphery of the plastid just beneath the innermost plastid membrane (Graham *et al*., 2009). Other common feature is the chrysolaminarin which is the carbohydrate storage product. Chrysolaminarin consists of 20-60 glucose units with β-1,3 linkages and some β-1,6 linked branches and it is dissolved within the vacuoles. Cytoplasmic reserves of lipid droplets are also common.

1.4.1 Cell division frustule development and auxospore generation

The diatoms possess a diplontic life cycle consisting of a long period (up to several years) during which diploid cells divide mitotically and a brief period (a few days) during which sexual reproduction may takes place. Diatoms use the dissolved silicate from marine and freshwater environment, where the predominant form of dissolved silicate is monosilicic acid ($Si(OH)_4$). The only known diatom that lacks an obligate requirement for silicate is the pennate *Phaeodactylum tricornutum* (Armbrust, 2009). Diatoms, excepting some endosymbiotic forms, are not able to live without their silica wall and thus cannot reproduce when the silicate concentration falls below 1 µM level (Martin-Jézéquel *et al.*, 2000). Another important feature of the diatom cell division is that it always happens in the plane of the valve, in consequence diatoms appear only as single cells or chain of cells joined at their valve. An individual characteristic of the cell division in diatoms take place during mitotic division. The two cells resulting from mitotic division retain one-half of the parental theca as an epitheca and both must

synthesize a new smaller hypotheca. Because of this particularity of the mitotic division in diatoms one of the daughter cells is always smaller than the parental cell or the other resulting cell. In consequence, over time the clonal diatom populations experience a reduction in mean cell size.

1.4.1.1 Frustule development

Diatom cell walls form intricately and ornately structured silica frustules on the nanometres scale. Hence, diatom cell division heavily depends on a sufficient supply of dissolved silicate. Global oceanic average concentration of monosilicic acid is 70 µM but this can drop significantly. Diatoms even at concentrations as low as 2 µM silicate, represent more than 70% of the phytoplankton community (Hildebrand, 2000).

Frustule composition is arranged on hierarchically organised silica structures (Sumper and Brunner, 2008). Biosilica involved in the biomineralisation process is made off a composite material which contains proteins such as silaffins, silacidins and long-chain polyamines as organic components. Silaffins are highly zwitterionic peptides capable of self-assembly driven by ionic interactions and able to guide silica formation and precipitation by building matrixes. The silacidin concentration present in the cells controls the size of the precipitating silica nanospheres while the specific role of polyamines is creating species-specific silica nanostructure (Sumper, 2002). The biomineralisation takes place in the silica deposition vesicles (SDV) which appears following fusion of the Golgi vesicles during mitosis. Valves are generally produced before girdle bands. In some diatoms silicification occurs from the margins inward, but it occurs uniformly across the valve in others. A separate SDV is generated when the valve is mature which will produce the girdle bands. Once the frustule is mature, diatoms grow by sliding the epitheca and hypotheca apart at the same time as new cingular bands are produced. From this point cell expansion can occur only at the region of their overlap at the cingulum. Frustule density seems to be influenced by external salinity (Vrieling *et al.*, 2007).

The sequencing of the *T. pseudonana* genome (Armbrust *et al.*, 2004) made possible the identification of three silaffin genes termed *sil1, sil2* and *sil3*. By alternative processing, five gene products (Sil-1L, Sil-1H, Sil-2L, Sil-2h and Sil-3) were found to be derived from these genes (Poulsen and Kröger, 2004). Based on these findings it is hypothesized that in diatoms is present an enzymatic machinery that transforms the amino acid

sequence information within a silaffin polypeptide into a pattern of positive or negative charges that may determines the assembly behaviour of these molecules.

Studies suggests that the parental epitheca can be recycled several times but not more than six times In one form of *Stephanodiscus* the parental valve was observed to last only six to eight generations (Jewson, 1992). Generations to generations the mean cell size in one of the daughter cells reduces as they inherit just the epitheca and generate smaller hypotheca. This size reduction resulting from continuous cell division is known as McDonald-Pfitzer rule. In conclusion, when diatoms reach a critical size, typically about one third of their maximal size (Lewis, 1984), they may undergo sexual reproduction. In nature, diatoms that are smaller than one third the maximal size for the species and are unable to restore cell size by sexual reproduction die (Mizuno and Okuda, 1985). However, such small sized diatoms can persists in laboratory cultures and it was hypothesized that many physiological and ecological experiments have been done with atypically small diatoms (Edlund and Stoermer, 1997).

The diatom life cycle was first described by Klebahn in 1896 in *Rhopalodia* and later by Karsten in 1912 who investigated *Surirella* (Graham *et al.*, 2009). Diatoms alternate a predominantly vegetative life cycle characterised by mitotic division of diploid cells with a gametic life cycle where haploid cells resulting from meiotic division undergo sexual reproduction as seen in Figure 1.7. Sexual reproduction is desired in most diatoms from two reasons: first it is the way how maximum size in diatom populations is regenerated and last but not least sexual reproduction generates genetic variability.

Environmental cues that may induce diatom sexual reproduction vary among species, but changes in temperature, day length (Ashworth *et al.*, 2013), nutrient availability (Smetacek 2012), presence of a mate or sexual hormones in the seawater (Frenkel *et al.*, 2014) or even biotic interactions with bacteria (Nagai and Imai, 1998) are common triggers. Only in a few cases nutrients stress has been reported to trigger sexual reproduction (Chepurnov and Mann, 2004). Centric diatoms are oogamous, producing one or two egg cells per parental cell as a result of the meiotic division. Once when gametes are mature the silica wall surrounding egg cells opens exposing the protoplast allowing fusion with freed flagellate cells which were released by the separating valves of sperm. Gamete fusion results in formation of a zygote known as an auxospore. The function of the auxospore is to shape a relatively large new frustule (Medlin and

Kaczmarska, 2004). In contrast pinnate diatoms are isogamous and can move towards each other while this phenomenon is rare in araphid diatoms (Sims *et al.*, 2006).

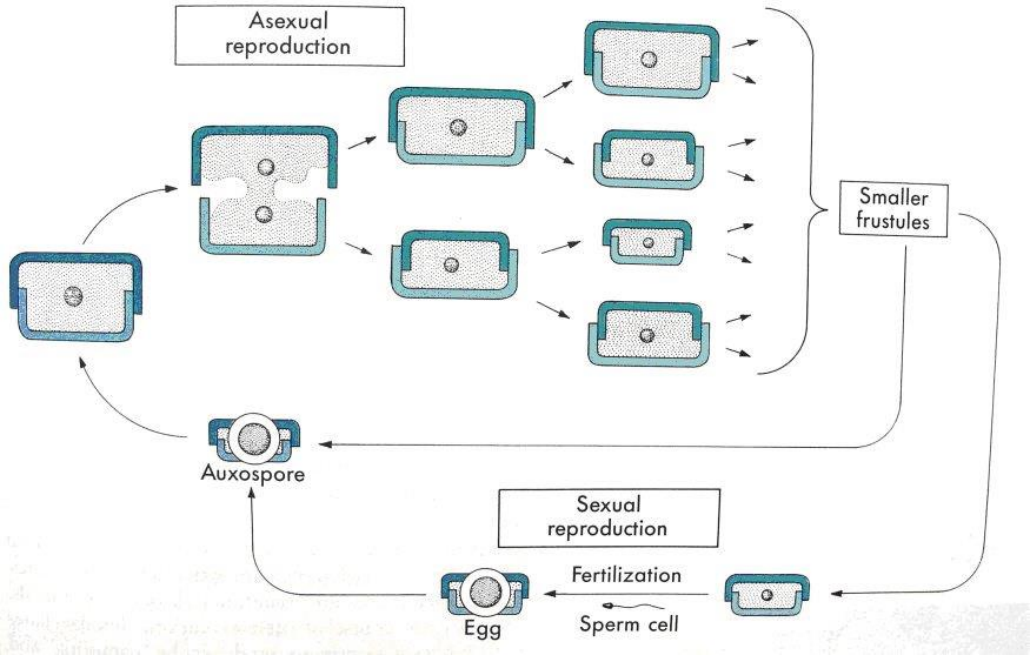

Figure 1.7: *Diagram of typical diatom life cycle. (Image credit Kooijman, 2000)*

Ongoing forward genetics studies of the pennate diatom *Seminavis robusta* in which the sexual cycle can be easily manipulated (Chepurnov *et al.*, 2008) seem to make it a promising candidate as a model system in elucidating the molecular mechanism associated with the cell size reduction, the switch from mitosis to meiosis and auxospore formation (Huysman *et al.*, 2013). This study complementing the existing knowledge about the identified diatom specific mitotic structures (De Martino *et al.*, 2009) along with the effects of nutrient limitation (Smetacek 2012) and daylight (Ashworth *et al.*, 2013) on cell cycle may shed more light on a set of genes for which no expression or functional data exists which is estimated to account a half of the identified gene repertoire in diatoms (Bowler *et al.*, 2008).

1.4.1.2 Mitosis and cytokinesis

The ultrastructural appearance of interphase nuclei in diatoms is similar to that of other eukaryotic algae but cells preparing to divide displays specific organisation of the

organelles involved in orchestrating the mitosis. Diatoms that approaches division lack centrioles, which organize the microtubular spindles of most eukaryotic organisms. This role is substituted by an electron-dense body often termed spindle precursor or microtubule organising center (Sluiman, 1993). In the prophase chromosomes are formed but they are not attached to the microtubules by kinetochores like in other organisms. Rather, diatom chromosomes seem to be attached by a dense material that extends from the chromatin to the pole (Pickett-Heaps *et al.*, 1990) encircling the central spindle as a collar (Huysman *et al.*, 2013). Cytoplasmic cleavage begins by ingrowth of a furrow extended from the cell membrane. Ultimately, cytokinesis is completed by emergence of nuclear envelopes.

1.4.2 Ecology and nutrition of diatoms

Over the year may appear periods that are not suitable for growth. Such periods may be induced by the stratification of the water column, nutrient depletion or lower. Diatoms may respond to these unfavourable environmental conditions by generating spores and resting cells (Hargrave and French, 1983; Smetacek, 1985). The development of diatom resting cells or spores does not usually involve sexual reproduction. Resting cells of some freshwater diatoms can survive in sediments for years. Such cells are generated condensing cytoplasm in a dark brown mass that is rich in lipid droplets and polyphosphate granules (Sicko-Goad *et al.*, 1986). Vegetative cells can suffer other alterations while forming resting cells as well. Such alterations are characterised by thickened frustule which may get a rounder shape and will exhibit less ornamentation than vegetative cells. Freshwater and pennate diatoms tend to produce resting cells, whereas coastal marine centric diatoms display preference to produce spores (Graham *et al.*, 2009). Spore production unlike resting cell production needs silicate for frustule thickening. Spores are believed to be able to survive for decades in sediments (Härnström *et al.*, 2011). The spores of marine diatoms often occur in marine snow playing important role in transporting or trapping organic carbon and silica to the sediments.

Diatom growth in open ocean water is commonly limited by silica, nitrate and iron concentration dissolved in the water. Many species of the diatom *Rhizosolenia* form mats that sink below the sunlit surface layer to reach subsurface nitrate pools. Then, nitrate replated cells rise back to the surface level to maximise again their

photosynthetic capacity, providing a previously unknown mechanism for the transport of nitrate from deep to surface waters (Graham *et al.*, 2009). Previous studies suggested that by this vertical migration up to 40 µmol N $m^{-2}day^{-1}$ could be conveyed to the surface (Villareal *et al.*, 1996). Other adaptation to low nitrate condition is represented by marine diatoms *Bacteriastrum* and *Chaetoceros* by forming symbiotic associations with nitrogen-fixing cyanobacteria *Richelia* and *Calothrix* (Foster and Zehr, 2006).

Some diatom species seem to possess intracellular silicon storage pools that might represent up to 50% of the total cellular biosilica, depending on species (Martin-Jézéquel *et al.*, 2000), others like *Thalassiosira oceanica* have adapted to low iron concentration by replacing the iron-containing electron transport substance cytochrome c_6 to copper-containing plastocyanin found in cyanobacteria (Peers and Price, 2006).

Some diatoms are able to populate areas where light conditions are significantly reduced like sea-ice, shaded streams and sediments where they feed heterotrophically. In these areas low light is the trigger that induces the uptake of organic carbon, process known as osmotrophy. One specific representative is *Cyclotella meneghiniana* in which glucose uptake is induced by several hours of darkness (Lylis and Trainor, 1973). Heterotrophic diatoms can be found attached to living or dead animals, aquatic plants or other algae.

The diatom *Thalassiosira rotula* and *Skeletonema costatum* seem that are able to produce polyunsaturated aldehydes to reduce the fitness of copepods grazers (Wichard *et al.*, 2007) but also displays antibacterial activity (Amin *et al.*, 2012) along with fatty acids palmitoleic acid and eicosapentaenoic acid, both of which are produced by *P. tricornutum* and inhibit growth of Gram-positive bacteria (Desbois *et al.*, 2009).

Last but not least some diatoms are known by their ability to produce toxins which are potentially harmful to the environment or humans. The most eloquent example of such a diatom is *Pseudo-nitzschia* spp, a ubiquitous genus of marine and estuarine diatom known to produce the amino acid neurotoxin domoic acid which cause amnesiac shellfish poisoning in humans and high animal mortality. The neurotoxin domoic acid occurs both in coastal and oceanic waters, and its concentration, associated with changes in *Pseudo-nitzschia* abundance, likely varies naturally with climate cycles, as well as with artificial iron fertilization. Thereby, consideration of the potentially serious

ecosystem impacts associated with domoic acid makes further iron fertilization projects prudent (Silver *et al.*, 2010).

1.5 The molecular underpinning of bloom formation in Diatoms

Albeit diatoms dominate spring phytoplankton blooms globally (Martin *et al.*, 2011) and their productivity drives high production rates of higher trophic levels (Armbrust *et al.*, 2004; Armbrust, 2009) genomics studies have so far examined only a tiny portion of existing diversity of diatoms. A recent plankton interactome study revealed that diatoms appear to exclude other organisms and thus to be more competitive than other phytoplankton groups, which seem to rely more on collaboration rather than competition (Lima-Mendez *et al.*, 2015). In addition, it was hypothesized that marine organisms adapt to dynamic environments by higher metabolic plasticity and increased number of transcriptional regulators (Maumus *et al.*, 2009). Insights into the molecular regulation of such processes have been made through whole genome sequencing of two model diatom species *Thalassiosira pseudonana* (Armbrust *et al.*, 2004), *Phaeodactylum tricornutum* (Bowler *et al.*, 2008) and the polar species *Fragilariopsis cylindrus* (Mock *et al.*, in press) complemented by the draft sequences of the toxigenic coastal species *Pseudo-nitzschia multiseries*, albeit the majority of genes are of unknown function yet. The unusual gene repertoire found in diatoms has been proposed to underpin their ecological success in the contemporary ocean (Armbrust *et al.*, 2004; Bowler *et al.*, 2008). However, the molecular machinery that made diatoms one of the most successful blooming phytoplankton group is limited.

Diatoms, like all marine microalgae, employ a carbon concentrating mechanism (CCM) to concentrate CO_2 to overcome the poor affinity of the photosynthetic enzyme RuBisCO (ribulose-1,5-biphosphate carboxylase/oxigenase) for CO_2 (Badger *et al.*, 1998; Giordano *et al.*, 2005). The activity of CCM is facilitated by low temperature, which promotes a high solubility of CO_2 in water and a low half-saturation constant for RuBisCO. The poor CO_2 buffering capacity, the slow diffusion of CO_2 and the slow enzymatic carboxylation rate may make the operation of the CCM particularly critical during phytoplankton blooms in cold water (Kranz *et al.*, 2014). A biophysical mechanism based on transformations between bicarbonate (HCO_3^-) and CO_2 via carbonic anhydrases coupled to transport of inorganic carbon within the cell was well

described in the green alga *Chlamydomonas reinhardtii* where the presence of a pyrenoid reduces diffusion losses of CO_2 (Parker *et al.*, 2008). In contrast, in the pennate diatom *P. tricornutum* a CCM seems to be based on a plastid-targeted carbonic anhydrase and a putative plastid-targeted sodium bicarbonate translocator. There is no evidence of targeting of either protein to the plastid in the centric diatom *T. pseudonana*, although the latest possesses multiple carbonic anhydrases, most of them appearing to be cytosolic with only one that appears to possess a signal peptide (Kroth *et al.*, 2008). An alternative way to deliver CO_2 to RuBisCO was proposed by a biochemical CCM cycle called C4 pathway through the fixation of CO_2 into phosphoenolpyruvate generating oxalacetic acid transported to the plastid by membrane transporters. The oxalacetic acid is converted into malate by malate dehydrogenase and subsequently decarboxylated by NADP-dependent malic-enzymes to generate the CO_2 fixed by RuBisCO along with pyruvate which is phosphorylated to regenerate phosphoenolpyruvate and exported to the cytosol (Parker *et al.*, 2008). However, in both diatoms the expected decarboxylating enzymes necessary for C4 metabolism such as phosphoenolpyruvate-carboxy-kinase and two members of the malic enzymes appear to be targeted to the mitochondria but no plastid-targeted translocators for oxalacetic acid were found. As a consequence it was suggested that a C4-like pathway in diatoms could concentrate CO_2 in the mitochondria before delivery to the plastid for fixation by RuBisCO (Kroth *et al.*, 2008).

A specific expansion of heat shock factors compared to other transcription factor families was identified in *T. pseudonana* (Rayko *et al.*, 2010). Heat shock factors (HSF) are evolutionarily conserved stress-response regulators which in eukaryotes are involved in the expression of genes with roles in cell maintenance and differentiation as well as in developmental processes. Heat-shock factors were the most abundant upregulated transcripts in *T. pseudonana* under temperature and nutrient limitations (Thamatracoln *et al.*, 2012; Dhyrman *et al.*, 2012). Enrichment of heat-shock factors may indicate the importance of transcriptional regulation in response to environmental stress in diatoms (Montsant *et al.*, 2007).

The *P. tricornutum* genome was found to be especially enriched in a diatom-specific class of copia retrotransposons, the expression of some of which are responsive to stress events such as nutrient starvation (Maumus *et al.*, 2009). Among nutrients nitrogen is indispensable for growth (Valenzuela *et al.*, 2012) being an essential component in

amino acids, proteins, nucleic acids and some signalling molecules such as NO. Nitrogen can be taken up in inorganic (NO_3, NO_2, NH_4) or organic form as urea or amino acids. Eukaryotic phytoplankton, excepting some nitrogen-fixing diatom symbioses between the host and a cyanobacteria, the diatom-diazotroph assotiations such as *Hemialurus* or *Rhizosolenia-Richelia*, are unable to utilize nitrogen in gaseous form. Generally, diatoms outcompete other phytoplankton for nitrate in nutrient rich coastal or upwelling zones but are rare in low nutrient, low chlorophyll environments (Smayda, 1997; Nunn *et al.*, 2009). Diatoms encode several transporters for nitrate, ammonium and urea which may lay at the base of their ability to populate turbulent often light limited waters. Nitrate transporters are highly expressed in the diatom *Skeletonema costatum* under both, nitrate replate and nitrate limiting conditions (Hildebrand and Dahlin, 2000) suggesting that diatoms are able to take up nitrate when it is both plentiful and scarce. Nitrate uptake and assimilation are both important to diatoms nutrition as well as an energy dissipation pathway where excess nitrate is used as an electron sink (Lomas and Gilbert, 1999; Lomas and Gilbert, 2000). Reviewed by Hopes and Mock (2015) some studies suggests that genes for transport of organic nutrients such as amino acids and purines (Armbrust *et al.*, 2004; Bowler *et al.*, 2008; Worden *et al.*, 2009) may help provide nitrogen during oscillating nutrient levels, whilst genes for a complete urea cycle, previously assumed to be an exclusively heterotrophic pathway for the detoxification of intracellular ammonia (Armbrust *et al.*, 2004), thought to originate from the host of secondary endosymbiosis, may allow rapid recovery after nitrogen (Allen *et al.*, 2011) and carbon (Parker *et al.*, 2008) deprivation. Recovery of nitrogen is suggested to occur in the plastid by the conversion of glutamate to glutamine or alternatively enters in the urea cycle as NH_3 and CO_2 resulted in photorespiration generating besides urea creatin-phosphates (storage molecules), long-chain polyamines (silica precipitation) or signalling molecules. It is suggested that the urea cycle could play a potential link in diatoms ability to switch between different pathways of energy dissipation depending on the availability of nitrogen sources (Parker and Armbrust, 2005). Also, a recent study demonstrated the importance of nitrate transporters to the survival of diatoms in dark and anoxic conditions (Kamp *et al.*, 2011).

Although several members of the common pathways in eukaryotic cells which couple nutrient sensing to cell division such as the Snf1 (sucrose-non-fermenting-1)/AMPK (AMP-activated protein kinase) (Hardie *et al.*, 2012) have been identified in the

genomes of *P. tricornutum* and *T. pseudonana* it is still unclear if they play a role in nutrient perception in diatoms (Huysman *et al.*, 2013). However, comparative genomics revealed that one of the expanded gene families in diatoms is represented by the cyclin gene family, along with histidine kinases and heat-shock transcription factors (Bowler *et al.*, 2008; Rayko *et al.*, 2010). The eukaryotic cell cycle control points represent the onset of DNA replication (the G_1-S transition) and mitosis itself (the G_2-M transition) (Buchanan *et al.*, 2000; Huysman *et al.*, 2013). Cyclins are proteins with particular oscillatory patterns of gene expression and protein destruction during the cell cycle (Evans *et al.*, 1983) which control the G_1-S and G_2-M transitions. Nitrate limitation causes an extended duration of the G_1 phase or an arrest at multiple G_1 checkpoints (Olson *et al.*, 1986; Vaulot *et al.*, 1987). In addition, a substantial number of diatom specific cyclin (dsCYC) genes were found many of them being up-regulated under certain environmental conditions (Bowler *et al.*, 2008; Huysman *et al*., 2010). The huge expansion of this gene family was suggested to reflect on the one hand the unique characteristics of diatom life cycles associated with constraints imposed by the rigid nature of their cell wall, such as the control of cell size reduction or the activation of sexual reproduction at a critical size threshold, and on the other hand the need to integrate a wide range of environmental cues into the cell cycle machinery (Huysman *et al.*, 2013).

A marked decrease in mechanisms that rely on iron-dependent enzymes such as photosynthesis and respiration was shown in the pennate diatom *P. tricornutum* (Bowler *et al.*, 2008). To reduce the production of reactive oxygen species (ROS) formed by the Fe-limited photosynthetic components excess electrons were channelled to mitochondrial alternative oxidase (AOX) and dissipated by upregulation of genes to increase nonphotochemical quenching (NPQ) capacity (Bowler *et al.*, 2008). Diatoms use an NPQ system that converts diadinoxanthin to diatoxanthin in the presence of a proton gradient (Goss and Lepetit, 2015) which is beneficial in coastal regions where spring blooms develop. Oceanic diatoms contain constitutively low levels of iron-rich photosystem I (PSI) complexes and some diatoms appear to replace the iron-rich cytochrome c_6 with the copper containing plastocyanin in the photosynthetic electron transport chain during conditions of chronic iron limitation (Strzepek and Harrison, 2004; Peers and Price, 2006). The presence and expression of genes such as *ferritin* and *LHCX* in some but not all diatoms allow survival in chronically nutrient limited or in

variable light environments (Bailleul *et al.*, 2010). *Fragilariopsis cylindrus*, a polar pennate diatom increases the number of genes for chlorophyll *a/c* light-harvesting complex (LHC) proteins (Mock *et al.*, in press) while a reduction of these proteins was described in other phytoplankton in response to stress (McKew *et al.*, 2013).

The environment could also induce additional variation, which could confer heritable phenotypic plasticity by epigenetic mechanisms, such as DNA methylation, histone modifications or involving small RNAs. Indeed, a dynamic regulation of DNA methylation was observed in response to nitrate starvation, with both genes and transposable elements being differentially methylated, suggesting a role in surviving nutrient limitation in the ocean (Veluchamy *et al.*, 2013). This finding is of special interest as termination of oceanic blooms are mostly associated with nitrate exhaustion from the water column. Furthermore, a recent study found that 66% of diverged alleles in the genome of *F. cylindrus* showed allele specific expression relative to optimal nutrient-replete growth and 45% of divergent alleles showed an allele specific expression in at least one of the tested conditions (such as temperature), suggesting the importance of differential allele expression in fine tuning gene regulation in response to the environment (Mock *et al.*, in press). The flexibility provided by epigenetic mechanisms and the presence of diverged alleles in the genomes of some diatoms in contrast to irreversible mutations may be particularly useful in a rapidly changing environment such as the ocean (Fuhrman, 2009; Bowler *et al.*, 2010; Tirichine and Bowler, 2011).

1.6 Applications of Diatoms

Diatoms grow quickly and are easy to genetically transform (Zaslavskaya *et al.*, 2000), characteristics which make them appealing systems for production of high value molecules. Diatoms are of great interest for several applications including the production of biofuels (Chisti, 2008; Radakovits *et al.*, 2010), biopolymers and computer chip manufacturing (Kroger and Poulsen, 2008; Gordon *et al.*, 2009), solar technology, microfluidics, catalyst production or bio-sensing. They are increasingly being used to produce polyunsaturated fatty acids (Harwood and Guschina, 2009; Hamilton *et al.*, 2013), polysaccharides (Raposo *et al.*, 2013), carotenoids or even vaccines (Specht and Mayfield, 2014). Over the centuries the sinking diatoms

constituted silica rich sediments known as diatomaceous earth widely utilised due to their structural and chemical composition as water filters during cholera epidemics, mild abrasives in toothpaste and metal polishes as well as stabiliser component in dynamite, but not least are also valuable model systems for studying cellular functions and cell division.

1.7 Thesis objectives

When environmental conditions become favourable for growth diatoms usually dominate sequential phytoplankton blooms in coastal upwelling and high latitude areas because they are able to grow faster than their competitors (Maranon *et al.*, 2012). However, the molecular machinery that made diatoms one of the most successful blooming phytoplankton group is unknown. Therefore identification of a possible regulatory mechanism which allows fast response of bloom forming diatoms to variable nutrient conditions and sudden changes in ocean may offer a better understanding of such processes.

The bloom inducer gene 1 (*big1*) was identified in a whole genome microarray study with the model centric diatom *Thalassiosira pseudonana* being strongly induced under silicate starvation (Mock *et al.*, 2008). A previous study confirmed that the encoding protein sequence of the *big1* does not show any significant similarity to other proteins (Hipkin, 2012). However, its activity was linked to diatoms' fast progression through the cell cycle post nutrient starvation and was found to differentially regulate about 30% of genes found in natural centric diatom blooms (Hipkin, 2012; Hipkin *et al.*, under revision).

Overexpressing genes is a widely accepted method in molecular biology to link function to genes and identify phenotypes (review Prelich, 2012) but the possibility to ascertain gene function through reverse genetics in diatoms represents a relatively new technique and a major advance for understanding their biology and the mechanisms underlying the success of these organisms in the oceans (De Riso *et al.*, 2009). Although the molecular tools for gentic manipulation in diatoms are now available for such studies experiments usually focus on investigating just one type of transformants (Poulsen *et al.*, 2006; Siaut *et al.*, 2007; Kroth, 2007). However, experiments conducted with transformants that

either overexpress or knock-down a gene allows a better understanding of the function of the gene and whether the expression of the gene is essential for viability.

The proteins as products of a given gene may possess the ability to affect multiple phenotypic characters endowing that gene with pleiotropic nature. Identification of such genes may help to elucidate intermediate ways on which a function of a protein pass through purifying selection. The knowledge acquired by such a process may play a crucial role in understanding the future phytoplankton successions in the oceans since the global sea surface temperature is approximately 1^0C higher now than 140 years ago, and is one of the primary physical impacts of climate change (Coppini *et al.*, 2007). Moreover, sea surface temperature in coastal seas is increasing more rapidly than in the global oceans (Lehmann *et al.*, 2011) potentially affecting the most productive and dynamic ecosystems on the oceans, the coastal upwelling zones, where diathoms thrive. In such a context, this study aimed to bring further insights in characterising the regulatory role of the BIG1 protein with emphasis on diatoms' ability to quickly respond to sudden changes in environment.

In **Chapter 2** I describe the laboratory and computational methods used in this work. First I present the materials and methods based on the experimental work performed in the framework of this thesis followed by the presentation of the statistical and bioinformatics approaches used for data analysis.

In **Chapter 3** I present results from nitrate limitation experiments. Diatoms cell cycle is intrinsically linked with the formation of their silica frustule and without silicate diatoms cannot enter the S-phase of the cell cycle, and therefore they will not divide (Hildebrand *et al.*, 2007). To synthesize their frustule, diatoms also require disolved nitrogen for proteins that precipitate silica and polyamines that aid the process of silica precipitation (Sumper and Kroeger, 2004). Thus, diatom cell division, and therefore their ability to form blooms are dependent on the availability of silicate (Allen *et al.*, 2005) and dissolved nitrate (Bruland *et al.*, 2001). Phytoplankton species compete with diatoms for nitrate in the ocean while limiting silicate impacts only on diatoms. Therefore, phenotyping experiments were conducted with the aim to determine a) how BIG1 functions in relation to simulated bloom conditions by nitrate starvation and subsequent re-addition, b) whether BIG1 impacts on cellular morphology and c) how nitrate limitation affects gene expression of *big1*.

In **Chapter 4** I present results from temperature experiments. Field studies are able to link biomass to temperature (Raven and Geider, 1988), but temperature was found to be strongly correlated with nutrient concentration, and it is not fully understood whether temperature itself or the associated indirect effect on nutrient depletion will be more influential (Finkel *et al.*, 2010; Lopez-Urrutia and Morán, 2015), although a recent study suggest that temperature is the main driver of the functional composition of the euphotic zone (Sunagawa *et al.*, 2015). In the intent to investigate the impact of temperature on the physiology of wild type and transgenic *T. pseudonana* lines temperature experiments were conducted over a temperature gradient (Eppley, 1972). I aimed to investigate a) the adaptive potential of BIG1 transgenic lines to temperature, b) to assess the conferred thermal limits and the niche width, c) the recoverying ability following exposure to the temperature tolerance limit and d) examine the expression of genes linked to the light reaction of photosynthesis, when the energy of light is captured and used to produce ATP and NADPH the 'energy currency' molecules of cells, and ultimately growth. This study is the first to assess thermal traits conferred by the BIG1 protein.

In **Chapter 5** I present preliminary results and limitations of chromatin immunoprecipitation followed by high-throughput DNA sequencing (ChIP-seq) of the DNA-binding protein BIG1. Chromatin immuno-precipitation (ChIP) has become a powerful tool to detect *in vivo* interactions between a DNA-associated protein and genomic DNA. ChIP combined with massively parallel sequencing is used to study gene regulatory networks active during development and/or in response to the environment (Lin *et al.*, 2012). The BIG1 DNA binding protein was integrally linked to growth in *T. pseudonana*. Thus, identification of the binding sites of BIG1 in the genome of *T. pseudonana* would provide new insights into genes responsible for bloom formation of diatoms in the ocean.

In **Chapter 6** I conclude with a summary of the major findings of the research and a general discussion of the main results. I attempt to give an integrative view on the ecological implications together with future research perspectives. The thesis ends with References.

CHAPTER 2: MATERIALS AND METHODS

2.1 Diatom species

The marine centric diatom *Thalassiosira pseudonana* (Hustedt) Hasle et Heimdal clone CCMP1335 was used for all experiments. This strain is available from the NCMA (National Center for Marine Algae and Microbiota; Boothbay Harbor, USA), formerly known as the Center for Culture of Marine Phytoplankton https://ncma.bigelow.org/. This clone was collected in 1958 from Moriches Bay (Long Island, New York, USA) and has been maintained continuously as axenic cultures in L1 medium at 14^0C (Hasle and Heimdal, 1970; https://ncma.bigelow.org/ncma-news/strain1/). Additionally this clone was cryopreserved on Aug 22 2000 using 12% DMSO as a cryoprotectant being available from cryopreserved stocks as well (https://ncma.bigelow.org/). It was the first eukaryotic marine phytoplankton used for whole genome sequencing by the JGI genome project and its genome sequence is available from http://genome.jgi-psf.org haps3 haps3.download.ftp.html.

Two genetically transformed strains of the *T. pseudonana* CCMP 1335 were used as well. The knock-in cell line which overexpress the protein encoded by the bloom inducer gene 1 (*big1*) was constructed with microparticle bombardement of the *T. pseudonana* by the vector (pTpNR) expression cassette (Poulsen et *al*., 2006). This cassette contains the regulatory sequence for nitrate reductase, the gene of interest tagged with eGFP and an antibiotic resistance gene against nourseothricin, making possible the selection of colonies with 100 µg/ml nourseothricin (clonNAT). The construction of plasmid was performed by Mock and Durkin and described by Hipkin (2012). The second cell line was obtained by knocking-down the *big1* gene (see 5.1 for details).

2.2 Culturing techniques

T. pseudonana clone CCMP1335 and both transformants, the overexpression and the knock-down of the BIG1 were grown in artificial seawater medium according to the North East Pacific Culture Collection (ocgy.ubc.ca/projects/nepcc/media.htm) at 20^0C under constant light at 80-90 mmol/photons $m^{-2}s^{-1}$ (Scalar PAR Irradiance Sensor QSL 2101, Biospherical Instruments Inc., San Diego, USA) in a MLR-350H Versatile Environmental Test Chamber (Sanyo Electric Biomedical Co. Ltd., Japan). Glassware was washed with detergent, thoroughly rinsed with hot water and rinsed three times with MilliQ water than air dried. Thereafter the glassware was autoclaved at 121^0C for 30 minutes prior to use. Culture transfers and sampling was performed in a Class II Microbiological Safety Cabinet (Class II, Walker, Glossop, UK).

2.2.1 Media preparation

All cultures of *T. pseudonana* were grown in NEPCC medium according to the North East Pacific Culture Collection (Harrison *et al.*, 1980). The NEPCC medium is composed of anhydrous and hydrous salts as well as macro and micronutrients. The macro and micronutrients were filter sterilised with a 0.22µm filter unit (Millipore) and stored as stock solutions at 4^0C. Appropriate quantity of NEPCC medium was made diluting the anhydrous and hydrous salts in MilliQ water stirred overnight. Next day the macro and micronutrients were added, stirred for 2-3 hours subsequently the pH was adjusted to 8.0-8.2 with hydrochloric acid. F/2 vitamins were added last ones and stirred again for 1 hour. Thereafter the media was filter sterilised passing in a series of filters Policap TC (0.45 µm) followed by Policap AS (0.2 µm) (GE Healthcare, UK) and an additional 0.22 µm filter unit (Millipore). This approach was chosen to remove unwanted or accidental precipitation of solvents following the autoclaving process.

Table 2.1: *Composition of NEPCC medium with the final micromolar concentrations, *solution sterilised by filtering through 0.22* µm *filter unit (Millipore)*

Compound	**Stock solution (g/L)**	**Quantity in 1L NEPCC**	**Final concentration in the NEPCC medium (µM)**
Anhydrous salts			
NaCl	--	20.8g	$0.36x10^6$
Na_2SO_4	--	3.5g	$0.25x10^5$
Hydrous salts			
$MgCl_2•6H_2O$	--	9.6g	$0.10x10^6$
$CaCl_2$	147.02	9.00mL	
KCl	223.62	2.66mL	$7.98x10^3$
Macronutrients			
$NaNO_3$	47	1mL	550
$Na_2SiO_3•9H_2O$	30	1mL	105
Na_2-Glycerophosphate*	0.60	1mL	27.78
Micronutients			
$Na_2SeO_3•5H_2O$	0.173	0.1mL	1.00
$SrCl_2•6H_2O$	21	1mL	78.8
H_3BO_3	25	1mL	404.3
Solutions:	**Quantity in 1L of stock**		
Trace metal solution*		1mL	--
$Na_2EDTA•2H_2O$	1.86		0.05
$ZnCl_2$	32.7mg		0.239
$CoCl_2•6H_2O$	20.2mg		0.156
$Na_2MoO_4•2H_2O$	126mg		1.3
$MnCl_2•4H_2O$	475mg		2.4
Iron solution*		1mL	10.85
$Na_2EDTA•2H_2O$	3.72g	--	
$FeCl_3•6H_2O$	1.76g	10.85	
NaF	3.00g	--	
KBr	85.00g	--	
Vitamins*		1mL	--

Thiamin•HCl (vit.B_1)		0.2g	0.296
Biotin (vit. H)	0.10g	10mL	$4.09x10^{-3}$
Cyanocobalamin (vit. B_{12})	1.00g	1mL	$1.48x10^{-3}$

2.3 Growth experiments

Cells from stock cultures were acclimated and subcultured approximately 20 generations. Cells were transferred three to four times during the exponential growth phase, and grown under light conditions specified above (see 2.1) at 20^0C in a culture chamber until they reached the exponentially growth stage and a photosynthetic efficiency of 0.6 Fv/Fm (see 3.1.2) or higher. The cultures were monitored daily. When cells reached Fv/Fm of 0.6 they were inoculated in triplicate at a final concentration of 25,000 cells/ml into 100 µM NO_3 limited media. Growth stage was followed with daily cell counts, microscopic counts for aggregation (see 3.1.3) and Fv/Fm measurements. Cultures were shaken in daily basis. Cells were maintained in stationary phase induced by nutrient limitation for a six days before an aliquote of 25,000 cells/ml was inoculated into nutrient replete NEPCC medium. The recovery and successive growth in nutrient replete medium was recorded every 12 hours with cell counts, microscopic analysis and Fv/Fm assessments. In order to get nutrient limited NEPCC media all nutrients were doubled excepting vitamins but the nutrient of interest, which was modified to the desired concentration. As nutrient replete media NEPCC was used at normal concentration according to the North East Pacific Culture Collection (Harrison *et al.*, 1980) (ocgy.ubc.ca/projects/nepcc/media.htm).

Figure 2.1*: The temperature gradient bar with the thermal gradient bar controller unit*

Temperature stress experiments were designed to test the *T. pseudonana* transgenic cell-lines and wild type response to temperature and acclimation. The experiments were completed in 55 ml culture tubes (Pyrex Brand 9826) in a temperature gradient bar (Buitenhuis, in prep.) across a temperature gradient between 5^0C and 40^0C and under constant light at 175 mmol/photons $m^{-2}s^{-1}$ (Scalar PAR Irradiance Sensor QSL 2101, Biospherical Instruments Inc., San Diego, USA) ± 5 mmol/photons $m^{-2}s^{-1}$, see Figure 2.1. Because the lower temperature tolerance limit was not achieved by the gradient bar settings supplemental temperature points at 5^0C and 7^0C were added using incubator chambers (see 2.2) for lower temperatures.

2.3.1 Cell characteristics

During all growth experiments cells were counted in a daily basis using a Beckman Coulter Counter (Beckman Multisizer 3 Coulter Counter, High Wycombe, UK) (see 3.1.1) and light adapted photosynthetic efficiency was measured with a Walz PHYTO-PAM Phytoplankton Analyzer linked to a PHYTO-ED Emitter-Detector Unit COMPCT version (Heinz Walz GmbH, Effeltrich, Germany) (see 3.1.2). Further physiological depiction including cell morphology was analysed with a microscope and random flow cytometry check for the presence of GFP was made as well (see 3.1.4).

2.3.1.1 Cell counts

The growth of cultures was monitored using a Beckman Coulter Counter with a 100 µm aperture tube. The particle counter uses a technology developed for counting and sizing

particles using impedance measurements (Graham, 2003). The technology was principally developed to count blood cells quickly by measuring the changes in electrical conductance as cells suspended in a conductive fluid passed through a small orifice. This change can be measured as a voltage pulse or a current pulse. The pulse height is proportional to the volume (or size) of the sensed particle. It can be used to measure any particulate material that can be suspended in an electrolyte solution. Particles as small as 0.4 µm and as large as 1600 µm in diameter can routinely be measured depending from the diameter of the aperture tube (Marshall Don. Graham, 2003). Preceding any counting a blank measurement was used to take in account the possible background noise. Afterwards an aliquot of cells were diluted to 1/10 ratio with 0.2 µm filtered NEPCC salt base. The goal of this step was to try to avoid clumping of cells during measurements. Specific growth rates per day (µ) were calculated from the linear regression of the natural log of cell counts related to time during exponential phase according to the equation:

$$\mu(d^{-1}) = \frac{\ln(C_1) - \ln(C_0)}{t_1 - t_0}$$

where C_1 represents the cell concentration at time t_1, C_0 the cell concentration at time t_0 and $t_1 - t_0$ the time difference in days between sampling intervals.

2.3.1.2 Maximum quantum yield of Photosystem II (F_v/F_m)

The maximum quantum yield of the Photosystem II (F_v/F_m) was measured with a Walz PHYTO-PAM Phytoplankton Analyzer fluorometer (Walz Gmbh, Effeltrich, Germany) equipped with a Phyto-ED head and visualized by the PHYTO-WIN software of the same company. Chlorophyll fluorescence is excited alternatingly at high repetition rates by microsecond LED-light pulses at four different wavelengths (470, 520, 645 and 665 nm light) and the photosynthetic performance is assessed by application of actinic light and saturation pulses. The *in vivo* photosynthetic performance and light-adaptation state of the various types of phytoplankton can be assessed from fluorescence readings of dark acclimated samples according to the established equation:

$$F_v/F_m = \frac{(F_m - F_0)}{F_m}$$

where F_m and F_0 represent the maximum and the minimum fluorescence level (Maxwell and Johnson, 2000).

2.3.1.3 Microscopic analysis of *T. pseudonana* cells

Microscopic analysis was carried out to analyse cell morphology and possible aggregation tendency. All analyses were performed under phase contrast microscopy using a Olympus BX40F-3 Research Microscope (Olympus Optical Co. Ltd., Japan) at a 200 times magnification. The microscope was equipped with a U-CMAD3 mount adapter, U-TV1X-2 direct image video port and an Olympus C-5060 Microscope Digital Camera Adapter to hold an Olympus Camedia C-7070 camera. In the course of nutrient limitation experiments, daily microscopic analysis was carried out in order to study the effects of nutrient limitation on stationary phase. The aggregation in *T. pseudonana* cells was monitored in recovery in nutrient replete NEPCC media as well. To facilitate counting of cells and aggregates, a counting chamber with cell depth of 0.1mm, area of 1/400mm^2 and an Improved Neubauer Ruling was used (Improved Neubauer cell haemocytometer BS748, Weber England, UK). Cells and aggregates were counted once a day during nutrient limitation stage and twice a day in the recovery stage following starvation. Total cell number and differential particle size was recorded and an aggregation ratio was calculated by dividing the total cell number with the number of aggregates. This value was used to correct the Coulter counter measurements, which are not able to distinguish between individual cells and aggregates.

2.3.1.4 Flow cytometer analysis

FACSCalibur (Beckton Dickinson) flow cytometer was used to confirm the presence of the green fluorescent pigment in exponentially growing BIG1 knock-in cells overexpression cell line. The green fluorescence emitted by the BIG1-GFP was measured in the FL1 channel using a 515-545nm emission filter. MilliQ water was used as a sheath fluid. The analyses were done on a low flow rate (20µl per minute calibrated with beads) and recorded for 2 min or until 100,000 events had been reached. The assays were diluted with 0.22 µm filtered NEPCC medium salt base. The µ control was performed to certify the presence of the BIG1 insert to avoid the accidental use of mixed cultures. If the BIG1-GFP construct lose the GFP following translation mixed

GFP lacking and expressing cultures may be present. In order to avoid any bias caused by such mixed cultures BIG1 knock-in was frequently monitored with flow cytometer.

2.4 Selection of single colonies

Single cell colony selection was applied to assure the use of only that BIG1 knock-in cultures which express GFP in the growth experiments and the followed molecular analysis, as this method allowed us to avoid confusion using cultures which may behave like the wild type. The selection was made on 0.8% agar plates. NEPCC media was diluted 1:1 with MilliQ water. Subsequently 0.4g agar was added and autoclaved at 121^0C for 30 min. When the agar-medium mix cooled to 40^0C macronutrients, micronutrients, vitamins and 100 µg/ml nourseothricin were added. The media mix was poured in petri dishes and air dried in the safety cabinet. When the agar solidified 20µl of BIG1 knock-in was inoculated and streaked with a sterilised wire loop on each plate. The plates were incubated at 20^0C under constant light at 80-90 mmol/photons $m^{-2}s^{-1}$ for 10-14 days. The resulting single cell colonies were transferred in liquid NEPCC media with 100 µg/ml clonNAT and tested with flow cytometer. Afterwards stock cultures were made from the positive ones and used in experiments.

2.5 Genetic transformation of *T. pseudonana* cells

2.5.1 Construction of plasmid (pTpFB1AS) performed by Amy Kirkman

The construction of knock-down cell lines was performed by amplifying a 249 bp fragment of the *big1* gene using the following primers:

*big1*KDF (ataagaatGCGGCCGCAAGCTTGAGGAGATTGCGTTCGAAAAGGC
*big1*KDR (ataagaatGCGGCCGCGATATCTGGTCGCAACGGGCATTGC

Primers were designed to contain restriction sites for NotI and HindIII (sense) and NotI and EcoRV (antisense), underlined and shaded, and additional nucleotides to aid NotI binding, lowercase). The resulting fragment was cloned into the parent vector pTpFCPNAT (Poulsen *et al.*, 2006) between the NAT nourseothricin resistance gene and the FCP terminator using the NotI restriction site. Resulting vectors were screened for the antisense orientation of the fragment using the EcoRV site introduced in the reverse primer, and the BglII restriction site located in the FCP terminator, yielding a

368 bp or 119 bp fragment for antisense or sense orientation respectively (see Appendix 1). The selected antisense vector was checked by sequencing with primer TpFCPt (CATTGGATCTTAGCTAGCCG) (Poulsen *et al.*, 2006) prior to transformation by microparticle bombardment. Colony PCR was used to confirm the presence of the antisense *big1* cassette in *T. pseudonana* CCMP 1335 genome (see 5.5.1) and to assess the reduction in protein expression Western blot (see 2.6.4) was performed.

2.5.2 Transformation of competent *E.coli* cells

The transformation protocol of the manufacturer (New England Biolabs Ltd., Herts SG4 0TY, UK) was followed in order to introduce the required vector expression cassette (pTpFB1AS, pTpNR) in *E.coli* plasmid DNA. Transformation was made using the Bio-Rad Biolistic PDS-1000/He Particle Delivery System (Bio-Rad, Hercules, CA, USA) fitted with 1350 psi and 1550 psi rupture discs as previously defined by (Poulsen *et al.*, 2006). For this purpose 0.05 ml of chemically competent NEB 5-alpha competent *E.coli* cells were thaw on ice for 10 minutes. Cells were carefully mixed with ≈100ng of plasmid DNA and incubated on ice for 30 minutes. The cells were heat shocked at 42^0C for 30 seconds and placed on ice for 5 minutes. The heat shocked cells were diluted with 950µl of room temperature SOC outgrowth medium (New England Biolabs) / pre-warmed LB medium (10 g/l tryptone, 5 g/l yeast extract, 10 g/l NaCl, pH 7) and incubated at 37^0C for 60 minutes under vigorous shake. Antibiotic selection was performed onto 1.5% LB-agar plates with 100 µg/ml ampicillin. One hundred µl of transformed *E.coli* cells were spread onto selection plates and incubated overnight at 37^0C.

2.5.3 Plasmid extraction

Three colonies of transformed *E.coli* cells from the 1.5% agar-ampicillin-LB medium selection plates were pick and grown overnight at 37^0C in liquid LB medium under antibiotic selection (100 µg/ml ampicillin) and constant shaking. High-quality plasmid DNA was isolated with the PureYield™ Plasmid Maxiprep System (Promega, Madison, WI 53711, USA) using a silica-membrane column from 200 ml of transformed bacterial culture following the manufacturer instructions. DNA was quantified utilizing a NanoDrop ND-1000 Spectrophotometer (Thermo Scientific, Rockford, lL 61105, USA) measuring absorbance at 260 nm to 280 nm wavelength.

2.5.4 Transformation of *T. pseudonana* cells

The centric diatom *T. pseudonana* CCMP 1335 (wild type) cells were grown to a cell density of around $1x10^6$ cells/ml in NEPCC media then $1x10^8$ cells were harvested by centrifugation at 3000xg for 10 minutes and resuspended in 250µl of NEPCC media. For each transformation the collected diatom cells were spread on a 1.2% agar plate (transformation plates) and let to dry in the safety cabinet and rotated every 5 minutes to get an even drying.

For particle bombardment, tungsten W-particles were washed and coated with plasmid DNA. Five µl of 1µg/µl plasmid DNA with the required vector was added to the washed W-particles beside 50µl 2.5M $CaCl_2$ and 20µl 0.1M Spermidine and vortexed continuously for 3 minutes. The particles were collected by a 10 seconds spin at 12,000xg, the supernatant removed, the pellet resuspended in 250µl ethanol and vortexed for 1 minute followed by another 10 seconds spin. Finally the pellet was resuspended in 50µl ethanol and stored on ice until use. The washing step comprised from resuspension of 10 mg W-particles in 500µl ethanol, spin for 30 seconds of the solution, discard the supernatant and resuspension of the pellet in 250µl ethanol followed by 1-2 minutes stirring. A 30 seconds spin was applied, the supernatant discarded and the pellet washed three times with 250µl sterile water. The particles were stored on ice in 50µl aliquots.

Before use all equipment was sterilised. The microcarrier holders, stopping screens and two pair of tweezers were autoclaved. The microcarriers and rupture disks were immersed in ethanol and air dried in the safety cabinet prior to use. The other parts and the interior of the Biolistic particle gun was thoroughly wiped with 70% ethanol.

The transformation plates with the dried diatom cells were placed in the Biolistic chamber at a distance of 7 cm from the stopping screen. For each plasmid two independent transformation was done with the different rupture disks (1350 and 1500 psi) and the DNA coated W-particles.

Cells from the agar plates were washed off with 2 ml NEPCC media and transferred for overnight recovery into 100 ml liquid NEPCC media without antibiotic selection under constant illumination. Next day $0.5x10^7$ cells per 0.8% agar plate containing 100 µg/ml CloneNAT were spread and incubated at 20^0C under constant illumination. After 10-14 days single cell colonies were transferred in liquid media under antibiotic selection.

2.5.5 Transformation efficiency of the *T. pseudonana* cells

TpFB1AS colonies were tested performing Western Blot analysis with rabbit anti-9619 serum (see 6.4) and with polymerase chain reaction (PCR). Candidate cell lines were preselected by growing in 50 µM Si depleted NEPCC medium, see Figure 2.2.

2.5.5.1 Amplification of *big1* sequences for knock-down candidate screening

Colony PCR confirming the presence of the antisense *big1* cassette in *T. pseudonana* CCMP 1335 genome was performed in a TECHNE TC-512 (Bibby Scientific Limited, Staffordshire, ST15 OSA, UK) thermal cycler with an initial denaturation of 3 minutes at 95^0C followed by 30 seconds denaturation at 94^0C, 30 seconds annealing at 52^0C and elongation at a temperature of 72°C in 35 cycles. A temperature of 72^0C was set for final elongation for 10 minutes and terminated at a final hold at 4^0C. The primers used were:

forward 5'-TCTGGTCGCAACGGGCATTGC-3' and
reverse 5'-CATTGGATCTTAGCTAGCCG -3'.

The reaction mixture used was made with GoTaq Flexi Buffer (Promega, Madison, WI, USA) and dNTPs (Invitrogen, Carlsbad, CA, USA) according to the following recipe:

***Table 2.2**: Composition of the PCR reaction mix for 25 µl final reaction volume*

Reagents	Amount
GoTaq buffer	5 µl
25 mM $MgCl_2$	2 µl
10 mM dNTPs	0.5 µl
Each primer	1 µl
gotaq	0.25µl
H_2O	15.75µl

DNA fragments resulting from PCR reactions were analysed applying gel electrophoresis on 1% TAE agarose gel (40mM Tris-acetate, 1mM EDTA, 0.5 µg/ml Ethidium bromide) at 70V for 1 hour and visualised with a UV light transmitter.

2.6 Protein extraction and analysis

2.6.1 Protein extraction

T. pseudonana cell culture was grown in 100 µM NO_3 depleted NEPCC medium. Two hundred ml of exponentially growing cells were filtered on 1.2 um RTTP filter (Merk Millipore Ltd., Tullagreen, Carrigrwohill Co. Cork, Ireland) as well as cells which reached the fourth day of stationary phase. Subsequently cells were washed with 4 ml of nitrate depleted media and centrifuged at 4000 rpm at 4^0C for 10 min. The supernatant was poured off and the cell pellet was either resuspended in lysis buffer (50mM Tris-HCl pH 6.8, 2% SDS and 1x EDTA free Protease Inhibitor Cocktail (Roche cat. No. 11973 580 001)) or flash frozen in liquid nitrogen and stored at -80^0C. The cell pellet was vortexed with the lysis buffer and incubated at room temperature for 30 minutes. In order to facilitate the cell lysis was briefly vortexed again during incubation. Following the incubation cells were spin at 13000 rpm at 4^0C for 30 minutes. The supernatant was transferred to a clean 1.5 ml eppendorf tube and stored on ice. From the resulting protein suspension 2µl was used to test the protein concentration according to the Thermo Scientific Pierce BCA Protein Assay protocol (Pierce Biotechnology, Rockford, lL 61105, USA).

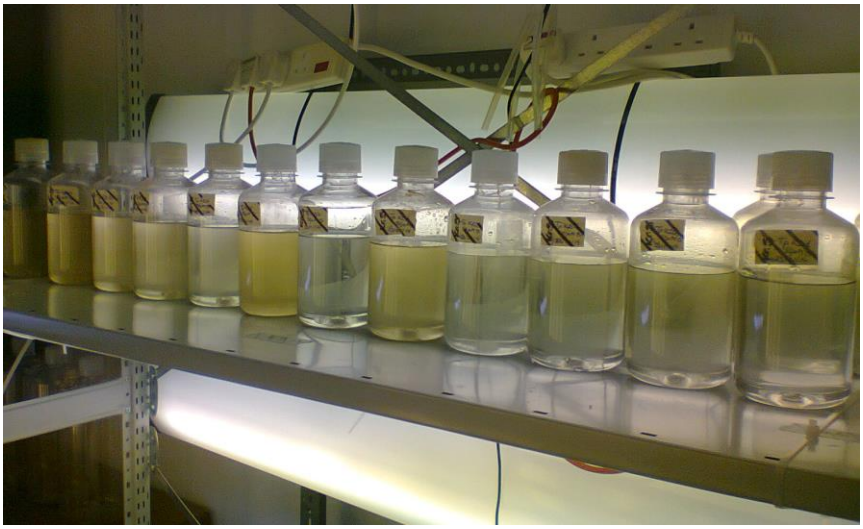

***Figure 2.2**: Growing biomass of T. pseudonana kock-down candidate cell lines for transformation efficiency control in 50 µM Si limited NEPCC medium at 20^0C. Those cell lines which showed significantly reduced growth indicated by less dense culutres were selected for subsequent PCR and Western Blot analysis*

2.6.2 Protein quantification

The extracted protein was quantified using a two-component, high-precision, detergent-compatible assay reagent set based on bicinchoninic acid (BCA) for the colorimetric detection and quantitation of total protein concentration compared to a protein standard with 1ml final volume, according to the manufacturer's instructions (Thermo Fisher Scientific Inc. PO Box 117, Rockford, lL 61105, USA). Bovine serum albumin (BSA) (Promega) was used to prepare standard curve in the range of 1µg/µl to 10µg/µl. The samples and standards were incubated in the reagent mix under standard condition at 37^0C for 30 minutes then, the absorbance of standards and samples were recorded with a spectrophotometer at 562 nm.

2.6.3 SDS-polyacrylamide gel electrophoresis (SDS-PAGE)

Polyacrylamide separating gel with 12% acrylamide concentration was used to perform the gel electrophoresis. The composition of the acrylamide gel consisting from the running gel and the stacking gel is shown in the *Table 3.*

Table 2.3: *Composition of the SDS-polyacrylamide separating gel used for gel electrophoresis*

Running gel		Stacking gel	
Reagents	**Amount**	**Reagents**	**Amount**
1.5M Tris-HCl pH 8.8	3.75 ml	0.5M Tris-HCl pH 6.8	1.25 ml
10% SDS	150µl	10% SDS	50µl
H_2O	5 ml	H_2O	2.75 ml
30% Acrylamide	6 ml	30% Acrylamide	1 ml
Temed	15µl	Temed	50µl
10% APS	150µl	10% APS	10µl

Laemmli sample buffer (Laemmli, U.K., 1970) (final concentration 2% SDS, 50mM Tris pH 6.8, Bromophenol blue 0.2 mg/ml, 10% v/v glycerol, 2.5% β-Mercaptoethanol (2-Mercaptoethanol)) was added to solubilized protein samples in $1/6^{th}$ ratio and boiled for 10 minutes at 98^0C prior to analysis by SDS-polyacrylamide gel electrophoresis. The protein samples were loaded into the gel accompanied by a prestained dual color molecular weight ladder with standard weights ranging between 10-250 kDa (Bio-Rad

Laboratories Gmbh, München, Germany). The gels were immersed in 1X Tris/Glycine/SDS running buffer (TGS) (25mM Tris, 192mM Gycine, 0.1% (w/v) SDS, pH 8.3) and ran for 35 minutes at 70V and 90 minutes at 100V voltage provided by a PowerPac™ Basic power supply (Bio-Rad).

2.6.4 Western blot analysis

The proteins from the SDS-PAGE gel were transferred on a nitrocellulose membrane (Amersham™ Protran™ 0.2µm, Germany) using a wet electrophoresis method (Bio-Rad). The transfer was made in pre-chilled transfer buffer (1xTGS, 10% methanol) for 1h and 45 min. When the transfer was complete the transfer of the proteins was imaged with Ponceau S (see 6.4.1). The membrane was blocked in 5% milk TBST (Tris-Buffered Saline (20 mM Tris and 150 mM NaCl), 0.1% Tween-20) at room temperature for 1 hour with gentle agitation. Thereafter the membrane was hybridised with the primary antibody (BIG1 anti-serum) produced in a rabbit against a 16 amino-acid long peptide sequence of BIG1 QPPTDYELSPEEAARR, at 1:1000 dilution with gentle swirling at 4^0C overnight. The membrane was subsequently washed three times with MilliQ water for 10 min with gentle agitation at room temperature. The secondary antibody was diluted in fresh 5% milk TBST and hybridised with gentle agitation for 1 hour at room temperature. The secondary antibody used was a horse radish peroxide (HRP) conjugated goat anti-rabbit antibody (Cell Signalling, Massachusetts, 01923, USA) to allow visualisation with chemiluminescence (see 2.6.4.2). The milk was poured off and the membrane was washed three times with MilliQ water for 10 min with gentle agitation at room temperature.

2.6.4.1 Visualisation of the protein transfer with Ponceau S

The protein loading was confirmed by staining the membrane following the blotting step with Ponceau S solution (0.1% w/v Ponceau S in 5% v/v acetic acid). The membrane was incubated under gentle agitation for 30 min at RT. Subsequently the membrane was washed indirectly with MilliQ water to remove the stain and let see the banding pattern of the proteins. Images were taken in white light than the remained stain was repeatedly washed off indirectly with MilliQ water.

2.6.4.2 Visualisation of blotted membranes

The Western Blot membranes were imaged with a chemiluminescent substrate (Thermo Scientific Pierce ECL Western Blotting Substrate, Pierce Biotechnology, Rockford, lL 61105, USA) for horseradish peroxidase (HRP) which is a two-component system consisting of a stable peroxide solution and an enhanced luminol solution (Thermo Scientific Pierce ECL Western Blotting Substrate, Pierce Biotechnology, Rockford, lL 61105, USA). To make a working solution, the two components were mixed together in a 1:1 ratio and poured over the blot. An increased incubation time of 4 minutes was applied compared to the instructions of the manufacturer and the excess removed. This method was adopted because on the blot a HRP-conjugated goat antibody was bound, which produced a light-emitting chemical reaction. Images were taken in a -30^0C cooled Fujifilm Las Imager 3000 camera at one minute exposure time.

2.7 RNA extraction and analysis

2.7.1 Total RNA extraction

Diatom cells were filtered onto 1.2 µm Isopore membrane filters (Millipore, Darmstadt, Germany) flash frozen in liquid nitrogen and stored at -80^0C. The RNA extraction was performed according to a modified Direct-zol™ RNA MiniPrep (Zymo Research, USA) extraction protocol. 1 ml of 65^0C preheated Trizol was added to the frozen filters, briefly shacked to wash off cells from the filters. Cell lysis was done by bead beating for 2 minutes at 4800 oscillations/min shaking speed (BioSpec 3110BX Mini-BeadBeater-1, Biospec Products, Bartlesville, OK). The resulted mixture was centrifuged for 2 minutes at 15,000 g at 4^0C. The supernatant was collected in clean tubes. One volume of pure ethanol was added to the sample homogenate and mixed thoroughly by vortexing. The sample mix was loaded onto separation columns placed in collection tubes and centrifuged for 1 min at 15,000 g at 4^0C. The columns were treated twice with 400 µl of the supplied RNA prewash buffer and centrifuge for 1 min at 15,000 g at 4^0C. The flow through was discarded. Subsequently the columns were washed with 700 uL RNA wash buffer and centrifuged for 1 min at 15,000 g at 4^0C. The columns were dried by a 2 minutes centrifugation at 15,000 g at 4^0C and transferred to clean RNAse free Eppendorf tubes. RNA was eluted in nuclease free water,

incubated for 5 minutes on room temperature and collected by centrifugation at 15,000 g for 1 minute.

The resulted RNA was treated with DNase I (Zymo Research, USA) for 1 hour at 37^0C in a thermal cycler, according to the following recipe:

***Table 2.4**: DNase reaction mix used to remove DNA contamination from RNA eluates.*

Reagents	Amount
RNA eluate	40 µl
10X DNase I Buffer	10 µl
DNase I stock 1U/µl	5 µl
H_2O	45 µl

The DNase was inactivated and selective recovery of total RNA was obtained by the use of a RNA Clean & Concentrator™-25 kit (Zymo Research, USA) which is based on a single-buffer system. The RNA was eluted from the Zymo-Spin™ IIC Column in nuclease free water. The RNA was quantified on a nanodrop (Thermo Scientific) at 260 nm to 280 nm and subsequently either used for RT-PCR or flash frozen and stored at -80^0C.

2.7.2 Real time quantitative polymerase chain reaction

Real time quantitative polymerase chain reaction (RT-qPCR) was performed for selected genes in the 9619 overexpression cell line compared to wild type and knock-down cell lines using an RT-qPCR protocol according to Nolan *et al*. (2006).

2.7.3 Reverse transcriptase reaction

First strand cDNA was reverse transcribed from 500 ng total RNA using SuperScript® III First-Strand Synthesis System for RT-PCR (Invitrogen, Carlsbad, CA, USA) with Anchored Oligo$(dT)_{20}$ (50µM) primer (Invitrogen, Carlsbad, CA, USA). The reverse transcription was performed according to the manufacturer's instructions for 10 µl reaction volume. The reaction mix was denatured at 65^0C for 5 minutes than chilled on ice for 1 minute. Ten µl of cDNA Synthesis Mix was prepared following the manufacturer's instructions and added to each RNA/primer mixture. The resulting

reaction mixture was gently mixed and collected by a brief centrifugation. cDNA synthesis was carried out at 50^0C for 50 minutes followed by inactivation at 85^0C for 5 minutes. The remaining RNA together with the RNA hybridized to DNA was removed by RNase H treatment at 37^0C for 20 minutes. The cDNA reverse transcriptase reaction mix was diluted 20-fold with molecular grade water and stored at -20^0C or used for qPCR.

2.7.4 Primer design and quantitative polymerase chain reaction

Oligonucleotides were designed targeting the 3' prime end using the web-based *PrimerQuest Tool* available at the IDT website (https://www.idtdna.com/Primerquest/Home/Index, Integrated DNA Technologies, Coralville, IA, USA) applying the following parameters: primer melting temperature of 62 – 68^0C with a TM optimum at 65^0C, GC content optimum of amplicon and primer of 50%, primer size 75 – 150 nucleotides and amplicon size 75 - 150 bp. Oligonucleotides were checked for self-dimers, hetero-dimers and hairpins using the OligoAnalyzer 3.1 tool of the same website (available at https://www.idtdna.com/calc/analyzer). The appropriate annealing temperature was controlled with the *TM Calculator* application of the New England Biolabs website (http:/ mcalculator.neb.com/#!/*).* All designed primers were subject to BLAST search against the *T. pseudonana* genome sequence *(*http://genome.jgi.doe.gov haps3 haps3.home.html*)* to make sure they are specific to the target gene, see Table 2.5. Primers were synthesized by Eurofins (Norwich, UK).

For qPCR reactions and second strand amplification 3 µl of the 20-fold diluted reverse transcriptase reaction mix was supplemented with 7.5 µl SYBR Green mastermix (SensiMix^{TM} SYBR No-ROX Master Mix (Bioline, London, UK) for 15µl total sample volume. Forward and reverse primers were added at a concentration of 200 nM. qPCR amplification reactions were performed in white 96-well plates on a CFX96 Touch™ Real-Time PCR Detection System (Bio-Rad, Hercules, CA, USA). The reaction parameters were: initial denaturation at 95^0C for 10 minutes followed by 40 amplification and quantification cycles of 15 seconds at 95^0C, 15 seconds at 60^0C and final extension at 72^0C for 10 seconds.

***Table 2.5**: Investigated genes and sequences of the oligonucleotides used to amplify target genes by qPCR*

Gene target/protein ID	Primer sequence (5' – 3')	Amplicon size (bp)
Bloom inducer	Fwd: ACGCCATACGATAAGGAGGA	
gene / 9619	Rev: CAACCTTTTCCTTTGGCTGAT	177
	(designed by Amy Kirkham)	
Tylakoid lumen	Fwd: CGGCACTGACGAAGAAGTTGAATCC	
protein / 24309	Rev: CTCCTCCGTAGTCTGCATCGTAACA	116
Rieske iron-sulfur	Fwd: TCAGCCGCCAACAACAAGTTCA	
protein / 38231	Rev: TCCACGTCGAGGTGAGATAGTTCAAG	116
NADP/FAD dependent	Fwd: GCTTAACAACGGTGCCCACATCTA	
oxidoreductase / 4914	Rev: CCACTCATCGTAATCCAATCCCTTGC	112
Photosystem II stability	Fwd: TTCTTCGGACTCGGTGGATTTGAG	
assembly factor/ 38769	Rev: AAGCCACATCCGTCAAGCCATA	92
Bacteriochlorophyll /	Fwd: TCTGTGCCGGATCTGTAACCTTGA	
chlorophyll synthetase/ 262279	Rev: ATCCAAGCAAGATTGCTGCGTATGT	93
CobN/magnesium	Fwd: ACGGCAGAGGAATGTGGGATACT	
chelatase / 34191	Rev: ACCCAAAGGACGATGCCACTTG	105
Mg-protoporphyrin IX	Fwd: AGTTCGGAGAGTTGTTCCCTGGT	
Methyltransferase / 261608	Rev: TGCAACCTCAAATCCAGCCTTCTTC	104
AOX2 / 42992	Fwd: TGTCGGGTGTGGCTCATGATACT	
	Rev: CTTCGTCTCGCTCCTCTCCATCATATC	110
Aktin like gene /	Fwd: ATCTCTGCTCCCCCTGAAAG	
269504	Rev: CATACTCGCTCTTCCCAACC	103
40s rRNA gene /	Fwd: CCAAAGACCATCGAAGGAGA	
	Rev: CGGAGAGATCGGTTACATGG	91

Fluorescence was measured in the final extension step. A melting curve analysis at 65^0C to 95^0C with increments of 0.5^0C and dwelling time for 5 seconds was performed to check for primer dimers and non-specific amplification. The reliability of the qPCR was verified by five point standard curves made by amplification from 1:10 serial dilutions of the cDNA reverse transcriptase reaction.

2.7.5 RNA expression analysis

The target gene's expression level was calculated based on pair wise fixed reallocation randomisation test using the Relative Expression Software Tool (REST-MCS © - version 2) (Pfaffl *et al*. 2002) and expressed in log2 values. To be able to quantify the gene expression the efficiencies of the qPCR reactions were calculated from the slope of the standard curves according to the equation:

$$E = 10^{[-1/slope]}$$

where E is the efficiency of the reaction (Rassmussen, 2001). E ranges from 1 – 2, 1 representing the minimal value and 2 the theoretical maximum and optimum value. The slope was determined from the linear regression of log(target concentration) versus cycle threshold (C_t). C_t values were automatically determined using the CFX Manager Software Version 1.1 (Bio-Rad, Hercules, CA, USA). If no PCR efficiency was determined, optimal efficiency of E = 2.0 was assumed. Finally, the relative expression ratio (R) of the target gene is calculated based on E (real-time PCR efficiency) and the CP (the cycle numbers of the crossing points) deviation of the sample versus a control, and expressed in comparison to a reference gene:

$$\text{ratio (R)} = \frac{(E_{target})^{\Delta CP_{target}(\text{control-sample})}}{(E_{ref})^{\Delta CP_{ref}(\text{control-sample})}}$$

where E_{target} is the real-time PCR efficiency of the target gene transcript; E_{ref} is the real-time PCR efficiency of the reference gene transcript; ΔCP_{target} is the CP deviation of control – sample of the target gene transcript; ΔCP_{ref} is the CP deviation of control –

sample of reference gene transcript. As reference gene was used an actin like housekeeping gene (gene id. 269504) or a 40s ribosomal RNA gene as suggested in a previous study on *T. pseudonana* gene expression (Durkin *et al.* 2008) which had the highest efficiency calculated.

2.8 Chromatin immunoprecipitation of BIG1 in *T. pseudonana* overexpression cell line

The chromatin immunoprecipitation of the BIG1 was performed according to the protocol developed by Lin *et al.* (2012) with minor modifications as follows. *Thalassiosira psedonana* culture was grown in NEPCC artificial seawater medium at 20^0C under constant light at 80 mmol/photons $m^{-2}s^{-1}$ (see 3). A concentration of 200,000 cells/ml was transferred in fresh 400 – 1000 ml NEPCC medium and grown for 24 hours under constant stirring and bubbled with air at ambient pressure until it reached an approximate concentration 1 million cells / ml. The DNA binding BIG1 protein was subsequently crosslinked to the DNA *in vivo*.

2.8.1 Formaldehyde crosslinking of BIG1 with DNA *in vivo* in *T. pseudonana*

Formaldehyde crosslinking was carried out adding 37% formaldehyde to a final concentration of 1% to the culture for 10 minutes at room temperature. The fixation was stopped by adding 2M Glycine to a final concentration of 0.125M for 5 minutes at room temperature. Cells were washed with 1xPBS solution twice by centrifugation at 4,000 rpm for 5 minutes at 4^0C, flash frozen in liquid nitrogen and stored at -80^0C.

2.8.2 Chromatin extraction

The formaldehyde crosslinked pellet from 1L culture was re-suspended in 20 ml of Extraction Buffer I (0.4 M sucrose, 1 Complete Mini Protease Inhibitor Cocktail tablet, EDTA free (Roche Applied Science, 68298 Mannheim Germany) dissolved in 1 ml sterile MilliQ H_2O, 10 mM $MgCl_2$, 5 mM 2-Mercaptoethanol, 10 mM Tris–HCl pH 8) and split in 4 aliquots of 5 ml. Alternatively, pellets from 400 ml culture were re-suspended in 5 ml Extraction Buffer I. The aliquots were chilled on ice for 5 minutes and centrifuged at 4000 rpm for 20 min at 4°C. The supernatant was discarded and the pellets were re-suspended in 1 ml of Extraction Buffer II (0.25 M sucrose, 10 mM Tris–HCl pH8, 10 mM $MgCl_2$, 1% triton, 1 Complete Mini Protease Inhibitor Cocktail tablet, EDTA free dissolved in 1 ml sterile MilliQ H_2O, 5 mM 2- Mercaptoethanol). The

suspension was centrifuged at 10,000 rpm for 10 min at 4°C. The resulted pellets were re-suspended in 300 µl of Extraction Buffer III (1.7 M sucrose, 1 Complete Mini Protease Inhibitor Cocktail tablet, EDTA free diluted in 1 ml sterile MilliQ H_2O, 0.15% Triton X-100, 2 mM $MgCl_2$, 5 mM 2-Mercaptoethanol, 10 mM Tris–HCl pH8) and the suspension was carefully layered on the top of 300 µl Extraction Buffer III avoiding to mix them and centrifuged at 13,200 rpm for 1 hour at 4°C. The pellets were re-suspended in 300 µl fresh Nuclei Lysis Buffer (50 mM Tris–HCl pH 8, 10 mM EDTA, 1 Complete Mini Protease Inhibitor Cocktail tablet, EDTA free diluted in 1 ml sterile MilliQ H_2O, 1% SDS). All these steps were carried out on ice.

2.8.3 Fragmentation of the fixed chromatin

The extracted formaldehyde fixed genomic DNA was sheared by sonication at a fragment size of up to 1000 bp. This step was done either by a BioruptorW UCD-200 sonicator (Diagenode, 4102 Seraing (Ougrée) – Belgium) set at 20 kHz (maximum power) performing 9 cycles of 30 seconds ON and 1 minute OFF for each cycle or by a Misonix X-2000 Series Ultrasonic Liquid Processor set at a power equivalent to 20 kHz performing 9 cycles of 30 seconds ON and 3 minute OFF for each cycle on ice. Five ul of the sonicated chromatin solution was analysed applying gel electrophoresis on 2% TAE agarose gel (40mM Tris-acetate, 1mM EDTA, 0.5 µg/ml Ethidium bromide) at 60V for 1.5 hour and visualised with a UV light transmitter.

2.8.4 Immunoprecipitation with BIG1 antibody

Twenty µl was taken off for total DNA control (Input) and stored at -20^0C until reverse crosslink step following centrifugation at 13,200 rpm for 5 minutes at 4^0C. Subsequently, the remaining volume of the chromatin solution was adjusted to 3 ml with fresh ChIP Dilution Buffer (1% Triton X-100, 1.2 mM EDTA, 167 mM NaCl, 16.7 mM Tris–HCl pH8) chilled on ice and split in 2 x 1 ml IP (antibody treatment) and 1 x 1 ml Mock (no antibody) control. 1.5 ml siliconized Eppendorf tubes (Eppendorf AG, 22331 Hamburg, Germany) were used to reduce the background noise. A volume of 45 µl Dynabeads protein A (Life Tecnologies AS, Oslo, Norway) was mixed with equal volume of Dynabeads protein G (Life Tecnologies AS, Oslo, Norway) per sample, washed with 200 µl of ChIP Dilution Buffer and re-suspended in 90µl of the same buffer. The pre-washed bead complexes were split for immune-capture (60 µl treated with 10 µl of BIG1 antibody) and chromatin preclearing (30 µl mixed with 1 ml of

diluted chromatin solution) and left under gentle rotation for 2 hours at 4^0C. Afterwards, the bead-antibody complexes were first washed with 1 ml and finally re-suspended in 60 µl ChIP Dilution Buffer prior to the addition of the precleared chromatin solution. The immunoprecipitation was carried out under gentle rotation at 4^0C overnight.

2.8.5 Purification of the immune complexes after immunoprecipitation and reverse crosslinking

Two washes were applied to the immune complexes with salt buffers, a quick one to remove the remnants of the previous buffer followed by a longer wash step under gentle rotation at 4^0C for 5 minutes with a volume of 1 ml of each buffer. In this intent freshly prepared and chilled Low Salt Wash Buffer (150 mM NaCl, 0.1% SDS, 20 mM Tris–HCl pH8, 2 mM EDTA, 1% Triton X-100), High Salt Wash Buffer (500 mM NaCl, 0.1% SDS, 1% Triton X-100, 20 mM Tris–HCl pH8, 2 mM EDTA), LiCl Wash Buffer (0.25 M LiCl, 1% IGEPAL CA-630 (Sigma Aldrich Co, St. Louis, MO 63103, USA), 10 Mm Tris–HCl pH8, 1 mM EDTA, 1% Sodium-deoxycholate (Sigma Aldrich Co, St. Louis, MO 63103, USA)) and TE Buffer (10 Mm Tris–HCl pH8, 1 Mm EDTA) were used in sequence.

The immune complexes were eluted twice with 250 µl freshly prepared Elution Buffer (1% SDS, 0.1 M $NaHCO_3$), mixed thoroughly and incubated for 15 minutes at 65^0C. When incubation was finished the beads were collected on a magnetic rack and the eluate transferred in clean regular 1.5 ml Eppendorf tubes. The Input DNA was thawed and its volume adjusted to the IP and Mock controls' volume with Elution Buffer. Reverse crosslinking was carried out at 65^0C with the addition of 20 µl 5M NaCl overnight.

2.8.6 DNA recovery

The eluates were treated with 10 µl of 0.5 M EDTA, 20 µl 1M Tris–HCl (pH 6.5), 1.5 µl of 20 mg/ml proteinase K (Thermo Fisher Scientific, LT-02241 Vilnius, Lithuania), and 1 µl of 10 mg/ml RNase A (Thermo Fisher Scientific, LT-02241 Vilnius, Lithuania) and incubated for one hour at 45°C. DNA was recovered performing AquaPhenol (MP Biomedicals, 67402 Illkirch Cedex, France), 1:1 volume of AquaPhenol/chloroform and chloroform extractions in sequence. 500 µl of each extraction solution was added, mixed by brief vortex and centrifuged 1 minute at 13,200 rpm at 4^0C. Following every

centrifugation the upper phase was carefully transferred in clean 1.5 ml Eppendorf tubes. At the end of extraction the two IPs were pooled. DNA was precipitated with 1 volume of Isopropanol and 1/10 volume of 3M Sodium-acetate pH 5.3 and cold incubated at −20°C overnight. At the end of the incubation samples were centrifuged 30 minutes at 13,200 rpm at 4^0C and the pellets were washed with 400 µl 70% ethanol. The DNA pellets were air dried either in a laminar flow cabinet or incubated for 20 minutes at 30^0C. The dried pellets were re-suspended in 20 – 30 µl molecular grade water, quantified using nanodrop or Qubit (Thermo Fisher Scientific, Rochford SS4 1ND, UK) and subsequently High precision DNA Assay (Invitrogen Life Technologies).

2.9 Statistics

All data were tested to control the normal distribution using a Shapiro-Wilk Normality Test. The variation in response of the different cell-lines used in this study over the whole temperature range was assessed using a Kruskal-Wallis Test, without assuming the data to have normal distribution in case they did not had a normal distribution, and tested at 0.05 significance level. A Mann-Whitney U test was performed as a post-hoc test. In calculating the significance at each temperature point a two samples t-test was used and the final values were obtained applying the Bonferroni correction which reduce the chances of obtaining false-positive results. The effects of different variables of experiments, were modelled to test which variable accounted for the observed traits. Generalized linear models (GLMs) of the R statistical package were used to relate the variation in growth rate and maximum efficiency of the photosystem II (Fv/Fm) to cell-line and temperature. This approach was the most appropriate to account for potential autocorrelation incorporating temperature as a nested random term. The best fitted model was selected using the 'MuMIn' package (Bartón, 2009) based on the Akaike Information Criterion (AIC) (Burnham and Anderson, 2002). According to this criterion, the equation with the lowest AICc value is most appropriate. We considered the R^2 (the percentage of the response variable variation that is explained by the linear model) as well.

The temperature optimum and maximum was determined using a non-linear regression model (`nls` from the `nlstools` package of the R platform) with a fixed formula for the pooled data frame containing all the data given by the temperatures, the associated

growth rates and a factor variable indicating each cell-lines. An equation as proposed by Yan and Hunt (1999) was used for fitting the data:

$$y = \frac{T_{max} - x}{T_{max} - T_{opt}} \left(\frac{x}{T_{opt}} \right)^{(T_{opt}/(T_{max} - T_{opt}))}$$

where *y* is the specific growth rate, *x* is the temperature, *Tmax* is the maximum temperature and *Topt* is the optimum temperature. The optimum and the maximum temperatures were subscripted by the factor variable being specified by the cell-lines. An ANOVA test was done to compare a fit to all the data against a fit to different cell-lines. The effect of the temperature on the temperature optimum and maximum values was assessed applying the Cohen's d rule on the predicted optimum/maximum temperatures and their standard errors according to the formula:

$$d = \frac{M_{group1} - M_{group2}}{SD_{pooled}}$$

$$SD_{pooled} = \sqrt{(SD^2_{group1} + SD^2_{group2})/2}$$

where d is the effect size, M_{group1} and M_{group2} are the mean temperatures returned by the model and SD is the standard error.

2.10 Bioinformatics

Single-end sequencing of four ChIP-DNA samples representing two IP samples and two Inputs (genomic DNA) as positive controls was performed on Illumina HiSeq2000 platform (Earlham Institute, formerly known as The Genome Analysis Centre (TGAC)) with a read length of 50 bp. This yielded an average of approximately 44 million reads each. Data for all ChIP samples and input were of good quality with mean quality scores of 30, with 50 % mean GC content.

For mapping and analysis *T. pseudonana* genome was downloaded from the Joint Genome Institute

(JGI) website (http://genome.jgi-psf.org haps3 haps3.download.ftp.html). Reads obtained from chromatin immuniprecipitation followed by high-throughput sequencing (ChIP-seq) were quality controlled with a standardized procedure using FastQC (Andrews, 2010). The reads were mapped onto the *T. pseudonana* genome using Bowtie2 (Langmead *et al.*, 2009) with mismatch permission of 1 bp. Unique mapping of reads was adopted. Regions that were significantly enriched were identified using MACS2 (Zhang *et al.*, 2008) on the High Performance Computing Cluster supported by the Research and Specialist Computing Support service at the University of East Anglia.

Unalysis of the unmapped reads was performed at TGAC. The reads were run against blastnt. The results were then loaded into a metagenomics analysis tool called MEGAN5 (Huson *et al.*, 2007).

CHAPTER 3: PHYSIOLOGICAL EFFECTS OF NITRATE YIELD LIMITATION ON WILD TYPE *T. PSEUDONANA* AND CELL LINES THAT OVEREXPRESS OR KNOCK-DOWN THE BIG1 PROTEIN

Hipkin, R., Sárközi, K.Cs., Kirkham, A.R., Toseland, A., Moulton, V., Barrz, K., Lindquist, E., Tringe, S.G., Tritt, A.J., Armbrust, E.V., Bowater, R. and Mock, T. A conserved DNA-binding protein regulates cell division in marine diatoms, Manuscript submitted to Nature Microbiology (under revision)

3.1 Introduction

Nitrogen is an essential nutrient for all organisms and is required for the biosynthesis of macromolecules such as proteins, nucleic acids and chlorophyll. The assimilation of inorganic nitrogen (N) into organic compounds is a key process regulating the growth and productivity of photosynthetic eukaryotes and requires coordinated expression and regulation of enzymes in the cytosol, chloroplast and mitochondria (Turpin, 1991; Hodges, 2002). With the exception of some species such as *Hemiaulus*, *Rhizosolenia* and *Chaetoceros*, which live in presumed symbiosis with diazotrophic cyanobacteria, diatoms are not able to acquire N from N_2 (Foster *et al.*, 2011). They rely on extracellular dissolved inorganic nitrogen pools, nitrate and ammonium, which in open ocean surface waters are present at extremely low concentrations but are supplied in pulses in coastal areas and upwelling regimes. The availability of inorganic nitrogen is a limiting factor in primary production (Doering *et al.*, 1995; Sarmiento *et al.*, 2006). Furthermore, it has an impact on biogeochemical cycling of CO_2 as the assimilation of inorganic nitrogen was demonstrated to be linked to carbon cycling (Gruber and Galloway, 2008). In highly productive coastal upwelling systems, wind-driven pulses of nutrient rich water periodically enhance the local productivity of phytoplankton populations, which are most often dominated by diatoms (Kudela and Dugdale, 2000; Bruland *et al.*, 2005; Allen *et al.*, 2006). While spring and autumn diatom blooms in coastal systems are recurrent processes and typically develop under conditions of high NO_3^- concentrations and a well-mixed water column (Lomas and Gilbert, 2000), in oligotrophic oceans diatom-cyanobacterial associations sustain occasional blooms when nutrients became available in the stratified water column (Villareal, 1994; Carpenter *et al.*, 1999; Villareal *et al.*, 2012). When the supply of nitrate decreases, phytoplankton may persist by using internal nutrient stores or regenerated forms of nitrogen such as ammonium or urea (Dickson and Wheeler, 1995; Bode *et al.*, 1997).

Although genome and proteome studies offer clues to the success of diatoms in the marine environment (Armbrust *et al.*, 2004; Bowler *et al.*, 2008; Nunn *et al.*, 2009), little is known about their adaptive response to changing environmental conditions (Hockin *et al.*, 2012). Various climate models predict that ocean warming will lead to changes in vertical stratification, resulting in reduced nutrient supply due to increased vertical stability and reduced vertical mixing. This could lead to a corresponding reduction in new primary production (Cox *et al.*, 2000; Sarmiento *et al.*, 2004; Doney,

2006). Since diatoms' ability to form extensive blooms has been hypothesized to be the key to their evolutionary success (Smayda, 1977), understanding the molecular base of this process became impetuous. Diatoms blooms are underpinned by fast growth response upon nutrient pulses.

The whole-genome sequence of the model centric diatom *Thalassiosira pseudonana* was published in 2004 (Armbrust *et al.*, 2004), providing a powerful tool to elucidate such processes. Furthermore, a new DNA binding protein was identified recently the activity of which was linked to diatoms' fast progression through the cell cycle post nutrient starvation. The bloom inducer gene 1 (*big1*) was identified in a whole-genome microarray study with *T. pseudonana* (Mock *et al.*, 2008). A previous study confirmed the presence of two splice variants of *big1* (Hipkin, 2012). The smaller splice variant was selected for further characterization because in a previous study it showed stronger differences in protein abundance in relation to different growth conditions while still containing the same type of repeats as identified in the bigger splice variant. Furthermore, the smaller splice variant of BIG1 appears to be formed only under silicate and nitrate starvation. Its presence had not been detected under nutrient replete growth (Hipkin *et al.*, under revision, see Appendix 5).

The use of molecular manipulation of genes in order to assess phenotypes is used in diatom studies in a similar manner to other organism groups. Transformation methods have been established for several species of diatoms including the pennate diatoms *Phaeodactylum tricornutum* (Apt *et al.* 1996; Falciatore *et al.*, 1999; Zaslavskaia *et al.*, 2000; Miyagawa *et al.*, 2009), *Cylindrotheca fusiformis* (Fischer *et al.*, 1999; Poulsen and Kröger 2005) and the centric diatoms *Cyclotella cryptica* (Dunahay *et al.*, 1995), *Chaetoceros* sp. (Miyagawa-Yamaguchi *et al.*, 2011) and *Thalassiosira pseudonana* (Poulsen *et al.*, 2006). To further assess the function of the *big1* gene in the centric diatom *T. pseudonana*, we generated knock-down mutants silencing the smaller splice variant of BIG1. Silencing was performed inserting an antisense sequence of the gene, a technique used successfully in the pennate diatom *P.tricornutum* (De Riso *et al.*, 2009). In this study, we focused on investigating any phenotypic trait conferred by knock-down constructs in relation to wild type and BIG1 knock-in with respect to one of the major limiting nutrient in the oceans, nitrate.

Phenotyping and molecular experiments were designed to determine any alteration induced by the introduction of the knock-down cassette in the *T. pseudonana* genome compared to its transgenic knock-in counterpart. Phenotyping experiments targeted the ability of diatoms to form blooms under nutrient limitation and initiation of growth upon re-addition of the limiting nutrient. Growth rates, cell density (cells ml^{-1}), cell size (µm) and maximum quantum yield of Photosystem II (Fv/Fm) were used as physiological parameters to characterise BIG1 knock-down. Phenotyping experiments were complemented by assessing protein and gene expression levels.

3.2 Results

3.2.1 Confirmation of the transformation of BIG1 knock-down line

Colony PCR was used to confirm the presence of the antisense *big1* fragment in the *T. pseudonana* genome. Immunoblot assays showed the reduction of the BIG1 protein compared to the wild type.

3.2.1.1 Identification of the BIG1 reverse transcript in *T. pseudonana* transformants

To identify whether the antisense fragment was present in colonies resulted from biolistic transformation of *T. pseudonana* wild type cells, the primers used were as seen in chapter 2 (Materials and Methods). The primers used assured that the expected PCR product will form only in the presence of the *big1* antisense fragment, see figure 3.1.

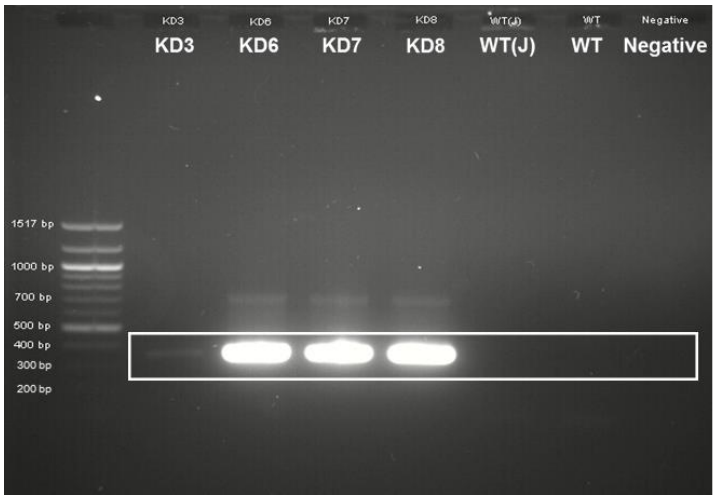

Figure 3.1*: Colony PCR of T. pseudonana BIG1 knock-down candidates. Lane one: 100 bp DNA ladder; lanes two-five: BIG1 knock-down candidates (KD3, KD6, KD7, KD8); lanes six-seven: two independent wild type lines used as positive controls (WT(J) and WT), lane eight: negative control containing H_2O instead of template (Negative).*

In wild type and negative control the absence of any product is due to the different binding sites of the forward and reverse primers in the genome which will extend upstream and downstream from their binding site, respectively. Based on the results, BIG1 knock-down 7 (KD7) was selected for further analysis unless stated otherwise.

3.2.1.2 Protein abundance in BIG1 knock-down and wild type lines of *T. pseudonana* under nitrate starvation

Previous work on BIG1 (Hipkin, 2012) showed that the larger splice variant (50 kDa) was constitutively translated while the translation of the smaller splice variant (37 kDa) increased over time reaching a maximum on the fourth day of the stationary phase. Therefore, we decided to measure the BIG1 knock-down protein expression on the fourth day of the nitrate limitation-induced stationary phase. This is the time point when we expected to observe maximal levels of both splice variants based on previous observation about the degradation level of the protein over a six day time course.

The immunoblot assay revealed strong reduction in translation of the larger splice variant (SV2). The smaller splice variant (SV1) reduction was less pronounced, see figure 3.2. No other protein bands were identified.

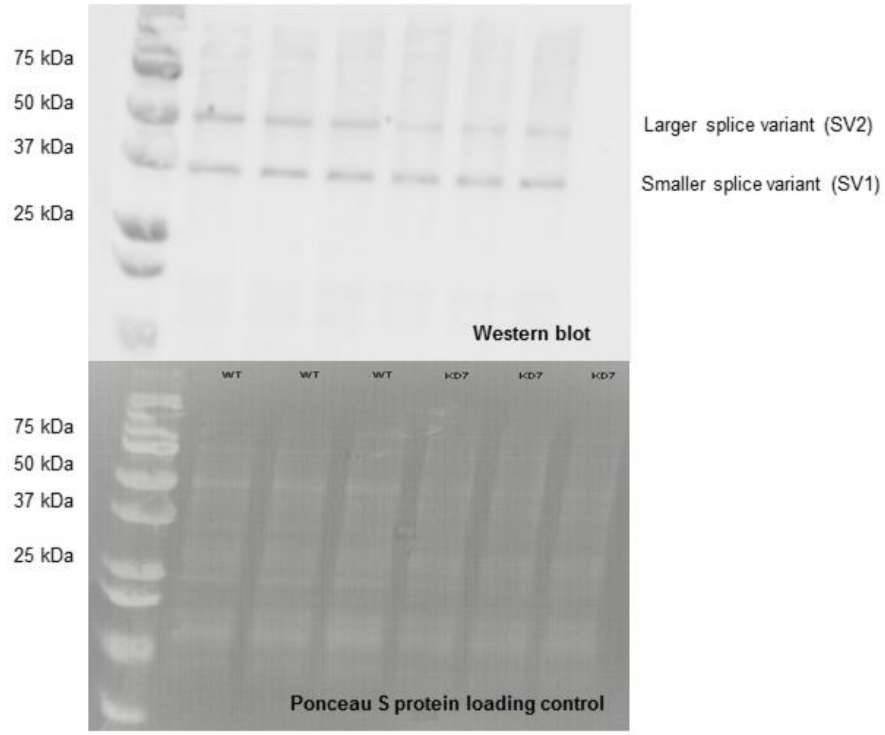

***Figure 3.2**: Western blot of 35 µg of protein from biological triplicates of T. pseudonana wild type and BIG1 knock-down lines on the fourth day of 100 µM nitrate limitation induced stationary phase. Top picture represents the Western blot image of both splice variants of the BIG1 protein Bottom picture displays Ponceau S used as protein loading control. Abbreviations denote the wild type (WT) and knock-down candidate (KD7) lines.*

The difference between protein bands was tested and quantified using the ImageJ software (Schneider *et al.*, 2012). Significant differences were seen for both splice variants compared to wild type, even though the difference between the wild type and BIG1 knock-down smaller splice variant was minor, see figure 3.3.

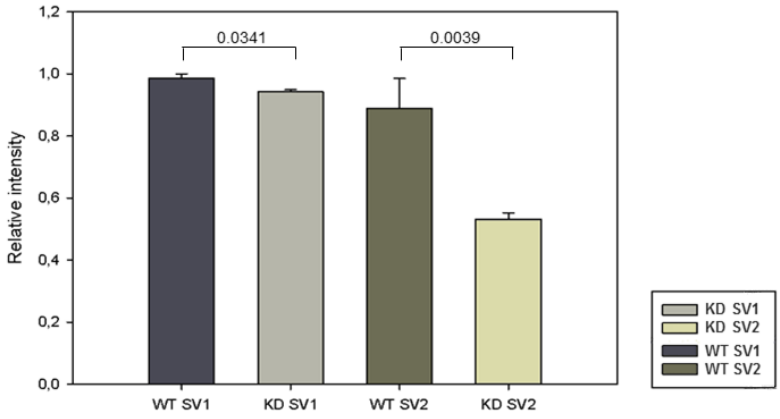

***Figure 3.3**: Relative intensity of protein bands from Western blot. Data corresponding to Figure 3. Abbreviations as follows: wild type (WT), BIG1 knock-down (KD), smaller splice variant (SV1) and larger splice variant (SV2). Error bars represent standard variation. Numbers denote significant difference at .05 level (Two samples t-test). N=3*

3.2.2 Physiological and morphological effects of nitrate yield limitation on BIG1 knock-in, BIG1 knock-down and wild type lines of *T. pseudonana*

Nitrate yield limitation means cultures were grown at a final concentration of 100 µM nitrate compared to a nutrient replete concentration of 550 µM. Limiting one of the essential nutrients makes cultures need longer to grow in the same medium. Therefore, in order to ensure that other nutrients did not become limiting, they were added in doubled concentration. Hipkin (2012) observed increased cell size in a treatment with excess cobalamin (vitamin B_{12}) and thiamine (vitamin B_1). In order to avoid any influence of excess vitamins on cell size in our experiments, they were added at 1x strength. We used standard f/2 vitamins.

3.2.2.1 Physiological effects of nitrate yield limitation on a BIG1 knock-in, BIG1 knock-down and wild type line

To assess the effects of nitrate starvation on both transgenic cell lines and wild type, cell counts, cell size and maximum quantum yield of the Photosystem II (Fv/Fm) were recorded. 25,000 cells/ml were inoculated in nitrate depleted NEPCC media (see 3.2.2) and monitored daily for nine days. Cultures were screened for aggregation starting at 96 hours after inoculation.

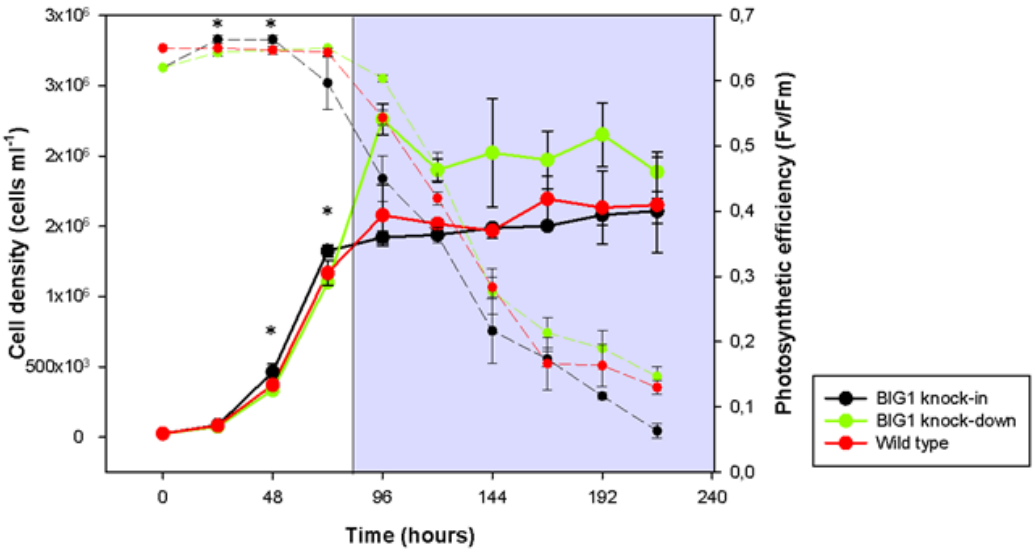

***Figure 3.4**: Mean cell density in 100 µM nitrate yield limitation. Dots and solid lines represent mean cell density of biological replicates of Thalassiosira pseudonana BIG1 knock-in (black), wild type (red) and BIG1 knock-down (green); dots and dashed lines represent the photosynthetic efficiencies of the cell lines, BIG1 knock-in (black), wild type (red) and BIG1 knock-down (green). Error bars indicate standard variation. Shading denotes stationary phase. Asterisks indicate significant difference in growth rate and photosynthetic quantum yield at .05 level (Two samples t-test). Asterisks refers to the BIG1 knock-in compared to the wild type. N=3.*

The BIG1 knock-in line ceased growth after 72 hours while the wild type and BIG1 knock-down stopped growing after 96 hours. The BIG1 knock-in line showed significantly higher Fv/Fm in mid-exponential phase ($p<0.03$). The exponential growth of the cell lines will be analysed later compared to the recovery, see 3.2.2.3.

The knock-down line displayed the longest growth period and reached the highest cell density. Wild type had similar cell density as the knock-in line throughout stationary phase, see Figure 3.4. The knock-in line was kept in stationary phase for 6 days compared to five days for wild type and knock-down. The discrepancy was caused by the difference in the length of the exponential phase. The first day of stationary phase was indicated by the cessation of growth which in the case of wild type and knock-down equalled the first drop in Fv/Fm. The Fv/Fm of BIG1 knock-in decreased (Fv/Fm 0.59) before the cells stopped growing. Fv/Fm values ranged between 0.06 and 0.65. Values between 0.55-0.6 indicate a maximally functional PSII and exponentially growing cultures, while decreasing values are associated with nutrient stress (Parkhill *et al.*, 2001).

The highest Fv/Fm value was recorded in knock-down lines at the end of the stationary phase, see Figure 3.4. Significant differences were observed between the knock-in line and wild type and knock-down, respectively. The latter ones showed no significant difference in Fv/Fm at the end of the starvation period, see Table 3.1

***Table 3.3**: Effect of nitrate yield limitation on Fv/Fm. Values represent means of biological triplicates. Abbreviations as follows: BIG1 knock-in (BIG1_KI), BIG1 knock-down (BIG1_KD) and wild type (WT). Significance calculated with Two samples t-test.*

BIG1_KI Fv/Fm	*WT Fv/Fm*	*BIG1_KD Fv/Fm*	*WT-BIG1_KI Fv/Fm*	*p-value*	*BIG1_KD-BIG1_KI Fv/Fm*	*p-value*	*WT-BIG1_KD Fv/Fm*	*p-value*
0.06±0.01	0.13±0.01	0.14±0.02	0.07	<0.001	0.08	<0.001	-0.01	0.21

3.2.2.2 Cellular morphology of the BIG1 knock-in, BIG1 knock-down and wild type line in nitrate yield limitation

Nitrate starvation resulted in an aggregating phenotype for BIG1 knock-down, see figure 3.5. Wild type showed moderate aggregating trend while the knock-in did not aggregate throughout the nitrate limitation-induced stationary phase, see Figure 3.6.

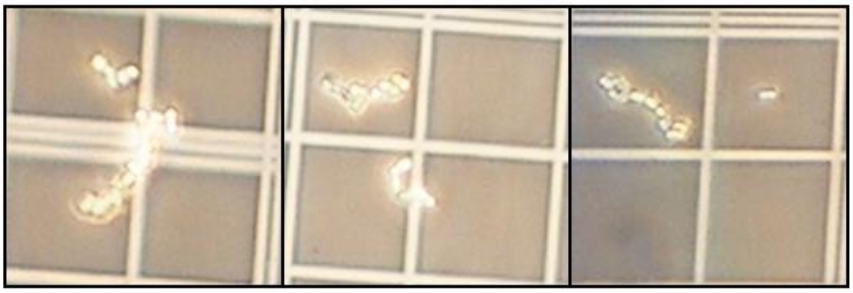

Figure 3.5*: Normal phase contrast images of BIG1 knock-down cell aggregates after 72 hours of 100 µM nitrate yield limitation. Squares are part of the central square of a Neubauer haemocytometer. Small squares represent 0.04 mm surface area.*

Nitrate limitation induced high aggregation rates in the knock-down line 48 hours after the initiation of stationary phase. Aggregation reached the maximum value at 72 hours following the cessation of growth. A significant difference was recorded between BIG1 knock-in and BIG1 knock-down starting from 48 hours of stationary phase until the end of starvation, see Figure 3.6. BIG1 knock-down and wild type differed significantly in cells per aggregate content only at 48 hours ($p=0.0206$) and 120 hours ($p=0.0291$) of stationary phase.

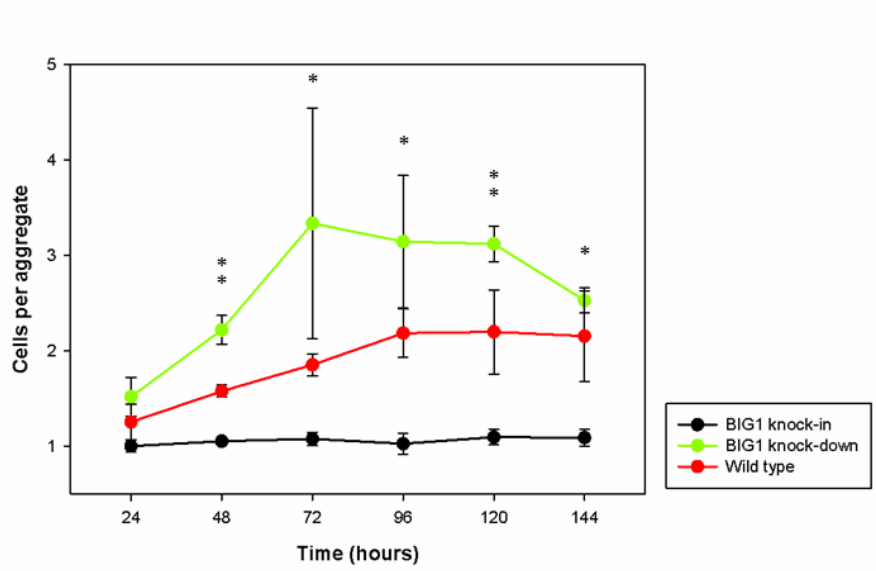

***Figure 3.6**: Aggregation trend during 6 days of 100 µM nitrate yield limitation induced stationary phase. Dots and solid lines represent mean cell density of biological replicates of* Thalassiosira pseudonana *BIG1 knock-in (black), wild type (red) and BIG1 knock-down (green); dots and dashed lines represent the photosynthetic efficiencies of the cell lines, BIG1 knock-in (black), wild type (red) and BIG1 knock-down (green). Error bars indicate standard variation; Asterisks indicate significant difference in growth rate and photosynthetic quantum yield ($p<0.05$) (Two samples t-test); * refers to the BIG1 knock-in compared to the Wild type;** refers to the BIG1 knock-down compared pairwise to the wild type and the BIG1 knock-in; N=3.*

Cell size was monitored throughout the nitrate yield limitation as well. BIG1 knock-in had bigger cell size at the beginning of the experiment. The smallest cell size was recorded for the BIG1 knock-down line at the start of the limitation experiment. Cell size of all cell lines had minor decrease by the end of the exponential phase 0.221±0.026 µm/0.148±0.001 µm/0.182±0.027 µm (knock-in/wild type/knock-down). Pairwise comparison showed significant difference between them over the exponential phase ($p<0.001$), see Figure 3.7.

Cell size altered differently in exponential phase compared to stationary phase under the nutrient limitation. BIG1 knock-in was significantly bigger in exponential phase than both other cell lines. Also, in stationary phase the cell size of the knock-in line had not varied. It showed exactly the same size as at the beginning of the experiment 4.833±0.136 µm. Significant difference between BIG1 knock-in, wild type ($p=0.002$)

and knock-down (p=0.0169) cell size was recorded at the end of the starvation period (Two samples t-test).

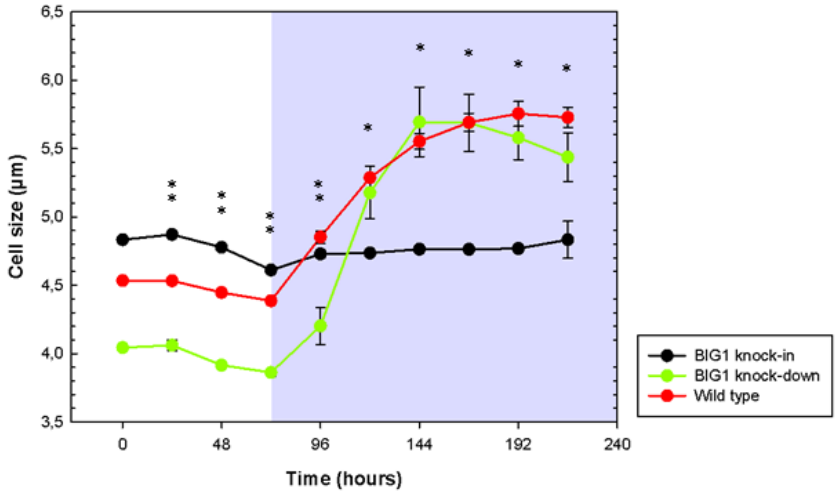

***Figure 3.7**: Cell size in nitrate limitation. Dots and solid lines represent mean cell size of biological replicates of Thalassiosira pseudonana BIG1 knock-in (black), wild type (red) and BIG1 knock-down (green). Error bars indicate standard variation. Asterisks indicate significant difference in size at .05 level (Two samples t-test). Shading indicates the stationary phase. * refers to the BIG1 knock-in compared to the wild type;** refers to the BIG1 knock-down compared pairwise to the wild type and the BIG1 knock-in; N=3.*

Conversely, the cell size of wild type (p=0.0013) and knock-down (p=0.0054) increased significantly during nitrate induced stationary phase, see figure 3.7. Significance level was tested using a Two samples t-test.

3.2.3 Growth recovery of the *T. pseudonana* BIG1 knock-in, BIG1 knock-down and wild type lines post nitrate starvation

After undergoing a stationary phase caused by nitrate yield limitation, cultures were transferred back to nitrate-replete medium. This was done by inoculating an aliquot of 25000 cells/ml into 100 ml of complete NEPCC. The recovery from yield limitation was assessed using the same physiological parameters as for stationary phase. This included cell counts, cell size, Fv/Fm and aggregation rate for 72 hours. Growth was monitored twice a day, see Figure 3.8.

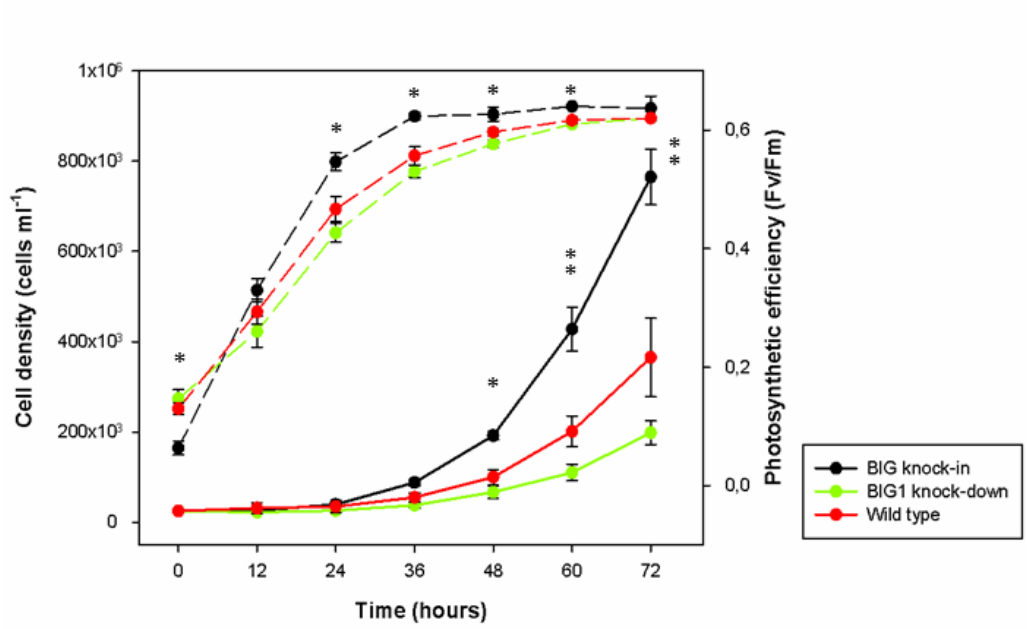

***Figure 3.8**: Recovery post nitrate starvation. Dots and solid lines represent mean cell density of biological replicates of Thalassiosira pseudonana BIG1 knock-in (black), wild type (red) and BIG1 knock-down (green); dots and dashed lines represent the photosynthetic efficiencies of the cell lines, BIG1 knock-in (black), wild type (red) and BIG1 knock-down (green). Error bars indicate standard variation; Asterisks indicate significant difference in growth rate and photosynthetic quantum yield ($p<0.05$) (Two samples t-test); * refers to the BIG1 knock-in compared to the wild type;** refers to the BIG1 knock-down compared pairwise to the wild type and the BIG1 knock-in; N=3.*

BIG1 knock-in reached higher Fv/Fm values through the recovery period, restoring the maximum quantum yield of PSII faster than wild type and knock-down. Significant difference in BIG1 knock-in Fv/Fm was recorded in mid-exponential phase ($p<0.02$) compared to wild type and BIG1 knock-down Fv/Fm. However, by the end of recovery, the difference in Fv/Fm was less distinct and was not statistically significant ($p=0.29$). Difference in Fv/Fm recovery of wild type and knock-down was not significant either.

Fv/Fm of BIG1 knock-in when was correlated to growth rate followed a linear regression (R^2adj 0.9824, $p<0.0001$) displayed significantly higher values than the wild type and BIG1 knock-down through the exponential phase see Figure 3.9. Also, the Fv/Fm of wild type and BIG1 knock-down differed significantly ($p<0.05$).

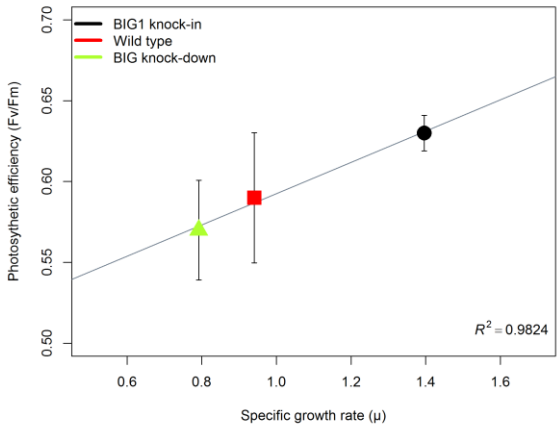

***Figure 3.9**: Modelled relation of the Fv/Fm of T. pseudonana wild type and transgenic lines related to growth rate in the exponential phase of recovery from nitrate yield limitation. Symbols are as follows: BIG1 knock-in (black circle), wild type (red squares), BIG1 knock-down (green triangle). Line represent the fitted model. Error bars indicate thestandard variation.*

The advantage of BIG1 knock-in in recovery was reflected by big differences in cell density as well, see growth curves in figure 3.8. The BIG1 knock-in cells/ml have been 209.38% and 385.18% higher than wild type and knock-down while wild type had 54.36% more cells/ml than knock-down. There was a lag phase of 12 hours observed in the BIG1 knock-in cell line while the knock-down and wild type showed a 24 hours lag phase.

Specific growth rates were calculated for all cell lines from a linear regression of the logarithmic nutrient saturated growth versus time for 12-60 hours. The growth rate of the BIG1 knock-in was significantly higher than both, wild type and knock-down. Furthermore, the wild type growth rate was significantly higher than BIG1 knock-down, see figure 3.10 and table 3.2.

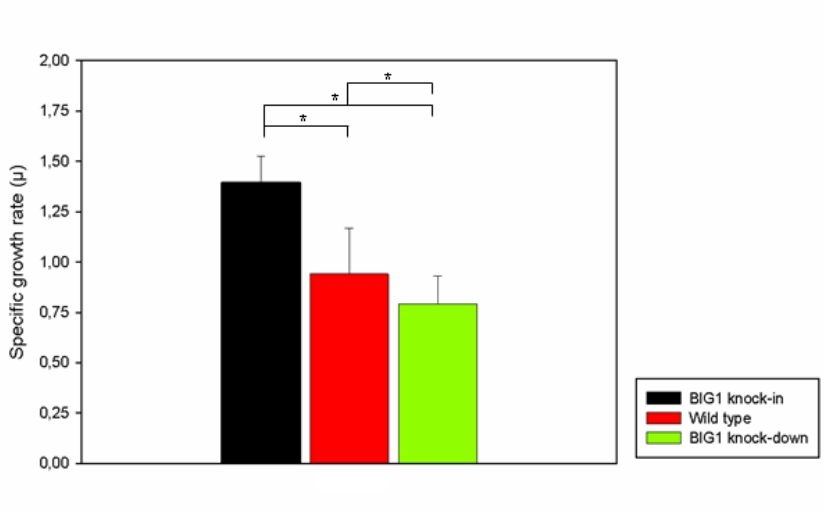

***Figure 3.10**: Growth rate in recovery post 100 µM nitrate yield limitation. Bars represent mean growth rate of three biological replicates, BIG1 knock-in (black), wild type (red) and BIG1 knock-down (green). Error bars indicate standard variation. Asterisks indicate significant difference in growth rate at level .05 (Two samples t-test).*

The growth of all cell lines was altered post yield limitation compared to the exponential growth recorded prior to nitrate limitation. The growth rate of wild type and BIG1 knock-down was significantly reduced post nitrate limitation while the growth rate of BIG1 knock-in was less affected (see Table 3.2).

***Table 3.4**: Changes in growth rates post and prior nitrate limitation. Values are shown are means of biological triplicates for recovery and the difference between no limited and recovery state. ± denotes standard variation.*

$\mu_{BIG1\_KI\_rec}$	μ_{WT_rec}	$\mu_{BIG1\_KD\_rec}$	$\mu_{BIG1\_KI\_lim}$- $\mu_{BIG1\_KI\_rec}$	*p-value*	μ_{WT_lim}- μ_{WT_rec}	*p-value*	$\mu_{BIG1\_KD\_lim}$- $\mu_{BIG1\_KD\_rec}$	*p-value*
1.40±0.13	0.94±0.22	0.79±0.14	0.06±0.12	0.530	0.41±0.21	0.035	0.50±0.15	0.025

3.2.3.1 Cellular morphology of BIG1 knock-in, BIG1 knock-down and wild type lines post nitrate starvation

We observed an aggregating trend induced by nitrate limitation throughout the starvation period in BIG1 knock-down and wild type. Consequently, the aggregation rate and associated cell size was monitored over the recovery period. As expected, decrease of cells per aggregates was noticed throughout recovery for wild type and BIG1 knock-down while the BIG1 knock-in showed no variation. After inoculation, knock-down (69.41%) and wild type (71.65%) cells per aggregate content decreased sharply over the next 12 h. Aggregation was gradually reduced in both cell lines during exponential growth with significant differences 48 hours after they have been transferred in nutrient replete media (p=0.0356). A significant difference was recorded throughout recovery between BIG1 knock-in and BIG1 knock-down, see figure 3.11. The aggregation rate of wild type was likewise significantly different from knock-in except for the 24 hours and 60 hours time-points.

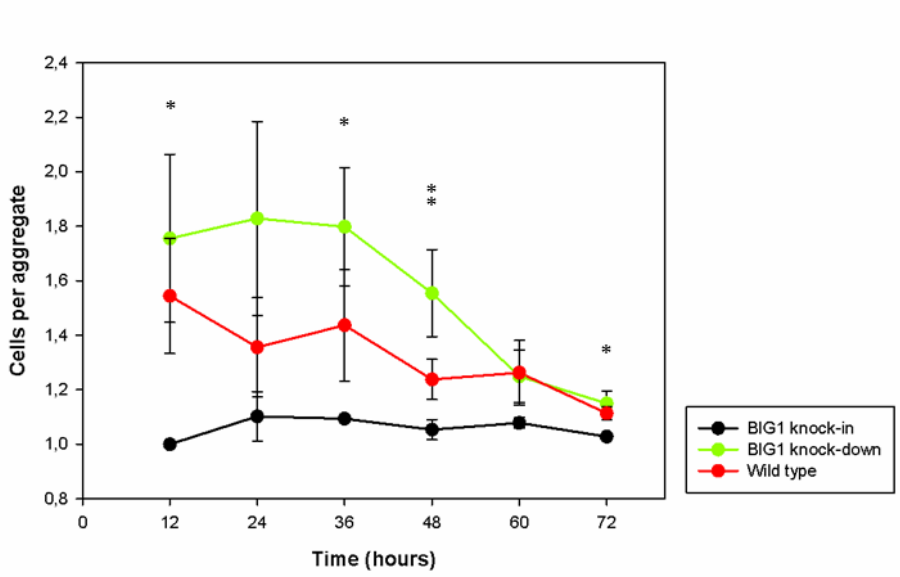

***Figure 3.11**: Aggregation trend following 6 days of 100 µM nitrate limitation induced stationary phase. Dots and solid lines represent mean cell density of biological replicates of Thalassiosira pseudonana BIG1 knock-in (black), wild type (red) and BIG1 knock-down (green); dots and dashed lines represent the photosynthetic efficiencies of the cell lines, BIG1 knock-in (black), wild type (red) and BIG1 knock-down (green). Error bars indicate standard variation; Asterisks indicate significant difference in growth rate and photosynthetic quantum yield (p<0.05) (Two samples t-test); * refers to the BIG1 knock-in compared to the wild type;** refers to the BIG1 knock-down compared pairwise to the wild type and the BIG1 knock-in; N=3.*

Cell size was also reduced during recovery post 100 µM nitrate limitation. BIG1 knock-down cell size decreased by 1.344±0.21 µm (p= 0.0067), wild type cell size by 1.227±0.11 µm (p= 0.0002) while BIG1 knock-in showed minor change with a decrease of 0.174±0.13 µm, Figure 3.12. Significant difference between BIG1 knock-in and wild type cell size was recorded at 60 hours (p=0.0485) and 72 hours (p=0.0274). BIG1 knock-down also differed significantly from wild type at these time points with p=0.0314 and p=0.0034, respectively.

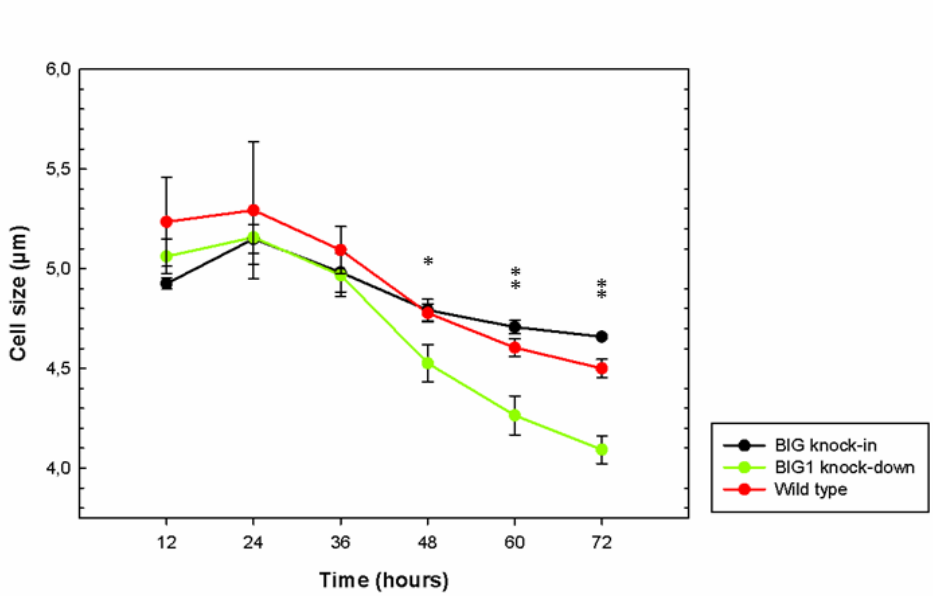

***Figure 3.12**: Cell size post nitrate starvation. Dots and solid lines represent mean cell density of biological replicates of Thalassiosira pseudonana BIG1 knock-in (black), wild type (red) and BIG1 knock-down (green. Error bars indicate standard variation; Asterisks indicate significant difference in growth rate and photosynthetic quantum yield (p<0.05) (Two samples t-test); * refers to the BIG1 knock-in compared to the wild type;** refers to the BIG1 knock-down compared pairwise to the wild type and the BIG1 knock-in; N=3.*

Also, comparing the cell size from the end of recovery to the onset of the nitrate limitation, we noticed a modest (0.174±0.008) but highly significant reduction in BIG1 knock-in cell size (p= 0.0007). This was not observed for wild type and BIG1 knock-down.

3.2.4 The expression of the *big1* gene under nitrate and silicate limitation in *T. pseudonana* BIG1 knock-in, BIG1 knock-down and wild type

It was investigated how the reduction of the BIG1 protein seen in Western blots compared to transcript levels of the gene. For this purpose we performed quantitative reverse transcription PCR (RT-qPCR) under two nutrient limitations, 100 µM nitrate, same as for the phenotyping experiment, and 50 µM silicate. Silicate limitation was used as a control because a strong induction (ca. 125 fold) was observed for BIG1 knock-in when it was first identified in microarray studies on *T. pseudonana* (Mock *et al.*, 2008). Also, in order to support the conclusions drawn about the BIG1 knock-down transcription level, we tested a random knock-down line (KD8) which had the antisense fragment inserted in their genome (see Figure 3.13).

The expression of the *big1* gene in knock-in and knock-downs was analysed from two perspectives. On one hand, it was compared to the expression of the gene in wild type under exponential and stationary phase, respectively, see figure 3.12. On the other hand, its expression was tested in exponential versus stationary phase for each cell line, see figure 3.14.

Compared to wild type we found relative gene expression of BIG1 knock-in to be co-expressed and upregulated under both exponential (log2 6.362 fold, $p<0.05$) and stationary phase (log2 5.045) under nitrate limitation. However, the gene expression was reduced by 20.70% in the stationary phase. It remained highly significant ($p<0.001$). Conversely, relative gene expression in knock-down lines was found to be downregulated in the exponential phase, showing a reduction of 102.70% (BIG1 knock-down) and 107.28% (KD8), see Figure 3.12.A. In stationary phase we noticed the same trend for the independent knock-down sample. This was not the case for the knock-down line where the gene expression of the *big1* gene was found to be upregulated. For both knock-down lines we observed just weak expression of the gene, see figure 3.12.B.

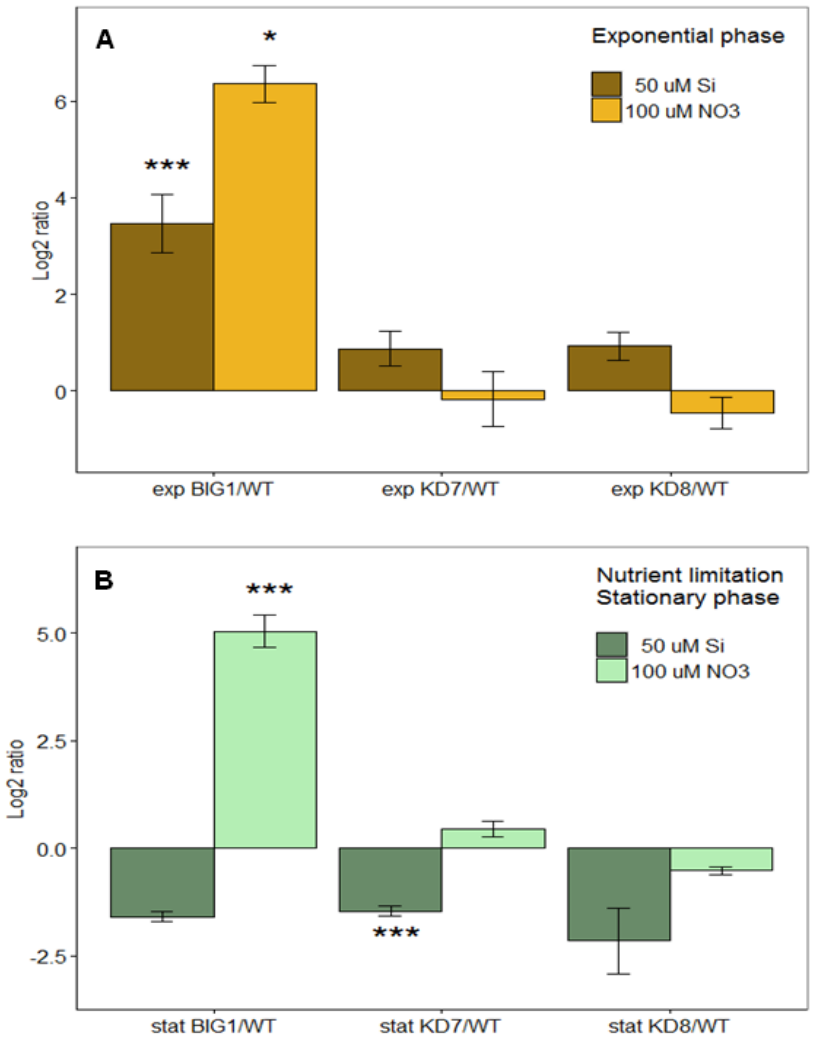

Figure 3.13**: Relative gene expression of big1 gene (**b**loom **i**nducer **g**ene 1) in Thalassiosira pseudonana cell lines that overexpress or knock-down the BIG1 protein under two experimental treatments. **A** Gene expression levels of the target gene in exponential phase, **B** Gene expression levels of the target gene in stationary phase. The analysed transcripts were compared to T. pseudonana wild type tested by a Pair Wise Fixed Reallocation Randomization Test and plotted using standard error estimation via a complex Taylor algorithm using Relative Expression Software Tool (REST) (Pfaffl et al., 2002). Asterisks (*,) indicate significant difference in gene regulation compared to the control at .05 and .001 level.*

Silicate limitation caused a more equilibrated gene expression pattern with all examined cell lines being upregulated in exponential phase and downregulated in stationary phase in relation to wild type. However, finding the knock-in line downregulated (log2 -1.587 fold) in stationary phase was unexpected. In exponential phase the BIG1 knock-in line was significantly upregulated (log2 3.468, $p<0.001$) while the relative gene expression

of knock-downs was reduced by 74.83% and 73.30% in the independent line. In stationary phase the BIG1 knock-down line was significantly downregulated (log2 -1.458, p<0.002) while the independent knock-down line had the *big1* gene expressed log2 -2.144 fold.

Relative gene expression under nitrate limitation was found to be upregulated relative to stationary phase in each cell line, while it was downregulated under silicate limitation with the exception of BIG1 knock-in, see figure 3.13. The expression of the gene in wild type was half (log2 1.066) the level in knock-in (log2 2.130, p<0.007) under nitrate limitation. The knock-down line displayed a weaker expression of the gene, with its expression being altered by 75.77% compared to BIG1 knock-in and 51.59% compared to wild type. Under silicate starvation relative gene expression of wild type (log2 -2.209, p<0.001) and knock-down was significantly downregulated with approximately halved expression level of the knock-down line (log2 -1.386, p<0.002).

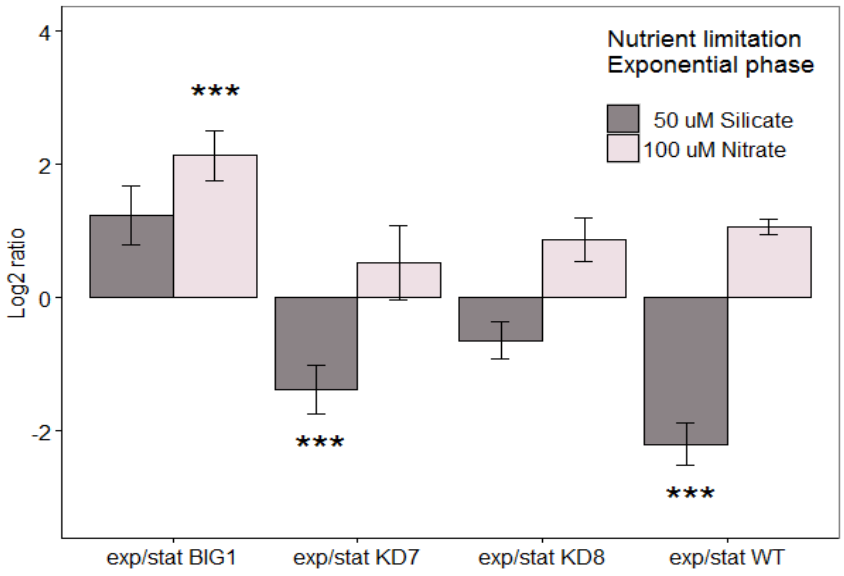

***Figure 3.14**: Relative gene expression of big1 gene (**b**loom **i**nducer **g**ene 1) in Thalassiosira pseudonana cell lines that overexpress or knock-down the BIG1 protein under two experimental treatments. Bars represent gene expression levels of the target gene in exponential phase compared to the stationary phase of the BIG1 knock-in line (exp/stat BIG1), two independent BIG1 knock-down lines (exp/stat KD7 and exp/stat KD8) and wild type (exp/stat WT). The analysed transcripts were tested by a Pair Wise Fixed Reallocation Randomization Test and plotted using standard error estimation via a complex Taylor algorithm using Relative Expression Software Tool (REST) (Pfaffl et al., 2002). Asterisks (***) indicate significant difference in gene regulation compared to the control at .001 level.*

3.3 Discussion

Nitrate uptake in marine ecosystems is of particular importance in oceanography and biogeochemistry because it sets an upper limit to biomass yield at higher trophic levels (Falkowski and Raven, 1997). In regions where high levels of nutrient supply are sustained, such as upwelling environments and continental margins, diatoms often constitute a large fraction of the photosynthetic biomass (Sarthou *et al.*, 2005). The occurrence of biomass burst commonly known as phytoplankton bloom depends not only on nutrient input but on the uptake of phytoplankton of these nutrients. Diatoms' ability to quickly respond to nutrient pulses following a starvation period is well established (Estrada and Blasco, 1979; Smayda, 1997; Smayda and Trainer, 2010). Although this property was extensively studied in nutrient limitation experiments (Parker and Armbrust, 2004; Shrestha *et al.*, 2012; Shi *et al.*, 2015), little is known about the molecular processes that regulate this aptitude of diatoms to successfully embrace an opportunistic growth and outcompete other phytoplankton groups.

Here, we report the results of an experiment which was based on the same approach, inducing a yield limited stationary phase in the growth of the diatom *T. pseudonana* by limiting one of the essential nutrients for protein and nucleic acid formation, nitrogen. In our approach, we focused on the effects of limitation and subsequent recovery in nutrient replete media. We applied genetic manipulation technique to gain transformants that knock-down the *big1* gene. This gene was previously found to be linked to diatoms' quick response to silicate and nitrate assimilation by differentially regulating genes involved in progression though the cell-cycle following a period of nutrient starvation (Mock *et al.*, 2008, Hipkin *et al*. under revision).

Inhibition of expression by nucleic acids has been known for more than three decades. The first report of sequence-specific binding of oligonucleotides to interfere with the translational machinery emerged 38 years ago (Stephenson and Zamecnik, 1978). Ever since, antisense strands of nucleotides have been used to manipulate gene expression and thereby identify gene function. The antisense technology is a molecular manipulation technique which allows the regulation of the quantities of a specific protein. In this technique, cDNA of a target gene is inserted into an appropriate vector in an orientation opposite to that of the native gene, after which the DNA construct is transferred into the host genome via microparticle bombardment (Muto *et al.*, 2013).

The antisense mRNA derived from the cDNA is then complementary to the sense transcript of the endogenous gene and thus interferes with the translation of the sense transcript, supressing translation of the native protein (Buchanan *et al.*, 2000). The first report of the successful use of this technique in diatoms was for the pennate diatom *P.tricornutum* (de Riso *et al.*, 2009). Our transformation efficiency using microparticle bombardment resembled the transformation efficiency observed by Falciatore (1999) with most transformants obtained using the maximal rupture disk pressure of helium (1550 psi) likely due to the thicker frustule of *T. pseudonana*.

The response of the BIG1 knock-in, BIG1 knock-down and wild type lines to nitrogen yield limitation and the subsequent recovery was analysed monitoring physiological parameters commonly used in phenotyping experiments such as cell density, growth rates, Fv/Fm and microscopic control to ascertain any additional trait. BIG1 knock-in recovered faster post nitrate starvation and its growth rate has not changed compared to that calculated at the onset of the experiment. BIG1 knock-down exhibited an aggregating phenotype and showed an opposite growth response. This morphotype has not been identified in knock-in cultures. Aggregation occurs in natural diatom communities at the onset of bloom termination (Smetacek, 1985). Its absence in BIG1 knock-in may potentially underlie a specific response of these cells to nutrient sensing. This discussion will focus on these features separately, concentrating on the growth aspect first, followed by the response of photosynthesis to nitrate limitation and lastly, the aggregating phenotype.

Growth is accomplished through cell division, and involves genetic, physiological, ecological and morphological events and their complex interactions. In the present study, it was found that cultures overexpressing the BIG1 protein had a higher growth rate. This was true both at the onset of nutrient limitation as well as during recovery after nitrate starvation. Conversely, growth rates of BIG1 knock-down were lower in both conditions, pointing towards a possible difference in regulation of the cell cycle or uptake of nutrients in the two transgenic cell-lines. Strikingly, the growth rates of the overexpression cell line showed only minor decrease following nitrate starvation (0.06 ± 0.012), compared to the decrease of 0.50 ± 0.15 and 0.41 ± 0.21 in growth rates of knock-down and wild type respectively. It was demonstrated that cells did not divide immediately after the addition of nitrate to nitrate-starved cultures, although they immediately began taking up the added nitrate, albeit at a reduced rate (De La Rocha *et*

al., 2010). A reduction of 70% in nitrate uptake post nitrate starvation was reported for *T. weissfogii* (De La Rocha *et al.*, 2010) which is higher than our results. This may indicate that *T. pseudonana,* and especially the BIG1 knock-in, mobilizes the pathway of nitrate assimilation differently.

Field and laboratory studies of phytoplankton, including diatoms, have revealed a temporal lag between increases in nitrogen assimilation and increased growth rates, following a transition to improved growth conditions (Duarte, 1990). The temporal lag means a period required for metabolic adjustment and has been used to examine specific enzyme systems and to examine cellular mechanisms implied in regulation of different metabolic pathways (Smith *et al.,* 1992). We noticed a 24 hours lag phase in growth of wild type and BIG1 knock-down lines which resembled the results reported by Brown and colleagues (2009) for *T. pseudonana* cells recovering post nitrate starvation. The authors found an increase in transcript levels of five genes encoding nitrogen-assimilating enzymes 24 hours after transfer to nitrate replete media, which is consistent with an increase in nitrate assimilation and incorporation reflected by growth (Berges and Harrison, 1995). An even longer lag phase was reported for *T. weissfogii* (De La Rocha *et al.,* 2010). This denotes that nitrate-starved cells suffers sever deficiency of carbon and chlorophyll (Harrison *et al.,* 1977), enzymes and proteins (Sakshaug and Holm-Hansen, 1977) and amino acids (Dortch, 1982). Also, it was reported that diatom cells do divide during nitrate starvation (De La Rocha *et al.,* 2004), recycling more internal nitrogen (Nunn *et al.*, 2009) and reducing nitrogen losses by release of a photorespiratory-specific nitrogenous compound, glycolate (Parker *et al.*, 2004). In addition, it was shown that *nia* (the gene encoding the nitrate reductase (NR)) transcript levels are highly sensitive to overall N availability but the mature NR protein is not processed and folded properly unless nitrate is available (Poulsen and Kröger, 2005). Furthermore, the lag phase of BIG1 knock-in observed in this study was shorter, just 12 hours, suggesting an enhanced nitrate assimilation and enzyme activity triggered by the presence of the BIG1 protein.

Nutrient uptake generally occurs during G1 and/or G2 phase of the cell cycle (Vaulot *et al.*, 1987; Brzezinksi *et al.*, 1990). The cell cycle consists of G1 (gap1), S (synthesis), G2 (gap2) and M (mitosis) phases. DNA is replicated during S phase, cell division takes place in M phase, while G1 and G2 phases are cell cycle arrest points. Progressively larger spans of time preceding DNA replication have been suggested to be a result of

increasingly earlier arrest points within G1 depending of nitrogen deficiency (Olson *et al.*, 1986; Vaulot *et. al.*, 1987). This alteration in arrest point during G1 ultimately increases the lag time before cell division. Considering the shorter lag phase and enhanced growth of the cell line that overexpress the BIG1 protein, it may be possible that BIG1 arrests cells in late G1 and initiates a quicker release from G1 and subsequent DNA synthesis required for division. Mechanisms triggering cell cycle arrest or progression upon nitrogen starvation/addition remain unknown, but presumably involve signalling processes that result in control over cell cycle-related genes (Falciatore *et al.*, 2000; Shrestha *et al.*, 2012). Comparative genomics in diatoms revealed expanded gene families belonging to the cyclin gene family, histidine kinases and heat shock transcription factors which are supposed to be involved in environmental sensing (Bowler *et al.*, 2008; Rayko *et al.*, 2010). Cyclins and cyclin-dependent kinases are evolutionarily conserved set of proteins which control the transfer through different phases of the cell cycle. Also, the cyclin gene family was found to be larger in *T. pseudonana* compared to the pennate diatom *P.tricornutum* likely as a result of a larger number of diatom-specific cyclins found in *T. pseudonana* (Huysman *et al.*, 2010). A previous microarray study (Hipkin, 2012) found that in BIG1 knock-in, a G1/S specific cyclin D (ID 268403) was upregulated while G2/M specific cyclin B (ID 3035) and cyclin A (ID 6211) were downregulated following nitrate limitation. The upregulation of G1-specific cell cycle regulators by BIG1 overexpressing cell line may be a further indication of its role in rapid initiation of cell division by a faster release of cells from G1, allowing DNA synthesis.

Fv/Fm values measured during our experiments resembled the growth trend at both the onset of nitrate limitation and recovery post yield limitation. It was found that the BIG1 knock-in line had higher Fv/Fm than wild type and knock-down. Furthermore, in mid-exponential phase BIG1 knock-in showed higher Fv/Fm than wild type and knock-down under all examined conditions, not just in yield limitation induced by nitrate depletion but in response to fluctuating temperature as well (see chapter 4.3). The lowest Fv/Fm values were noted for the knock-down line at the start of the experiment and post nitrate limitation but its value decreased slower during starvation than for the other cell lines. The Fv/Fm data shows a declining pattern of PSII activity, similar to that observed in *T. weissflogii* (Berges and Falkowski, 1998) and *T. pseudonana* (Franklin *et al.*, 2012), likely indicating a process of intracellular protein degradation caused by nitrogen

deprivation. It is of special interest that the Fv/Fm of BIG1 knock-in recovers quicker upon release from stress. Additionally, the higher Fv/Fm indicates that Photosystem II is more efficient when BIG1 is overexpressed and may influence photosynthesis in a yet unknown manner (for more details see discussion in chapter 4). There is a consensus among photosynthetic eukaryotes that nitrogen starvation causes down-regulation of photosynthesis, irrespective of nitrogen source (Sun *et al.*, 2002; Li *et al.*, 2008). Nitrate assimilation and fixation into amino acids is an energy-consuming process. Since proteins that facilitate the electron transport and catalyse photosynthetic reactions require nitrogen to fix carbon, lower protein content due to nitrate starvation may limit the flow of electrons through the photosynthetic apparatus, causing increased production of reactive oxygen species. Thus, the resultant metabolic imbalance stimulates an increased oxidative stress (Logan *et al*., 1999). A sharp decrease of Fv/Fm was observed for all cultures during the nitrate depletion-induced stationary phase. The biggest decline was noticed in BIG1 knock-in. Increased chlorophyll degradation (Walker *et al.*, 2004) may be a possible explanation for the affected photosynthetic apparatus as it was suggested in previous nitrogen limitation experiments on *T. pseudonana* (Franklin *et al.*, 2012). They revealed a more rapid decrease in chlorophyll relative to carotenoids, suggesting that an increase in chlorophyll alteration may serve as early indicators of loss of cell viability (Franklin *et al.*, 2012).

Additionally, diatoms are known to store carbon as chrysolaminaran (Kroth *et al.*, 2008) or as lipids (Armbrust *et al.*, 2004) outside of the plastids but under nitrogen starvation *T. pseudonana* appeared to remobilise carbon. Conversely, plants and green algae increase their carbon stores in response to nitrogen stress (Eberhard *et al.*, 2008). It was found that protein (Hockin *et al.*, 2012; Shi *et al.*, 2015) and transcript (Mock *et al.*, 2008) abundance associated with the Krebs cycle increased at the onset of nitrogen starvation. In addition to producing cellular energy, the Krebs cycle provides carbon skeletons for nitrogen assimilation and the biosynthesis of compounds. Although it was suggested that this response is specific for diatoms, a similar response was described in a marine cyanobacteria under nitrogen limitation (Tolonen *et al.*, 2006), suggesting that breakdown of intracellular carbon stores is more efficient for the assimilation of nitrogen than photosynthesis (Parker and Armbrust, 2005; Tolonen *et al.*, 2006). In addition, diatoms, uniquely among eukaryotes with the exception of metazoans, possess a full urea cycle (Armbrust *et. al.*, 2004; Bowler et al., 2008). The urea cycle is thought

to be involved in mobilizing nitrogen and carbon produced by cell processes back into central metabolism (Allen *et al.*, 2006, 2011). Summarising the characteristics of the BIG1 knock-in line under nitrogen starvation, a possibly different mechanism of nitrogen recruitment is suggested. These characteristics include i) unchanged cell size, ii) higher Fv/Fm and iii) a decrease in lipid accumulation during nutrient starvation.

In bloom forming diatoms, declining growth is accompanied by an increase in sinking rate (Smayda, 1970; Walsby and Reynolds, 1980). Amorphous aggregates of small particles, including phytoplankton cells, termed 'marine snow' are major vehicles of global sinks of carbon and nitrogen. It was described that diatoms' life cycle includes a resting stage (Hensen, 1887) either in the form of vegetative cells or spores prevalent among blooming diatoms (Hargrave and French, 1983). Formation of aggregates and resting stages was associated with the terminal phase of phytoplankton blooms as a process that rapidly removes the population from an inhospitable environment characterised by nutrient limitation (Smetacek, 1985; Kiørboe *et al.*, 1990). The sinking rate of some diatoms reduces when they encounter higher nutrient concentration and lower light levels (Bienfang *et al.*, 1983; Richardson and Cullen, 1995). Nutrient uptake and storage at low light allow the initiation of cell division upon illumination (Malone, 1980, Doney, 2006) as well as the formation of the subsurface chlorophyll maxima (Carmack *et al.*, 2004; Martin *et al.*, 2010). Aggregates tend to disintegrate into individual cells (Margalef, 1978), mediated by frustule dissolution (Hurd *et al.*, 1979). This may be an explanation for the decreasing aggregation observed in BIG1 knock-down line by the end of the starvation period. The maximum aggregation rate of BIG1 knock-down was observed at 144 hours from the onset of the experiment. This may be the point when nitrate was depleted from the media, thus triggering a mechanism which under natural conditions would allow cells to escape from waters that run out of nutrients and sink to lower levels. Since this trait is not shared with BIG1 knock-in, which did not form aggregates in response to nitrate depletion, it seems that reduced BIG1 protein level reactivates a flocculation mechanism observed mostly in diatoms (reviewed by Kiørboe and Hansen, 1993). This mechanism allows diatom cells to thrive longer under unfavourable conditions even if their growth is reduced.

It was revealed that among diatoms *Thalassiosira* species were the most nutrient-sensitive in natural assemblages, and their sinking rates increased most dramatically upon nitrate depletion (Waite *et al.*, 1992). Nitrogen depletion was seen as the main

trigger for generation of vegetative cells in diatoms (Hargraves and French, 1983, Lewis *et al.*, 1999). However, formation of spores was observed at high ambient nitrate concentration in *Thalassiosira antarctica* (Doucette and Fryxel, 1983), suggesting that nitrogen depletion causes sporulation only in temperate but not polar species (Smetacek, 1985). Conversely, several studies noted a high fraction of diatom resting spores within the subsurface chlorophyll maxima, suggesting either a moribund community (Heiskanen and Keck, 1996; Booth, *et al.*, 2002) or active photosynthesis and new production (Hill and Cota, 2005; Palmer *et al.*,2013) by an active, photosynthetically competent subsurface diatom community (Brown *et al.*, 2015). Either way, the different morphotypes observed in the two transgenic lines shows how variable the response to changing environmental conditions may be not just at interspecific but intraspecific level as well.

In addition to the observed three main traits, some features related to cell size and differential regulation of gene expression needs to be mentioned. Some may point towards the BIG1 knock-in initiating faster growth by its property to not form aggregates, saving time that cells need to dissociate. However, a bigger cell size was observed for the BIG1 knock-in in relation to BIG1 knock-down at the onset of nutrient limitation as well as under nutrient replete conditions which is in contradiction with the paradigm that smaller cells divide quicker. It is worthwhile mentioning that nitrate starvation caused the *big1* gene to be significantly upregulated and co-expressed in BIG1 knock-in in exponential and stationary phase (log2 6.362/5.045 fold) relative to wild type, which indicates that although the level of BIG1 protein is reduced in stationary phase, the mRNA level remains high, initiating quicker translation of proteins when nutrient levels recover (Poulsen *et al.*, 2006). Moreover, the co-regulation of the expression of genes was suggested to be interpreted as a mechanism to ensure that subunits of multi-protein complexes are synthesized in matching amounts (Biehl *et al.*, 2005).

The ability of diatoms to thrive in upwelling-induced, periodically nutrient reach conditions makes them the basis for the shortest and most energy efficient food webs of the world (Mann, 1993; Allen *et al.*, 2006; Armbrust, 2009). Diatoms, like many other marine phytoplankton, rely on the utilisation of nitrate as one of the primary nitrogenous nutrient. However, the concurrently warming effect caused by rising CO_2 may suppress nitrate reduction due to the inverse temperature dependency of NR

(Lomas and Glibert, 1999), the essential enzyme for nitrate incorporation. Furthermore, it was suggested that under increased atmospheric anthropogenic ammonium ($NH4^+$) and less input of nitrate from deep waters as a consequence of global warming (Doney, 2006; Duce *et al.*, 2008) phytoplankton, including diatoms, may shift their preference from nitrate to ammonium (Shi *et al.*, 2015). In conclusion, it would be worthwhile repeating the experiment with another nitrogen source, such as ammonia, as its uptake was suggested to be more energy conserving (Parker and Armbrust, 2005).

The phenotyping experiment revealed a net advantage of BIG1 knock-in in recovery post nitrate starvation. BIG1 knock-down caused an opposite phenotype confirming the role of its encoded protein in progression through the cell cycle. The identification of different phenotypes for BIG1 transformants may indicate clues about diatoms' ability to outcompete other phytoplankton groups as well as their ability to quickly initiate blooms when environmental conditions turn favourable.

CHAPTER 4: PHYSIOLOGICAL EFFECTS OF TEMPERATURE-INDUCED STRESS ON WILD TYPE *T. PSEUDONANA* AND CELL LINES THAT OVEREXPRESS OR KNOCK-DOWN THE BIG1 PROTEIN

4.1 Introduction

Physical properties of the upper ocean such as temperature, mixed-layer depth, and seasonal stratification of the surface layer are predicted to be strongly modified by climate warming in the coming century (Behrenfeld, 2014) and accompanied by altered seasonal patterns (Roemmich *et al.*, 2012; Wells *et al.*, 2015). The link between increasing water temperatures and phytoplankton growth rates has long been recognized, and it is expected that increased potential growth rates will accompany warming (Eppley, 1972; Bissenger *et al.*, 2008). Temperature influences physiological processes such as nutrient uptake and photosynthesis (Raven and Geider, 1988; Beardall and Raven, 2004). Phytoplankton species have a temperature niche described by optimal, lethal and tolerable water temperatures, with tolerable meaning that cells do not grow well, but still survive (de Boer, 2005; Fehling *et al.*, 2004; Magaña and Villareal, 2006). Their growth and diversity depend on temperature optima, the thermal niche width (Thomas *et al.*, 2012) and on physical constrains for the supply of nutrients such as stratification and mixing (Falkowski *et al.*, 1998). The surface ocean is divided into distinct temperature zones from the tropics to the poles as seen in Figure 4.1. This zoning according to temperature regimes sets the biogeographical boundaries between phytoplankton species (Longhurst, 1998; Okolodkov 1999).

Most knowledge about the distribution and dynamics of phytoplankton biomass is provided by satellite observations. Ocean-colour sensors measure the electromagnetic spectrum of sunlight scattered back to space from below the surface. The resulting surface chlorophyll data is combined in empirical models to estimate phytoplankton growth rates or net primary production (Doney, 2006). Although remote sensing is a valuable tool to analyse the distribution and succession of phytoplankton, it does not offer data about blooming species. Conversely, the *Tara* Oceans expeditions (2009-2013) collected an overwhelming amount of samples from different water layers over 3 years. One of the outcomes of this project was the generation of an extensive database of species-specific 18S ribosomal barcodes. They estimated that the euphotic zone of the ocean harbour ~150,000 DNA-based taxa of small eukaryotes (Vargas *et al.*, 2015). Among them diatoms, an exceptionally divers lineage of predominantly photoautotrophic heterokonts (Mann and Vanormelingen, 2013), were found to be one of the most abundant (Vargas *et al.*, 2015). Also, the analysis of the extensive generated

dataset concluded that temperature is the major driving force of phytoplankton, and as such diatoms, distribution (Sunagawa *et al.*, 2015).

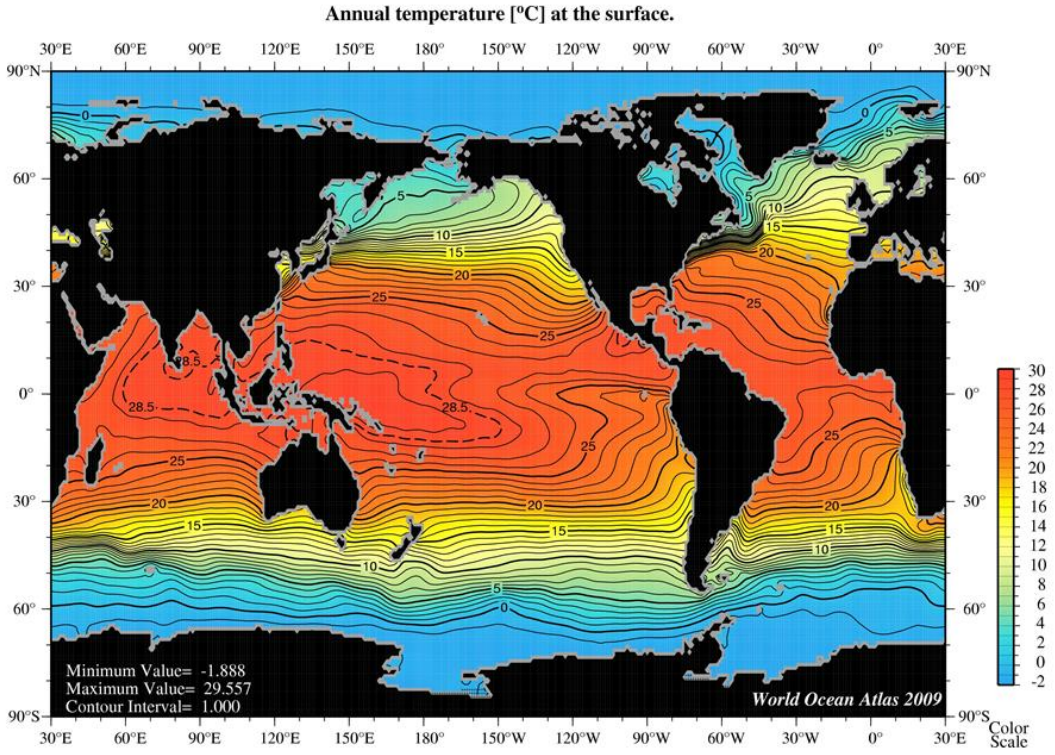

***Figure 4.1**: Surface ocean temperature distribution map. Image credit: The World Ocean Atlas 2009 (http://data.nodc.noaa.gov/woa/WOA09F emperature/JPEG _0_0_1.jpg), National Oceanic and Atmospheric Administration / Department of Commerce*

Such species diversity in a wide variety of habitats requires a very efficient use of energy to fuel cells activity. Diatoms, like many other phytoplankton, use photosynthesis to convert light energy into chemical energy which is ultimately stored in carbohydrates. Photosynthesis is a biological process that uses the energy generated by water oxidation to capture CO_2 and convert it into carbohydrates. Oxygen is a by-product of this "water-splitting" reaction. Photosynthesis is an endergonic reaction. In eukaryotes, it takes place in a specialised cell compartment called chloroplast. Photosynthesis occurs in two phases. In the first phase, termed light reaction, the energy of light is captured and used to produce the energy storage molecules ATP and reducing equivalents in the form of NADPH. In the second phase, the Calvin cycle, the energy of these products is used to capture and reduce CO_2. Light reactions in plants and algae

take place in thylakoids which are membrane bound compartments inside the chloroplast.

Chloroplasts share some features across plants and algae. Such features are the presence of the multiprotein photosynthetic complexes, Photosystem I and II (PSI and PSII). The two photosystems cooperate in the transfer of electrons from water to $NADP^+$ involving a linear electron transfer. In addition to the photosystems, the photosynthetic electron transport chain contains a transmembrane cytochrome complex (cytochrome b_6f), a water soluble copper protein (plastocyanin) in the lumen of the thylakoid membrane, and a lipid soluble quinone (plastoquinone) pool (Eberhard *et al.*, 2008). During electron transfer protons are pumped into the lumen of thylakoids generating a proton gradient which drives ATP synthesis. The two photosystems further carry pigment-protein complexed, called light-harvesting antennae (LHCs), which contain chlorophyll *a* and *c* in diatoms, alongside carotenoids. Photons absorbed by LHCs can take three alternative routes. Mainly, they are used for photochemistry inside the photosystems and driving electron transport, as described above. This process is also referred to as photochemical quenching. Excessive excitation energy, however, can also be dissipated as heat or chlorophyll fluorescence. The thermal dissipation process is termed non-photochemical quenching (NPQ) (Horton *et al.*, 1996) and was described to be highly efficient in the pennate diatom *P. tricornutum* (Ruban *et al.*, 2004; Bowler *et. al.*, 2008). Fluorescence only dissipates a minor fraction of excitation energy. It can be used, however, as a measure to assess the relative contribution of photochemical and non-photochemical quenching and thus photosynthetic performance. This relative measure of PSII photosynthetic performance is referred to as Fv/Fm (see Materials and Methods 2.1.2). Within the photosynthetic electron transport chain, over-reduction can be prevented by electrons being rerouted towards the respiratory chain by mitochondrial alternative oxidase (AOX), a process believed to be predominant in diatoms (Bailleul *et al.*, 2015). Chloroplasts are also capable of synthesizing ATP via a cyclic electron pathway that involves only PSI without net NADPH production (Shikanai, 2007), although in diatoms this pathway has been described as less active (Wilhelm *et al.*, 2006; Lepetit *et al.*, 2011) or even claimed to be lacking (Bailleul *et al.*, 2015).

Photosynthetic organisms fix CO_2 using the key enzyme Ribulose-1,5-bisphosphate carboxylase/oxygenase (RubisCO). However, diatom plastids originate from secondary endosymbiosis with a red alga, therefore they have an ID form of RubisCO. Form ID

RubisCO has higher affinity for CO_2, high CO_2/O_2 selectivity and a relatively low CO_2-saturated specific reaction rate compared to the IB form found in green algae (Roberts *et al.,* 2007). In addition, the activity of RubisCO is temperature sensitive (Badger *et al.*, 1998) while some enzymes involved in CO_2 fixation require activation by light (Buchanan *et. al*., 2000). RubisCO has an oxygenase or photorespiration activity that competes with carboxylation and leads to the loss of fixed carbon and the dissipation of photochemical energy (reviewed by Reinfelder, 2011).

The above underlines the importance of understanding light harvesting and energy conversion as well as the energy requirements of diatoms under dynamic environmental conditions. Additionally, despite the significance of temperature for life in surface oceans, our understanding on its impact on growth strategies, metabolism and composition of eukaryotic marine phytoplankton is limited (Toseland *et al.,* 2013). Furthermore, it was shown that phytoplankton species can display strong intraspecific differences in temperature tolerance and responses (de Boer, 2005).

Eppley (1972) used data of approximately 130 species to review the influence of temperature on phytoplankton between 2°C and 40°C to calculate the maximum growth rate of the phytoplankton community. Since then his assumptions form the basis of many ecosystem models and were proved to be appropriate, although phytoplankton growth rate tends to be higher (Bissinger *et al.*, 2008). While some studies focus on the optimal growth temperature of phytoplankton (Thomas *et al.*, 2012) there is little information on the temperature limits of phytoplankton although its importance has long been recognized (Li, 1980). Analogous to optimal growth temperatures, temperature limits can also be viewed as species functional traits that might be useful in understanding ecological responses to environmental factors (Chen, 2015). Thus, the physiological response of wild type and transgenic *T. pseudonana* lines was investigated in accordance to the existing literature with the aim of determining BIG1 thermal niche width for the first time. Also, by covering a wide range of temperatures information about its adaptive potential was gained. The monitored physiological parameters were the same as used in chapter 3. Phenotyping experiments were complemented by gene expression analysis of selected photosynthesis genes.

4.2 Results

4.2.1 Temperature-induced changes in growth

The physiological response of *T. pseudonana* wild type and *T. pseudonana* cell lines that overexpress (knock-in) or knock-down the BIG1 protein was investigated at 13 temperature points ranging from 5^0C to 33.6^0C with an average increasing step of 2.15^0C. Cell counts, cell size, and maximum photosynthetic efficiency of photosystem II were recorded until the cultures reached stationary phase. The illumination light intensity was set to 180 µmol photons $m^{-2}s^{-1}$ which assured a favourable growth condition and avoided co-limitation. Two treatments were applied, one measuring the response of the cell lines to temperature stress and one which investigated the response to temperature following a short acclimation period of approximately 10 generations (three transfers in late exponential phase). Stagnation in stationary phase was avoided as we tried to minimise potential physiological changes due to frequent genetic adaptation which diatoms are prone to exhibit (Lakeman *et al.*,2009).

Examining the length of the exponential growth phase as a function of temperature revealed that the BIG1 knock-in cell-line needed on average 11.54 hours less than the wild type and 12.46 hours less than the knock-down to progress through the exponential phase. The growth period of the BIG1 knock-in cell-line was shorter at all examined temperature points. Only at 14.5^0C it needed the same time as the wild type as seen in Figure 4.2. The wild type and the knock-down cell lines showed an alternating pattern of time used for growth at every second temperature point, also, their growth took the same time from 29^0C to 33.60^0C.

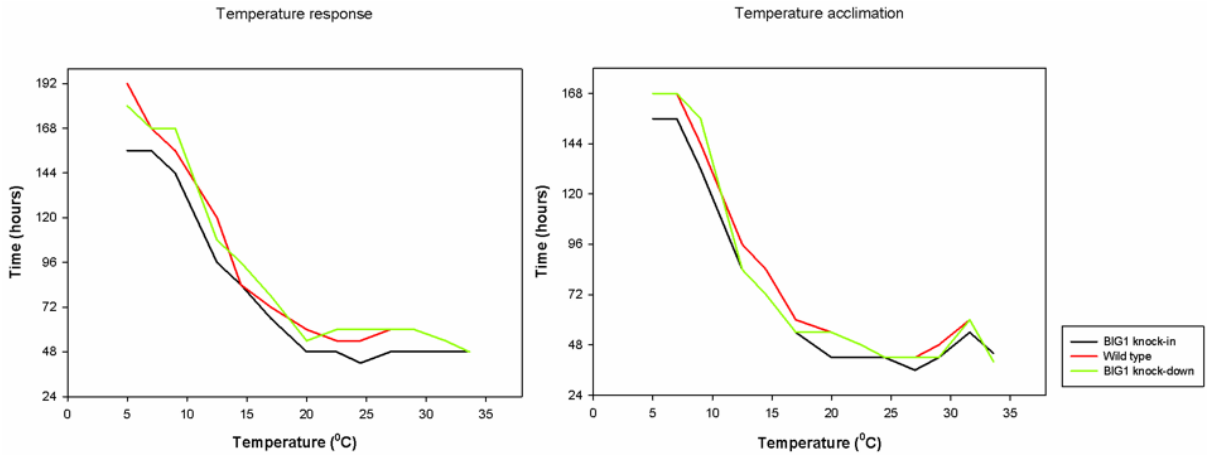

***Figure 4.2**: Length of the exponential growth in relation to the temperature in the centric diatom T. pseudonana that overexpress the BIG1 protein (BIG1 knock-in) and knock-down the expression of the BIG1 protein (BIG1 knock-down) and wild type under two conditions: temperature response and temperature acclimation.*

Acclimation to specific temperature points reduced the time of the exponential phase with an average of 5.84 hours for the BIG1 knock-in, 9.84 hours for the wild type and 12.62 hours for the knock-down cell line. However, these alterations in growth time have not changed the fact that the BIG1 knock-in cell line had the shortest growth time. Also, the knock-down cell-line needed the same time to grow as the knock-in at five temperature points spread across the two imminent sides of the optimum temperatures (12.5^0C, $14.\ 5^0$C, 17^0C, 24.5^0C and 29^0C).

4.2.1.1 The effect of temperature acclimation on growth of BIG1 knock-in, BIG1 knock-down and wild type *T. pseudonana* cell lines

The specific growth rate was calculated for the BIG1 knock-in, BIG1 knock-down and wild type cell lines. The results plotted as a function of time for the two treatments showed that acclimation to specific temperatures had minor effect on the growth of the BIG1 knock-in cell-line. Acclimation resulted in significantly higher growth rate just at 12.5^0C and 14.5^0C (Figure 4.3.A).

Temperature acclimation resulted in enhanced growth in the case of the wild type and the BIG1 knock-down cell-lines, as seen in Figure 4.3.B and Figure 4.3.C.

The outcome of the acclimation on the growth of the BIG1 knock-down cell-line was significantly higher in half of the examined temperature points, mostly on the lower optimum range, Figure 4.3.C.

Although there were significant differences between the growth rates of the three cell lines, the overall response was similar for the two conditions, as shown in Figure 4.4. The wild type performed better in the temperature range 14.5^0C – 24.5^0C in temperature response, while in acclimation this range was 12.5^0C – 22.5^0C. The BIG1 knock-down cell line grew better under 27^0C – 31.5^0C (temperature response) compared to 24.5^0C – 29^0C in acclimation. A decrease of 2.5^0C of the preferred temperature range was observed in BIG1 knock-down as a result of the acclimation. Similar to the knock-down line, acclimation reduced the optimal growth temperature range by 2^0C in wild type.

Conversely, the knock-in cell line performed best at the limit temperatures, 5^0C – 9^0C and 33.5^0C (temperature response) while under acclimation its advantage was reduced to two temperature points at the lower tolerance limit (5^0C and 7^0C) as seen in Figure 4.4. None of the cultures were able to acclimatise to 33.5^0C.

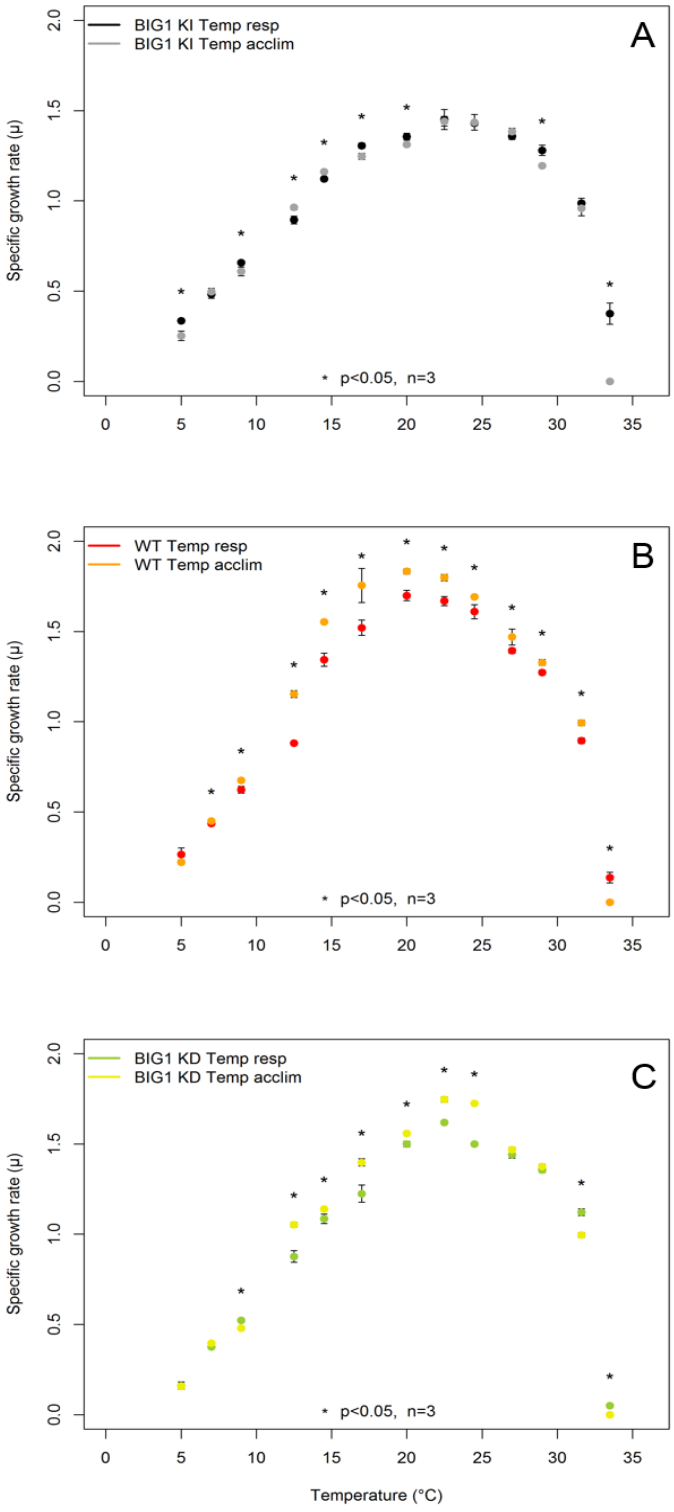

***Figure 4.3**: Specific growth rates in function of a temperature range of 5 – 33.5^{0}C of three cell lines of the diatom Thalassiosira pseudonana at temperature response and temperature response following acclimation. **A** BIG1 knock-in cell line, **B** Wild type cell line, C) BIG1 knock-down cell line. Dots represents mean growth rate of three biological replicates. Asterisks indicate significant difference in growth rate (Two samples t-test)*

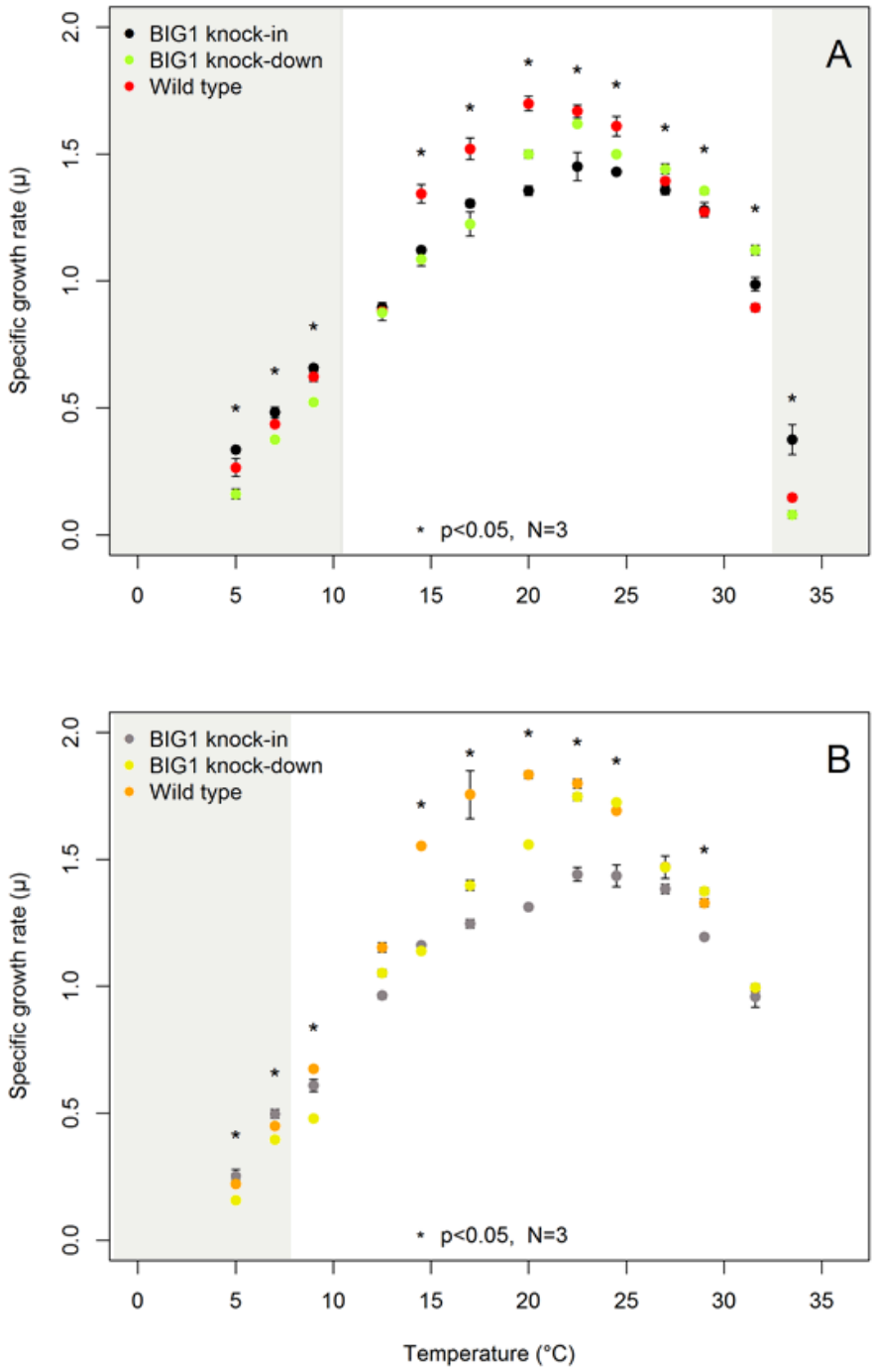

***Figure 4.4**: Specific growth rates in function of temperature in range of 5 – 33.5^{0}C of the BIG1 knock-in, BIG1 knock-down and Wild type cell lines of the diatom Thalassiosira pseudonana. **A** Temperature response; **B** Temperature acclimation. Dots represents mean growth rate of three biological replicates. Shading indicates advantage of the BIG1 knock-in cell line. Asterisks indicate significant difference in growth rate (Two samples t-test).*

Temperature acclimation enhanced the growth rate in wild type and BIG1 knock-down cell lines while in the knock-in cell-line it had little effect. Moreover, the knock-in cell-line performed better in temperature response, Figure 4.5.

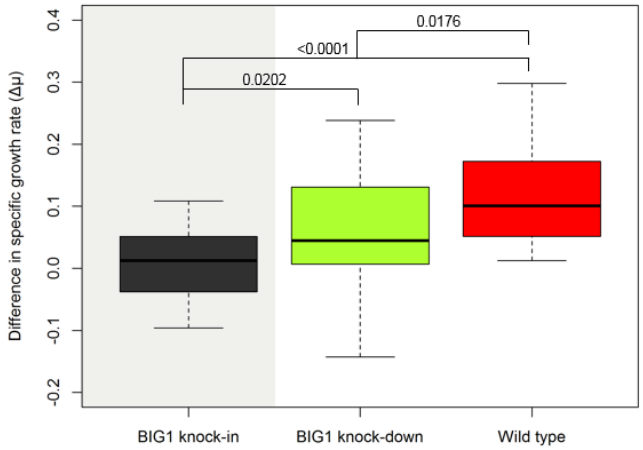

***Figure 4.5**: Means of the difference between growth rates calculated at temperature acclimation minus temperature response applied to a range of temperature of 5-33.5^{0}C. Boxplots represents mean of growth difference at 13 temperature points of three biological replicates of BIG1 knock-in, BIG1 knock-down and Wild type cell line. p value are indicated on figure (Mann-Whitney U test). Shading indicates contrasting trend, mean growth rates of temperature response higher than of temperature acclimation.*

4.2.1.2 Predicted and observed temperature optimum and maximum

Different windows of optimal temperature range for growth were identified for the wild type and the two transgenic cell lines of *T. pseudonana*, as described previously. Before the temperature response and acclimation experiments the cultures were kept at 20^{0}C. Therefore, no data about their optimal growth temperature were available. This lack of information was filled by experimental and modelled results. The optimum growth temperature of each cell-line was identified from the growth rates as a function of temperature. Under both treatments, temperature response and acclimation, the transgenic cell lines showed an optimum growth at 22.5^{0}C while the optimum temperature for wild type was acquired at 20.10^{0}C. The maximum growth temperature was recorded at 33.6^{0}C in temperature response for all analysed cell lines while the

maximum temperature that all cell lines were able to acclimate to was at 31.6^{0}C. No acclimation occurred at 33.6^{0}C.

Shifts in temperature optimum and temperature maximum were investigated by uploading the growth rate as a function of temperature in a non-linear regression model. The model returned a significant difference in the knock-down optimum temperature and a significant difference in the predicted maximum temperature in the case of the knock-in cell-line, as seen in Figure 4.6.

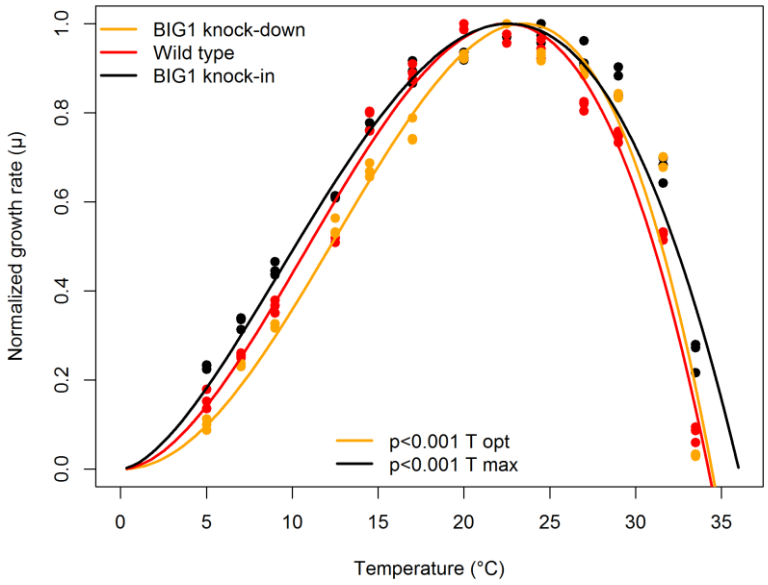

***Figure 4.6**: Modelled relation of the optimum and maximum temperature of T. pseudonana wild type and transgenic lines calculated from normalised growth rate in function to temperature. Dots represent biological replicates of wild type (red), knock-in (black) and knock-down (orange). Lines represent the fitted model. Significant differences are shown on numbers for optimum temperature (T opt) and maximum temperature (T max). N=3*

The predicted growth optimum and maximum temperature were compared to the experimental optimum and maximum recorded from plotting the growth rate as a function of temperature for both treatments, temperature response and acclimation.

Table 4.1: *List of the observed optimum and maximum temperatures along with the values calculated by the model for the Thalassiosira pseudonana cells overexpressing the BIG1 protein, wild type and cells that knock down the BIG1 protein exposed to temperature stress and acclimation to specific temperatures.*

Cell-lines	***Observed optimum temperature (^{0}C)***	***Modelled optimum temperature (^{0}C)***	***Observed maximum temperature (^{0}C)***	***Modelled maximum temperature (^{0}C)***
Temperature response BIG1 knock-in	22.50	22.62	33.60	36.02
Temperature response Wild type	20.10	22.48	33.60	34.25
Temperature response BIG1 knock-down	22.50	23.49	33.60	34.45
Temperature acclimated BIG1knock-in	22.50	22.33	31.60	34.63
Temperature acclimated Wild type	20.10	21.99	31.60	34.03
Temperature acclimated BIG1 knock-down	22.50	23.17	31.60	34.02

The predicted values were close to the observed ones in the case of optimum temperature. The best prediction was made for the BIG1 knock-in cell-line where the optimum temperature differed with (+)0.12^{0}C in temperature response and (-)0.17^{0}C in acclimation. The biggest difference compared to the observed optimum was predicted for the wild type with (+)2.38^{0}C at temperature response and (+)1.89^{0}C for acclimated cultures. Also, the estimated optimum temperature at temperature response and acclimation differed significantly (p-value 0.02872) for wild type. Values predicted for the knock-down cell-line stood between these limits, with (+)0.99^{0}C at temperature response and (+)0.67^{0}C following acclimation. In the case of the maximum temperature, the model predicted higher differences compared to the observed data. The model concluded that the highest difference for the knock-in cell-line was (+)3.03^{0}C at acclimation and (+)2.42^{0}C at temperature response. The wild type and the knock-down cell-line had a close outcome with (+)0.65^{0}C and (+)0.85^{0}C at temperature response. The predicted values for the wild type and knock-down cell lines were almost identical at temperature acclimation, notably (+)2.43^{0}C and (+)2.42^{0}C respectively.

However, analysing the relation between the estimated maximum temperatures of the temperature response and acclimation, there were significant differences in the case of the knock-down (p-value 0.04417) and knock-in (p-value 0.00037) cell-lines. In both

cases temperature had a strong negative effect, exerting a stronger effect on the knock-in cell line (d= –3.51) than on the knock-down cell-line (d= –1.72). We compared the predicted optimum temperature of the cell lines and found that the knock-down had highly significant difference in the estimated optimum temperature under both, temperature response (p-value 0.00182) and temperature acclimation (p-value 0.00001) compared to the wild type cell-line which was not the case for the BIG1 knock-in cell-line at any condition. Temperature had a strong positive effect on the optimum temperature exerting a stronger effect on acclimation (d = 4.56) than on temperature response (d = 3.00). In contrast, a large, statistically significant difference in the predicted maximum temperature was found just in the case of the BIG1 knock-in cell-line compared to the wild type with the stronger effect on temperature response (d = 6.55) than on acclimation (d = 1.83).

The highest tested temperature of the experiments was 36.4^0C at which temperature the BIG1 knock-down cell line died in twelve hours from the initial inoculation. In BIG1 knock-in and wild type cell lines photosynthesis ceased six hours later.

4.2.1.3 The effect of temperature on the growth of the BIG1 knock-in, BIG1 knock-down and wild type *T. pseudonana* cell lines in temperature response

The temperature response treatment can be interpreted as stress because cells were moved from steady 20^0C growth conditions to specific temperatures ranging from 5^0C to 33.6^0C. The response of the cells to the created stress condition was reflected by their growth rates and maximum photosynthetic quantum yield of photosystem II (Fv/Fm).

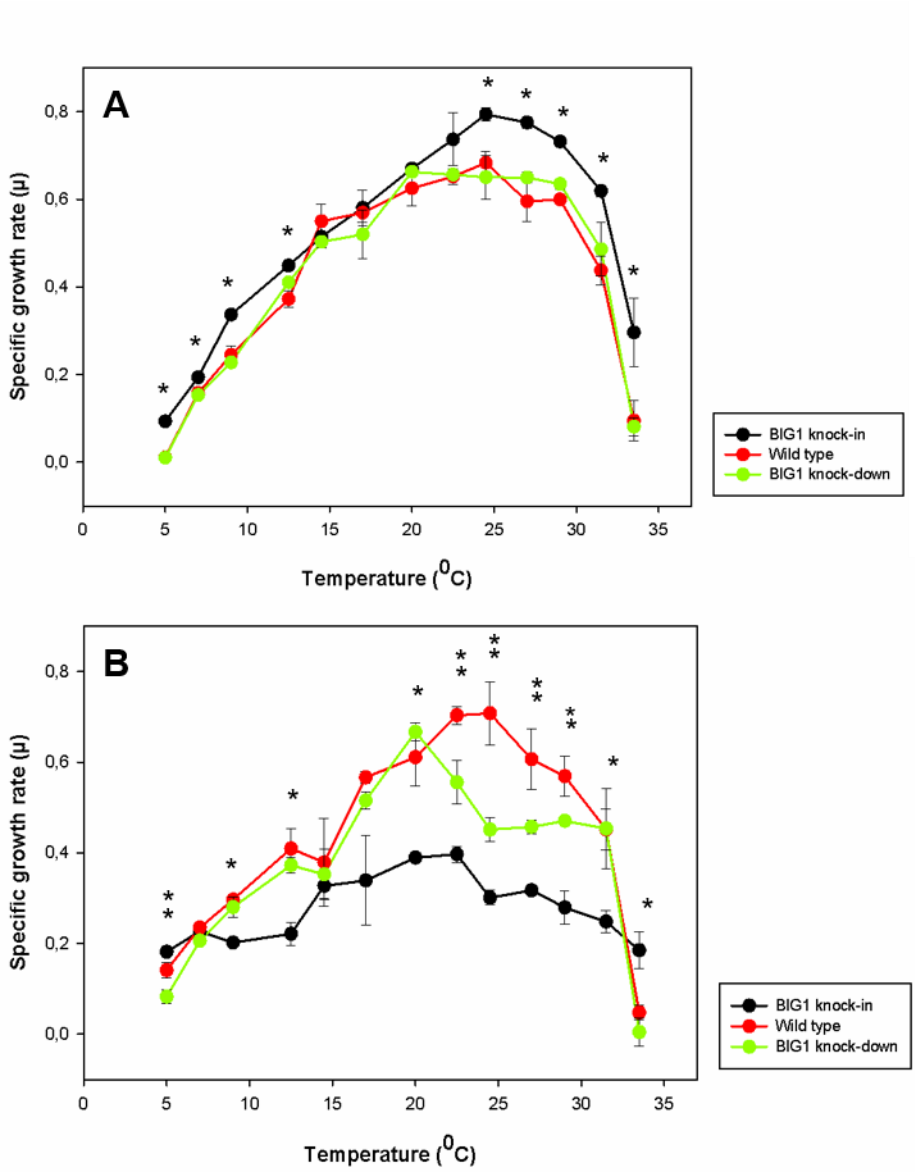

***Figure 4.7**: Mean specific growth rates in temperature response over a temperature range of 5 – 33.5^{0}C of three biological replicates of three cell-lines of the diatom Thalassiosira pseudonana. **A** Mean specific growth rates of the first half of the exponential phase; **B** Mean growth rates of the second half of the exponential phase; Black dots represent BIG1 knock-in; red dots Wild type, green dots BIG1 knock-down. Asterisks indicate significant difference in growth rate (Two samples t-test), * refers to the BIG1 knock-in compared pairwise to the Wild type and the BIG1 knock-down; ** refers to the Wild type compared to the BIG1 knock-down; N=3*

The growth rate at temperature response showed a distinct pattern for the first half of the exponential phase compared to the second half of the exponential phase (see Figure 4.7). A slow-down in growth of the BIG1 knock-in cell line was identified at all examined temperature points. This was seen at 30 hours following the inoculation at the temperatures between 33.5^0C – 14.5^0C and at 72 hours at the lower temperatures. An initial advantage of BIG1 knock-in in the first half of the exponential phase and a subsequent loss of it was mirrored in Fv/Fm as well (see supplementary materials). This aspect will be analysed later (see 4.2.5). According to this observation, the specific growth rate at temperature response was analysed separate for the time period before the observed break and the time period after that point. The specific growth rate was calculated from the slope of a linear regression of the natural logarithm of cell counts versus time. For this calculation an interval of 12 hours between subsequent cell counts was used in order to be able to split the exponential phase in two parts. This approach was imposed by the short duration of the exponential phase at some temperature points (see Figure 4.2.).

The growth in the first half of the exponential phase was led by the BIG1 knock-in cell line which outperformed both, wild type and knock-down at all temperature points except 14.5^0C. At 17^0C and 20^0C the BIG1 knock-in cell line grew at a similar speed as the wild type and the knock-down cell line. No statistically significant differences were seen between the Wild type and the knock-down cell line at any of the examined temperature points. In contrast, the BIG1 knock-in cell line showed statistically significant difference from both, wild type and knock-down at a significance level of $p<0.05$. Interestingly, the knock-in and wild type cell lines had the highest growth response at 24.5^0C, which is 2.5^0C and 4.5^0C higher than the temperature where the maximum growth response was calculated from the cell counts.

The growth of the knock-in cell line in the second part of the exponential phase, on the contrary, was outperformed by both wild type and BIG1 knock-down cell lines at all temperature points. This was statistically significant ($p<0.05$) except for the tolerance limit temperatures 5^0C and 33.5^0C. At this temperatures the BIG1 knock-in cell line grew significantly faster ($p<0.013$ and $p<0.027$). The highest growth rates were calculated for the wild type, though its advantage over the knock-down cell line was evident just between 22.5^0C and 29^0C. Reporting the growth rate in the second half of the exponential phase over all temperature points, the growth of the BIG1 knock-in cell

line was significantly lower than the Wild type ($p<0.03$) and the knock-down ($p<0.05$). A Mann-Whitney U test (Field, 2000) was used to examine the significance level over all temperature points. In a statistical sense, no difference was seen between the wild type and the BIG1 knock-down cell line over the whole temperature range.

Generalized linear models (GLM) of the R statistical package were used to relate variation in growth rates of cell lines as a function of temperature. By this method we tried to elucidate which variable, the genetic difference between the transgenic lines and wild type or the temperature, accounts for the difference in growth in the two halves of the exponential phase to a higher degree.

***Table 4.2**: Results of GLMs predicting the relationship between a) the cell lines and temperature on growth rate on the first half of the exponential phase; b) the cell lines and temperature on growth rate on the second half of the exponential phase; Abbreviations are BIG1 knock-down (BIG1 KD) and BIG1 knock-in (BIG1 KI)*

a) Growth rate in the first half of the exponential phase in temperature response

Predictors	**Estimate**	**SE**	**t value**	**Pr(>| t |)**
Intercept	0.758	0.028	27.463	<0.001
BIG1 KD cell-line	-0.009	0.039	0.234	0.815
BIG1 KI cell-line	-0.093	0.039	2.375	0.019
Difference from the optimum temperature	-0.040	0.003	-14.071	<0.001
BIG1 KD : Difference from the optimum	-0.0006	0.004	-0.153	0.871
BIG1 KI : Difference from the optimum	0.00003	0.004	0.009	0.992
Variance explained (R^2_{GLM}): 84.24%				

b) Growth rate in the second half of the exponential phase in temperature response

Predictors	**Estimate**	**SE**	**t value**	**Pr(>| t |)**
Intercept	0.732	0.018	41.761	<0.001
BIG1 KD cell-line	-0.119	0.028	-4.812	<0.001
BIG1 KI cell-line	-0.355	0.025	-14.319	<0.001
Difference from the optimum temperature	-0.033	0.002	-17.747	<0.001
BIG1 KD : Difference from the optimum	0.007	0.003	2.501	0.014
BIG1 KI : Difference from the optimum	-0.021	0.003	8.132	<0.001

Variance explained (R^2_{GLM}): 87.38%				

The models showed a significant ($p<0.001$) negative effect of temperature on the growth rate of the transgenic cell lines. This effect was more or less equal for the two parts of the exponential phase. Although, temperature had more pronounced effect on the first half of the exponential phase. An increase of one degree Celsius causes -0.040 decrease in growth rate by mid-exponential phase. By the end of the exponential phase an increase of 1^0C lowers the growth rate by -0.033, see Table 4.2. Temperature interacts significantly ($p<0.001$) with BIG1 knock-in in the second half of the exponential phase. The models showed that in the first part of the exponential phase the difference between the knock-in and knock-down genotype is responsible for the observed difference in growth rate. Conversely, in the second part of the exponential phase the difference between the genotypes is accentuated by temperature with a significant ($p=0.014$) positive effect on knock-down and a significant ($p<0.001$) negative effect on knock-in growth rates. The model explained 84% of data for the first half of the exponential phase (R^2_{adj} 0.8424, $p<0.001$) and 87% of the data (R^2_{adj} 0.8738, $p<0.001$) for the second half of the exponential phase. Also, for the second part of the exponential phase all variables were significant. Model residuals were normally distributed and variances of residuals were homogenous in both models.

4.2.1.4 The effect of temperature on the photosynthetic quantum yield of photosystem II (Fv/Fm)

The maximum photosynthetic efficiency of photosystem II (Fv/Fm) was monitored during the exponential growth phase of the *T. pseudonana* BIG1 knock-in, BIG1 knock-down and Wild type cell lines over 13 temperature points and under two treatments: temperature response and temperature acclimation at the same intervals as for growth rate.

A Kruskal-Wallis rank sum test showed a statistically significant difference in the maximum photosynthetic efficiency of photosystem II (Fv/Fm) between the three cell lines under two different treatments, temperature response and temperature acclimation as follows:

- Maximum acquired Fv/Fm at temperature response, $p<0.002$,
- Maximum acquired Fv/Fm at temperature acclimation, $p<0.03$,
- Fv/Fm recorded at the end of the exponential phase at temperature response, $p<0.003$

At the end of the exponential phase under temperature acclimation no significant difference was seen between the three cell-lines.

Due to the different behaviour observed in the early to mid-exponential phase and late exponential phase described earlier, the Fv/Fm was analysed accordingly. The photosynthetic efficiency of the PSII of the three cell lines was compared using a Mann-Whitney U test as seen in Figure 4.8.E-H. At temperature response condition the maximum acquired Fv/Fm of theBIG1 knock-down cell line was found to be the lowest. It was statistically significant compared to the knock-in and wild type ($p<0.003$; $p<0.007$). Also, the Fv/Fm recorded at the end of the exponential phase was significantly different compared to knock-in and wild type under the same condition ($p<0.005$ and $p<0.002$ respectively).

The same trend was observed in temperature acclimation. Under temperature acclimation, the only significant difference was seen between the Wild type and the BIG1 knock-down cell line ($p<0.009$). Within the same test outliers were identified at the temperature limits (5^0C and 33.5^0C) and removed from further analysis. These data points were analysed individually.

The maximum Fv/Fm of BIG1 knock-in was higher in temperature response over the whole examined temperature range. The photosynthetic efficiency of BIG1 knock-in was lowered sequentially as the cultures were acclimated. In late exponential phase in temperature acclimation the lowest Fv/Fm values were of BIG1 knock-in, see Figure 4.8.A-D.

GLM models were used to investigate whether the genetic difference or the temperature cause bigger effects on Fv/Fm in relation to temperature. The temperature response treatment was normalized by subtracting the Fv/Fm value of each temperature point from the maximum value recorded over all temperatures for each cell-line. The Fv/Fm response in temperature acclimation treatment was identified to follow a fifth degree polynomial trend and normalised accordingly.

The model showed a significant ($p<0.001$) negative effect of temperature on Fv/Fm in temperature response. Increasing one degree of temperature causes -0.0017 decrease in Fv/Fm compared to its value under optimal temperature. Temperature also interacts significantly ($p<0.001$) with genotype BIG1 knock-down exerting a positive effect on it. The model explains around 90% of the data (R^2_{adj} 0.8957, $p<0.001$). The model residuals were normally distributed and variance of residuals were homogeneous. There were no significant effects on BIG1 knock-in. All the other variables were been assigned as highly significant, Table 4.3.a.

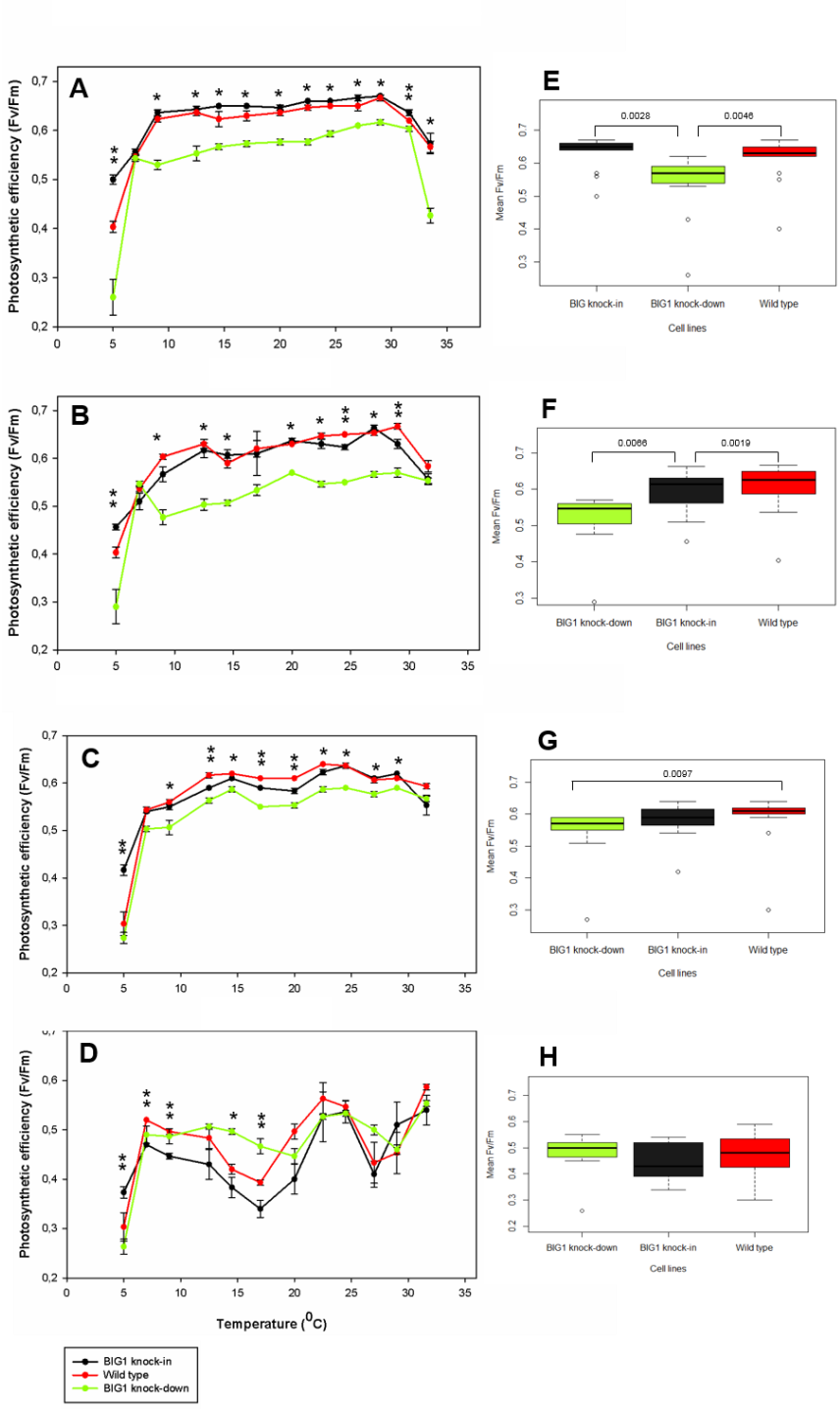

Figure 4.8*: Means of the Fv/Fm in temperature acclimation over a temperature range of 5 – 33.5^{0}C of three biological replicates of the diatom Thalassiosira pseudonana.* ***A*** *Maximum Fv/Fm recorded in exponential phase (temperature response);* ***B*** *Fv/Fm recorded at the end of the exponential phase (temperature response);* ***C*** *Maximum Fv/Fm recorded in exponential phase (acclimation);* ***D*** *Fv/Fm recorded at the end of the exponential phase (acclimation)* ***E*** *Means of the maximum photosynthetic efficiency from 13 temperature points;* ***F*** *Means of the photosynthetic efficiency from 13 temperature points at significance level .05 (E, F,G and H, Mann-Whitney U test). Black dots represents the BIG1 knock-in; red dots the Wild type, green dots the BIG1 knock-down. Asterisks indicate significant difference in Fv/Fm (Two samples t-test), * refers to the BIG1 knock-down compared pairwise to the Wild type and the BIG1 knock-in; ** refers to the BIG1 knock-in compared to the Wild type; N=3*

***Table 4.3**: Results of GLMs predicting the relationship between the cell lines and temperature on maximum photosynthetic efficiency of the photosystem II (Fv/Fm) a) in temperature response; b) at the end of the exponential phase in temperature response; c) in temperature acclimation; d) at the end of the exponential phase in temperature acclimation*

a) Maximum Fv/Fm in temperature response

Predictors	**Estimate**	**SE**	**t value**	**Pr(>| t |)**
Intercept	0.0592	0.0070	8.437	<0.001
BIG1 KD cell-line	0.0544	0.0099	5.481	<0.001
BIG1 KI cell-line	*0.0126*	*0.0099*	*-1.255*	*0.2234*
Temperature	-0.0017	0.0003	-4.681	<0.001
BIG1 KD : Temperature	-0.0022	0.0004	-4.616	<0.001
BIG1 KI: Temperature	*<-0.0001*	*0.0004*	*0.143*	*0.8879*
Variance explained (R^2_{GLM}): 89.57%				

b) Maximum Fv/Fm at the end of the exponential phase in temperature response

Predictors	**Estimate**	**SE**	**t value**	**Pr(>| t |)**
Intercept	0.5729	0.0171	33.493	<0.001
BIG1 KD cell-line	-0.1304	0.0241	-5.392	<0.001
BIG1 KI cell-line	*-0.0247*	*0.0241*	*-1.024*	*0.3192*
Temperature	0.0029	0.0008	3.375	0.0003
BIG1 KD : Temperature	*0.0009*	*0.0012*	*0.787*	*0.4415*
BIG1 KI : Temperature	*-0.0008*	*0.0012*	*-0.695*	*0.4959*
Variance explained (R^2_{GLM}): 92.09%				

c) Maximum Fv/Fm in temperature acclimation

Predictors	**Estimate**	**SE**	**t value**	**Pr(>| t |)**
Intercept	0.6200	0.0027	221.576	<0.001
BIG1 KD cell-line	-0.0450	0.0039	-11.372	<0.001
BIG1 KI cell-line	-0.0125	0.0039	-3.159	0.0196
Temperature (5^{th} order poly)5	0.0386	0.0137	2.813	0.0306
BIG1 KD : Temperature (5^{th} order poly)5	*0.0241*	*0.0193*	*1.243*	*0.2601*
BIG1 KI : Temperature (5^{th} order poly)5	*0.0189*	*0.0193*	*0.979*	*0.3654*

Variance explained (R^2_{GLM}): 90.39%%				

d) Maximum Fv/Fm at the end of the exponential phase in temperature acclimation

Predictors	**Estimate**	**SE**	**t value**	**Pr(>| t |)**
Intercept	0.4777	0.0107	44.436	<0.001
BIG1 KD cell-line	*0.0155*	*0.0152*	*1.023*	*0.3330*
BIG1 KI cell-line	-0.0322	0.0152	-2.119	0.0631
Temperature (5^{th} order poly)5	0.1917	0.0558	3.431	0.0075
BIG1 KD : Temperature (5^{th} order poly)5	-0.1738	0.0790	-2.200	0.0553
BIG1 KI : Temperature (5^{th} order poly)5	*0.0143*	*0.0790*	*0.180*	*0.8607*
Variance explained (R^2_{GLM}): 68.35%				

The effect of temperature grew increasingly with acclimation gradually becoming positive. It was also significant at mid-exponential and late exponential phase in both conditions, temperature response and acclimation ($p<0.05$), see Table 4.3. An opposite trend was shown for the effect of the genotype on Fv/Fm. The difference caused by knocking down the BIG1 protein showed a significant decreasing effect ($p<0.001$) on Fv/Fm with acclimation, see Table 4.3.a-c. The interrelation of genotype – temperature was significant just for BIG1 knock-down ($p<0.001$) in temperature response at mid-exponential phase, see Table 4.3.a.

At the end of the exponential phase in temperature response (R^2_{adj} 0.9209, $p<0.001$) the BIG1 knock-down cell-line showed a significant negative response ($p<0.001$) while the temperature had a significant positive effect ($p<0.001$) on the photosynthetic efficiency. The genotype – temperature interrelation was significant for any of the transgenic lines.

The models explained 68-90% of data in temperature acclimation as follows: (R^2_{adj} 0.9039, $p<0.002$) at mid-exponential phase and (R^2_{adj} 0.6835, $p<0.02$) at the end of the exponential phase.

4.2.1.5 Cellular morphology of the BIG1 knock-in, BIG1 knock-down and wild type cell lines in temperature response and acclimation

The cell size showed little fluctuation over the temperature response. The three examined cell lines displayed more or less identical response at first contact with different temperatures. Interestingly, the cell size of the BIG1 knock-in cell-line was on average 1-1.6 µm bigger than the sizes of the BIG1 knock-down and wild type cell lines over all temperatures under both temperature response and acclimation, see Table 4.4. In contrast, at temperature acclimation both genetically modified strains showed differences. Notably, the knock-in cell line had a sharp cell size reduction in the 9^0C – 29^0C temperature range, while the knock-down cell-line showed the opposite, increased its cell size at all temperatures except 33.5^0C, as seen in Figure 4.9 and Figure 4.10.

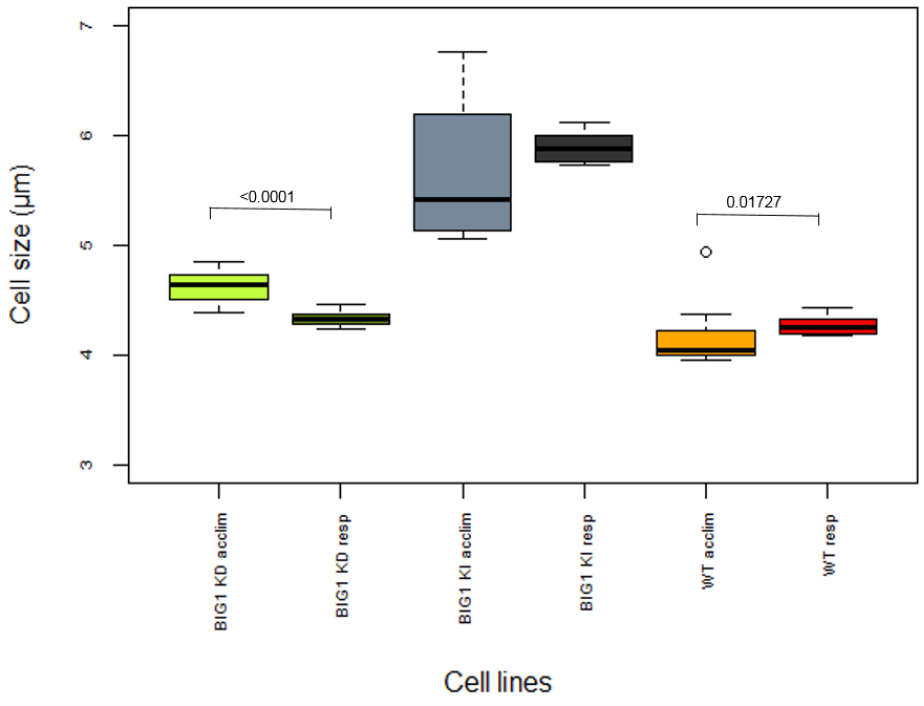

***Figure 4.9**: Average cell size measured in triplicates at 13 temperature points at temperature response and temperature acclimation. Abbreviations represents as follows: BIG1 knock-in at temperature response (BIG1 KI resp), BIG1 knock-in at temperature acclimation (BIG1 KI acclim), BIG1 knock-down at temperature response (BIG1 KD resp), BIG1 knock-down at temperature acclimation (BIG1 KD acclim), Wild type at temperature response (WT resp) and Wild type at temperature acclimation (WT acclim). Significant differences are shown in numbers (Mann-Whitney U test)*

***Table 4.4**: Differences in average cell size compared to BIG1 knock-in cells measured in triplicate at 13 temperature points. Standard errors are shown after ± sign, p-value denotes significance level (Mann-Whitney U test).*

Cell lines	*Cell size (µm)*			
	Temperature response	*p-value*	*Temperature acclimation*	*p-value*
Wild type	1.601±0.023	<0.0001	1.468±0.019	<0.0001
BIG1 knock-down	1.550±0.027	<0.0001	1.004±0.013	<0.0001

The recorded average cell size was compared to the cell size measured at the beginning of the experiments. This relation is presented in Figure 4.10.

The cell size of the wild type and knock-down cell lines at temperature response showed little change in relation to the starting cell size except at 33.5^0C, where a difference of 0.587±0.036 µm and 0.572±0.069 µm was recorded for the wild type and knock-down respectively. In the case of the BIG1 knock-in cell-line a change of 0.495±0.098 µm and 0.458±0.065 µm was recorded at 33.5^0C and 9^0C. On the whole, any of these changes in cell size represent a considerable shift from the starting size.

Temperature acclimation caused little change in cell size of the BIG1 knock-down cell line. All the noted differences were below 0.6 µm as seen in Figure 4.10. The results of the wild type were similar, the only exception was at 31.5^0C, where the cell size increased with 1.053±0.018 µm compared to the start of the experiment. The BIG1 knock-in cell-line showed changes of 1.736±0.028 µm (31.5^0C, $p<0.001$), 1.152±0.021 µm (29^0C, $p<0.001$), 1.285±0.038 µm (7^0C, $p<0.001$) and 1.194±0.017 µm (5^0C, $p<0.001$). This resulted in an equilibrated pattern with increasing cell size at the margins of the temperature tolerance. These results indicate an average of 2.73-fold increase in cell size compared to the wild type and 3.16-fold increase in cell size compared to knock-down cell-line at the same temperatures.

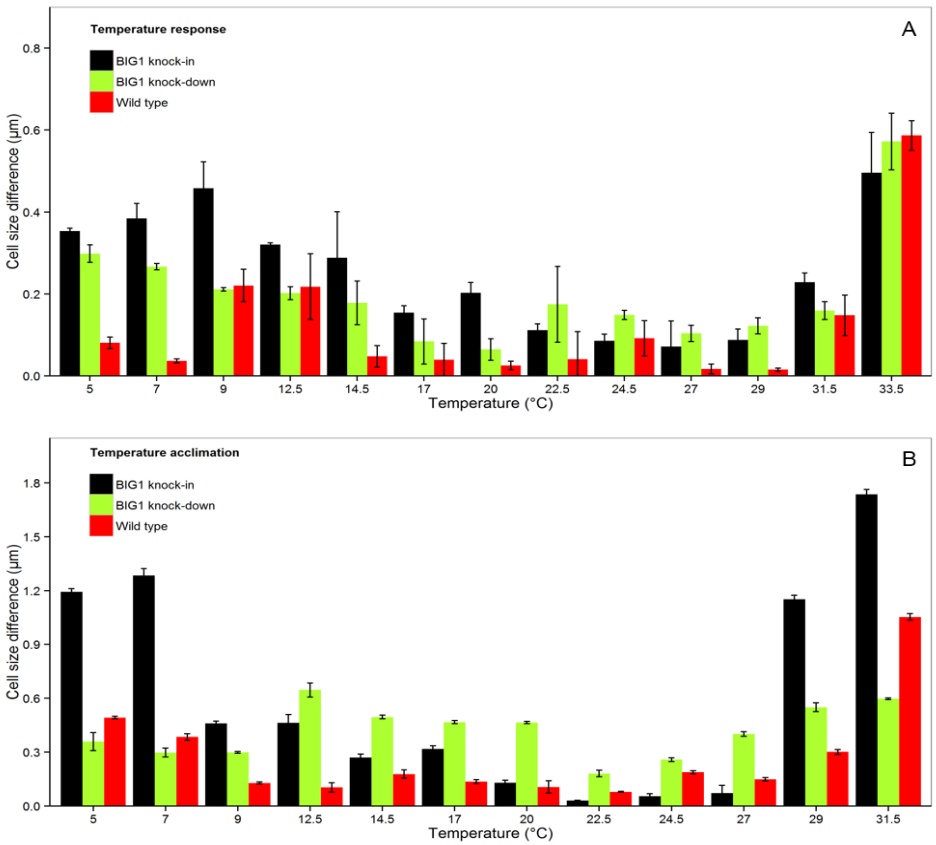

Figure 4.10*: Cell size difference between the start and the end of the temperature stress experiment.* ***A*** *Temperature response;* ***B*** *Temperature acclimation. Error bars indicate standard variation. Cell size differed significantly for all temperatures in acclimation at .01 level except 20^{0}C (Two samples t-test); N=3.*

Possible aggregation in relation to temperature was tested in temperature acclimated cultures. The results showed that no aggregation occurred (supplementary materials).

4.2.2 Response of *T. pseudonana* BIG1 knock-in, BIG1 knock-down and wild type to fluctuating temperature

Subsequent to the identification of the minimum and maximum temperatures at which a measurable growth rate was acquired for all the three examined cell lines under both temperature response and acclimation, we tested the cell lines' response to high fluctuation in temperature. For this purpose, 250,000 cells of exponentially growing cultures with Fv/Fm ≥ 0.6 were inoculated in 150 ml of NEPCC media and exposed to short time temperature stress at 5^{0}C and 33.5^{0}C for 24 hours. After 24 hours, 25,000

cells of each culture was inoculated in fresh 100 ml NEPCC media in replicates and kept at 20^0C. Their recovery was monitored for the next 60 hours and recorded every 12 hours. The monitored physiological parameters were the same as for the acclimation.

All cell lines displayed a lag phase in growth in the first 12 hours post temperature stress. Analysing the slope of the log-transformed cell number as a function of time at 5^0C the lag phase was not as distinct as it was at 33.5^0C. In contrast, the cell number during recovery following exposure to 33.5^0C displayed a continuous increase without break points which was not the case in recovery following 5^0C. Here, a clear break point was identified at 36 hours following the temperature stress. This breaking point as well as the presence of a lag phase, even if it had not been so pronounced, was taken into account when growth rates were calculated for the examined period. Two samples t-test were used pair wise (BIG1 knock-in – wild type; wild type – BIG1 knock-down) to calculate the significance between the growth rates and the recorded Fv/Fm values.

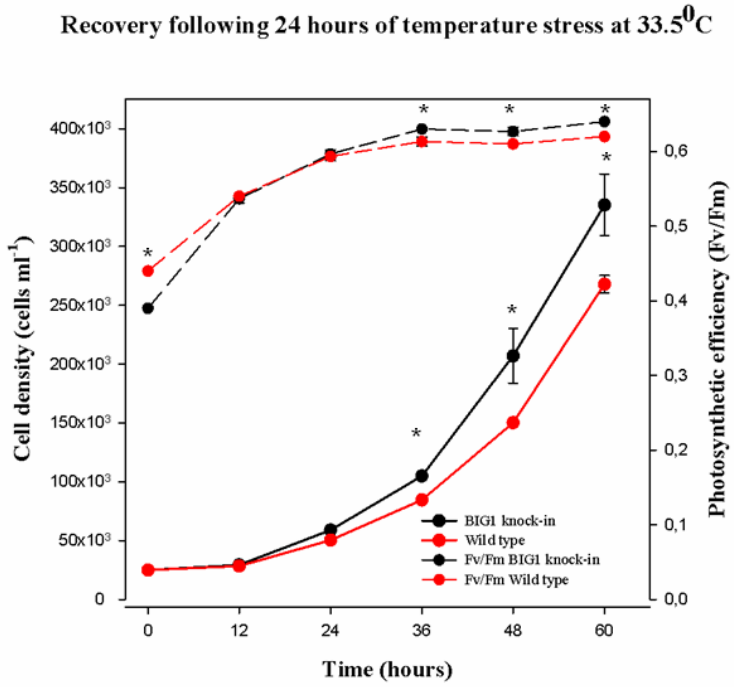

***Figure 4.11**: Recovery at 20^0C following 24 hours of temperature stress at 33.5^0C. Dots and solid lines represent mean cell density of biological replicates of Thalassiosira pseudonana BIG1 knock-in (black), wild type (red); dots and dashed lines represent the photosynthetic efficiencies of the two cell lines, BIG1 knock-in (black), wild type (red). Error bars indicate standard variation, asterisks indicate significant difference in growth rate and photosynthetic quantum yield ($p<0.05$); N=3.*

The BIG1 knock-down cell line died at the end of the third hour following the temperature stress and inoculation into fresh media at 20^0C. Because in this experiment the knock-down line did not produce measurable dataset it was omitted from Figure 4.11, Figure 4.12 and Table 4.5. The knock-in cell line recovered better, had higher cell number and growth rates, as well as recovered better in photosynthetic efficiency of PS II. Fv/Fm value of BIG1 knock-in was lower than the wild type (0.39 compared to 0.44) at the onset of recovery following 24 hours temperature stress at 33.5^0C. Also, Fv/Fm recovered quicker in the BIG1 knock-in cell line than the wild type at both limit temperatures as seen in Figure 4.11 and Figure 4.13.

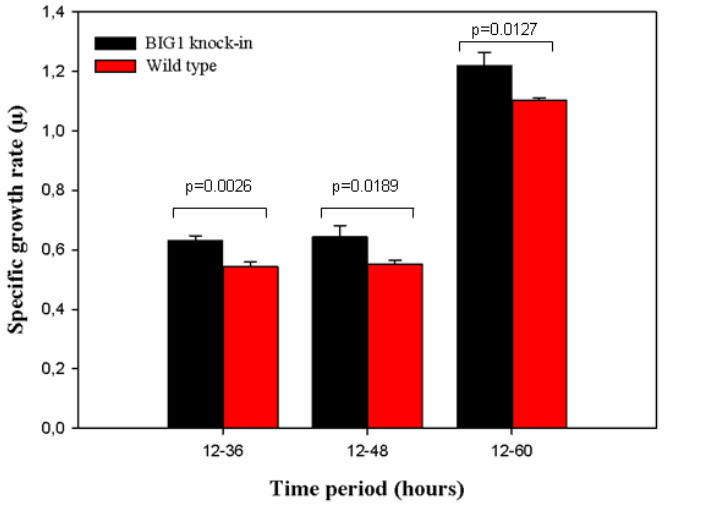

***Figure 4.12**: Specific growth rates at 36, 48 and 60 hours of recovery following 24 hours temperature stress at 33.5^0C. Bars represent the mean growth rates of biological replicates of Thalassiosira pseudonana BIG1 knock-in (black), wild type (red) cell lines at the specified time period. Error bars indicate standard variation, p values show significant differences in growth rate calculated with two samples t-test, N=3.*

Almost no difference in growth rate between the first 36 hours and 48 hours was calculated from the measurements, with only slightly higher variation at 48 hours as seen in Figure 4.12. At 60 hours the growth rate was approximately double the rate at 48 hours. Higher cell density was recorded, matching the higher growth rate. The difference in cell number between the BIG1 knock-in and wild type was expressed in percentage calculated according to the formula: cell number of BIG1 knock-in minus the value of WT/BIG1*100 and is summarised in Table 4.5.

***Table 4.5**: Summary of the acquired growth rate in the time period of 12 – 60 hours following 24 hours temperature stress at 33.5^{0}C. Data shown for the BIG1 knock-in and Wild type cell lines: specific growth rate (μ), standard deviation (SD), difference between the two cell lines expressed in growth rate difference and percentage of cells and error of the percentage.*

Temp stress	***BIG1***		***WT***		***Difference***		
	μ_{BIG1}	***SD***	μ_{WT}	***SD***	μ_{BIG1-} μ_{WT}	***%***	***Error***
33.5^{0}C	1,22	0,05	1,10	0,01	0,12	22,14	4,43

The recovery from 5^{0}C temperature stress showed some differences compared to the 33.5^{0}C recovery. The photosynthetic quantum yield of PSII showed higher stress after 24 hours at 5 C than 33.5C. A sharp drop was recorded from the exponentially growing cells Fv/Fm value of 0.6 to Fv/Fm 0.17 (BIG1 knock-in), 0.27 (wild type) and 0.12 (BIG1 knock-down), respectively, as seen in Figure 4.13. Although, the Fv/Fm starting values for the recovery experiment from 5^{0}C were considerably lower than for the 33.5^{0}C, all cell lines performed better in the first 12 hours. The photosystem II of the knock-in cell line achieved the stage of a healthy exponentially growing culture almost at its maximum value (Fv/Fm 0.64) within 12 hours from the onset of recovery. The Fv/Fm of the wild type and the knock-down were lower, both reached an Fv/Fm of 0.57 at 12 hours after temperature stress. Interestingly, the Fv/Fm recorded in the recovery from 33.5^{0}C for BIG1 knock-in and wild type equalled 0.54 at that point.

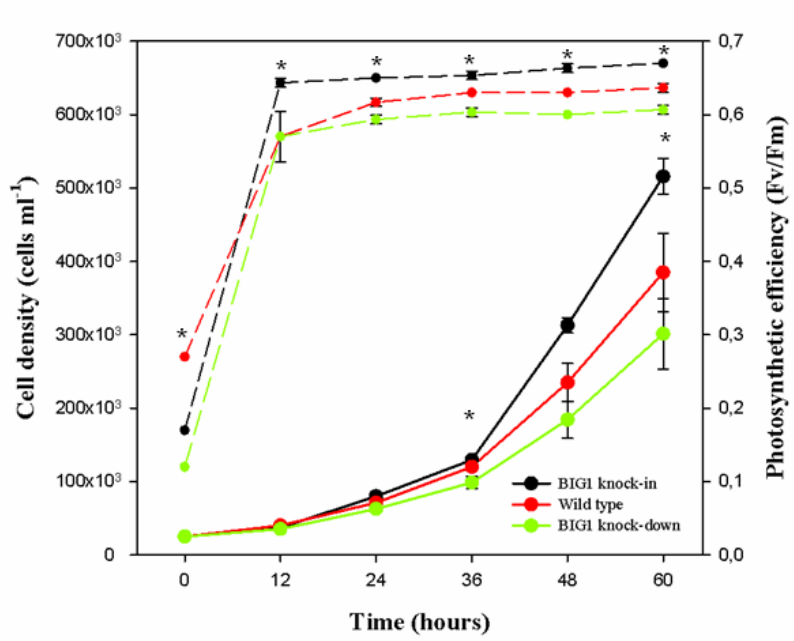

***Figure 4.13**: Recovery at 20^{0}C following 24 hours of temperature stress at 5^{0}C. Dots and solid lines represent mean cell density of biological replicates of Thalassiosira pseudonana BIG1 knock-in (black), wild type (red) and BIG1 knock-down (green); dots and dashed lines represent the photosynthetic efficiencies of the two cell lines, BIG1 knock-in (black), wild type (red) and BIG1 knock-down (green). Error bars indicate standard variation, asterisks indicate significant difference in growth rate and photosynthetic quantum yield (p<0.05); N=3.*

At 24 hours from the start of the recovery the photosynthetic efficiency reached the exponentially growing stage for all three cell lines, recording Fv/Fms of 0.65, 0.62 and 0.59 for the knock-in, wild type and knock-down respectively and were consistently higher than in 33.5^{0}C recovery, as seen in Figure 4.13.

The BIG1 knock-in cell line recovered better than the two other cell lines in both the first part and the complete exponential phase ($p<0.05$). Interestingly, the knock-in growth rate was a bit higher in the second half of the exponential phase, as seen in Table.4.6 and Figure 4.14, which was in contrast with the tendency observed in the temperature response and acclimation experiments.

***Table 4.6**: Summary of the acquired growth rate in the two parts of the exponential time period of 12 – 60 hours following 24 hours temperature stress at 5^0C. Data shown: the BIG1 knock-in (μ_{BIG1}), Wild type (μ_{WT}) and BIG1 knock-down (μ_{KD}) cell lines: specific growth rate, standard deviation (SD).*

Time in hours	BIG1		WT		BIG1 k-d	
	μ_{BIG1}	SD	μ_{WT}	SD	μ_{KD}	SD
12-36h	0,63	0,01	0,55	0,05	0,51	0,03
36-60h	0,69	0,03	0,58	0,06	0,56	0,04

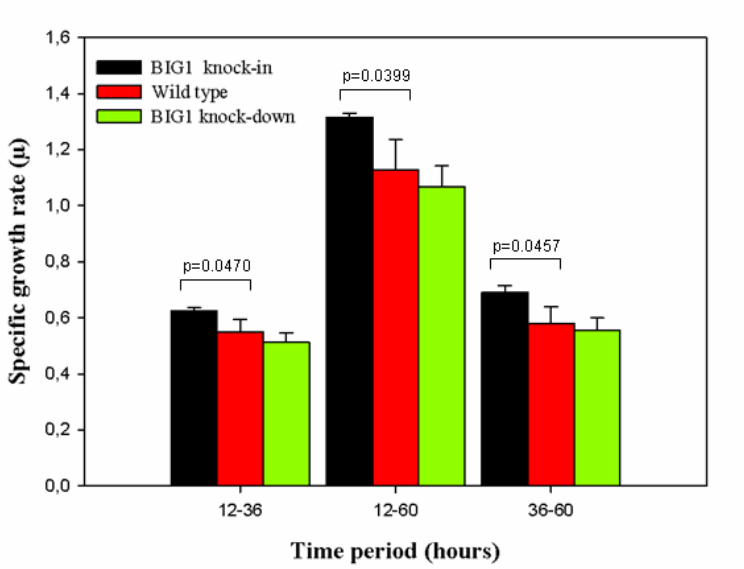

***Figure 4.14**: Specific growth rates at 36 and 60 hours of recovery following 24 hours temperature stress at 5^0C. Bars represent the mean growth rates of biological replicates of Thalassiosira pseudonana BIG1 knock-in (black), wild type (red) and BIG1 knock-down (green) cell lines at the specified time period. Error bars indicate standard variation, p values show significant differences in growth rate calculated with two samples t-test, N=3.*

***Table 4.7**: Summary of the acquired growth rate in the time period of 12 – 60 hours following 24 hours temperature stress at 5^0C. Data shown for the BIG1 knock-in, Wild type and BIG1 knock-down cell lines: specific growth rate (μ), standard deviation (SD), difference between the pairs of cell lines expressed in growth rate difference and percentage of cells and error of the percentage.*

Temp stress	BIG1		WT		BIG1 k-d		Difference					
	μ_{BIG1}	SD	μ_{WT}	SD	μ_{KD}	SD	μ_{BIG1}-μ_{WT}	%	Error	μ_{WT}-μ_{KD}	%	Error
5^0C	1,32	0,02	1,13	0,11	1,07	0,07	0.19	25,42	8,77	0.06	20,09	19,93

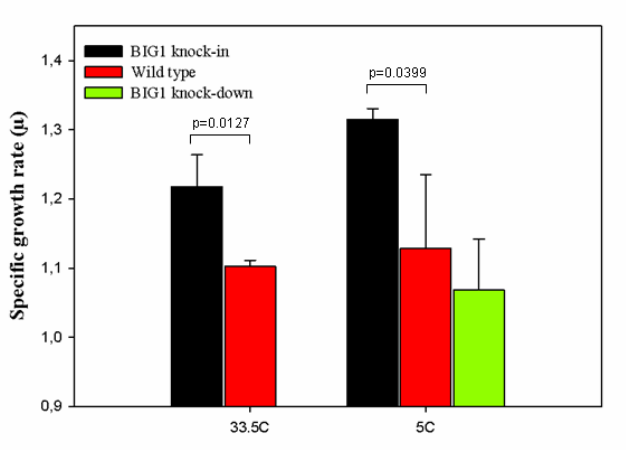

***Figure 4.15**: Mean specific growth rates at 33.5^{0}C and 5^{0}C. Bars represent growth rates of biological replicates of BIG1 knock-in (black), Wild type (red) and BIG1 knock-down (green). Numbers denote statistically significant differences (Two samples t-test).N=3*

Although the Fv/Fm values revealed a higher temperature stress at 5^{0}C, growth rates were higher than for recovery following 24 hours temperature stress at 33.5^{0}C. BIG1 knock-in recovered significantly better after temperature stress induced by low and high temperature (Figure 4.15).

24 hours of temperature stress at 5^{0}C and 33.5^{0}C caused no alterations in cell size in either investigated cell line. The recorded changes in the mean cell size measured in the recovery period and the cell size measured at the beginning of the temperature stress are shown in Table 4.8.

***Table 4.8**: Summary of the cell size evolution following 24 hours temperature stress at 5^{0}C and 33.5^{0}C. Data represents the difference between cell size before temperature stress and the mean cell size recorded in the recovery period, BIG1 knock-in (BIG1), Wild type (WT) and BIG1 knock-down (BIG1 kd), ±error given by standard deviation*

Temp stress	***Cell size BIG1 (µm)***	***Cell size WT (µm)***	***Cell size BIG1 kd (µm)***
5^{0}C	(-) 0.026±0.038	(-) 0.095±0.031	(-) 0.031±0.035
33.5^{0}C	(+)0.365±0.038	(+)0.144±0.057	---

The warming and cooling pace of the artificial seawater medium was correlated to the time that it needed to reach a steady state at 20^0C. Both, the warming and cooling pace followed an exponential trend. The goodness of the fit was described by the coefficient of determination with values of R^2=0.9885 and R^2=0.9894 for 33.5^0C and 5^0C treatments, respectively, as seen in the Figure 4.16. The time period required to reach a steady-state temperature was equilibrated. In both cases, the temperature of 20^0C was reached in 140 minutes counted from the transfer of the inoculums.

Additionally, the photosynthetic quantum yield was recorded every 15-30 minutes starting right after the inoculation of the 24 hours temperature stressed cells into fresh NEPCC media for 4 hours. The BIG1 knock-in cell line displayed an enhanced ability to restore a fully functional photosystem II following stress condition induced by both temperature limits. The Fv/Fm of the wild type recovered at lower values than the knock-in especially from 5^0C. The BIG1 knock-down cell line consistently had a lower photosynthetic quantum yield as seen in Figure 4.17.

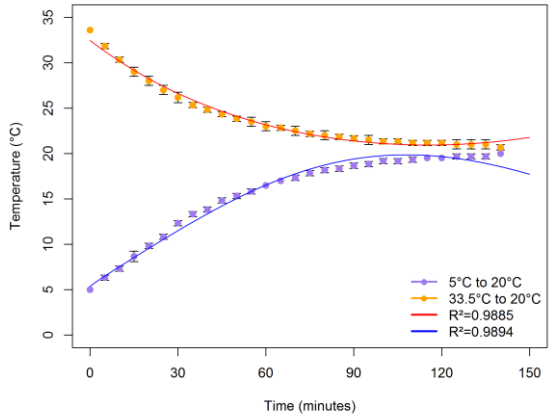

***Figure 4.16**: Alteration of the temperature in function to the time needed to reach a steady 20^0C incubation condition starting from the upper limit (33.5^0C) and lower limit (5^0C) of temperature tolerance of the Thalassiosira pseudonana strains. Dots represent mean temperature of replicates, warming pace (purple), cooling pace (orange), exponentially increasing trend (blue line), exponentially decreasing trend (red line). Error bars indicate standard variation, N=3.*

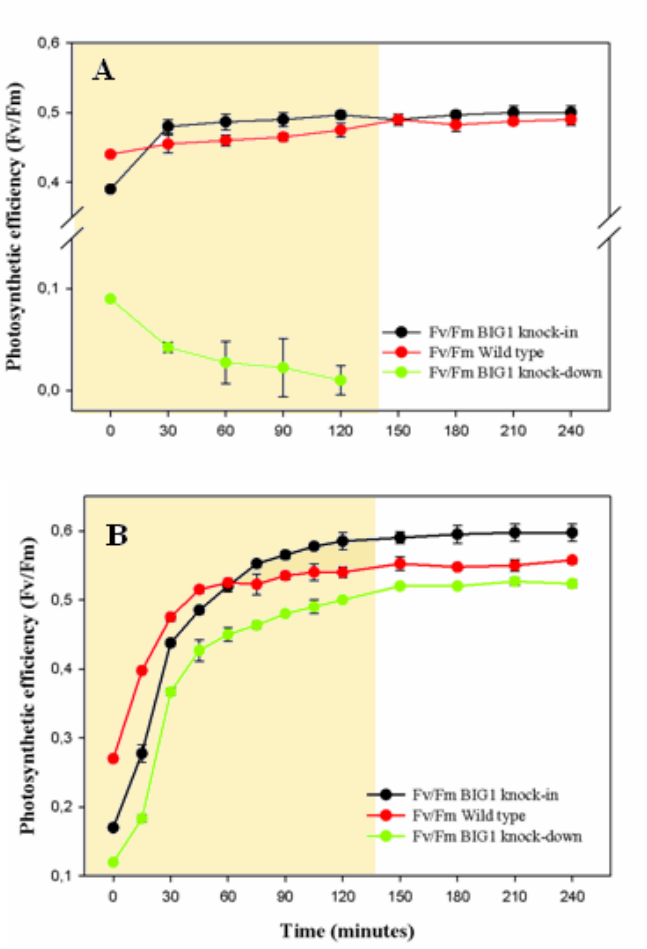

***Figure 4.17**: Recovery of the photosystem II following 24 hours exposure to temperature stress induced by the identified temperature tolerance limits. **A** Fv/Fm recovery after 24 hours exposure to 33.5^{0}C; **B** Fv/Fm recovery after 24 hours exposure to 5^{0}C. Dots represent means of biological replicates of. T. pseudonana BIG1 knock-in (black), wild type (red) and BIG1 knock-down (green) lines. Shading denotes the time where temperature reached 20^{0}C in cultures.*

The 5^{0}C treated cells started to recover from Fv/Fm values of 0.17 (BIG1 knock-in), 0.27 (wild type) and 0.12 (BIG1 knock-down) compared to Fv/Fm of 0.39 (BIG1 knock-in) and 0.44 (wild type) at 33.5^{0}C. The lower Fv/Fm values observed at 5^{0}C indicate that the temperature stress was higher at low temperature than at high temperature. Conversely, after 140 minutes when the media reached a steady 20^{0}C all the three cell lines acquired higher photosynthetic efficiency than their 33.5^{0}C treated counterparts. Although the 33.5^{0}C treatment caused a more or less equal recovery of the photosystem II of the BIG1 knock-in and wild type cells by the end of the first hours,

difference in recovery was present in both treatments in favour of the BIG1 knock-in cells as seen in Table 4.9.

***Table 4.9**: Summary of the maximum photosynthetic quantum yield following 24 hours temperature stress at 5^0C and 33.5^0C at the beginning of the recovery, at steady 20^0C and at 4 hours from the start. Data represents the mean Fv/Fm values recorded, BIG1 knock-in (BIG1), Wild type (WT) and BIG1 knock-down (BIG1 kd), standard deviation (SD), N=3.*

Time	5^0C						33.5^0C			
	BIG1		WT		BIG1 kd		BIG1		WT	
	Fv/Fm_{BIG1}	SD	Fv/Fm_{WT}	SD	Fv/Fm_{KD}	SD	Fv/Fm_{BIG1}	SD	Fv/Fm_{WT}	SD
0 min	0.17	0.00	0.27	0.00	0.12	0.00	0.39	0.00	0.44	0.00
140 min	0.59	0.01	0.55	0.01	0.52	0.00	0.49	0.01	0.49	0.01
240 min	0.60	0.01	0.56	0.01	0.52	0.01	0.50	0.01	0.49	0.01

4.2.3 Analysis of the expression of genes involved in photosynthetic processes

Previous experiments (see 4.2.2 and Chapter 3) revealed differences in Fv/Fm values between wild type and transgenic cell lines under temperature and nutrient stress. The BIG1 knock-in line recovered quicker from physical and chemical stress, showing higher photosynthetic efficiency of PSII. Therefore, we selected genes linked to the light reaction of photosynthesis to get better insight into the processes which may underlie the observed characteristics. Genes involved in chlorophyll biosynthesis along with genes for energy conversion and electron transfer were investigated through RT-qPCR. The list of genes with associated functions is shown in Table 4.10. The expression of genes was analysed under two aspects. First, gene expression under stress conditions (7^0C and 33.5^0C) was compared to the optimum growth condition (20^0C). Second, the analysis was complemented with the expression ratio of the transgenic lines compared to that of the wild type.

Most of the examined genes were downregulated at high temperature and upregulated at low temperature. At 33.5^0C six out of the eight tested genes were significantly downregulated in knock-down cell lines, while at 7^0C showed an opposite trend, see Figure 4.18. At 7^0C genes have not been significantly different expressed compared to the 20^0C excepting the cobalamin/magnesium chelatase (ID 34191). In contrast, at low temperatures wild type showed significantly different expression of six genes, which

were mostly upregulated. However, the fold change of the gene expression exceeded 1.0 in log2 ratio just in case of the chloroplast ferredoxin dependent NADH oxidoreductase (ID 4914), a putative cytochrome b_6f complex iron-sulfur subunit (ID 38231) and bacteriochlorophyll/chlorophyll synthetase (ID 262279).

Gene ID	GO Description	Biological Process	Molecular Function
4914	Putative chloroplast ferredoxin NADP(+) reductase	Electron transport	oxidoreductase activity
38231	Rieske iron-sulfur protein (RISP), PETC2	Electron transport	oxidoreductase activity
24309	Unknown thylakoid lumen protein, chloroplast precursor	Oxygen-evolving complex-related	N/A
42992	Mitochondrial alternative oxidase cyanide insensitive [AOX2]	Respiratory gaseous exchange	oxidoreductase activity
38769	Photosystem II stability/assembly factor HCF136	Chloroplast precursor	Twin-arginine translocation pathway signal
34191	CobN/magnesium chelatase	Chlorophyll biosynthesis	N/A
261608	Putative magnesium-protoporphyrin IX methyltransferase	Chlorophyll biosynthesis	S-adenosylmethionine-dependent methyltransferase activity
262279	UbiA	Chlorophyll biosynthesis	Bacteriochlorophyll/chlorophyll synthetase

Table 4.10*: List of genes used in this study with annotated function in Thalassiosira pseudonana genome related to photosynthesis.*

The expression of the cobalamin/magnesium chelatase (ID 34191) gene was the most significantly downregulated in the BIG1 knock-in at 20^0C and strongly downregulated at 7^0C compared to the wild type. Compared to the expression level from 20^0C at 33.5^0C it was highly upregulated. At 33.5^0C, compared to the expression level at 20^0C, the only other highly upregulated gene was found to be the ubiquinol cytochrome *c* reductase, a putative cytochrome b_6f complex iron-sulfur subunit (gene ID 38231) which plays a role in electron transport, see Figure 4.18. This gene was not expressed at 7^0C and just weakly expressed at 20^0C and 33.5^0C compared to the wild type, as seen in Figure 4.19.

A putative magnesium-protoporphyrin IX methyltransferase (ID 261608) was highly downregulated at 20^0C in BIG1 knock-in. The gene turned out to be upregulated at high and low temperatures with a higher expression level at 7^0C compared to the wild type. When it was compared to 20^0C at high temperature, the expression level was reduced in knock-in but showed significant downregulation in the case of wild type and knock-down compared to 20^0C. At low temperature it was highly upregulated in knock-in and downregulated in knock-down and wild type, being significant in the latter.

Bacteriochlorophyll/chlorophyll synthetase (ID 262279) was the second highest upregulated gene at low temperature in BIG1 knock-in cell line compared to ambient temperature. Also, it was significant and upregulated for wild type. It was not expressed at any of the examined temperatures when its expression was analysed compared to wild type.

The chloroplast ferredoxin dependent NADH oxidoreductase (ID 4914) was highly expressed at 20^0C in BIG1 knock-in cells compared to wild type. At 33.5^0C, this gene was 1.23-fold downregulated in the BIG1 knock-in. At the same time it was the only gene still expressed at 33.5C. No other genes showed significant regulation at 7^0C or 33.5^0C in either transgenic cell line.

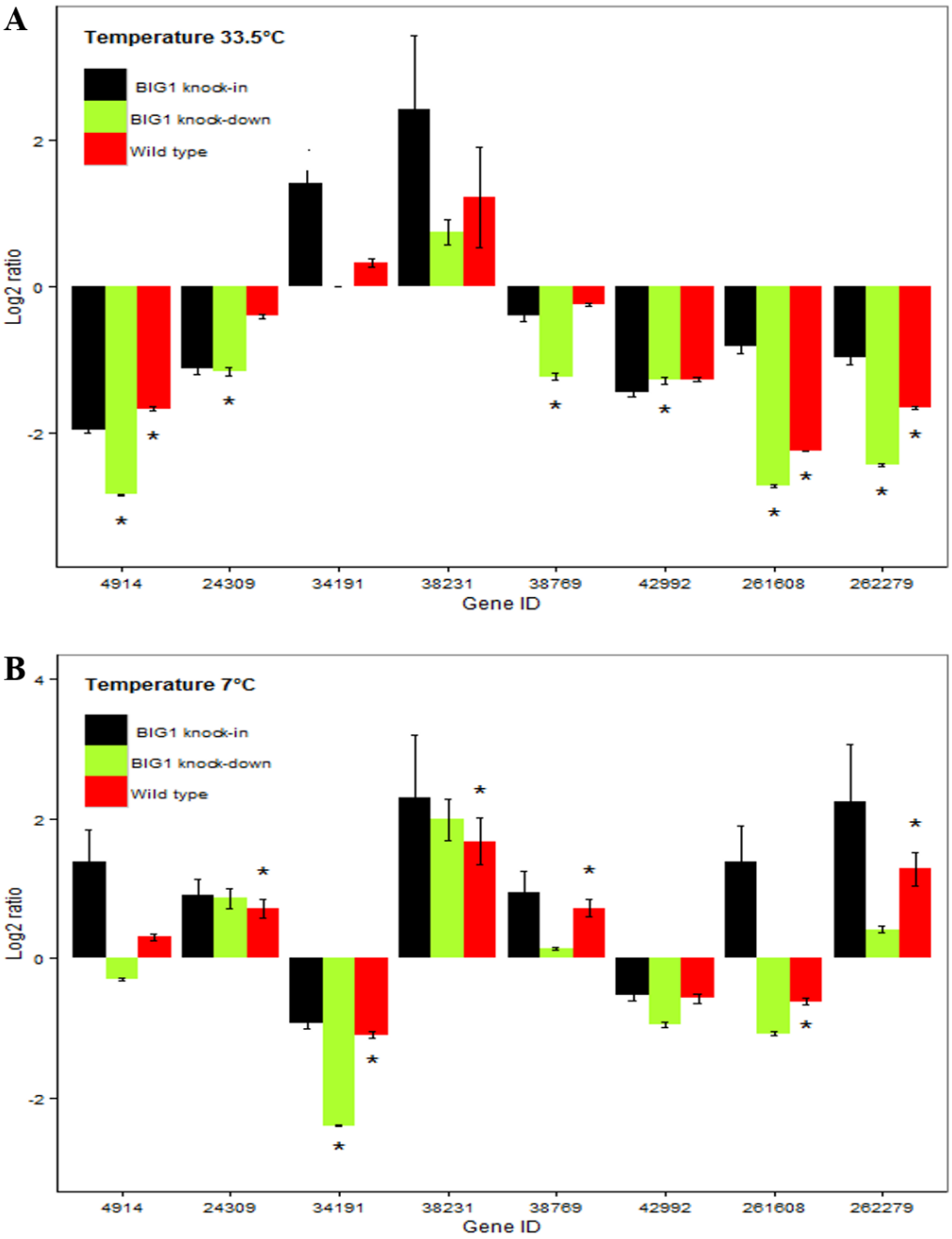

***Figure 4.18**: Relative gene expression of eight genes involved in photosynthesis in Thalassiosira pseudonana cell lines that overexpress or knock-down the big1 gene (Bloom Inducer Gene 1) under three experimental treatments. **A** Gene expression levels of the target genes at 33.5^{0}C, **B** Gene expression levels of the target genes at 7^{0}C. 20^{0}C was used as control treatment for each cell line and all analysed transcripts were tested by a pair Wise Fixed Reallocation Randomization Test and plotted using standard error estimation via a complex Taylor algorithm using Relative Expression Software Tool (REST) (Pfaffl et al., 2002). Asterisks (*) indicate significant difference in gene regulation compared to the control.*

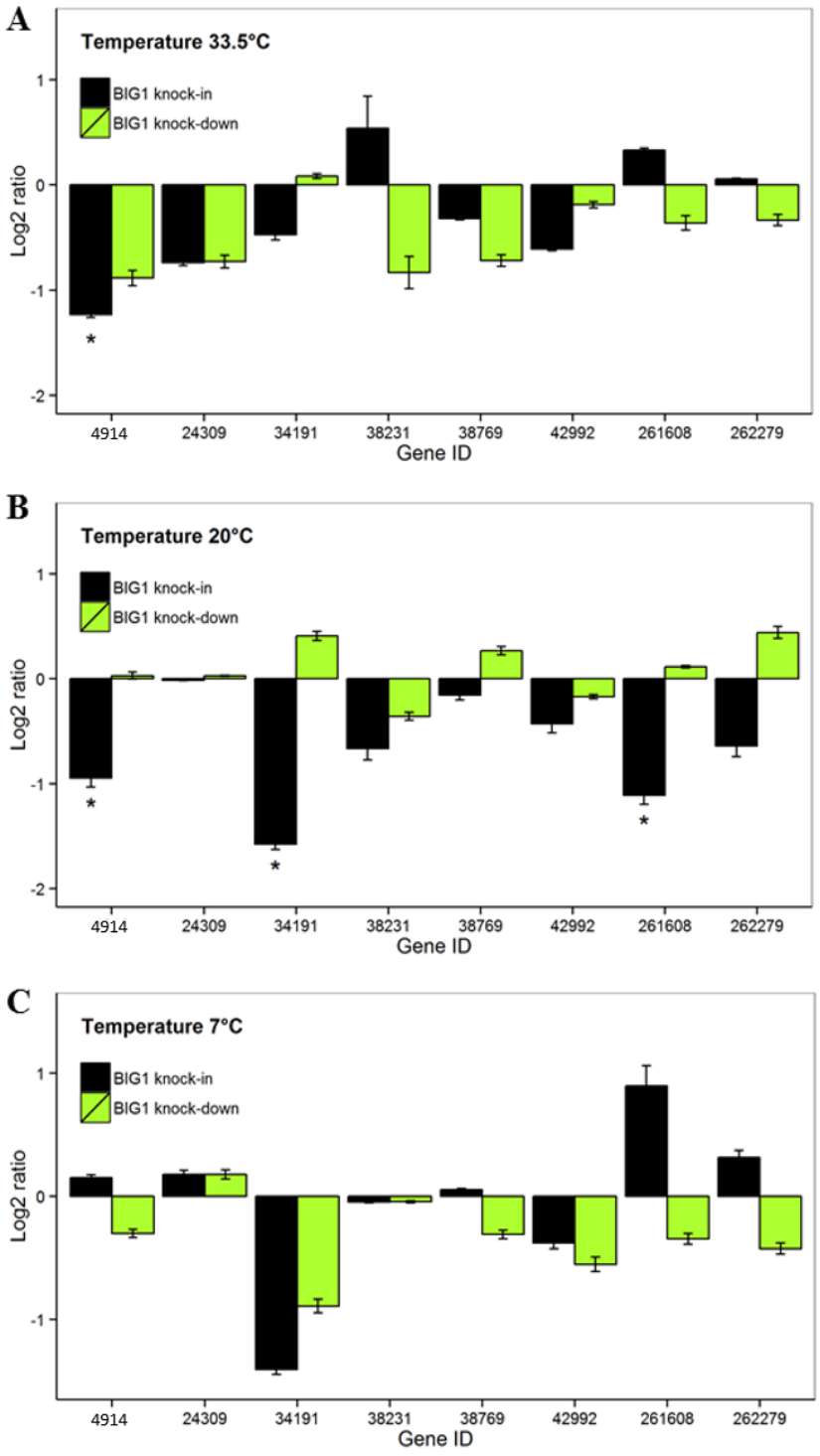

***Figure 4.19**: Relative gene expression of eight genes involved in photosynthesis in Thalassiosira pseudonana cell lines that overexpress or knock-down the big1 gene (Bloom Inducer Gene 1) under three experimental treatments. **A** Gene expression levels of the target genes at 33.5^{0}C, **B** Gene expression levels of the target genes at 20^{0}C, **C** Gene expression levels of the target genes at 7^{0}C. The analysed transcripts were compared to T. pseudonana Wild type tested by a Pair Wise Fixed Reallocation Randomization Test and plotted using standard error estimation via a complex Taylor algorithm using Relative Expression Software Tool (REST) (Pfaffl et al., 2002). Asterisks (*) indicate significant difference in gene regulation compared to the control.*

The thylakoid lumen protein (gene ID 24309), photosystem II stability/assembly factor (gene ID 38769) and mitochondrial alternative oxidase (gene ID 42992) showed low and not significant expression levels compared to the wild type at any temperature. At 33.5^0C they were downregulated in both BIG1 knock-in and knock-down, being significant for knock-down compared to 20^0C. At 7^0C compared to 20^0C the thylakoid lumen protein (gene ID 24309) and photosystem II stability/assembly factor (gene ID 38769) were upregulated and significant for the wild type. The mitochondrial alternative oxidase was downregulated but not significant at low temperature.

4.3 Discussion

There is a consensus that there will be significant changes in temperature based on projections from climate models (Boyd *et al.*, 2013) obtained from global modelling experiments and, to a lesser extent, from time series data. However, both global modelling experiments (Sarmiento *et al.*, 1998, Behrenfeld, 2014) and time series data (Kraberg *et al.*, 2015) reveal that ocean warming is a present and undoubtable phenomenon (Sarmento *et al.*, 2010). The temperature of the upper ocean has a fundamental control on phytoplankton metabolic processes (Raven and Geider, 1988) and sets the biomes of major phytoplankton groups (Needoba *et al.*, 2007). Thus temperature has a significant effect on phytoplankton processes such as growth or photo-physiology (Sunda and Huntsman, 1995; Moisan *et al.*, 2002). Also, it was predicted that in waters colder than 21^0C the photosynthesis/respiration ratio tends to decline with increasing temperature (Regaudie-de-Gioux and Duarte, 2012). It suggests that planktonic communities will allocate a larger fraction of carbon flow to respiration as temperature increases as a consequence of increasing CO_2 in the atmosphere acting as a CO_2 source in the tropics and subtropics (Duarte and Prairie, 2005). This prediction is in accordance with the observation that bacterial growth efficiency will decrease by 2.5% per 1^0C increase in temperature (Rivkin and Legendre, 2001). In addition, Harris *et al.* (2006) predicted a 16% decrease in photosynthesis/respiration ratio in warmer waters as well as planktonic communities becomingmore heterotrophic. Given that phytoplankton photosynthesis and nitrogen fixation make major contributions to global carbon and nitrogen cycling, understanding their response to warming waters became impetuous. Although the diatom genus *Thalassiosira* was extensively studied

physiologically and genetically with respect to *Thalassiosira pseudonana* (Sakshaug *et al.*, 1987; Armbrust *et al.*, 2004) or *Thalassiosira weissflogii* (Strzepek and Harrison, 2004), most comparative studies examining the influence of temperature on phytoplankton physiology were conducted decades ago (Eppley, 1972; Admiraal, 1977).

This study is the first to assess thermal traits of the BIG1 knock-in. The response of the BIG1 knock-in, BIG1 knock-down and wild type lines to temperature stress and acclimation, as well as the recovery after exposure to the identified tolerance temperatures, was analysed monitoring the same physiological parameters used in Chapter 3. Such parameters were cell density, growth rates, Fv/Fm and cell size. Stress conditions imbalance the cellular homeostasis. Imbalances in cellular energy supply and demand may result in over-reduction of photosynthetic electron acceptors, generation of reactive oxygen species (ROS) and finally to photooxidative stress, a major deterrent to growth. Thus, physiological data were complemented by gene expression analysis of selected genes involved in light reaction of photosynthesis. The aim was to shed more light on which processes are dominant in the cell lines studied by us.

We found some interesting traits from phenotyping experiments with respect to the effect of temperature on BIG1 knock-in. BIG1 knock-in recovered faster from exposure to 24 hours of low and high temperature stress similar to post nitrate starvation potentially indicating that temperature stress triggers very similar if not the same processes as nitrate starvation does. Temperature acclimation had little effect on growth of BIG1 knock-in compared to temperature stress. Conversely, wild type growth rates increased in a wide range of temperatures following acclimation. Changes induced in growth rates were mirrored by Fv/Fm in wild type. We found that BIG1 foster growth under suboptimal temperatures, especially under low temperature. Knocking down the gene produced an opposite effect, cells growing better under higher temperatures. Additionally three intriguing observations were made: first, in temperature response BIG1 enhanced stress response up to mid exponential phase in the knock-in line but its growth significantly slowed down in late exponential phase. This phenotypic trait was not observed in wild type. The second very interesting observation revealed a contradiction in BIG1 knock-down between the previously observed pattern that higher growth rate is accompanied by higher Fv/Fm. A consistently lower efficiency of PSII compared to BIG1 knock-in was measured for the knock-down line throughout the

whole temperature gradient under both temperature response and acclimation associated with higher growth. Finally we found interesting that the expression of a cytochrome b_6f complex related gene did not vary under high or low temperature. This is particularly intriguing because the cytochrome b_6f is considered a switching point between different patways where the photosynthetic electrons can be channelled. This discussion will focus on these features separately.

Prior to the discussion, the limitations of the experimental design of phenotyping under temperature response and acclimation need to be acknowledged. In the temperature response and acclimation experiments, light intensity needed to be increased compared to the other experiments performed in this study. This approach was necessary to allow cultures to reach their maximum growth at each examined temperature point. In order to reduce biases in results by possible co-limitation effects, cultures were kept in exponential phase (Lakeman *et al.*, 2009).

Growth rate represents the most direct measure of reproductive success and therefore of fitness in environment. Thus growth rate represents the most appropriate way to assess diatom physiology in response to temperature (Boyd *et al.*, 2013).

Phenotyping experiments conducted under a wide temperature gradient revealed that BIG1 knock-in grew better under high temperature stress (5^0C-9^0C and 33.5^0C) compared to the culturing temperature 20^0C. Conversely, knocking down the gene kept cultures more susceptible to higher temperatures, while wild type dominated at a $\pm10^0$C range from the optimal temperature. Additionally, a temperature optimum shift of 2.5^0C was observed for the transgenic lines compared to wild type. This observation may be in line with previous measurements which showed that in diatoms higher growth rate can occur at higher temperatures than those at which the species or strains live in nature (Samyda 1969; Durbin, 1974) or, in our case, in culturing conditions. Also, low temperatures, as expected, induced lag phase in growth. The BIG1 knock-in line had lag in growth response to temperature just at 5^0C while wild type and BIG1 knock-down displayed 12-60 hours lag in the temperatures ranging from 12^0C to 5^0C in temperature response. Acclimation reduced the lag in growth by 12 hours on average at these temperatures. No lag phase was observed under high temperatures for either cell line. Also, the temperature gradient used by us is in accord with the temperatures investigated by Boyd *et al.* (2013) and Litchman *et al.* (2012). A previous study found

that *T. pseudonana* displayed significant differences in growth rate at varying temperatures, excepting at 15^0C, 20^0C and 24^0C (Boyd *et al.*, 2013). Our results contrast these observations as we recorded higher growth at all of these temperature points. Furthermore, growth rates recorded over the temperature gradient were higher than previously reported in the mentioned study. However, it needs to be acknowledged that our results may be biased by the light adjustment (Smayda, 1969) which was used to get the maximal growth rates. As no information on the light setting used in previous experiments is available, the comparison may be inappropriate. If indeed, the light adjustment biased the growth response to temperature, it is even more intriguing that BIG1 knock-in had significantly lower growth rates at most of the examined temperature points. This may reflect that BIG1 knock-in is more responsive under low light.

All cultures recovered better after exposure to low temperature than to high temperature. Interestingly, the growth rate of the BIG1 knock-in was 0.0402± 0.0336 lower in recovery from 5^0C and 0.1375± 0.0626 lower in recovery from 33.5^0C than its growth rate recorded at continuous 20^0C growth. The specific growth rate of wild type in recovery following temperature stress was decreased with 0.5705± 0.1116 (from 5^0C) and 0.5967± 0.0376 (from 33.5^0C). A similar trend was observed for BIG1 knock-down with a decrease of 0.4316± 0.0746 in growth rate in recovery from 5^0C stress. Although BIG1 knock-in recovered faster from stress at both limit temperatures, it seems to offer more advantage under lower temperatures. Furthermore, 24 hours exposure to low or high temperature induced a lag phase of the same length as nitrate yield limitation did. This behaviour resembles how BIG1 knock-in recovered in nutrient replete media post nitrate yield limitation (see Discussion Chapter 3). Temperature seems to have a negative effect on growth of BIG1 knock-in. Wild type showed an opposing trend. Moreover, we found that the growth rate of BIG1 knock-in during recovery following temperature stress is lower than the growth rate recorded after nitrate yield limitation, albeit this difference was small (0.1018±0.0716). This is particularly interesting because the outcome of the two experiments suggest a very conserved and quick response of BIG1 knock-in to favourable changes in environmental conditions. This may indicate that temperature stress pauses BIG1 knock-in cells in the same arrest point in the cell cycle (close to the G1/S transition) as nitrate limitation does (see discussion in chapter 3).

An intriguing observation was that BIG1 knock-in showed enhanced response to the whole temperature gradient up to mid exponential phase while in late exponential phase it was outcompeted by wild type and knock-down lines. However, interactions between genotype and temperature were not detected by mixed effect models for either cell line. This may be a further clue that BIG1 knock-in stagnates in late G1 and is able to synthesise DNA quicker than wild type. Its fast response to changes in environment, further indicate an efficient sensing mechanism which triggers its immediate response to fluctuations in environment. However, as the loss of advantage in the second half of the exponential phase showed, these mechanisms should involve high energy demand which does not seem to be fuelled by the breakdown of internal storages. Hipkin (2012) demonstrated that BIG1 knock-in store less lipids than wild type. However, this observation does not exclude the employment of other storage compounds or other mechanisms (such as optimal photosynthesis rate) in generating the necessary energy to sustain the enhanced response to stress conditions.

It was suggested that investing into the cellular machinery responsible for growth (ribosomes) may limit investment into the light-harvesting machinery (chloroplasts) (Klausmeier *et al.*, 2004). A simultaneous production of heat shock proteins in response to rising temperatures may limit the investment into photo-protective compounds. However, heat shock proteins were suggested to be useful in photoprotection (Schroda *et al.*, 1999). Furthermore, a specific expansion of heat shock factors compared to other transcription factor families was identified in *T. pseudonana* (Rayko *et al.*, 2010). Heat shock factors (HSF) are evolutionarily conserved stress-response regulators which in eukaryotes are involved in the expression of genes with roles in cell maintenance and differentiation as well as in developmental processes. They form a homotrimer that binds to gene promoters containing a heat shock element (HSE) (Pelham, 1982; Sakurai and Enoki, 2010). HSEs were found to be indispensable for the regulation of the heat shock response in *Chlamydomonas* (Lodha *et al.*, 2008). HSF proteins contain two evolutionarily conserved functional modules: a DNA-binding domain at the amino-acid terminus and the oligomerization domain in the central region of the protein (Fujimoto and Nakai, 2010). The transcriptional activity of the HSF is regulated at two steps: DNA-binding and acquisition of the transactivating ability under physiological conditions. *In vitro* analysis demonstrated that inactive monomeric HSF directly senses heat and oxidative stress and becomes able to trimerize and bind to the HSE (Morimoto

et al., 1992; Sakurai and Enoki, 2010). Furthermore, heat-shock factors were the most abundant upregulated transcripts in *T. pseudonana* under nutrient and temperature limitations (Mock *et al.*, 2008, Thamatracoln *et al.*, 2011; Dhyrman *et al.*, 2012) as well as eco-toxicological stress (Carvalho *et al.*, 2011). Enrichment of heat-shock factors may indicate the importance of transcriptional regulation in response to environmental stress in diatoms (Montsant *et al.*, 2007). Also, it was suggested that heat shock proteins can act in stabilization of proteins and may assist in protein refolding under stress conditions (reviewed by Wang *et al.*, 2004; reviewed by Hartl *et al.*, 2011). It was hypothesized that the accumulation of HSP in G1/S transition of the cell cycle may have a preparatory role for cells to deal with the increased protein synthesis in S phase (reviewed by Srinivas and Swamynathan, 1996). This aspect is particularly interesting as BIG1 knock-in was found to arrest at this cell cycle stage (Hipkin *et al.*, under revision, see Appendix 5). Additionally, it was found in *A. thaliana* that adjoining genes can co-express each other, likely by shared promoters (Chen *et al.*, 2010). This is of particular interest as *big1* is flanked by a heat shock factor (ID 264072) and a gene (ID 24726) with no significant homology ($p<e^{-5}$) in the Pfam database. However, it is currently unknown whether *big1* is regulated by other elements or its regulation is a response to temperature or primarily nutrient limitation.

Besides heat-shock factors, helicase-associated domains were reported to be upregulated in *T. pseudonana* (Mock *et al.*, 2008). DNA/RNA helicases catalyse the unwinding of duplexes and secondary structures of nucleic acids. A function in the control of secondary structures of DNA/RNA under low temperature to keep transcription and translation active may be consistent to that suggested for *F. cylindrus* (Mock *et al.*, 2005). Topography of chromatin has been found to be important in changing potential transcriptional activity in local genomic regions, as found in *Drosophila* where heat shock factors could only bind open chromatin (Guertin and Lis, 2010). Association of the DNA with nucleosomal proteins is enhanced by deacetylation of lysine residues in the histone tails. In heat shocked cells, HSF1 binds to histone deacetylase (HDAC), and their histone-deacetylase activities increase. The heat-induced deacetylation of histone H4 is not observed in HSF1 knockout mouse cells (Fritah *et al.*, 2009). The relationship between HSF1 and histone deacetylases has also been shown in human breast cancer cells linked to metastasis. Therefore, HSF1 is a potent regulator of global histone acetylation / deacetylation in stressed and unstressed cells (Sakurai and Enoki, 2010).

Furthermore, a HDAC (ID 32098) belonging to the RPD3 HDAC family was found to be upregulated in a previous microarray study in BIG1 knock-in. It was found to be co-expressed in exponential and stationary phase with log2 1.18 and 1.45, respectively, but the gene was not expressed in wild type (Hipkin, 2012). This group of HDACs are associated with regulators of global transcription (Pazin and Kadonaga, 1997; Pandey *et al.*, 2002) and are found in all eukaryotes. Moreover, it was found to be one of the most represented genes in diatom bloom libraries (Hipkin, 2012). This gene seems to be expressed in actively growing diatom communities, which is particularly interesting considering that excepting 5^0C BIG1 knock-in did not have lag phase in temperature response. Thus, *big1* may enhance transcription especially under stress or when cells are released from limitation induced by either chemical or physical stresses.

The photo-physiological parameters observed by us recover slower from temperature stress (140 min) than CO_2 deficiency (100 min) (Kustka *et al.*, 2014). Previous studies demonstrated the presence of an active carbon concentrating mechanism (CCM) in diatoms (Fielding *et al.*, 1998; Burkhardt *et al.*, 2001). The activity of CCM is facilitated by low temperature, which promotes a high solubility of CO_2 in water and a low half-saturation constant for RubisCO. Also, the CCM of diatoms depends critically on high permeability of membranes to CO_2 but low permeability for HCO_3^- although the membrane permeability of diatoms is neither species nor temperature specific (Kranz *et al.*, 2014). The diatom silica cell wall presents a proton buffering role (Milligan and Morel, 2002), providing protons involved in the interconversion between HCO_3^- and CO_2 more efficiently than water (Tripp and Ferry, 2000). The affinity of enzymes for their substrate decreases with temperature with a factor of ~3.33 in the case of RubisCO (Young *et al.*, 2014) that fixes CO_2 in the pyrenoid (an electron-dense, sub-cellular compartment found in chloroplasts stroma of many algae) (Jenks and Gibbs, 2000). Its turnover rate can decrease with a factor of 10 between 20 and 0^0C (Young *et al.*, 2016). However, some cold adapted enzymes such as the carbonic anhydrase that catalyse the inter-conversion of CO_2 and HCO_3^- within the cell and at the cell surface may maintain relatively high kinetics in psychrophilic diatoms (Kranz *et al.*, 2014). These results are consistent with previous studies (Badger *et al.*, 1998) which states that temperature rather than intrinsic properties among different species are responsible for the low turnover rate of RubisCO.

Furthermore, several studies have consistently shown that the temperature optimum for NR in the diatom *Skeletonema costatum* is about 15^0C (Packard *et al.*, 1971; Kristiansen 1983; Gao *et al.*, 1993, 2000). However, Kristiansen (1983) suggest that the temperature optimum of NR is largely invariant with growth temperature (Lomas and Gilbert, 2000). The lower temperature optima for NR was suggested as a possible physiological adaptation to thrive in cool, nitrate rich environments while warmer temperatures may be approaching the physiological limits of NO_3 uptake in diatoms (Lomas and Gilbert, 1999). Also, it was suggested that increasing cellular concentration of ribosomal proteins partially compensate for the reduced translation efficiency of *T. pseudonana* under low temperatures (Toseland *et al.*, 2013). This has implications for how fast cells are able to progress through the cell cycle. Indeed, we found that total RNA synthesis was negatively correlated to temperature in our samples. All of the above mentioned findings indicate that diatoms are particularly successful in cold waters where the BIG1 knock-in cell line was found to grow better. This characteristic, along with the ability of BIG1 knock-in to recover faster after a short period of temperature stress, may indicate that the overexpression of BIG1 may confer advantage in maintaining a more efficient translation under highly fluctuating environmental conditions.

Since body size is a major determinant of many biological processes, climate-warming related changes in cell size could imbalance multiple levels of ecological organization (Daufresne *et al.*, 2009). It is widely accepted that metabolic rate increases with temperature (Brown *et al.*, 2004), thus if nutrient levels remain the same growth will be limited, and organisms will become smaller to compensate for the increased metabolic demand (Adams *et al.*, 2013). Also it was suggested that reduced body size is a universal ecological response to warming in aquatic ecosystems (Gillooly *et al*, 2001; Brown *et al.*, 2004; Daufresne *et al.*, 2009). Indeed, a decrease in cell size was observed related to temperature acclimation. However, suboptimal temperatures increased the cell size of the wild type at 31.5^0C and of BIG1 knock-in line at 5^0C, 7^0C, 29^0C and 31.5^0C. Our observations are consistent with older studies which showed that diatom and phytoplankton cells can increase with temperature (Durbin, 1977; Thompson *et al.*, 1992) as well as some more recent studies (Gardner *et al.*, 2011; Rüger and Sommer, 2012; van Ruth *et al.*, 2012; Adams *et al.*, 2013). Furthermore, it was demonstrated that large cells can acquire nutrients more rapidly (Malone, 1980; Finkel *et al.*, 2005) which ultimately results in higher growth rates or longer survival. This hypothesis was

sustained by competition experiments which showed that bigger diatom cells outcompete smaller ones (van Ruth *et al.*, 2012). Our results suggest that BIG1 knock-in may partially follow Bergmann's rule which states that larger phytoplankton species tend to be found at colder temperatures but contrasts James' rule which states that cell size will tend to decrease at intraspecific level (Blackburn *et al.*, 1999). Moreover, bigger cells are able to sustain growth more efficiently in environments were nutrients are delivered in pulses such as coastal upwelling zones (Falkowski and Raven, 2007) where fluctuations in nutrients are often accompanied by fluctuations in temperature. The increase in cell size observed for BIG1 knock-in close to both temperature tolerance limits raise the question whether this increase in cell size is linked to a sensible environmental sensing mechanism. The existence of such mechanism is yet unknown related to BIG1 knock-in. However, in transcriptome analysis of BIG1 among the top ten upregulated genes were genes putatively involved in signalling. Besides an EF-hand domain (ID.260844), most likely associated with calcium signalling (Bhattacharya *et. al.*, 2004) which was upregulated log2 7.61 fold, was found a transcript with predicted cyclic adenosine monophosphate (cAMP)-dependent protein kinase regulator activity (ID. 32880) upregulated log2 4.65 fold. cAMP activity facilitates the entrance of Ca^{+2} in cytosol or mobilize intracellular Ca^{+2} with effects on chlorine channels. Moreover a putative plastid terminal oxidase belonging to the membrane associated bestrophin protein family was found in thylakoid membrane proteome of *T. pseudonan* and *P. tricornutum*. Bestrophins act as chloride channels (Tsunenari *et al.*, 2003) and thus may be involved in the transport of chloride anions to maintain cellular osmolyte homeostasis (Boetius and Joye, 2009). They also possess plastid targeting signals and present homology to low CO_2 inducible proteins from *C. reinhardtii* (Grouneva *et. al.*, 2011).

An interesting observation was that higher growth rate compared to BIG1 knock-in was achieved by knock-down cells throughout a wide range of temperatures although their Fv/Fm was lower. This observation is in contradiction to the previously observed trend that higher growth rates are associated with higher Fv/Fm (see chapter 3). Although it is a very distinct and consistent pattern observed in both temperature response and acclimation we cannot explain this feature.

Transcriptomic analysis from the microarrays of Mock *et al.* (2008) under nutrient limitation and low temperature revealed that the majority of the down-regulated genes

encoded proteins related to photosynthetic processes such as light harvesting. Our analysis based on RT-qPCR of selected photosynthesis genes are in contrast, showing upregulation tendency under low temperature. Exposure to high temperature showed the earlier described trend. In addition, recent DNA microarray study effectuated in recovery after nitrate starvation (Hipkin 2012) identified only three photosynthesis-related differentially expressed genes. Among these genes were the -1.55 fold downregulated magnesium chelatase (ID 34191) associated to stationary phase and a putative magnesium-protoporphyrin IX methyltransferase (ID 261608) which was co-expressed and upregulated 1.61/1.0 fold. The co-regulation of the expression of genes for photosynthetic proteins and of genes for plastid ribosomes was suggested to be interpreted as a mechanism to ensure that the subunits of those multi-protein complexes are synthesized in matching amounts (Biehl *et al.*, 2005). In this study we aimed to link the regulation of the expression of these genes to temperature in addition to nutrient limitation.

In photosynthesis a tight control of the ATP/NADPH ratio is a prerequisite for the efficient conversion of carbon dioxide into carbohydrates. Chloroplasts can synthesize ATP by using either linear electron transfer with a concomitant synthesis of oxygen and NADPH (Arnon *et al.*, 1957), or cyclic electron transfer with ATP as the only net product (Allen, 2002). Noncyclic ATP synthesis is coupled to electron transport between PSI and PSII (Hill and Bendall, 1960). In contrast, the cyclic electron transport pathway was described as one that involves only PSI, a putative ferredoxin-plastoquinone oxidoreductase and the cytochrome b_6f complex (Shikanai, 2007). ATP is produced by the proton gradient generated through plastoquinol oxidation (Krieger-Liszkay *et al.*, 2008). The ratio of ATP/NADPH generated by noncyclic electron flow is considered to be insufficient to assure CO_2 import into the plastid and assimilation by the Calvin cycle (Allen, 2002; Lucker and Kramer, 2013). Therefore something else must account for about 14% of the total ATP required (3 ATP per 2 NADPH molecules) (Allen, 2002). There is growing evidence that cyclic electron transfer can be a constitutive activity, increasing under stress conditions such as low temperature and drought in plants (Kramer *et al.*, 2004; Shikanai, 2007; Eberhard *et al.*, 2008). It was suggested that diatoms may perform a PSI cyclic electron transport of the same type as the green alga *C. reinhardtii* (Grouneva *et al.*, 2011) or optimise photosynthesis by a partial re-routing of the electron flow to mitochondria followed by the import of

mitochondrial ATP into the plastid (Bailleul *et al.*, 2015). Recent studies identified key genes in cyclic electron flow in plants. The protein products are termed proton gradient regulation5 (PGR5) (Munekage *et al.*, 2002) and proton gradient regulation like1 (PGRL1) (DalCorso *et al.*, 2008). PGR/PGRL proteins mediate a form of cyclic electron transport (CET) that transfers electrons from ferredoxin-$NADP^+$-oxidoreductase (FNR) (Zhang *et al.*, 2001) to the platoquinone pool-cytochrome b_6f complex (Munekage *et al.*, 2002). However, particularities of this predicted pathway were also identified. Cyanobacteria appear to lack the PGRL1 protein. In the green alga Chlamydomonas PGRL1 (but not PGR5) has been detected in a PSI-Cyt b_6f super-complex (Leister and Shikanai, 2013). In all cases, these complexes seem to mediate a switch between linear and cyclic electron transport (DalCorso *et al.*, 2008; Dang *et al.*, 2014). The PSI cyclic electron transport was suggested to be mainly PGR-mediated throughout diatom species and additionally assisted by type II dehydrogenases (NAD(P)H dehydrogenases) in centric diatoms and green algae (Jans *et al.*, 2008). Moreover, a recent study revealed the presence of PGR5 and PGRL1 homologues in *T. pseudonana* and *P. tricornutum* thylakoid membranes (Grouneva *et al.*, 2011).

A recent study showed strong evidence of the action of mitochondrial alternative oxidase (AOX) in diatoms as electron supplier for ATP production (Bailleul *et al.* 2015). Thus the expression level of AOX (ID 42292) was analysed in the present study as well. The expression of the mitochondrial alternative oxidase (ID 42992) was downregulated at both temperature extremes. Furthermore, at low temperature it was weakly expressed. AOXs act as protective enzymes which prevent over-reduction of the PQ pool responsible for energy conservation by directing electrons towards mitochondria and dissipating excess as described for *Phaeodactylum tricornutum* (Bowler *et al.*, 2008). Also, AOXs play a role in optimising photosynthesis under suboptimal temperatures by regulation of reactive oxygen species (ROS) in *Pisum sativum* (Dinakar *et al.*, 2016). However, our results suggest that this mechanism is not employed by BIG1 knock-in, moreover, by any of the cell lines investigated by us, contrasting Bailleul *et al.* (2015) findings. The authors suggested the involvement of mitochondrial respiration in the optimization of photosynthesis being a general and conserved feature in diatoms. Our results do not support this hypothesis and points towards a cyclic electron flow as potential process in optimising photosynthesis. Additionally, protein expression analysis may help to further clarify this aspect.

The cyclic electron flow is driven by PSI which returns electrons to itself through the site of proton translocation and ATP synthesis (Allen, 2002). As stress conditions imbalance the demand for energy this process seems to allow high benefits. The most intriguing observation was the finding that the ubiquinol cytochrome *c* reductase, a putative cytochrome b_6f complex iron-sulfur subunit (ID 38231), a high potential electron carrier Rieske Fe-S protein (nuclear encoded) that oxidises the quinol molecule to semiquinone on the luminal side of the thylakoid membrane expression, was highly upregulated under suboptimal temperatures at both low and high temperatures. The expression of this gene was considerably lower in wild type and knock-down at 33.5^0C (log2 1.22 and 0.75) but remains consistent in the knock-in line. This observation seems to indicate that its regulation is independent of temperature when BIG1 is expressed. The cytochrome b_6f complex was described and hypothesized to be the switch on/off point in triggering CET (Lavaud, 2007). As the cytochrome b_6f complex seems to play a key role in directing electrons through different pathways this observation is very interesting. The upregulation of this gene (log2 2.29 at 7^0C and log2 2.42 at 33.5^0C) indicates a constant electron flow through the cytochrome b_6f complex. Algae containing chlorophyll *c* may lack plastocyanin and contain a functionally equivalent Fe-containing homologue, cytochrome c_6 which is believed to be the sole electron transport protein between cytochrome b_6f and PSI in diatoms (Raven *et al.*, 1999). All diatoms which have sequenced genomes have the gene for iron containing lumen localised cytochrome c_6 as the catalyst of electron transfer from the cytochrome b_6f complex to the PSI (Blaby-Haas and Merchant, 2012). Diatoms possess only PsaF, the likely docking site for plastocyanin (Grouneva *et al.*, 2014). The pennate diatom *F.cylindrus* has the gene for the alternative electron carrier plastocyanin which contains copper instead of iron as well as the gene for cytochrome c_6 (Blaby-Haas and Merchant, 2012). The centric diatom *T. oceanica* (Peers and Price, 2006) only contains plastocyanin with undetectable levels of the alternative electron carrier cytochrome c_6 (Raven, 2013). Another adaptive (genetic) variation is the low expression of the iron-rich photosystem I and cytochrome b_6f complex relative to iron poor photosystem II in *T. oceanica* (Strzepek and Harrison, 2004). However, in organisms containing both cytochrome c_6 and plastocyanin, transfer of electrons to PSI occurs at the same rate regardless of which carrier is functional (Peerce and Price, 2006). Strzepek and Harrison (2004) hypothesized that the decreased content of PSI and the cytochrome b_6f complex in the pelagic diatom *T. oceanica* relative to the coastal *T. weissflogii* might be

attributed to decreased ability to acclimate to fluctuations in photosynthetically active radiations. During the cyclic electron flow (CEF), electrons from either NADPH or ferredoxin are cycled around PSI into the plastoquinone pool and regenerate ATP without reducing $NADP^+$ (Golbeck *et al.*, 2006). The nuclear encoded putative cytochrome b_6f complex iron-sulfur subunit (ID 38231), PETC2, investigated in our study possess a Rieske subunit. It shares 80.3% sequence similarity with PETC encoding the cytochrome b_6f complex iron-sulfur subunit in *T.pseudonana* (Uniprot). Presequences of nucleus encoded plastid proteins consist of a signal peptide followed by a transit peptide-like domain (Pancic and Strotmann 1993). Although Gruber *et al.* (2015) assigned it to not have plastid signal it contains a partial ASAFAP motif. The ASAFAP sequence motif is considered to be conserved and a good marker for nuclear-encoded plastid proteins (Gruber *et al.*, 2007). Proteins with partial signal peptides can keep their ability to be directed to plastids besides a missing full signal (Gruber *et al.*, 2007). Keeping a phenylalanine residue at +1 position after the signal peptide cleavage site was described crucial for successful plastid protein import (Kroth, 2002; Apt *et al.*, 2002). Indeed, the AF residue is present in the Rieske subunit analysed by us. Although Gruber and colleagues (2015) assembled a comprehensive dataset we question some of their predictions. With respect to our data the mentioned dataset does not contains entries for two enzymes, part of the chlorophyll biosynthesis pathway (ID 34191 and 261608) although members of this pathway are chloroplast localised. In chloroplasts, most of the enzymes of chlorophyll biosynthesis are either bound to the chloroplast envelope or are soluble in the chloroplast stroma (reviewed in Joyard *et. al.*, 1998; Vavilin *et. al.*, 2002). The magnesium-protoporphyrin IX methyltransferase (ID 261608) seem to have dual action. On the one hand methylates the Mg-protoporphyrin resulted from the activity of magnesium-chelatase representing the second step following the branch point for the synthesis of heme and chlorophyll (Malkin and Niyogi, 2000). On the other hand, it is associated to methylation of the L11 ribosomal subunit by the PrmA domains in the plastids of eukaryotes playing important role in the protein synthesis in the plastid of *A. thaliana* (Pesari *et al.*, 2001). Furthermore Mg-protoporphyrin was found to act as a signal mediating communication between plastids and the nucleus (reviewed by Mochizuki *et al.*, 2010) synchronizing nuclear DNA replication with organellar DNA replication in the red alga *Cyanidioschyzon merolae* (Kobayashi *et al.*, 2009), green alga *Chlamydomonas* (Kropat *et. al.*, 1997) and tobacco (Kobayashi *et al.*, 2009). The expression of this gene is particularly interesting

considering that AOX did not seem to be highly expressed. Taking all together, this points towards the possibility that BIG1 involves CET in optimising photosynthesis, thus growth.

Moreover, the expression of a gene responsible for NADPH production by linear electron flow was found weakly expressed under low temperature (log 2 0.86) while under high temperature was downregulated (log2 -1.17). The noncyclic photosynthetic electron transfer, in fact, an exergonic electron transport which produces a proton electrochemical gradient fuelled by the activity of cytochrome b_6f complex which permits the translocation of two protons for every electron transferred to plastocyanin drives synthesis of ATP by the transmembrane ATP synthase through the oxidation of water. ATP synthase is located almost entirely in the stroma-exposed thylakoid membrane. An intermediate product of this chain reaction, reduced ferredoxin, serves as an electron donor in many reactions such as reduction of the regulatory disulphide protein thioredoxin, assimilation of nitrogen but ultimately the reduction of $NADP^+$. The ferredoxin transfers electrons to $NADP^+$ by an intermediate enzyme the ferredoxin-$NADP^+$ reductase (FNR). FNR which easily dissociates from the thylakoid membrane is a FAD containing enzyme which is reduced by two electrons to $FADH_2$ consecutively passing these electrons to $NADP^+$. The ferredoxin-NADPH-oxidoreductase (FNR) was found to bind tightly to the cytochrome b_6f complex suggesting the formation of a complex together with ferredoxin, which would then create a bridge for the electron transfer to the PQ pool (Zhang *et al.*, 2001). Our study revealed that the NADP/FAD dependent oxidoreductase (FNR) is also negatively correlated to temperature in transgenic cell-lines of *T. pseudonana* that either overexpress or supress the BIG1 protein in relation to wild type and optimal temperature denoted by 20^0C. These results may suggest that temperature stress suppressed NADPH production compromising the energy supply of cells. However, an enhanced growth response of BIG1 knock-in under suboptimal temperatures as well as its faster recovery following temperature stress was observed. This seems to be in contradiction with the upregulation of the Rieske subunit which indicates that energy is still fuelled around PSI.

It is noteworthy that the analysed genes were significantly downregulated in the knock-down line at high temperature. Taking into account that this line could not recover at 20^0C after 24 hours exposure to high temperature further indicates that electrons remain trapped in the photosystems generating ROS, damaging the photosynthetic apparatus

with eventual chloroplast disassembly (Franklin et al., 2012). Diatom chloroplast exhibit some particularities compared to plants and green algae. The most important feature is represented by the absence of stacked and unstacked granal regions and they apparent lack of spatial segregation between photosystem I and II (Pyszniak and Gibbs, 1992). This characteristic of the thylakoid membranes deprive diatoms of state transitions (Miloslavina *et al.*, 2009), reversible phosphorylation of a small pool of the light harvesting complex II (LHC-II) an auxiliary antenna for PSII. This process which balances the absorbed light energy between photosystems is present in plants, green and red algae (Owens, 1986). Also, recent studies suggest that state transitions may have a role in the absence of PGRL1-mediated cyclic electron flow activity in green algae (Takahasi *et al.*, 2013). The loss of the process from cyanobacteria and diatoms raise the possibility for the existence of a mechanism for excitation energy distribution between the two photosystems in diatoms (Grouneva *et al*., 2011). Therefore as an alternative, the PSII stability/assembly factor (ID 38769) was tested and found to be weakly expressed and negatively correlated to temperature in relation to both wild type and stock conditions representing optimal growth temperature (20^0C) in BIG1 knock-in and knock-down lines. The weak expression seems to further sustain that chloroplasts may be disassembled.

Genes involved in chlorophyll biosynthesis pathway (ID 34191) CobN/magnesium chelatase and chlorophyll synthase (ID 262279) showed an antagonistic relation to temperature. Also, the gene expression suggest different relation to temperature at the end of the chlorophyll biosynthesis pathway compared to the branching point of the heme and chlorophyll synthesis. Bacteriochlorophyll/chlorophyll synthetase (gene ID 262279) initiates the final step of the chlorophyll *a* synthesis and involves esterification of the hydrophobic phytol side chain while the magnesium chelatase inserts a magnesium atom into the protoporphyrin IX, the common branch point for the synthesis of heme and chlorophyll. The absorption properties of different chlorophyll species are altered by small changes in chemical structure. This may point the maintenance of an equilibrated chlorophyll synthesis.

Most of the biochemical, biophysical and molecular biological information about photosynthetic processes relies on studies of higher plants and a few model algae, including *Synechocystis*, *Chlamydomonas*, *Chlorella* and *Phaeodactylum* (Kaplan and Reinhold, 1999; Harris, 1989, Rochaix, 1995; Grossman, 2000). Genome sequence

studies offer a broad range of knowledge about the expressed genes under diverse treatments. However, the conclusions drawn from such studies need prudence. In the case of *T. pseudonana* it was suggested that C_4 type photosynthesis may occur (Armbrust *et al*., 2004) based on the finding that *T. pseudonana* possesses the enzymatic apparatus to operate C_4 photosynthesis of the kind suggested for *T. weissflogii* (Reinfelder *et al.*, 2000; Morel *et al.*, 2002). The occurrence of these genes was also reported for *P. tricornutum* (Montsant *et al.*, 2005) and the green alga *Ostreococcus tauri* (Derelle *et al.*, 2006). Nonetheless, Roberts *et al.* (2007) concluded that *T. pseudonana* performs exclusively C_3 photosynthesis based on gene transcripts and protein abundances of C_4-metabolic enzymes and RubisCO. The findings of Roberts and colleagues were recently questioned (Kustka *et al.*, 2014). The authors rendered previous suggestions that diatoms rapidly interconvert OAA and malate which compete equally for CO_2 fixation (Reinfelder *et al*., 2004). Although under bloom conditions denoted by low CO_2 level the photosynthetic affinity for inorganic carbon increases in *T. pseudonana* (Fielding *et al.*, 1998) and the freshwater green alga *Chlamydomonas reinhardii* (Vance and Spalding, 2005) under low temperature, the energetic benefit of switching from CO_2 to HCO_3^- uptake, associated to C_4 photosynthesis during bloom conditions, has not been obvious and had little effect on organic carbon production (Kranz *et al.*, 2014).

Bailleul *et al.* (2015) hypothesized that photosynthesis in diatoms is optimised by a partial re-routing of photosynthetic electron flow to mitochondria, followed by the import of mitochondrial ATP into the plastid. The study suggested the involvement of mitochondrial respiration in optimisation of photosynthesis to be a conserved feature in *T. pseudonana* and other four diatoms. Indeed, we found that *T. pseudonana* wild type cells maintain an equilibrated growth over the whole exponential phase in temperature response and display an enhanced growth under temperature acclimation. This may indicate a conserved mechanism to proportionate the energy flow between cell compartments. The process seems to be present at $\pm 10^0$C temperature range from optimal growth temperature. This temperature range is wide enough to allow diatoms to outcompete other phytoplankton in natural phytoplankton assemblages. However, the responsiveness of BIG1 knock-in to sudden changes in environmental conditions points to the employment of a different mechanism in balancing the energy demand and supply of cells. Thus a cyclic electron transport may overtake the regulator role of the

ATP/NAPH ratio more efficiently as we propose to happen in our BIG1 knock-in line which exhibit enhanced response to rapid changes in environmental conditions and stress. It was proposed that PGRL1-mediated cyclic electron flow in *Chlamydomonas reinhardtii* may allow rapid adaptation of the photosynthetic electron transport chain in response to sudden changes in the environment (Dang *et al.*, 2014). In the same study was hypothesized that PGRL1-dependent cyclic electron transfer is not essential for steady-state growth but may play a key role under fluctuating environment. However, before we confidently accept the hypothesis of the presence of BIG1-mediated CET further studies are needed to investigate whether PGR5-PGRL1 proteins are expressed in the transgenic lines in relation to wild type. Also, further investigation is needed for a wider range of proteins associated to energy conversion and electron transfer in chloroplasts complemented by gene expression analysis.

CHAPTER 5: PRELIMINARY RESULTS FOR THE ANALYSIS OF CHROMATIN IMMUNOPRECIPITATION (CHIP) FOLLOWED BY HIGH-THROUGHPUT DNA SEQUENCING (CHIP-SEQ) OF BIG1

5.1 Introduction

Genome-wide mapping of protein-DNA interactions and epigenetic marks is essential for understanding of transcriptional regulation. As reviewed by Park (2009) a precise map of binding sites for transcription factors, core transcriptional machinery and other DNA-binding proteins is vital for deciphering gene regulatory networks that lies behind various biological processes. The combination of nucleosome positioning and dynamic modification of DNA and histones plays a key role in gene regulation (Li *et al.*, 2007) and guides development and differentiation (Allis *et al.*, 2007). Chromatin states can influence transcription directly by altering the packaging of DNA to allow or prevent access to DNA-binding proteins; or they can modify the nucleosome surface to enhance or impede recruitment of effector protein complexes (Park, 2009). Recent advances suggest that this interplay between chromatin and transcription is dynamic (Veluchamy *et al.*, 2013). The main tool for investigating these mechanisms is chromatin immunoprecipitation (ChIP) which with the rapid advances made in the next generation sequencing platforms became widely used coupled with high-throughput DNA sequencing generating tens of millions of short sequence reads.

Chromatin immunoprecipitation (ChIP) followed by high-throughput DNA sequencing (ChIP-seq) has become a valuable and widely used approach for mapping the genomic location of transcription-factor binding and histone modifications in living cells (Landt *et al.*, 2012). The method allows in vivo determination where a protein binds in the genome. In ChIP assays, a transcription factor, cofactor, or other chromatin protein of interest is enriched by immunoprecipitation from cross-linked cells, along with its associated DNA. Genomic DNA sites enriched in this manner were initially identified by DNA hybridization to a microarray (ChIP-chip) (Ren *et al.*, 2000) and more recently by DNA sequencing (ChIP-seq) (Barski *et al.*, 2007). ChIP-seq first cross links bound protein to chromatin, fragments the chromatin, captures the DNA fragments boundt to the investigated protein using an antibody specific to it and sequences the ends of the captured fragments using next generation sequencing (Bailey *et al.*, 1013).

5.2 Results

5.2.1 Validation of the nuclear localization of the BIG1

The *T. pseudonana* vector (pTpNR) expression cassette was designed to tag the inserted gene with eGFP, therefore screening for eGFP. A previoous study (Hipkin, 2012) showed the nuclear localization of the BIG1-GFP fusion protein. The fastest screening for GFP is using a flow cytometer. Therefore, cells were screen on flow cytometer to control if they are in exponential phase and for the expression of the GFP fusion protein previous they were harwested for ChIP extraction.

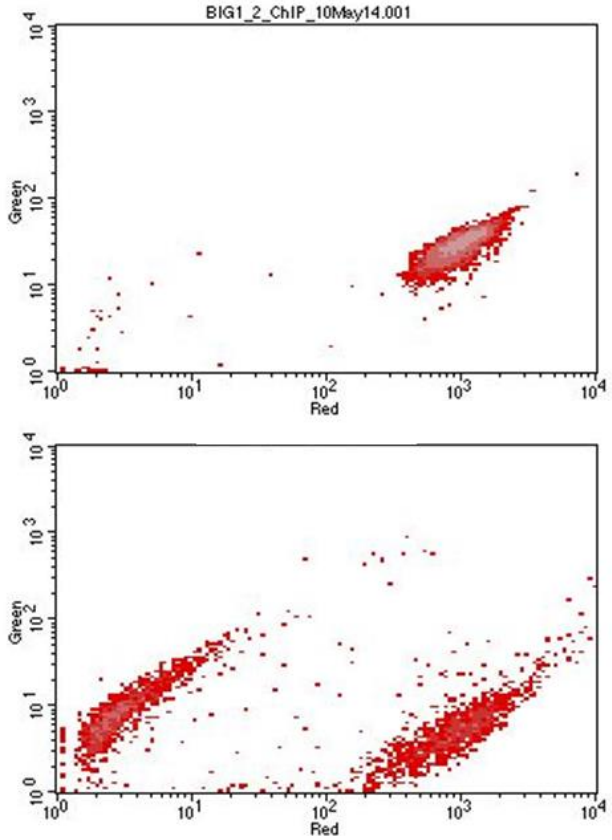

***Figure 5.1**: A representation of biparametric plot of green flurescence related to red fluorescence. The upper image with the higher green fluorescence represents BIG1 knock-in expressing GFP, the lower panel represents cells which do not express GFP.*

5.2.2 Validation of the antibody

Previous work on BIG1 (Hipkin, 2012) showed that under exponential phase the smaller splice variant forms a dimer of ~75 kDa. The selectivity of the antibody was tested

performing immunoblot assay on total protein extract of BIG1 knock-in and wild type. Cultures were grown in complete NEPCC media and harvetsed at mid exponential phase. The immunoblot assay confirmed the selectivity of the antibody as seen in Figure 5.2. Only one protein band was observed for BIG1 knock-in and no bands were seen for wild type.

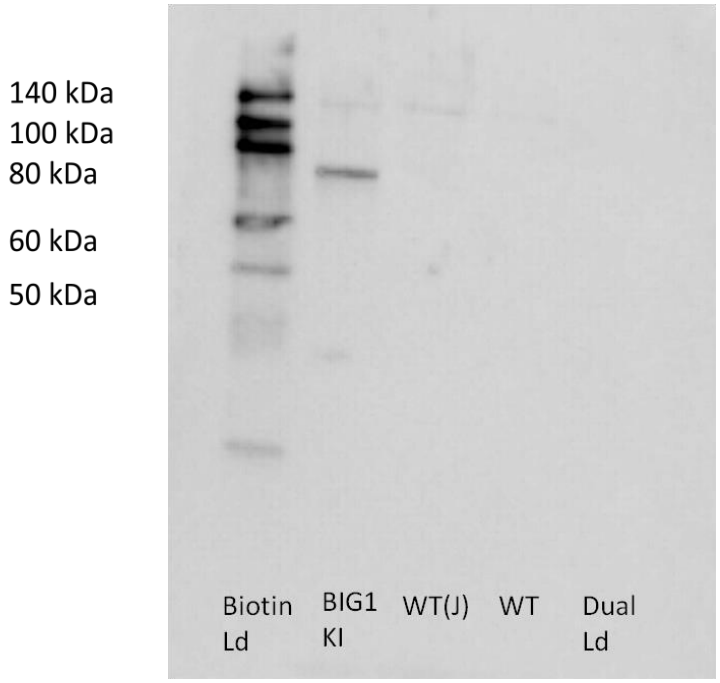

***Figure 5.2**: Western blot of 35 µg of protein from T.pseudonana BIG1 knock-in, two wild types lines grown in NEPCC media and harwested at 36 hours after inoculation.*

5.2.3 Partial result of the analysis

The High throughoutput sequencing generated 8.96 Gb data with a total of 179.230.679 reads for four libraries constructed from our two treatments (IPs) and two controls (Inputs) with an average of ~44 Million reads per sample. Reads were quality controlled with FastQC (Andrews, 2010). The results for the general statistics resuming some features which may rise wornings are shown in Table 5.1. Results from mapping the reads against the *T. pseudonana* genome are shown in Figure 5.3.

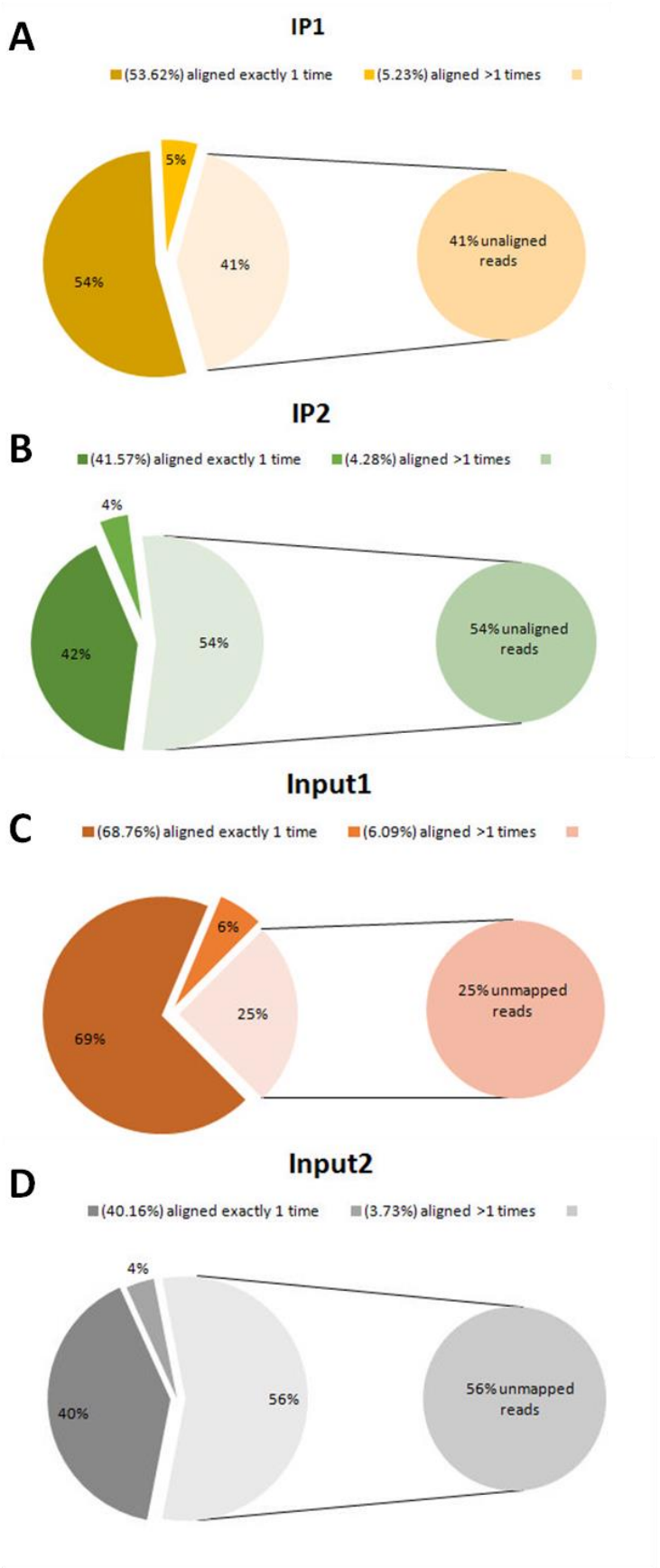

***Figure 5.3**: Results of mapping the sequences against the genome of T. pseudonana. Bowtie2 was used to performe the mapping.*

***Tabel 5.1**: Statistics representing the efficiency of the ChIP extraction and the basic statistics over the results of the sequencing*

Sample ID	*Entry ChIP-DNA (ng)*	*Reads generated*	*Depth/Coverage*	*Sequence duplication (%)*
IP1	2.318	46,122,590	67.82	83.02
Input1	855	38,370,228	56.42	42.43
IP2	2.09	48,388,424	71.16	84.61
Input2	229.9	46,349,437	68.16	52.15

The unmapped reads were further analyzed in order to determine which group they belonged to. The results of a subset of these data are shown in Table 5.2.

***Tabel 5.2**: Results of the analysis done on a subset of unmapped reads*

Sample ID	***Stramenopiles***	***Bacteria***	***Viridiplantae***	***Opisthokonta***	***No hits***	***Not assigned***
IP1	0.2	10.63	4.18	44.84	30.54	7.57
Input1	14.01	17.15	0.02	1.26	63.38	0.28
IP2	4.48	17.05	1.67	39.10	30.09	6.83
Input2	13.28	23.63	0.02	1.19	59.46	0.22

5.3 Discussion

Mapping the chromosomal locations of transcription factors, nucleosomes, histone modifications, chromatine remodelling enzymes, chaperones, and polymerases is one of the key tasks of modern biology, as evidenced by the Encyclopedia of DNA elements (ENCODE) Project. To this end, chromatin immunoprecipitation followed by high-throughput sequencing (ChIP-seq) is the standard methodology (Bailey *et al.*, 2013). ChIP-seq represenths the most widely used procedure for genome-wide asseys of protein-DNA interactions (Furey, 2012) and fostered paricularly the epigenetics reasearch (Ku *et al.*, 2011). Although ChIP-seq is a versatile tool to analyse chromatin-DNA interactions its use in the field of diatom research became a validated technique from 2012 (Lin *et al.*, 2012) used in mapping histone modifications (Veluchamy *et al.*, 2013, 2015). Currently other protein-DNA interactions analised by ChIP-seq are unknown related to diatoms. Thus our study would potentially bring new insights in the regulatory mechanisms that make diatoms one of the most successfull group of phytoplankton by identifying the mapping location of one protein that seems to play a regulatory role in their fast initiation of growth following nutrient stress.

Mapping such protein-DNA interactions *in vivo* using ChIP-seq presents multiple challenges. A successful mapping has many pitfalls not only in sample preparation but in computational analysis. One of the major impediment in application of this procedure is represented by the difficuly of generating sufficient amount of DNA for sequencing. The sample preparation step highly depend on selectivity of the anibody for the analysed protein as well. The antiboby used in our study showed high selectivity for BIG1 as evidenced by western blotts (see 3.2.2 and 3.2.1). However, the generated ChIP-DNA used in this study was very low (2 ng). Unfortunately this proned further analysis to be biased. Such consequence is revealed by quality control and the success of mapping the obtained sequenced reads against the reference genome. A low percentage of uniquely mapped reads offen is due either to excessive amplification in the PCR step in library preparation, problems with the sequencing platform or in case of some proteins it is unavoidable if the protein binds freqently in repetitive DNA (Bailey *et. al.*, 2013). Our results raised concerns as the quality control revealed ~84% sequence duplication level in treatments. This may be a result either by PCR artefacts or repetitive DNA. An other reason for concern that 40-52% and 49-72% of uniquely mapped reads

were generated for treatments and controls respectively. The very low mapping percentage in one of the input (control) sample may indicate a contamination of the samples either in the extraction process, library preparation or crosscontamination during sequencing. We do not know the origins of the other samples used to fill the flow cell (the place where the sequencing chemistry occurs) when our samples were sequenced. Indeed, the IP1 and IP2 treatment samples had 20% and 23% reads mapping to the human genome respectively, while the Input1 and Input2 did not contain any human (<1% mapping) (Chris Watkins, personal communications). Furthermore, analysis of a subset of reads showed that the treatment samples mapped in high percentage to opisthokonts, a broad group of eukaryotes including both the animal and fungus kingdoms which in IP1 was subdivided to 39% mapping to Chordata. Given that all samples were extracted at the same time using exatly the same chemicals and equipment it is unusual that the contamination was found in treatment samples but not in controls.

Reads which mapped to the genome of *T. pseudonana* generated 580 (IP1) and 265 (IP2) peaks denoting regions with significant number of mapped reads. The peaks showed a false discovery rate (FDR) <5%, a commonly accepted value for peaks of good quality (Chakraborty and Nagal, 2015). However, they seem to fail another intuitive measure of peak quality scoring <10 fold change compared to a 20-fold enrichment used as an indicator of good ChIP enrichment (Chakraborty and Nagal, 2015).

Our results thus far indicate that: i) we obtained high quality reads from sequencing even though the entry DNA amount was low, ii) the samples were contaminated, iii) peak calling was possible but further analysis is needed to asses if they are reliable before other analyzes are carried out.

Given the presented obstacles attempts to optimize the extraction protocol were done with the aim of gaining higher amount of ChIP-DNA. This optimization would reduce the possibility of introducing PCR related bias in sample preparation pipeline. We found that increasing the culture biomass to 1L gives a good yield in case that resequencing will be needed. However, we need to acknoledge that our extraction technique used to optmize the extracted DNA amount is still not the optimal as the sheared DNA

fragments were bigger then 1000 bp, the recommanded maximum. However, this aspect is related to the sonication facility used and can be fixed finding a more reliable one.

CHAPTER 6: GENERAL DISCUSSION

General discussion

The evolutionary success of diatoms in the oceans was suggested to be partly underpinned by their fast growth response upon a pulse of nutrients in the euphotic zone (Katz *et al.*, 2004). Diatoms have a "mix-and-match" genome (Armbrust, 2009) that provides them with a range of potentially useful attributes from a silicified cell-wall to resting stage formation. Diatoms populate a wide range of habitats but they are particularly common in nutrient reach regions encompassing polar as well as upwelling and coastal areas (Smetacek, 2012). In these areas, they constitute a major part of seasonal blooms, outcompeting other phytoplankton groups. The publication and annotation of the genome of *Thalassiosira pseudonana* (Armbrust *et al.*, 2004) enabled the analysis of genes that may be linked to diatoms' success in occupying a wide range of ecological niches and biomes. However, little is known about the molecular base of diatoms' ability to dominate the mentioned oceanographic regimes. Thus, identification of a potential regulatory element, the DNA binding protein BIG1 involved in diatoms growth response upon nutrient additions may provide insights into regulatory processes that govern their opportunistic growth.

This study aimed to add new insights into characterising a recently identified DNA-binding protein, BIG1, found to be transcriptionally regulated in response to silicate starvation and showing cell cycle-dependent expression. In this intent transgenic strains of the centric diatom *T. pseudonana* that either overexpress or knock-down the BIG1 protein response to nitrogen limitation and temperature was investigated. On the other hand, it was addressed the question whether short time acclimation to a broad range of temperatures would foster growth. From this purpose cellular physiology, along with genes involved in the light reaction of the photosynthetic pathway, were investigated.

Phenotyping experiments revealed a net advantage of BIG1 knock-in in recovery post nitrate starvation and post temperature stress. Compared to the onset of the experiments, the growth rates of the overexpression cell line showed only minor decrease under both conditions, following nutrient starvation and temperature stress. Moreover, under temperature stress a shorter growth period was observed in cultures overexpressing the BIG protein compared to wild type. Temperature stress induced an intriguing growth pattern with enhanced growth response up to mid exponential phase and subsequent

slow-down in late exponential phase in BIG1 knock-in. This response to temperature was not seen in wild type. Knocking down the protein caused an opposite effect, pointing towards a possible difference in regulation of the cell cycle or uptake of nutrients when BIG1 is overexpressed. Furthermore, the temperature stress experiments revealed that the presence of the BIG1 protein gives advantage under suboptimal growth temperatures, especially under low temperature. Field and laboratory studies of phytoplankton, including diatoms, have revealed a temporal lag between increases in nitrogen assimilation and increased growth rates, following a transition to improved growth conditions (Duarte, 1990). A shorter temporal lag period of the BIG1 knock-in cultures compared to wild type was observed in both phenotyping experiments, pointing to an enhanced nutrient assimilation and enzyme activity triggered by the presence of the BIG1 protein. The upregulation of G1-specific cell cycle regulators by BIG1 overexpressing cell line identified in a previous study, (Hipkin, 2012) along with its quick response to improved growth conditions, led us to the conclusion that BIG1 may arrest cells in late G1 phase of the cell cycle, allowing rapid DNA synthesis, and therefore faster growth.

Temperature stress experiments revealed that growth of BIG1 knock-in had less variation in temperature response and acclimation. Conversely, the wild type displayed an enhanced growth in acclimation to a wide temperature gradient, including 20^0C, its identified optimum temperature of growth. Due to the necessity to increase light intensity to get maximal growth rates we cannot exclude the possibility of introducing a bias in our results. If indeed, the light adjustment biased the growth response to temperature, due to the fact that BIG1 knock-in had significantly lower growth rates at most of the examined temperature points we suggest that BIG1 knock-in is more responsive under low light.

Additionally, an aggregating phenotype was identified in BIG1 knock-down line in nitrate limitation. It seems that reduced BIG1 protein level reactivates a flocculation mechanism observed mostly in diatoms (reviewed by Kiørboe and Hansen, 1993). This mechanism allows diatom cells to thrive longer under unfavourable conditions even if their growth is reduced as we observed in nutrient replete conditions.

An interesting feature was observed linked to Fv/Fm of BIG1 knock-down. In all phenotyping experiments performed in our study, a consistently lower Fv/Fm was

observed for cultures with reduced BIG1. Following recovery from chemical or physical stress, represented by nitrate limitation and temperature stress, Fv/Fm mirrored growth rates. A discrepancy between Fv/Fm and growth was observed in temperature acclimation where at most of the examined temperature points the knock-down cell line outperformed the knock-in cell line. We do not have an explanation for this observation. However, our experiments indicate that Photosystem II is more efficient when BIG1 is overexpressed and may influence photosynthesis.

An intriguing observation of our study is the finding that BIG1 may influence the expression of genes linked to the light reaction of photosynthesis. We found that a putative cytochrome b_6f complex Rieske iron-sulfur protein gene was upregulated in BIG1 knock-in and its expression seemed not to be affected by high fluctuation of temperature. This is of particular interest as cytochrome b_6f represents a switching point between linear and cyclic electron flow. High fluctuation of temperature exerts stress on phytoplankton cells. Under stress conditions, the ATP homeostasis is imbalanced and alternative pathways are engaged to redirect the excess of photosynthetic electrons to reduce the damaging effect of accumulating reducing agents. Cyclic electron flow is one such alternative pathway. Considering that AOX was found to be downregulated under suboptimal temperatures, the involvement of mitochondrial respiration to photosynthesis does not seem to have role in our results. Therefore, we suggest that a cyclic electron flow may be involved in maintaining the advantage offered by the presence of BIG1 in photosynthesis and thus growth.

Future prospects:

At this stage we are not able to predict the outcome of the ChIP-seq as the analysis of data is not finished yet. However, concerns regarding the low amount of entry DNA used for sequencing were raised. Thereafter, following the completion of the analysis, we highly recommend repeating the ChIP-seq with increased ChIP-DNA amount. We consider this necessary in order to validate the results of the analysis as low amount of entry DNA is prone to bias the results (Jakobsen *et al.*, 2015). Our study highlights the potential regulatory role of BIG1 in growth and photosynthesis. Thereafter, the localization of the binding site of BIG1 in the genome of *T. pseudonana* would give

valuable insights about the function of BIG1, especially if it is coupled to previous transcriptomic studies.

Our results suggest that BIG1 may offer advantage under low light. It would be worthwhile to explore this aspect by designing a light gradient experiment similar to the temperature gradient experiment used in this study to test whether higher or lower light influence the growth of cells that either overexpress or knock-down the BIG1 protein compared to wild type. The result of such experiment would complete our knowledge about how BIG1 influences growth as the major limitations of the planktonic metabolism are light, nutrient availability and temperature (Field *et al.*, 1998).

We would also suggest repeating the nutrient limitation experiment with another nitrogen source, such as ammonia, as its uptake was suggested to be more energy conserving (Parker and Armbrust, 2005).

Last but not least we suggest the analysis of gene expression levels of PGR5/PGRL1 proteins as they were identified to be direct regulators of the cyclic electron flow around PSI. Also, we recommend analysis of additional genes members of the cytochrome b_6f complex. The extended RT-qPCR analysis would help to shed light on which members of the cytochrome complex may be additionally regulated by BIG1. This analysis may foster our understanding of the underlying processes that seem to induce a more efficient involvement of PSII in photosynthesis in cells overexpressing BIG1. Also, we would suggest the investigation of protein expression levels of photosynthetic and respiratory complexes complemented with in vivo electro-chromic shift (ECS) measurements (Bailleul *et al.*, 2010, 2015).

BIBLIOGRAPHY

Adams, G.L., Pichler, D.E., Cox, E.J., O'Gorman, E.J., Seeney, A., Woodward, G. And Reuman, D.C. (2013) Diatoms can be an important exception to temperature-size rules at species and community levels of organization, *Global Change Biology*, **19**: 3540-3552.

Admiraal, W. (1977) Influence of Light and Temperature on the Growth Rate of Estuarine Benthic Diatoms in Culture, *Marine Biology*, **39**: 1-9.

Alexopoulos, C.J., Mims, C.W. and Blackwell, M.M. (1996) Introductory Mycology, 4th Edition, Wiley, New York, pp880.

Alldredge, A.L., and Silver, M.W. (1988) Characteristics, dynamics and significance of marine snow. *Prog. Oceanogr.*, **20**(1):41–82.

Allen, A.E., Dupont, C.L., Obornik, M,, Horák, A., Nunes-Nesi, A., McCrow, J.P. *et al.*(2011) Evolution and metabolic significance of the urea cycle in photosynthetic diatoms, *Nature*, **473**: 203–207.

Allen, A.E., Vardi, A. and Bowler, C. (2006) An ecological and evolutionary context for integrated nitrogen metabolism and related signalling pathways in marine diatoms, *Current Opinion in Plant Biology*, **9**:264–273.

Allen, J.F. (2002) Photosynthesis of ATP electrons, protons, pumps, rotors and poise. *Cell* **110**, 273-276

Allen, J.T., Brown, L., Sanders, R., Moore, C.M., Mustard, A., Fiedling, S., Lucas, M., Rixen, M., Savidge, G., Henson, S., Mayor, D. (2005) Diatom carbon export enhancement by silicate upwelling in the northeast Atlantic. *Nature*, **437**:728-732.

Allis, C.D., *et al.*, (2007) editors. Epigenetics. Cold Spring Harbor Laboratory Press, Cold Spring Harbor, New York.

Amin, S.A, Parker, M.S and Armbrust, E.V (2012) Interactions between Diatoms and Bacteria, *Microbiol. Mol. Biol. Rev.*, **76**(3): 667-684.

Andrews, S. (2010) FastQC: a quality control tool for high throughput sequence data. Available online at: http://www.bioinformatics.babraham.ac.uk/projects/fastqc

Apt, K.E., Grossman, A.R. & Kroth-Pancic, P.G. (1996) Stable nuclear transformation of the diatomPhaeodactylum tricornutum, Molec. Gen. Genet., **252**: 572.

Archibald, J.M., Rogers, M.B., Toop, M., Ishida, K. and Keeling, P.J (2003) Lateral gene transfer and the evolution of plastid-targeted proteins in the secondary plastid-containing alga Bigelowiella natans, *PNAS*, **100**(13): 7678-7683.

Armbrust, E.V. (2009) The life of diatoms in the world's oceans, *Nature*, **459**: 185-192.

Armbrust, E.V., Berges, J.A., Bowler, C., Green, B.R., Martinez, D., Putnam, N.H., Zhou, S.G., Allen, A.E., Apt, K.E., Bechner, M., *et al* (2004) The genome of the diatom *Thalassiosira pseudonana*: ecology, evolution, and metabolism. *Science* **306**: 79–86

Arnon, D.I. 1959. Conversion of light into chemical energy in photosynthesis. *Nature* **184**: 10–21.

Arrigo, K.L., Perovich, D.K., Pickart, R.S., Brown, Z.W., van Dijken, G.L., Lowry, K.E., Mills, M.M. *et al.* (2012) Massive phytoplankton blooms under Arctic sea ice, *Science*, **336**(6087) pp. 1408.

Ashworth, J., Coesel, S., Lee, A., Armbrust, E.V., Orellana, M.V. and Baliga, N.S. (2013) Genome-wide diel growth state transitions in the diatom *Thalassiosira pseudonana*. *Proceedings of the National Academy of Sciences of the United States of America*, **110**: 7518–7523.

Backhaus, J.O., Hegseth, E.N., Wehde, H., Irigoien, X., Hatten, K. and Logemann, K. (2003) Convection and primary production in winter, *Mar. Ecol.-Prog. Ser.*, **251**:1–14.

Badger, M.R., Andrews, T.J., Whitney, S.M., Ludwig, M., and Yellowlees, D.C., (1998) The diversity and co-evolution of Rubisco, plastids, pyrenoids and chloroplast-based CO_2-concentrating mechanisms in the algae. *Canadian Journal of Botany* **76**, 1052-1071.

Bailey S, Melis A, Mackey KR, Cardol P, Finazzi G, *et al.* (2008) Alternative photosynthetic electron flow to oxygen in marine Synechococcus. Biochim. Biophys. Acta.

Bailey, T., Krajewski, P., Ladunga, I., Lefebvre, C., Li, Q., Liu, T., Madrigal, P., Taslim, C. and Zhang, J. (2013) Practical Guidelines for the Comprehensive Analysis of ChIP-seq Data. *PLoS Comput Biol.*, **9**(11):e1003326.

Bailleul, B., Berne, N., Murik, O., Petroutsos, D., Prihoda, J., Villanova, V. *et al.*, (2015) Energetic coupling between plastids and mitochondria drives CO_2 assimilation in diatoms. *Nature* **524**, 366-369.

Bailleul, B., Cardol, P., Breyton, C. and Finazzi, G. (2010) Electrochromism: a useful probe to study algal photosynthesis, *Photosynth Res.*, **106**(1-2):179-89.

Ban, A., Aikawa, S., Hattori, H., Sasaki, H., Sampei, M., Kashino. Y. (2006) Comparative analysis of photosynthetic properties in ice algae and phytoplankton inhabiting Franklin Bay, The Canadian Arctic, with those in mesophilic diatoms during CASES 03-04. *Polar Biosci.*, **19**, 11-28.

Banse, K. (1976) Rates of growth, respiration and photosynthesis of unicellular algae as related to cell-size - a review. *J. Phycol.*, **12**:135–40.

Barber, R.T. and Hiscock, M.R. (2006) A rising tide lifts all phytoplankton: Growth response of other phytoplankton taxa in diatomdominated blooms. *Global Biogeochem. Cy.*, **20**, GB4S03.

Barski, A., Cuddapah, S., Cui, K., Roh, T., Schones, D.E., Wang, Z., Wei, G., Chepelev, I., Zhao, K. (2007) High-resolution profiling of histone methylations in the human genome, *Cell*, 129: 823–837.

Barton, A.D., Finkel, Z.V., Ward, B.A., Johns, D.G. and Follows, M.J. (2013) On the roles of cell size and trophic strategy in North Atlantic diatom and dinoflagellate communities. *Limnol. Oceanogr.*, **58**(1): 254-266.

Bartón, K (2009) MuMIn: multi model inference. R package, version 0.12.2

Beardall, J., Stojkovic, S. and Larsen, S. (2009) Living in a high CO2 world: impacts of global climate change on marine phytoplankton, *Plant Ecol. Diversity*, **2**(2):191–205.

Behrenfeld, M. J., O'Malley, R. T., Siegel, D. A. *et al*. (2006), Climate-driven trends in contemporary ocean productivity. *Nature*, **444**:752–755.

Behrenfeld, M.J. (2010) Abandoning Sverdrup's Critical Depth Hypothesis on phytoplankton blooms. *Ecology*, **91**:977–89.

Behrenfeld, M.J. (2014) Climate-mediated dance of the plankton. *Nature Climate Change*, **4**:880–887.

Behrenfeld, M.J. and Boss, E.S. (2014) Resurrecting the ecological underpinnings of ocean plankton blooms, *Annual Review of Marine Science*, **6**: 167-194.

Behrenfeld, M.J. and Falkowski, P.J. (1997) Photosynthetic rates derived from satellite-based chlorophyll concentration, *Limnol. Oceanogr.*, **42**(l): 1-20.

Berges, J.A. and Falkowski, P.G. (1998) Physiological stress and cell death in marine phytoplankton: Induction of proteases in response to nitrogen or light limitation, *Limnol. Oceanogr*., **43**: 129-135.

Berges, J.A., Gibson, C.E. and Stewart, B.M. (2004) Physiological responses of phytoplankton communities in the Irish Sea to simulated upwelling, *Hydrobiologia* **517**: 121-132

Biello, D. (2010) What causes the North Atlantic plankton bloom? *Scientific American*, January 29, 2010.

Bilger, W. and Bjorkman, O. (1994) Relationships among violaxanthin deepoxidation, thylakoid membrane conformation, and nonphotochemical chlorophyll fluorescence quenching in leaves of cotton (*Gossypium hirsutum* L.), *Planta*, **193**: 238-246.

Bissenger, J.E., Montagnes, S.J. and Atkinson, D. (2008) Predicting marine phytoplankton maximum growth rates from temperature: improving on the Eppley curve using quantile regression, *Limnol. Oceanogr.*, **53**: 487–493.

Blaby-Haas, C.E., Merchant, S.S., (2012) The ins and outs of algal metal transport. *Biochimica et Biophysica Acta Bioenergetics* **1823**, 1531–1552.

Blackburn, T., Gaston, K.J. and Loder, N. (1999) Geographic gradients in body size: a clarification of Bergmann's rule, *Diversity and Distribution*, **5**: 165-174.

Bode, A., Botas, J.A. and Fernandez, E. (1997) Nitrate storage by phytoplankton in coastal upwelling environment, *Mar. Biol.*, **129**: 399-406.

Booth, B.C., Larouche, P., Belanger, S., Klein, B., Amiel, D., Mei, Z.-P. (2002) Dynamics of *Chaetoceros socialis* blooms in the North Water. *Deep-Sea Res.* Part II **49**: 5003–5025.

Bowler, C *et al.*, (2008) The *Pheodactylum* genome reveals the evolutionary history of diatom genomes. *Nature* **456**, 239-244.

Bowler, C., Allen, A.E., Badger, J.H., Grimwood, J., Jabbari, K., Kuo, A., Maheswari, U., Martens, C., Maumus, F., Otillar, R.P., *et al* (2008) The *Phaeodactylum* genome reveals the evolutionary history of diatom genomes, *Nature*, **456**: 239–244

Bowler, C., Vardi, A. and Allen, A.E. (2010) Oceanographic and biogeochemical insights from diatom genomes. *Ann. Rev. Mar. Sci.*, **2**:333-365.

Boyd, P.W., Jickells, T., Law, C.S., Blain, S., Boyle, E.A., Buesseler, K.O., Coale, K.H., Cullen, J.J., De Baar, H.J.W., Follows, M., Harvey, M., Lancelot, C., Levasseur, M., Owens, N.P.J., Pollard, R., Rivkin, R.B., Sarmiento, J., Schoemann, V., Smetacek, V., Takeda, S., Tsuda, A., Turner, S., Watson, A.J. (2007) Mesoscale iron enrichment experiments 1993-2005: Synthesis and future directions, *Science*, **315**: 612-617.

Boyd, P.W., Law, C.S., Wong, C.S., Nojiri, Y., Tsuda, A., *et al.* (2004) The decline and fate of an iron-induced subarctic phytoplankton bloom. *Nature*, **428**, 549–553.

Boyd, P.W., Rynearson, T.A., Armstrong, E.A., Fu, F., Hayashi, K., Hu, Z., Hutchins, D.A *et al.*, (2013) Marine Phytoplankton Temperature versus Growth Responses from Polar to Tropical Waters – Outcome of a Scientific Community-Wide Study, *PLoS ONE*, **8**(5): e63091.

Brown, C.W. and Yoder, J.A. (1994) Coccolithophorid blooms in the global ocean. *J. Geophys. Res.*, **99**:7467−7482.

Brown, J. H. (1995) *Macroecology*, The University of Chicago Press, Chicago.

Brown, J. H., J. F. Gillooly, A. P. Allen, V. M. Savage, and G. B. West (2004), Toward a metabolic theory of ecology, *Ecology*, **85**(7), 1771–1789.

Browna, Z.W., Lowry, K.E., Palmer, M.A., van Dijken, G.L., Mills, M.M., Pickart, R.S. and Arrigo, K.R. (2015) Characterizing the subsurface chlorophyll *a* maximum in the Chukchi Sea and Canada Basin, *Deep-Sea Research* II **118**: 88–104.

Bruland, K.W., Rue, E.L. and Smith, G.J. (2001) Iron and macronutrients in California coastal upwelling regimes: implications for diatom blooms. *Limnol. Oceanogr*., **46**:1661-1674.

Bruland, K.W., Rue, E.L., Smith, G.J. and DiTullio, G.R. (2005) Iron, macronutrients and diatom blooms in the Peru upwelling regime: brown and blue waters of Peru, *Mar. Chem.*, **93**: 81-103.

Brunet, C. and Lavaud, J. (2010) Can the xanthophyll cycle help extract the essence of the microalgal functional response to a variable light environment?, *J. Plankton Res.*, **32**(12): 1609-1617.

Brzezinksi, M.A., Olson, R.J. and Chisholm, S.W. (1990) Silicon availability and cell-cycle progression in marine diatoms, *Mar. Ecol. Prog. Ser*., **67**: 83-96.

Buchan, A., LeCleir, G.R., Gulvic, C.A. and González, J.M. (2014) Master recyclers: features and functions of bacteria associated with phytoplankton blooms. *Nature Reviews Microbiology*, **12**:686–698.

Buchanan, B.B., Gruissem, W. and Jones, R.L. (2000) Biochemistry and molecular biology of plants. *American Society of Plant Physiologists*, Rockwille, Maryland, USA.

Büchel, C. (2003) Fucoxanthin-chlorophyll proteins in diatoms: 18 and 19 kDa subunits assemble into different oligomeric states, *Biochemistry*, **42**: 13027-13034.

Burnham, K.P. & Anderson, D.R. (2002) Model Selection and Multi-Model Inference: A Practical Information-Theoretic Approach. *Springer*, New York.

Carpenter EJ, Montoya JP, Burns JA, Mulholland M, Subramaniam A, Capone DG. (1999) Extensive bloom of a N_2-fixing diatom/cyanobacterial association in the Tropical Atlantic Ocean, Mar. Ecol. Prog. Ser., **185**: 273–283.

Cassar, N., Bender, M.L, Barnett, B.A, Songmiao, F, Moxim, W.J, Levy, H, II and Tilbrook, B. (2007) The Southern Ocean biological response to aeolian iron deposition, *Science*, **317**: 1067–1070.

Cavalier-Smith, T. (1999) Zooflagellate phylogeny and the systematic of protozoa, *Biological Bulletin*, **196**: 393-396.

Chakraborty, P. and Nagal, A. (2015) Software innovations in clinical drug development and safety, Medical Information Science Reference (an imprint of IGI Global) USA, pp 235-236.

Chan, C.X., Baglivi, F.L., Jenkins, C.E. and Bhattacharya, D. (2013) Foreign gene recruitment to the fatty acid biosynthesis pathway in diatoms, *Mob. Genet. Elements*, **3**(5): e27313.

Chan, C.X., Reyes-Prieto, A. and Bhattacharya, D. (2011) Red and green algal origin of diatom membrane transporters: Insights into environmental adaptation and cell evolution, *PLoS One*, **6**(12): e29138.

Charlson, R., Lovelock, J., Andreae, M. and Warren, S. (1987) Oceanic phytoplankton, atmospheric sulphur, cloud albedo and climate. *Nature*, **326**:655–661.

Chavez, F.P., Messié, M. and Pennington, J.T. (2011) Marine primary production in relation to climate variability and change. *Annu. Rev. Mar. Sci*., **3**:227–60.

Chen, B. (2015) Patterns of termal limits of phytoplankton, *J. Plankton Res.*, **37**(2): 285-292.

Chen, W.H., de Meaux, J. and Lercher, M.J. (2010) Co-expression of neighbouring genes in Arabidopsis: separating chromatin effects from direct interactions, *BMC Genomics*, **11**:178.

Chepurnov, V.A. and Mann, D.G. (2004) Auxosporulation of *Licmophora communis* (Bacillariophyta) and a review of mating systems and sexual reproduction in araphid pennate diatoms, *Phycol. Res.*, **52**: 1–12.

Chepurnov, V.A., Mann, D.G, von Dassow, P., Vanormelingen, P., Gillard, J., Inzé, D., Sabbe, K. and Vyverman, W. (2008) In search of new tractable diatoms for experimental biology, *BioEssays*, **30**: 692–702.

Chisholm, S.W. (1992) Phytoplankton size. In *Primary Productivity and Biogeochemical Cycles in the Sea*, ed. PG Falkowski, AD Woodhead, New York: Plenum, pp. 213–37.

Chisti, Y. (2008) Biodiesel from microalgae beats bioethanol. *Trends Biotechnol.*, **26**:126-131.

Coale, K.H., Johnson, K.S., Fitzwater, S.E. *et al.* (1996) A massive phytoplankton bloom induced by an ecosystem-scale iron fertilization experiment in the equatorial Pacific Ocean. *Nature*, **383**:495–501.

Coleman, M.L., Sullivan, M.B., Martiny, A.C., Steglich, C., Barry, K., DeLong, E. and Chisholm, W. (2006) Genomic island and the ecology and evolution of *Prochlorococcus*, *Science*, **311**:1768-1770.

Coppini, G., Pinardi, N., Marullo, S. and Loewe, P. (2007) Sea surface temperature, Compiled for EEA by the Instituto Nazionale di Geofisica e Vulcanologia (INGV) based on datasets made available by the Hadley Center, HADISST1: http://hadobs.metoffice.com/hadisst/data/download.html.

Dang, K.V., Plet, J., Tolleter, D., Jokel, M., Cuiné, S., Carrier, P. et al., (2014) Combined increases in mitochondrial cooperation and oxygen photoreduction compensate for deficiency in electron flow in *Chlamidomonas reinhardtii*. *Plant cell* **26**, 3036-3050.

Daniels, C.J., Poulton, A.J., Esposito, M., Paulsen, M.L., Bellerby, R., John, M.St. and Martin, A.P. (2015) Phytoplankton dynamics in contrasting early stage North Atlantic spring blooms: composition, succession, and potential drivers. *Biogeosciences*, **12**:2395–2409.

Daufresne, M., Lengfellner, K. and Sommer, U. (2009) Global warming benefits the small in aquatic ecosystems, *Proceeding of the National Academy of Science of the USA*, **106**: 12788-12793.

de Baar, H.J.W., Boyd, W.P., Coale, K.H., Landry, M.R., Tsuda, A., *et al.* (2005) Synthesis of iron fertilization experiments: From the Iron Age in the Age of Enlightenment. *J. Geophys. Res.*, **110**:C09S16.

de Boer, M.K. (2005) Temperature responses of three *Fibrocapsa japonica* strains (Raphidophyceae) from different climate region, *J. Plankton Res.*, **27**(1): 47–60.

De La Rocha, .L., Terbrüggen, A., Völker, C. and Hohn, S. (2010) Response to and recovery from nitrogen and silicon starvation in Thalassiosira weissflogii: growth rates, nutrient uptake and C, Si and N content per cell, Mar. Ecol. Progr. Ser. 412: 57-68.

De La Rocha, C.L. and Passow, U. (2004) Recovery of *Thalassiosira weissflogii* from nitrogen and silicon starvation. *Limnol. Oceanogr*. **49**: 245-255.

De Martino, A., Amato, A. and Bowler, C. (2009) Mitosis in diatoms: rediscovering an old model for cell division, *BioEssays*, **31**: 874–884.

De Riso, V., Raniello, R., Maumus, F., Rogato, A., Bowler, C. and Falciatore, A. (2009) Gene silencing in the marine diatom *Phaeodactylum tricornutum*. *Nucleic Acids Res.*, **37**(14):e96.

de Vargas, C., Audic, S., Henry, N., Decelle, J., Mahé, F., Logares, R., Lara, E., Berney, C. *et al.*, (2015) Ocean plankton. Eukaryotic plankton diversity in the sunlit ocean, Science, **348**(6237):1261605.

Delwiche, C.F. (1999) Tracing the thread of plastid diversity through the tapestry of life. *Am. Nat.*, **154**, S164–S177.

Desbois, A., Mearns-Spragg, A. and Smith, V. (2009) A fatty acid from the diatom *Phaeodactylum tricornutum* is antibacterial against diverse bacteria including multi-resistant *Staphylococcus aureus* (MRSA), *Mar. Biotechnol*., **11**:45–52.

Dickson, M.L. and Wheeler, P.A. (1995) Ammonium uptake and regeneration rates in a coastal upwelling regime, *Mar. Ecol. Progr. Ser.*, **121**: 239-248.

Dinakar, C., Vishwakarma, A., Raghavendra, A. and Padmasree, K., (2016) Alternative oxidase pathway optimises photosynthesis during osmotic and temperature stress by regulating cellular ROS, malate valve and antioxidative systems. *Front. Plant Sci.* **7**:68.

Doering, P.H., Oviatt, C.A., Nowicki, B.L., Klos, E.G. and Reed, L.W. (1995) Phosphorus and nitrogen limitation of primary production in a simulated estuarine gradient, *Mar. Ecol. Progr. Ser.*, **124**: 271-287.

Doney, S.C. (2006) Plankton in warmer world, *Nature*, **444**: 695-696.

Dore, J.E., Letelier, R.M., Church, M.J., Lukas, R. and Karl, D.M. (2008) Summer phytoplankton blooms in the oligotrophic North Pacific Subtropical Gyre: Historical perspective and recent observations, *Progress in Oceanography*, **76**: 2–38.

Dortch, Q. (1982) Effect of growth conditions on accumulation on internal nitrate, ammonium, amino acids and protein in three marine diatoms, *J. Exp. Mar. Biol. Ecol*., **61**: 243-264.

Douglas, S., Zauner, S., Fraunholz, M., Beaton, M., Penny, S., Deng, L.T., Wu, X., Reit, M., Cavalier-Smith, T. and Maier, U.G. (2001) The highly reduced genome of an enslaved algal nucleus, *Nature*, **410**: 1091–1096.

Duarte, C. M. (1990) Time lags in algal growth: generality, causes and consequences, *J. Plankton Res.*, **12**: 873-883.

Duarte, C. M., and Y. T. Prairie (2005), Prevalence of heterotrophy and atmospheric CO2 emissions from aquatic ecosystems, *Ecosystems*, **8**: 862–870.

Duce, R.A, LaRoche, J., Altieri, K., Arrigo, K.R. Baker, A R. *et al.*, (2008) Impacts of atmospheric anthropogenic nitrogen on the open ocean, *Science*, **320**: 893-897.

Dunahay, T. G., Jarvis, E. E. and Roessler, P. G. (1995), Genetic transformation of the diatoms Cyclotella cryptica and Navicula saprophyla., Journal of Phycology, **31**: 1004–1012.

Durbin, E. (1977) Studies on the autecology of the marine diatom *Thalassiosira nordenskoldii* Cleve. II. The influence of cell size on growth rate, and carbon, nitrogen, chlorophyll *a* and silica content, *J. Phycol.*, **33**: 897-918.

Durbin, E.G. (1974) Studies on the autecology of the marine diatom *Thalassiosira nordenskoldii* Cleve. I. The influence of daylight, light intensity, and temperature on growth, *J. Phycol.*, **10**:220-225.

Durkin, C.A., Mock, T., and Armbrust, E.V. (2009) Chitin in diatoms and its association with the cell wall, *Eukaryotic Cell*, **8**: 1038-1050.

Duysens, L.N.M. (1956) The flattening of the absorption spectrum of suspensions, as compared to that of solutions. *Biochim. Biophys. Acta*, **19**:1–12.

Dyhrman, S.T., Jenkins, B.D., Rynearson, T.A., Saito, M.A., Mercier, M.L., *et al.* (2012) The transcriptome and proteome of the diatom *Thalassiosira pseudonana* Reveal a diverse phosphorus stress response. *PLoS ONE,* **7**(3): e33768

Eberhard S., Finazzi G., and Wollman F.-A., (2008) The Dynamics of Photosynthesis, *Annu. Rev. Genet*., **42**:463–515.

Egge, J.K. and Aksnes, D.L. (1992) Silicate as regulating nutrient in phytoplankton competition. *Marine Ecol. Prog. Ser.*, **83**:281-289.

Eppley, R.W. (1972) Temperature and phytoplankton growth in the sea, *Fish. Bull.*, **70**: 1063–1085.

Eppley, R.W. and Peterson, B.J. (1979) Particulate organic matter flux and planktonic new production in the deep ocean. *Nature*, **282**:677–680.

Estrada, M. and Blaco, D. (1979) 2 phases of the phytoplankton community in the Baja California upwelling, *Limnol. Oceanogr*., **24**: 1065-1080.

Evans, G.T. and Parslow, J.S. (1985) A model of annual plankton cycles, *Biological Oceanography*, **3**(3): 327-347.

Falciatore,A., Casotti,R., Leblanc,C., Abrescia,C. and Bowler,C. (1999) Transformation of nonselectable reporter genes in marine diatoms, Marine Biotech.,**1**: 239–251.

Falkovski, P.G and Raven, J.A (1997) Aquatic photosynthesis, Malden, M.A.: Blackwell Sciences

Falkovski, P.G and Raven, J.A (2007) An introduction to photosynthesis in aquatic systems. Princeton University Press.

Falkowski, P.G. (1997) Evolution of the nitrogen cycle and its influence on the biological sequestration of CO2 in the ocean. *Nature*, **387**:272-275.

Falkowski, P.G. and Oliver, M.J. (2007) Mix and meci: how climate selecs phytoplankton. *Nature Reviews Microbiology*, **5**:813–819.

Falkowski, P.G., Barber, R.T. and Smetacek, V. (1998) Biogeochemical controls and feedbacks on ocean primary production. *Science*, **281**:200–6.

Falkowski, P.G., Boyle, E., Canadell, J. *et al.* (2000) The global carbon cycle: a test of our knowledge of the Earth as a system. *Science*, **290**:291–294.

Falkowski, P.G., Fenchel, T. and Delong E.F. (2008) The microbial engines that drive Earth's biogeochemical cycles. *Science*, **320**:1034-1039.

Falkowski, P.G., Katz, M.E., Knoll, A.H., Quigg, A. Raven, J.A., Schoefield, O. And Taylor, F.J.R. (2004) The evolution of modern eukaryotic phytoplankton, *Science*, **305**: 354-360.

Fehling, J., Green, D.H., Davidson, K., Bolch, C.J. and Bates, S.S. (2004) Domoic acid production by *Pseudo-nitzschia seriata* (Bacillariophyceaae) in Scottish waters, *J. Phycol.*, **40**: 622–630.

Field, A. (2000). 3.1. Mann-Whitney test. Research Methods 1: SPSS for Windows part 3: Nonparametric tests. Retrieved from https://www.discoveringstatistics.com/repository/nonparametric.pdf

Field, C.B., Behrenfeld, M.J., Randerson, J.T. and Falkowski, P.G. (1998) Primary production of the biosphere: integrating terrestrial and oceanic components. *Science* **281**:237–40.

Finkel, Z. V., Beardall, J., Flynn, K. J. *et al*. (2010) Phytoplankton in a changing world: cell size and elemental stoichiometry. *J. Plankton Res.*, **32**:119–137.

Finkel, Z.V. (2007) Does phytoplankton cell size matter? The evolution of modern marine food webs. In Evolution of aquatic photoautotrophs (eds P.G. Falkowski and A.H. Knoll), San Diego, CA, USA: Academic Press, pp.333-350.

Finkel, Z.V., Katz, M., Wright, J. *et al.* (2005) Climatically driven macroevolutionary patterns in the size of marine diatoms over the Cenozoic. *Proc. Natl Acad. Sci. USA*, **102**:8927–8932.

Finkel, Z.V., Katz, M.E., Wright, J.D., Schofield, O.M.E. and Falkowski, P.G. (2005) Climatically driven macroevolutionary patterns in the size of marine diatoms over the Cenozoic. *Proceedings of the National Academy of Sciences of the USA*, **102**: 8927-8932.

Finkel, Z.V., Sebbo, J., Feist-Burkhardt, S. *et al.* (2007b) A universal driver of macroevolutionary change in the size of marine phytoplankton over the Cenozoic. *Proc. Natl Acad. Sci. USA*, **104**:20416–20420.

Finkel, Z.V., Vaillancourt, C.-J., Irwin, A.J. *et al.* (2009) Environmental control of diatom community size structure varies across aquatic ecosystems. *Proc. R. Soc. B.*, **276**:1627–1634.

Fischer, H., Robl, I., Sumper, M., Kröger, N., (1999) Targeting and covalent modification of cell wall and membrane proteins heterologously expressed in the diatom *Cylindrotheca fusiformis* (Bacillariophyceae). *J. Phycol*. **35**: 113–120.

Fisher, T.R., Peele, E.R., Ammerman, J.W. and Harding, L.W. Jr. (1992) Nutrient limitation of phytoplankton in Chesapeake Bay, *Mar. Ecol. Prog. Ser.*, **82**:51–63.

Foster, R. A., Kuypers, M. M. M., Vagner, T., Paerl, R. W., Musat, N., & Zehr, J. P. (2011). Nitrogen fixation and transfer in open ocean diatom–cyanobacterial symbioses, The ISME Journal, **5**(9): 1484–1493.

Foster, R.A. and Zehr, J.P. (2006) Characterization of diatom-cyanobacteria symbioses on the basis of *nifH*, *hetR* and 16s rRNA sequences, *Environmental Microbiology*, **8**:1913-1925.

Franklin, D,J., Airs, R.L., Fernandes, M., Bell, T.G., Bongaerts, R.J, Berges, J.A and Malin, G. (2012) Identification of senescence and death in *Emiliana huxleyi* and *Thalassiosira pseudonana*: Cell staining, chlorophyll alterations and dimethylsulfoniopropionate (DMSP) metabolism, *Limnol. Oceanogr*., **57**(1): 305-317.

Furey, T.S. (2012) ChIP-seq and beyond: new and improwed methodologies to detect and characterize protein-DNA interactions, *Nat. Rev. Genet.*, **13**: 840-852.

Fuhrman, J.A. (2009) Microbial community structure and its functional implications. *Nature*, **459**:193-199.

Gao, Y., Smith, G.J. and Alberte, R.S. (1993) Nitrate reductase from the marine diatom *Skeletonema costatum* biochemical and immunological characterization, *Plant Physiol.*, **103**: 1437–45.

Gao, Y., Smith, G.J. and Alberte, R.S. (2000) Temperature dependence of nitrate reductase activity in marine phytoplankton: biochemical analysis and ecological implications, *J. Phycol.*, **36**: 304–13.

Gardner, J.L., Peters, A., Kearney, M.R., Joseph, L. and Heinsohn, R. (2011) Declining body size: a third universal response to warming? *Trends in ecology & evolution*, **26**: 285-291.

Geider, R.J., Osborne, B.A. and Raven. J.A. (1986) Growth, photosynthesis and maintenance metabolic cost in the diatom *Phaeodactylum tricornutum* at very low light levels. *J. Phycol.*, **22**:39–48.

Genovesi-Giunti, B. and Vaquer, A. (2006) The benthic resting cysts: A key actor in harmful dinoflagellate blooms, *Vie et Milieu*, **56**(4): 327-337.

Giering, S.L.C., *et al.* (2014) Reconciliation of the carbon budget in the ocean's twilight zone. *Nature*, **507**(7493):480–483.

Giering, S.L.C., Sanders, R., Martin, A.P., Lindemann, C., Möller, K.O., Daniels, C.J., Mayor, D.J. and St. John, M.A. (2016), High export via small particles before the onset of the North Atlantic spring bloom, *J. Geophys. Res. Oceans*, **121**:6929–6945.

Gillooly, J. F., J. H. Brown, G. B. West, V. M. Savage, and E. L. Charnov (2001), Effects on size and temperature on metabolic rate, *Science*, **293**: 2248–2251.

Giordano, M., Beardall, J. and Raven, J.A. (2005) CO_2 concentrating mechanisms in algae: mechanisms, environmental modulation, and evolution. *Annual Review of Plant Biology*, **56**:99–131.

Glibert, P. M. and Terlizzi.D. E. (1999) Cooccurence of elevated urea levels and dinoflagellate blooms in temperate estuarine aquaculture ponds, *Appl. Environ. Microbiol.*, **65**: 5594–5596.

Golbeck, J., Joliot. P., Joliot, A. and Johnson, G. (2006) Cyclic electron transfer around photosystem I. In Photosystem I, Vol 24. Springer, Houten, The Netherlands, pp 639–656.

Gordon, R., Losic, D., Tiffany, M.A., Nagy, S.S. and Sterrenburg, F.A. (2009) The Glass Menagerie: diatoms for novel applications in nanotechnology. *Trends Biotechnol.*, **27**:116-127.

Goss, R. and Lepetit, B. (2015) Biodiversity of NPQ. *J. Plant Physiol*., **172**:13–32.

Graham, L.E., Graham, J.M. and Wilcox, L.W. (2009) Algae, Second edition, Pearson Education, Inc., San Francisco, CA 94111.

Graham, M.D., (2003) The coulter principle: Foundation of an industry. *Journal of the Association for Laboratory Automation*, Vol. **8**, Issue 6, 72-81.

Gray, M.W., Burger, G. and Lang, B.F. (1999) Mitochondrial evolution, *Science*, **283**: 1476–1481.

Grouneva, I., Rokka, A., and Aro, E.-M. (2011) The thylakoid membrane proteome of two marine diatoms outlines both diatom-specific and species-specific features of the photosynthetic machinery, *J. Proteome Res*., **10**, 5338-5353.

Gruber, A., Vugrinec, S., Hempel, F., Gould, S.B., Maier, U.G. and Kroth, P.G. (2007) Protein targeting into complex diatom plastids: functional characterisation of a specific targeting motif, *Plant Mol. Biol.*, **64**: 519–530.

Gruber, N., Galloway, J.N. (2008) An Earth-system perspective of the global nitrogen cycle, *Nature*, **451**, 293–296.

Guiry, M.D. (2014) AlgaeBase. Guiry, M.D., and Guiry, G.M.(eds). Galway: World-wide electronic publication, National University of Ireland. http://www.algaebase.org.

Hackett, J.D., Anderson, D.M., Erdner, D.L. and Bhattacharya, D. (2004) Dinoflagellates: A remarkable evolutionary experiment, *American Journal of Botany*, **91**: 1523–1534.

Hamilton, M.L., Haslam, R.P., Napier, J.A. and Sayanova, O. (2014) Metabolic engineering of *Phaeodactylum tricornutum* for the enhanced accumulation of omega-3 long chain polyunsaturated fatty acids. *Metab. Eng.*, **22**:3-9.

Hamme, R.C., Webley, P.W., Crawford, W.R., Whitney, F.A., DeGrandpre, M.D., Emerson, S.R., Eriksen, C.C., Giesbrecht, K..E., Gower, J.F.R., Kavanaugh, M.T., Pena, M.A., Sabine, C.L., Batten, S.D., Coogan, L.A., Grundle, D.S., and Lockwood, D.

(2010) Volcanic ash fuels anomalous plankton bloom in subarctic northeast Pacific, *Geophys. Res. Lett.*, **37**, L19604.

Han S, Tang R, Anderson LK, Woerner TE, Pei ZM (2003) A cell surface receptor mediates extracellular $Ca^{(2+)}$ sensing in guard cells, Nature, **425**:196–200.29.

Hardie, D.G., Ross, F.A. and Hawley. S.A. (2012) AMPK: a nutrient and energy sensor that maintains energy homeostasis, *Nature Reviews Molecular Cell Biology*, **13**: 251–262.

Härnström, K., Ellegaard, M., Andersen, T.J. and Godhe, A. (2011) Hundred years of genetic structure in a sediment revived diatom population, *Proceedings of the National Academy of Sciences of the United States of America*, **108**(10): 4252–4257.

Harris, L. A., C. M. Duarte, and S. W. Nixon (2006), Allometric laws and prediction in estuarine and coastal ecology, *Estuaries Coasts*, **29**(2): 340–344.

Harrison, P.J., Conway, H.L., Holmes, R.W. and Davis, C.O. (1977) Marine diatoms grown in chemostats under silicate or ammonium limitation. III. Cellular chemical composition and morphology of *Chaetoceros debilis*, *Skeletonema costatum*, and *Thalassiosira gravida*, *Mar. Biol*. **43**: 19-31.

Harrison, P.J., Waters, R.E. and Taylor. F.J.R. (1980) A broad spectrum artificial medium for coastal and open ocean phytoplankton, *J. Phycol.*, **16**:28-35.

Harrison, W.G. and Cota, G.F. (1991) Primary production in polar waters: relation to nutrient availability. in Sakshaug, E., Hopkins. C. C. E. & Oritsland. N. A. (eds.): Proceedings of the Pro Mare Symposium on Polar Marine Ecology. Trondheim. 12-16 May 1990. Polar Research l0(1). pp. 87-104

Hartl., F.U., Bracher, A. and Mayer-Hartl, M. (2011) Molecular chaperones in protein folding and proteostasis, *Nature*, **475**: 324–332

Harwood, J.L. and Guschina, I.A. (2009) The versatility of algae and their lipid methabolism. *Biochemie*, **91**:679-684.

Hasle, G.R. and Heimdal, B.R. (1970) Some species of the centric diatom genus Thalassiosira studied in the light and electron microscopes, *Nova Hedwigia*, 31: 543-581.

Hasle, G.R. and Syvertsen, E.E. (1997) Marine diatoms. In: Tomas, C.R. (ed) *Identifying marine phytoplankton*, Academic Press, San Diego CA, Chapter 2.

Hedges, S.B., Chen, H., Kumar, S.,Wang, D., Thompson, A. and Watanabe, H. (2001) A genomic timescale for the origin of eukaryotes. *BMC Evol. Biol.* **1**:4.

Heiskanen, A.-S., Keck, A. (1996) Distribution and sinking rates of phytoplankton, detritus, and particulate biogenic silica in the Laptev Sea and Lena River (Arctic Siberia), *Mar. Chem*. **53**: 229–245.

Henson, S.A., Cole, H., Beaulieu, C. and Yool, A. (2013) The impact of global warming on seasonality of ocean primary production. *Biogeosciences*., **10**:4357–69.

Henson, S.A., Dunne, J.P. and Sarmiento, J.L. (2009) Decadal variability in North Atlantic phytoplankton blooms. *J. Geophys. Res.*, **114**:C04013.

Hildebrand, M. and Dahlin, K. (2000) Nitrate transporter genes from the diatom Cylindrotheca fusiformis (Bacillariophyceae): mRNA levels controlled by nitrogen source and by the cell cycle, *J. Phycol*., **36**:702–713.

Hildebrand, M., Frigeri, L.G. and Davis, A.K. (2007) Synchronized growth of *Thalassiosira pseudonana* (Bacillariophyceae) provides novel insights into cell-cycle synthesis processes in relation to the cell cycle. *J. Phycol*., **43**:730-740.

Hill, V., and Cota, G. (2005) Spatial patterns of primary production on the shelf, slope and basin of the Western Arctic in 2002, *Deep. Sea Res*. PartII, **52**:3344–3354.

Hilligsøe, K.M., Richardson, K., Bendtsen, J., Sørensen, L.-L., Nielsen, T.G. and Lyngsgaard, M.M. (2011) Linking phytoplankton community size composition with temperature, plankton food web structure and sea-air CO_2 flux. *Deep Sea Res.* I, **58**:826-838.

Hipkin, R. (2012) The identification of a novel DNA binding protein that underpins bloom formation in the centric diatom Thalassiosira pseudonana, PhD Thesis. University of East Anglia

Hodges, M. (2002) Enzyme redundancy and the importance of 2-oxoglutarat in plant ammonium assimilation, *J. Exp. Bot.*, **53**: 905-916.

Hofmann, M. and Schellnhuber, H.J. (2009) Oceanic acidification affects marine carbon pump and triggers extended marine oxygen holes, *PNAS*, **106**(9): 3017–3022.

Hopes A., Mock T. (2015) Evolution of Microalgae and Their Adaptations in Different Marine Ecosystems. eLS,

Horton, P., Ruban, A.V. and Walters, R. (1996) Regulation of light harvesting in green plants, *Annu. Rev. Plant Physiol. Plant Mol. Biol.*, **47**: 655–684.

http://www.statisticshell.com/docs/nonparametric.pdf.

Huisman, J., van Oostveen, P. and Weissing, F.J. (1999) Critical depth and critical turbulence: two different mechanisms for the development of phytoplankton blooms. *Limnol. Oceanogr.*, **44**:1781–87.

Huson, D.H., Auch, A.F., Qi, J. and Schuster, S.C. (2007). MEGAN analysis of metagenomic data, *Genome Research*, **17**(3): 377–386.

Huysman, M. J., Martens, C., Vandepoele, K., Gillard, J., Rayko, E., Heijde, M., Vyverman, W. *et al.* (2010). Genome-wide analysis of the diatom cell cycle unveils a

novel type of cyclins involved in environmental signalling, *Genome Biology*, **11**(2), R17.

Huysman, M. J., Vyverman, W. and De Veylder, L. (2013) Molecular regulation of the diatom cell cycle, *J. Exp. Botany*, doi:10.1093/jxb/ert387.

Ichimi, K., Kawamura, T., Yamamoto, A., Tada, K., and Harrison, P. (2012) Extremely high growth rate of the small diatom *Chaetoceros salsugineum* isolated from an estuary in the Eastern Seto Inland Sea, Japan, *Journal of Phycology*, **48**(5):1284-1288.

Irwin, A.J., Finkel, Z.V., Schofield, O.M.E. *et al.* (2006) Scaling-up from nutrient physiology to the size-structure of phytoplankton communities. *J. Plankton Res.*, **28**:459–471.

Jakobsen, A., Larsen, A., Martinez-Martinez, J., Verity, P.G. and Frischer, M.E. (2007) Susceptibility of colonies and colonial cells of *Phaeocystis pouchetii* (Haptophyta) to viral infection, *Aquatic Microbial Ecology*, **48**(2): 105-112.

Jakobsen, J.S., Bagger, F.O. Hasemann, M.S., Schuster, M.B., Frank, A.-K., Waage, J., Vitting-Seerup, K. and Porse, B.T. (2015) Amplification of pico-scale DNA mediated by bacterial carrier DNA for small-cell-number transcription factor ChIP-seq, BMC Genomics, **16**:46.

Jewson, D.H. (1992) Life cycle of a *Stephanodiscus* sp. (Bacillariophyta), *Journal of Phycology*, **28**: 856-866.

Jiroutová, K., Horák A., Bowler, C., Oborník, M. (2007) Tryptophan biosynthesis in stramenopiles: eukaryotic winners in the diatom complex chloroplast, *J. Mol. Evol.*, **65**:496–511.

Joliot P, Joliot A. (2006) Cyclic electron flow in C_3 plants, *Biochim. Biophys. Acta* **1757**: 362–68.

Joyard, J., Teyssier, E., Miege, C., Berny-Seigneurin, D., Marechal, E., Block, M.A., Dorne, A.J., Rolland, N., Ajlani, G., Douce, R. (1998) The biochemical machinery of plastid envelope membranes, *Plant Physiol.*, **118**: 715–723.

Kamp, A., de Beer, D., Nitsch, J.L., Lavik, G. and Stief, P. (2011) Diatoms respire nitrate to survive dark and anoxic conditions, *Proceedings of the National Academy of Sciences of the USA*, **108**(14): 5649–5654.

Karentz, D. and Smayda, T.J. (1984) Temperature and seasonal occurrence patterns of 30 dominant phytoplankton species in Narragansett Bay over a 22-year period (1959–1980). *Mar. Ecol. Prog. Ser.* **18**:277–93.

Karentz, D., Cleaver, J E. and Mitchell, D.L. (1991) Cell survival characteristics and molecular responses of Antarctic phytoplankton to ultraviolet-B radiation. *J. Phycol.*, **27**:326–341.

Katz, M.E.F., Finkel, Z.V., Grzebyk, D., Knoll, A.H. and Falkowski, P.G. (2004) Evolutionary trajectories and biogeochemical impacts of marine eukaryotic phytoplankton. *Annu. Rev. Ecol. Evol. Syst.*, **35**:523-556.

Keeling, P.J. (2009) Chromalveolates and the evolution of plastids by secondary endosymbiosis, *Journal of Eukaryotic Microbiology*, **56**: 1–8.

Kimmance, S. A., Wilson, W. H. and Archer, S. D. (2007) Modified dilution technique to estimate viral versus grazing mortality of phytoplankton: limitations associated with method sensitivity in natural waters. *Aquat. Microb. Ecol.*, **49**:207 – 222.

Kiørboe, T. (2001) Formation and fate of marine snow: Small-scale processes with large-scale implications, *Sci. Mar.*, **65**(Supp. 2):57–71.

Klausmeier, C.A. and Litchman, E. (2001) Algal games: The vertical distribution of phytoplankton in poorly mixed water columns. *Limnol. Oceanogr.*, **46**:1998-2007.

Klausmeier, C.A., Litchman, E., Daufresne, T. and Levin, S.A. (2004) Optimal nitrogen-to-phosphorus stoichiometry of phytoplankton, *Nature*, **429**: 171−174.

Kooistra, W.H.C.F., Gersonde, R., Medlin, L.K. and Mann, D.G. (2007) The origin and evolution of the diatoms: Their adaptation to a planktonic existence. In: Falkowski, P.G., and A.H. Knoll (eds), *Evolution of primary producers in the sea*, Academic Press, New York, pp. 210-249.

Kørboe, T. And Hansen, J.L.S. (1993) Phytoplankton aggregate formation: observations of patterns andnmechanisms of cell sticking and the significance of exopolymeric material, *Journal of Plankton Research*, **15**(9): 993-1018.

Kørboe, T., Andersen, K.P. and Dam, H.G. (1990) Coagulation efficiency and aggregate formation in marine phytoplankton, *Mar. Biol.*, **107**:235-245

Kraberg, A, Baumann, M. and Dürselen C.-D. (2010) Coastal phytoplankton. Photo guide for Northern European Seas, Verlag Dr. Friedrich Pfeil, München, pp204.

Kraberg, A.C., Rodriguez, N. and Salewski C.R. (2015) Historical phytoplankton data from Helgoland Roads: Can they be linked to modern time series data? *Journal of Sea Research*, **101**: 51–58.

Kranz, S.A., Young, J.N., Hopkinson, B.M., Goldman, J.A.L., Tortell, P.D. and Morel, F.M.M. (2014) Low temperature reduces the energetic requirement for the CO_2 concentrating mechanism in diatoms. *New Phytologist*, **205**:192–201.

Krieger-Liszkay A, Fufezan C, Trebst A (2008) Singlet oxygen production in photosystem II and related protection mechanism, Photosynth Res., **98**: 551–564.

Kristiansen, S. (1983) The temperature optimum of the nitrate reductase assay for marine phytoplankton. Limnol. Oceanogr. **28**:776–80.

Kroger, N. and Poulsen, N (2008) Diatoms-from cell wall biogenesis to nanotechnology. *Annu. Rev. Genet.*, **42**:83-107.

Kroth, P.G. (2007) Genetic transformation: a tool to study protein targeting in diatoms. *Methods Mol. Biol.*, **390**:257–267.

Kroth, P.G., Chiovitti, A., Gruber, A., Martin-Jezequel, V., Mock, T., *et al* (2008) A model for carbohydrate metabolism in the diatom Phaeodactylum tricornutum deduced from comparative whole genome analysis, *PLoS* ONE, **3**(1): e1426.

Ku, C.S., Naidoo, N., Wu, M. and Soong, R. (2011) Studying the epigenome using next generation sequencing, *J. Med. Genet.*, 48:721-730.

Kuczynska, P., Jemiola-Rzeminska, M. and Strzalka, K., (2015) Photosynthetic pigments in diatoms, *Marine Drugs*, **13**: 5847-5881.

Kudela, R.M. and Dugdale, R.C. (2000) Nutrient regulation of phytoplankton productivity in Monterey Bay, California, *Deep-Sea Res.* Part II, **47**:1023-1053.

Kustka, A.B., Milligan, A.J., Zheng, H., New, A.M., Gates, C., Bidle, K.D., and Reinfelder, J.R., (2014) Low CO2 results in a rearrangement of carbon metabolism to support C4 photosynthetic carbon assimilation in *Thalassiosira pseudonana*, *New Phytologist*, **204**, 507-520.

Laemmli, U.K., (1970) Cleavage of structural proteins during the assembly of the head of bacteriophage T4, *Natur*, **227**: 680-685.

Lakeman, M.B., von Dassow, P. and Cattolico, R.A., (2009) The strain concept in phytoplankton ecology, *Harmful Algae*, **8**(5), pp.746-758.

Landt, S.G., Marinov, G.K., Kundaje, A., Kheradpour, P., Pauli, F., Batzoglou, S., *et al.* (2012) ChIP-seq guidelines and practices of the ENCODE and modENCODE consortia, *Genome Res.*, **22**(9): 1813–1831.

Langmead, B., Trapnell, C., Pop, M. and Salzberg, S.L. (2009) Ultrafast and memory-efficient alignment of short DNA sequences to the human genome, *Genome Biol.*, **10**:R25.

Lavaud J. (2007) Fast regulation of photosynthesis in diatoms: mechanisms, evolution and ecophysiology, *Funct. Plant Sci. Biotech.*, **1**: 267-287.

Lavaud J., Kroth P. G. (2006) In diatoms, the transthylakoid proton gradient regulates the photoprotective non-photochemical fluorescence quenching beyond its control on the xanthophyll cycle, *Plant Cell Physiol.*, **47**: 1010-1016.

Lavaud J., Rousseau B., van Gorkom H. J., et al. (2002) Influence of the diadinoxanthin pool size on photoprotection in the marine planktonic diatom *Phaeodactylum tricornutum*, *Plant Physiol.*, **129**: 1398-1406.

Lavaud, J. (2007) Fast regulation of photosynthesis in diatoms: Mechanisms, evolution and ecophysiology, *Functional Plant Science and Biotechonology*, **1**, pp.267-287.

Laws, E.A., Falkowski, P.G., Smith, W.O.J., Ducklow, H. and McCarthy, J.J. (2000) Temperature effects on export production in the open ocean. *Global Biogeochem. Cycles*, **14**:1231-1246.

Leblanc, K., Hare, C.E., Feng, Y., Berg, G.M., DiTullio, G.R., Neeley, A., *et al.* (2009) Distribution of calcifying and silicifying phytoplankton in relation to environmental and biogeochemical parameters during the late stages of the 2005 North East Atlantic Spring Bloom. *Biogeosciences*, **6**:2155–2179.

Lehman, A., O'Rouke, N., Hatcher, L. & Stepanski, E. J. (2005) JMP for Basic Univariate and Multivariate Statistics: A Step-by-Step Guide, SAS Institute Inc., Cary, North Carolina, 481 pp

Lehmann, A., Getzlaff, K. and Harlaß, J. (2011) Detailed assessment of climate variability in the Baltic Sea area for the period 1958 to 2009. *Clim Res.*, **46**: 185–196.

Lessard, E.J., Merico, A. and Tyrrell, T. (2005) Nitrate:phosphate ratios and *Emiliana huxleyi* blooms. *Limnol. Oceanol.*, **50**:1020-1024.

Letelier, R.M., Karl, D.M., Abbott, M.R., Flament, P., Freilich, M., Lukas, R. and Strub, T. (2000) Role of late winter mesoscale events in the biogeochemical variability of the upper water column of the North Pacific Subtropical Gyre, *J. Geophys. Res.*, **105**: 28,723-28,739.

Lewis, J., Harris, A.S.D., Jones, K.J. and Edmonds, R.L. (1999) Long-term survival of marine planktonic diatoms and dinoflagellates in stored sediment samples, *J. Plank. Res.*, **51**: 343-354.

Lewis, W.M. Jr. (1984) The diatom sex clock and its evolutionary significance, *The American Naturist*, **123**(1): 73-80.

Li, B., *et al.* (2007) The role of chromatin during transcription. *Cell*, **128**(4):707–19.

Li, W.K.W., McLaughlin, F.A., Lovejoy, C., Carmack, E.C. (2009) Smallest algae thrive as the Arctic Ocean freshens. *Science*, **326**:539.

Lima-Mendez, G., Faust, K., Henry, N., Decelle, J., Colin, S., Carcillo, F., Chaffron, S., Ignacio-Espinosa, J.C., Roux, S., Vincent, F. *et al.* (2015) Ocean plankton. Determinants of community structure in the global plankton interactome. *Science*, **348**:1262073.

Lin, X., Tirichine, L. and Bowler, C., (2012) Protocol: Chromatin immunoprecipitation (ChIP) methodology to investigate histone modifications in two model diatom species, *Plant Methods*, **8**:48.

Lindell, D., Sullivan, M.B., Johnson, Z.I., Tolonen, A.C., Rohwer, F. And Chisholm S.W. (2004) Transfer of photosynthesis genes to and from *Prochlorococcus* viruses, *Proceeding of the National Academy of Sciences of the United States of Amerika*, **101**: 11013-11018.

Litchman, E. and Klausmeier, C.A. (2008) Trait-based community ecology of phytoplankton, *Annu. Rev. Ecol. Evol. Syst*., **39**:615–39.

Litchman, E., Edwards, K.F., Klausmeier, C.A. and Thomas, M.K. (2012) Phytoplankton niches, traits and eco-evolutionary responses to global environmental change, *Mar. Ecol. Progr. Ser.*, **470**:235-248.

Litchman, E., Klausmeier, C.A., Schofield, O.M. and Falkowski, P.G. (2007) The role of phytoplankton functional traits in structuring phytoplankton communities: scaling from cellular to ecosystem level. *Ecol. Lett.* **10**:1170–81.

Lochte, K., Ducklow, H.W., Fasham, M.J.R. and Stienen, C. (1993) Plankton succession and carbon cycling at 47 ◦ N 20 ◦ W during the JGOFS North Atlantic Bloom Experiment. *Deep-Sea Res. II*, **40**:91–114.

Lodha, M., Schulz-Raffelt, M. and Schroda, M. (2008). A new assay for promoter analysis in *Chlamydomonas* reveals roles for heat shock elements and the TATA box in HSP70A promoter-mediated activation of transgene expression, *Eukaryot. Cell*, **7**: 172–176.

Logan, B.A., Demmig-Adams, B., Rosenstiel, T.N. and Adams, W.W. III (1999) Effect of nitrogen limitation on foliar antioxidants in relationship to other metabolic characteristics, *Planta*, **209**: 213-220.

Lomas, M.W (2004) Nitrate reductase and urease enzyme activity in the marine diatom *Thalassiosira weissflogii* (Bacillariophyceae): interactions among nitrogen substrates, *Mar. Biol.*, **144**: 37-44

Lomas, M.W. and Gilbert, P.M. (1999) Temperature regulation of nitrate uptake: A novel hypothesis about nitrate uptake and reduction in cool-water diatoms, *Limnol. Oceanogr*. **44**: 556-572.

Lomas, W.L. and Gilbert, P.M. (2000) Comparisons of nitrate uptake, storage and reduction in marine diatoms and flagellates, *J. Phycol.*, **36**: 903–913

Longhurst, A. (1998) Ecological Geography of the Sea. Academic Press, San Diego, 398 pp.

Lopez-Urrutia, Á. and Morán, X.A.G. (2015) Temperature affects the size-structure of phytoplankton communities in the ocean. *Limnol. Oceanogr.*, **60**:733-738.

Losh, J.L., Young, J.N., and Morel F.M.M. (2013) Rubisco is a small fraction of total protein in marine phytoplankton, *New Phytologist*, **198**, 52-58.

Lucker, B. and Kramer, D.M. (2013) Regulation of cyclic electron flow in *Chlamydomonas reinhardtii* under fluctuating carbon availability, *Photosynth. Res*., **117**, 449-459.

Lylis, J.C. and Trainor, F.R. (1973) The heterotrophic capabilities of *Cyclotella meneghiniana*, *Journal of Phycology*, **9**(4): 365-369.

Lyon, B.R. and Mock, T. (2014) Polar Microalgae: New approaches towards understanding adaptations to an extreme and changing environment, *Biology*, **3**(1), 56-80.

Mackas, D., Batten, S. and Trudel, M. (2007) Effects on zooplankton of a warmer ocean: recent evidence from the Northeast Pacific. *Prog. Oceanogr.*, **75**:223–52.

Magaña, H.A. and Villareal, T.A. (2006) The effect of environmental factors on the growth rate of *Karenia brevis* (Davis) G. Hansen and Moestrup, *Harmful Algae*, **5**(2): 192–198.

Mahadevan, A., D'Asaro, E., Lee, C. and Perry, M.J. (2012) Eddy driven stratification initiates North Atlantic spring phytoplankton blooms. *Science*, **337**:54–58.

Malkin, R. and Niyogi, K., (2000) Photosynthesis. Biochemistry & Molecular Biology of Plants, B. Buchanan, W. Gruissem, R. Jones, Eds. American Society of Plant Physiologists, p568-628.

Malone, T.C. (1980) Algal size. In Morris I, ed. 1980. *The Physiological Ecology of Phytoplankton*. Oxford, Blackwell, pp. 433–63.

Malone, T.C. (1980) Algal size. In: Morris, I. (ed) *The physiological ecology of phytoplankton*, University of California Press, Berkeley, pp 433-463.

Mann KH (1993) Physical oceanography, food chains, and fish stocks: a review, *ICES J. Mar. Sci.*, **50**: 105–119.

Mann, D.G. and Vanormelingen, P. (2013) An inordinate fondness? The number, distributions, and origins of diatom species, *J. Eukaryot. Microbiol.*, **60**: 414-420.

Marañon, E., Cermeño, P., Latasa, M. and Tadonléké, R.D. (2012) Temperature, resources, and phytoplankton size structure in the ocean. *Limnol. Oceanogr.*, **57**:1266-1278.

Margalef, R. (1978) Life-forms of phytoplankton as survival alternatives in an unstable environment, *Oceanol. Acta* , **1**: 493–509.

Martin, A. (2012) The seasonal smorgasbord of the seas. *Science*, **337**:46–47.

Martin, P., Lampitt, R.S., Perry, M.J., Sanders. R., Lee. C. and D'Asaro, E. (2011) Export and mesopelagic particle flux during a North Atlantic spring diatom bloom. *Deep-Sea Res. I,* **58**:338–49.

Martin-Jézéquel, V., Hildebrand, M. and Brzezinski, M.A. (2000) Silicon metabolism in diatoms: Implications for growth, *Journal of Phycology*, **36**: 821-840.

Martiny, A.C., Coleman, M.L. and Chisholm, S.W. (2006) Phosphate acquisition genes in Prochlorococcus: Evidence for genome-wide adaptation, *Proc. Natl. Acad. Sci. USA*, **103**:12552–12557.

Maumus, F., Allen, A.E., Mhiri, C., Hu, H., Jabbari, K., Vardi, A., Grandbastien, M.A. and Bowler, C. (2009) Potential impact of stress activated retrotransposons on genome evolution in a marine diatom. *BMC Genom*, **10**:624.

McFadden, G.I. (2001) Chloroplast origin and integration, *Plant Physiol.*, **125**: 50–53.

McKew, B.A., Davey, P., Finch, S.J., Hopkins, J., Lefebvre, S.C., Metodiev, M.V., *et al.* (2013) The trade-off between light-harvesting and photoprotective functions of fucoxanthin-chlorophyll proteins dominates light acclimation in *Emiliania huxleyi* (clone CCMP 1516), *New Phytol.*, **200**: 74–85.

McLemore, V.T. (2008) Basics of Metal Mining Influenced Water. Management technologies for metal mining influenced water, Vol.1, Society for Mining, Metallurgy, and Exploration (U.S.), 43pp

Miller, C.B. (2003) Biological Oceanography, Wiley-Blackwell, Oxford.

Miller, T.R., Hnilicka, K., Dziedzic, A., Desplats, P. and Belas, R. (2004) Chemotaxis of *Silicibacter* sp. strain TM1040 toward dinoflagellate products. *Appl. Environ. Microbiol.* **70**:4692–4701.

Milligan, A.J. and Morel, F.M.M. (2002) A proton buffering role for silica in diatoms, *Science*, **297**: 1848-1850.

Miloslavina, Y., Grouneva, I., Lambrev, P.H., Lepetit, B., Goss, R., Wilhelm, C. and Holzwarth, A.R. (2009) Ultrafast fluorescence study on the location and mechanism of non-photochemical quenching in diatoms, *Biochimica et Biophysica Acta*, **1787**: 1189-1197.

Mitra, A. and Flynn, K.J. (2005) Predator-prey interactions: is 'ecological stoichiometry' sufficient when good food goes bad? *J. Plankton Res.*, **27**:393–399.

Miyagawa, A., Okami, T., Kira, N., Yamaguchi, H., Ohnishi, K., Adachi, M., (2009) High efficiency transformation of the diatom Phaeodactylum tricornutum with a promoter from the diatom Cylindrotheca fusiformis, Phycol. Res., **57**: 142–146.

Miyagawa-Yamaguchi, A., Okami, T., Kira, N., Yamaguchi, H., Ohnishi, K. and Adachi, M. (2011), Stable nuclear transformation of the diatom Chaetoceros sp.. Phycol. Res., **59**: 113–119.

Mizuno, M. and Okuda, K. (1985) Seasonal change in the distribution of cell size of *Cocconeis scutellum* var ornate (Bacillariophyceae) in relation to growth and sexual reproduction, *Journal of Phycology*, **21**: 547-553.

Mock, T. and Junge, K., (2007) Psychrophilic diatoms: Mechanisms for survival in freeze-thaw cycles. J. Seckbach (Ed). Algae and cyanobacteria in extreme environments, Springer, pp343-364.

Mock, T. and Medlin, L.K. (2012) Genomics and genetics of diatoms, *Advances in Botanical Research*, **64**:245-284.

Mock, T., Otillar, R.P., Strauss, J., McMullan, M., Paajanen, P., Schmutz, J., Salamov, A., Sangers, R., Toseland, A., Ward, B.J., Allen, A.E. *et al.* Evolutionary genomics of the cold adapted diatom *Fragillariopsis cylindrus*. (in press).

Mock, T., Samanta, M.P., Iverson, V., Berthiaume, C., Robison, M., Holterman, K., *et al.* (2008) Whole-genome expression profiling of the marine diatom *Thalassiosira pseudonana* identifies genes involved in silicon bioprocesses. *Proc. Natl Acad. Sci. USA*, **105**(5): 1579-1584.

Moisan, J.R., Moisan, T.A. and Abbot, M.R. (2002) Modelling the effect of temperature on the maximum growth rates of phytoplankton populations, *Ecol. Model.*, **153**: 197-215.

Montsan, A., Allen, A.E., Coesel, S., De Martino, A., Falciatore, A., Mangogna, M., Siaut, M., Heijde, M., *et al.* (2007) Identification and comparative genomic analysis of signalling and regulatory components in the diatom *Thalassiosira pseudonana*, *Journal of Phycology*, **33**:512-519.

Moore, C.M., Mills, M.M., Milne, A., Langlois, R., Achterberg, E.P., Lochte, K., Geider, R.J., and La Roche, J. (2006) Iron limits primary productivity during spring bloom development in the central North Atlantic. *Glob. Change. Bio.*, **12**:626–634.

Moore, J. K., Doney, S. C., Glover, D. M., and Fung, I. Y. (2002). Iron cycling and nutrient-limitation patterns in surface waters of the World Ocean. *Deep Sea Res. II*, **49**:463–507.

Morimoto, R.I., Sarge, K.D. and Abravaya, K. (1992) Transcriptional regulation of heat shock genes. A paradigm for inducible genomic responses, *Journal of Biological Chemistry*, **267**: 21987–21990.

Moustafa, A., Beszteri, B., Maier, U.G., Bowler, C., Valentin, K. and Bhattacharya, D. (2009) Genomic footprints of a cryptic plastid endosymbiosis in diatoms, *Science*, **324**: 1724–1726.

Munekage Y., Hojo M., Meurer J., Endo T., Tasaka M., Shikanai T. (2002). PGR5 is involved in cyclic electron flow around photosystem I and is essential for photoprotection in Arabidopsis, Cell, **110**: 361–371.

Munk, W.H. and Riley, G.A. (1952) Absorption of nutrients by aquatic plants. *J. Mar. Res.*, **11**:215–240.

Muto, M., Fukuda, Y., Nemoto, M., Tomoko Yoshino, T., Matsunaga, T., and Tanaka, T. (2013) Establishment of a Genetic Transformation System for the Marine Pennate Diatom Fistulifera sp. Strain JPCC DA0580—A High Triglyceride Producer, Mar Biotechnol., **15**: 48.

Nagai, S. and Imai, I. (1998) Enumeration of bacteria in seawater and sediment from the Seto Inland Sea of Japan that promote sperm formation in *Coscinodiscus wailesii* (Bacillariophyceae), *Phycologia*, **37**: 363–368.

Neeboda, J.A., Foster, R.A., Sakamoto, C., Zehr, J.P. and Johnson, K.S. (2007) Nitrogen fixation by unicellular cyanobacteria in the temperature oligotrophic North Pacific Ocean, *Limnol. Oceanogr.*, **52**:1317-1327.

Nolan, T., Hands, R.E, and Bustin, S.A. (2006) Quantification of mRNA using real-time RT-PCR, *Nature Protocols*, **1**: 1559-1582.

Norton, T.A., Melkonian, M. and Andersen, R.A. (1996) Algal biodiversity, *Phycologia*, **35**: 308-326.

Nunn, B.L., Aker, J.R., Shaffer, S.A., Tsai, S., Strzepek, R.F., Boyd, W. et al., (2009) Deciphering diatom biochemical pathways via whole-cell proteomics, *Aquat. Microb. Ecol.*, **55**(3): 241-253.

Oborník, M. and Green, B.R. (2005) Mosaic origin of the heme biosynthesis pathway in photosynthetic eukaryotes, *Mol. Biol. Evol.*, **22**(12):2343-53.

Okolodkov, Y.B. (1999) Species range types of recent marine dinoflagellates recorded from the Arctic, *Grana*, **38**(2–3): 162–169.

Olson, R.J., Vaulot, D. and Chisholm, S.W. (1986) Effects of environmental stresses on the cell cycle of two marine phytoplankton species. I: Cell division patterns, *J. Phycol.*, **19**: 522-528.

Orellana, M.V., Matrai, P.A., Leck, C., Rauschenberg, C.D., Lee, A.M. and Coz, E. (2011) Marine microgels as a source of cloud condensation nuclei in the high Arctic. *Proc. Natl Acad. Sci. USA*, **108**:13612–13617.

Packard, T.T., Blasco, D., MacIsaac, J.J. and Dugdale, R.C. (1971) Variations of nitrate reductase activity in marine phytoplankton., *Inv. Pesq.*, **35**:209–19.

Palmer, J.D. (2003) The symbiotic birth and spread of plastids: how many times and howdunit? *J. Phycol.*, **39**:4–11.

Palmer, M.A., van Dijken, G.L., Mitchell, B.G., Seegers, B.J., Lowry, K.E., Mills, M.M. and Arrigo, K.R. (2013) Light and nutrient control of photosynthesis in natural

phytoplankton populations from the Chukchi and Beaufort Seas, Arctic Ocean, *Limnol. Oceanogr*., **58**: 2185–2205.

Pancic, P.G. and Strotmann, H. (1993) Structure of the nuclear encoded γ subunit of CF0CF1 of the diatom Odontella sinensis including its presequence, *FEBS Lett*., **320**:61–66.

Pandey R1, Müller A, Napoli CA, Selinger DA, Pikaard CS, Richards EJ, Bender J, Mount DW, Jorgensen RA. (2002) Analysis of histone acetyltransferase and histone deacetylase families of Arabidopsis thaliana suggests functional diversification of chromatin modification among multicellular eukaryotes, *Nucleic Acids Res.*, **30**(23):5036-55.

Park, P.J. (2009) ChIP-Seq: advantages and challenges of a maturing technology. *Nat. Rev. Genet.*, **10**(10): 669–680.

Parker, M.S. and Armbrust. E.V. (2005). Synergistic effects of light, temperature and nitrogen source on transcription of genes for carbon and nitrogen metabolism in the centric diatom *Thalassiosira pseudonana* (Bacillariophyceae), *Journal of Phycology*, **41**: 1142-1153.

Parker, M.S., Armbrust, E.V., Piovia-Scott, J. and Keil, R G. (2004). Light regulation of a photorespiratory gene (glycine decarboxylase) in the centric diatom *Thalassiosira weissflogii* (Bacillariophyceae), *Journal of Phycology*, **40**:557-567.

Parker, M.S., Mock, T. and Armbrust, E.V. (2008) Genomic insights into marine microalgae, *Annual Review of Genetics*, **42**(1): 619-645.

Parkhill, J.-P., Maillet, G. and Cullen, J.J., (2001) Fluorescence-based maximal quantum yield for PSII as a diagnostic of nutrient stress, *J. Phycology*, **37**, 517-529.

Pazin, M..J. and Kadonaga. J.T. (1997) What's up and down with histone deacetylation and transcription? *Cell*, **89**:325–328.

Peers, G., and Price, N.M., (2006) Copper-containing plastocyanin used for electron transport by an oceanic diatom., *Nature*, **441**, 341-344.

Pelham H.R. (1982). A regulatory upstream promoter element in the Drosophila hsp70 heat-shock gene, *Cell*, **30**: 517–528.

Pennington, F., Guillard, R.R.L., and Liaaen-Jensen, S., (1988) Carotenoid distribution patterns in Bacillariophyceae (Diatoms), *Biochemical Systematics and Ecology* **16**, 7/8, p589-592.

Pfaffl, M.W., Horgan, G.W. and Dempfle, L. (2002) Relative expression software tool (REST) for group-wise comparison and statistical analysis of relative expression results in real-time PCR, *Nucleic Acids Res.*, **30**, e36.

Pickett-Heaps, J., Schmid, A.-M.M. and Edgar, L.A. (1990) The cell biology of diatom valve formation, *Progress in Phycological Research*, **7**:1-157.

Pickett-Heaps, J.D., Hill, D.R.A. and Wetherbee, R. (1986) Cellular movement in the centric diatom *Odontella sinensis*, *Journal of Phycology*, **6**:189-215.

Platt, T., Fuentes-Yaco, C. and Frank, K. (2003) Spring algal bloom and larval fish survival. *Nature*, **423**:398–99.

Poulsen, N. and Kröger, N. (2004) Silica morphogenesis by alternative processing of silaffins in the diatom *Thalassiosira pseudonana*, *J. Biol. Chem*., **279**(41): 42993-42999.

Poulsen, N., and Kröger, N. (2005) A new molecular tool for transgenic diatoms – control of mRNA and protein biosynthesis by an inducible promoter-terminator cassette, *FEBS J.*, **272**: 3413-3423.

Poulsen, N., Chesley, P.M. and Kroger, N. (2006) Molecular genetic manipulation of the diatom *Thalassiosira pseudonana* (Bacillariophyceae). *J. Phycol.*, **42**:1059–1065.

Poulsen, N., Chesley, P.M., and Kröger, N. (2006) Molecular genetic manipulation of the diatom *Thalassiosira pseudonana* (Bacillariophyceae), *Journal of Phycology*, **42**, 1059-1065.

Prelich, G. (2012) Gene Overexpression: Uses, Mechanisms, and Interpretation. *Genetics*, **190**(3):841–854.

Prihoda, J., Tanaka, A., de Paula, W.B.M., Allen, J.F., Tirichine, L. and Bowler, C. (2012) Chloroplast-mitochondria cross-talk in diatoms. *J. Exp. Bot*. **63**: 1543-1557.

Quigg, A., Finkel, Z.V., Irwin, A.J. *et al.* (2003) The evolutionary inheritance of elemental stoichiometry in marine phytoplankton. *Nature*, **425**:291–294.

Radakovits, R., Jinkerson, R.E., Darzins, A. and Posewitz, M.C. (2010) Genetic engineering of algae for enhanced biofuel production. *Eukaryot. Cell*, **9**:486-501.

Raposo, M.F., de Morais, R.M. and Bernardo de Morais, A.M. (2013) Bioactivity and applications of sulphated polysaccharides from marine microalgae. *Mar. Drugs*, **11**:233-252.

Rassmussen, R. (2001) Quantification on the LightCycler. In Rapid Cycle Real-time PCR, *Methods and Applications*. Meuer,S., Wittwer, C., and Nakagawara, K. (Eds). Heidelberg: Springer, pp21-34.

Raven, A.J., Evans, M.C.W., and Korb, R., (1999) The role of trace metals in photosynthetic electron transport in O_2-evolving organisms, *Photosynthesis Research*, **60**:111-149.

Raven, J.A, (2013) Iron acquisition and allocation in stramenopile algae, *Journal of Experimental Botany*, Vol. **64**, No. 8, 2119-2127.

Raven, J.A. (1987) The role of vacuoles. *New Phytol.*, **106**:357–422.

Raven, J.A. and Geider, R.J. (1988) Temperature and algal growth, *New Phytol.*, **110**: 411–416.

Raven, J.A. and Waite A.M. (2004) The evolution of silicification in diatoms: Inescapable sinking and sinking as escape? *New Phytologist*, **162**: 45-61.

Rayko, E., Maumus, F., Maheswari, U., Jabbari, K. and Bowler, C. (2010), Transcription factor families inferred from genome sequences of photosynthetic stramenopiles, *New Phytologist*, **188**: 52–66.

Razeto-Barry, P., Díaz, J., Cotoras, D. and. Vásquez, R. A. (2011) Molecular evolution, mutation size and gene pleiotropy: A geometric re-examination, *Genetics*, **187**(3): 877–885.

Redfield, A.C. (1958) The biological control of chemical factors in the environment. *American Scientist*, **46**(3):205–221.

Regaudie-de-Gioux, A. and Duarte, C. M., (2012) Temperature dependence of planktonic metabolism in the ocean, *Global Biogeochem. Cycles*, **26**: GB1015.

Reinfelder, J.R., Kraepiel, A.M.L., and Morel, F.M.M. (2000) Unicellular C_4 photosynthesis in a marine diatom, *Nature*, **407**: 996-999.

Ren, B., Robert, F., Wyrick, J.J., Aparicio, O., Jennings, E.G., Simon, I., Zeitlinger, J., Schreiber, J., Hannett, N., Kanin, E., *et al.* (2000) Genome-wide location and function of DNA binding proteins, *Science*, **290**: 2306–2309.

Reynolds, C.S. (1984) *The Ecology of Freshwater Phytoplankton*. Cambridge, UK: Cambridge Univ. Press.

Richardson, T.L. and Cullen, J.J. (1995) Changes in buoyancy and chemical composition during growth of a coastal marine diatom: ecological and biogeochemical consequences, *Mar. Ecol. Prog. Ser.*, **128**: 77-90.

Rivkin, R. B., and L. Legendre (2001) Biogenic carbon cycling in the upper ocean: Effects of microbial respiration, *Science*, **291**: 2398–2400.

Roberts, K., Granum, E., Leegood, R. C., & Raven, J. A. (2007). C3 and C4 pathways of photosynthetic carbon assimilation in marine diatoms are under genetic, not environmental control, *Plant Physiology*, **145**(1): 230–235.

Roemmich, D., Gould, W.J., Gilson, J. (2012) 135 years of global ocean warming between the Challenger expedition and the Argo Programme, *Nat. Clim. Change*, **2**(6): 425-428.

Rothschild, L.J. and. Mancinelli, R.L. (2001) Life in extreme environments, *Nature*, **409**: 1092-1101.

Round, F.E., Crawford, R.M. and Mann, D.G. (1990) The diatoms: biology and morphology of the genera, Cambridge University Press, London, pp747.

Rousseaux, C.S. and Gregg, W.W. (2013) Interannual variation in phytoplankton primary production at a global scale. *Remote Sens.*, **6**:1-19.

Ruban, A., Lavaud. J., Rousseau, B., Guglielmi, G., Horton, P., Etienne, A.L. (2004) The super-excess energy dissipation in diatom algae: comparative analysis with higher plants, *Photosynth Res.*, **82**(2):165-75.

Rüger, T. and Sommer, U. (2012) Warming does not always benefit the small – Results from a plankton experiment, *Aquatic Botany*, **97**: 64-68.

Rynearson, T., Richardson, K., Lampitt, R., Sieracki, M., Poulton, A., Lyngsgaard, M., and Perry, M. (2013) Major contribution of diatom resting spores to vertical flux in the sub-polar North Atlantic, *Deep-Sea Res. Pt. I*, **82**:60–71.

Rynearson, T.A. and Armbrust, E.V. (2004) Genetic differentiation among populations of the planktonic marine diatom *Ditylum brightwellii* (Bacillariphyceae), *J. Phycol.*, **40**:34-43.

Sakshaug, E. and Holm-Hansen, O. (1977) Chemical composition of *Skeletonema costatum* (Grev.) Cleve and *Pavlova* (*monochrysis*) *lutheri* (Droop) as a function of nitrate-, phosphate-, and iron limited growth, *J. Exp. Mar. Biol. Ecol*., **29**: 1-34.

Sakshaug, E., Demers, S. and Yentsch, C.M. (1987) Thalassiosira oceanica and Thalassiosira pseudonana: Two different photoadaptational responses, *Mar. Ecol. Progr. Ser.*, **41**: 275-282.

Sanders, R., Henson, S. A., Koski, M., De La Rocha, C. L., Painter, S. C., Poulton, A. J., Riley, J., Salihoglu, B., Visser, A., Yool, A., Bellerby, R., and Martin, A. (2014) The biological carbon pump in the North Atlantic, *Prog. Oceanogr.*, **129**:200–218.

Sardet, S. (2015) Plankton: Wonders of the drifting world, The University of Chicago Press Books.

Sarmento, H., Montoya, J.M. Vazquez-Dominguez, E., Vaque, D. and Gasol, J.M. (2010) Warmin effects on marine microbial foodweb processes: how far can we go when it comes to predictions? *Phil. Trans. R. Soc. B.*, **365**: 2137-2149.

Sarmiento, G., da Silva, M.P., Naranjo, M.E. and Pinillos, M. (2006) Nitrogen and phosphorus as limiting factors for growth and primary production in a flooded savanna in the Venezuelan Llanos, *Journal of Tropical Ecology*, **22**(2), pp. 203–212.

Sarmiento, J.L., Hughes, T.M.C., Stouffer, R.J. and Manabe, S. (1998) Simulated response of the ocean carbon cycle to anthropogenic climate warming, *Nature*, **393**: 245-249.

Sarthou, G., Timmermans, K.R., Blain, S. and Treguer, P. (2005) Growth physiology and fate of diatoms in the ocean: a review, *J. Sea. Res.*, **53**: 25-42.

Schmidt, A.-M.M. (2003) Endobacteria in the diatom *Pinnularia* (Bacillariophyceae.) I. "Scattered ct-nucleoids" explained: DAPI-DNA complexes stem from exoplastidial bacteria boring into the chloroplast, *Journal of Phycology*, **39**:122-138.

Schneider, C. A.; Rasband, W. S. & Eliceiri, K. W. (2012) NIH Image to ImageJ: 25 years of image analysis, Nature methods, **9**(7): 671-675, PMID 22930834.

Schoemann, V., Becquevort, S., Stefels, J., Rousseau, W. and Lancelot, C. (2005) *Phaeocystis* blooms in the global ocean and their controlling mechanisms: a review. *J. Sea Res.*, **53**:43-66.

Schreiber, U., Schliwa, U. and Bilger, W. (1986) Continuous recording of photochemical and nonphotochemical chlorophyll fluorescence quenching with a new type of modulation fluorometer, *Photosynth. Res.*, **10**: 51-62.

Schroda, M., Vallon, O., Wollman, F.A. and Beck, C.F. (1999) A chloroplast-targeted heat shock protein 70 (HSP70) contributes to the photoprotection and repair of photosystem II during and after photoinhibition, *Plant Cell*, **11**: 1165−1178.

Shi, D., Li, W., Hopkinson, B.M., Hong, H., Li, D., Kao, S. and Lin, W. (2015) Interactive effects of light, nitrogen source, and carbon dioxide on energy metabolism in the diatom *Thalassiosira pseudonana*, *Limnol. Oceanogr*., **60**: 1805-1822.

Shikanai, T. (2007) Cyclic electron transport around photosystem I: genetic approaches, *Annu. Rev. Plant. Biol*., **58**: 199-217.

Shrestha, R.P., Tesson, B., Norden-Kirichmar, T., Federowicz, S., Hildebrand, M. and Allen, A.E (2012) Whole transcriptome analysis of the silicon response of the diatom *Thalassiosira pseudonana, BMC Genomics*, **13**:499

Shutler, J.D., Land, P.E., Brown, C.W., Findlay, H.S., Donlon, C.J. *et al*. (2013) Coccolithophore surface distributions in the North Atlantic and their modulation of the air–sea flux of CO_2 from 10 years of satellite Earth observation data. *Biogeosciences*, **10**:2699–2709.

Siaut, M., Heijde, M., Mangogna, M., Montsant, A., Coesel, S., Allen, A., Manfredonia, A., Falciatore, A. and Bowler, C. (2007) Molecular toolbox for studying diatom biology in *Phaeodactylum tricornutum*. *Gene*, **406**:23–35.

Sicko-Goad, L., Stoermer, E.F. and Kociolek, J.P. (1986) Diatom resting cell rejuvenation and formation: Time course, species, records and distribution, *J. Plankton Res.*, **11**(2): 385-389.

Silver, M.W, Bargu, S., Coale, S.L., Benitez-Nelson, C.R., Garcia, A.C., Roberts, K.J., Sekula-Wood, E., Bruland, K.W. and Coale, K.H. (2010) Toxic diatoms and domoic acid in natural and iron enriched waters of the oceanic Pacific, *Proc. Natl. Acad. Sci. USA*, **107**(48): 20762–20767.

Sims, P.A., mann, D.G. and Medlin, J.K. (2006) Evolution of the diatoms: Insights from fossil, biological, and molecular data, *Phycologia*, **45**:361-402.

Sinninghe Damsté J.S., Muyzer, G., Abbas, B., Rampen, S.W., Massé, G., Allard, W.G., Belt, S.T., Robert, J.M., Rowland, S.J., *et.al.* (2004) The rise of the rhizosolenid diatoms, *Science*, **304**: 584-587.

Sluiman, H. (1993) Nucleus, nuclear division, and cell division. In: Berner, T. (ed) *Ultrastructure of microalgae*, CRC Press, Boca Raton, Fl, pp 221-268.

Small, L.F., Knauer, G.A. and Tuel, M.D. (1987) The role of sinking fecal pellets in stratified euphotic zones, *Deep-Sea Research*, **34**: 1705–1712.

Smayda, T.J. (1969) Experimental observations on the influence of temperature, light and salinity on cell division of the marine diatom *Detonula confervacea* (Cleve) Gran. *J. Phycol*., **5**: 150-157.

Smayda, T.J. (1970) The suspension and sinking of phytoplankton in the sea. *Oceanogr. Mar. Biol. Annu. Rev.*, **8**:353–414.

Smayda, T.J. (1997) Harmful algal blooms: their ecophysiology and general relevance to phytoplankton blooms in the sea. *Limnol. Oceanogr.* **42**:1137–53.

Smayda, T.J. and Trainer, V.L. (2010) Dinoflagellate blooms in upwelling systems: seeding, variability, and contrasts with diatom bloom behaviour, *Prog. Oceanogr*., **85**(1–2), 92–107.

Smayda, T.J., (1997) What is a bloom? A commentary, *Limnol. Oceanogr*., **42**(5), 1132–1136.

Smetacek, V., 1999. Diatoms and the ocean carbon cycle, *Protist*, **150**: 25–32.

Smetacek, V., Klaas, C., Strass, V.H., Assmy, P., Montresor, M., Cisewski, B., *et al.* (2012) Deep carbon export from a Southern Ocean iron-fertilized diatom bloom. *Nature*, **487**:313–319.

Smetacek, V., Klaas, C., Strass, V.H., Assmy, P., Montresor, M., Cisewski, B., Savoye,N., Webb, A. *et al.* (2012) Deep carbon export from a Southern Ocean iron-fertilized diatom bloom, *Nature*, **487**: 313–319.

Smetacek, V.S. (1985) Role of sinking in diatom life-history cycles: ecological, evolutionary and geological significance. *Mar. Biol.*, **84**:239–251.

Smith, D.C., Simon, M., Alldredge, A.L. and Azam, F. (1992) Intense hydrolytic enzyme activity on marine aggregates and implicates for rapid particle dissolution. *Nature*, **359**:139–142.

Smith, G.J., Zimmerman, R.C. and Alberte, R.S. (1992) Molecular and physiological responses of diatoms to variable levels of irradiance and nitrogen availability: growth of Skeletonema costatum in simulated upwelling conditions, *Limnol. Oceanogr.*, **37**: 989-1007.

Smith, W. and Nelson, D. (1985) Phytoplankton bloom produced by receding ice edge in the Ross Sea: spatial coherence with the density field. *Science* **227**:163–66.

Smyth, T.J., Allen, I., Atkinson, A., Bruun, J.T., Harmer, R.A., Pingree, R.D., Widdicombe, C.E., and Somerfield, P.J. (2014) Ocean net heat flux influences seasonal to interannual patterns of plankton abundance. PLoS ONE, **9**, e98709.

Sommer, U., Gliwicz, Z.M., Lampert, W. and Duncan, A. (1986) The PEG-model of seasonal succession of planktonic events in fresh waters. *Arch. Hydrobiol.* **106**:433–71.

Specht, E.A. and Mayfield, S.P. (2014) Algae-based oral recombinant vaccines. *Front. Microbiol.*, **5**:60.

Srinivas, U.K. and Swamynathan, S.K. (1996) Role of heat shock transcription factors in stress response and during development, *J. Biosci.*, **21**(2): 103–121.

Stael S, *et al.* (2012) Cross-talk between calcium signalling and protein phosphorylation at the thylakoid, J. Exp. Bot., **63**:1725–1733.

Stephenson, M. L., Zamecnik, P. C. (1978) Inhibition of Rous sarcoma viral RNA translation by a specific oligodeoxyribonucleotide, Proc. Natl. Acad. Sci. USA,**75**(1), 285-288.

Sterner, R.W. and Elser, J.J. (2002) Ecological Stoichiometry: The Biology of the Elements from Molecules to the Biosphere. Princeton University Press, Princeton.

Stommel, H. (1951) An elementary explanation of why ocean currents are strongest in the west. Am. Meteorol. Soc. Bull., 32:21-23.

Strzepek, R.F and Harrison, P. (2004) Photosynthetic architecture differs in coastal and oceanic diatoms, *Nature*, **431**, 689-692.

Strzepek, R.F, (2003) Photosynthetic iron requirements of marine diatoms. Thesis, Univ. British Columbia.

Sumper, M and Brunner, E. (2008) Silica biomineralisation in diatoms: The model organism *Thalassiosira pseudonana*, *ChemBioChem*, **9**(8): 1187-1194.

Sumper, M. (2002) A phase separation model for the nanopatterning of diatom biosilica, *Science*, **295**: 2430-2433.

Sumper, M. and Kroeger, N. (2004) Silica formation in diatoms: the function of long-chain polyamines and silaffins. *J. Mater. Chem*., **14**:2059-2065.

Sunagawa, S., Coelho, L.P., Chaffron, S., Roat Kultima, J., Labadie, K., Salazar, G., *et al.* (2015) Structure and function of the global ocean microbiome, *Science*, Vol. **348**, Issue 6237.

Sunda, V.G and Huntsman, S.A, (1995) Iron uptake and growth imitation in oceanic and coastal phytoplankton, *Mar. Chem.*, **50**: 189-206.

Sunda, V.G and Huntsman, S.A, (1995) Regulation of copper concentrations in the oceanic nutricline by phytoplankton uptake and regeneration cycles, *Limnol. Oceanogr*., **40**: 132-137.

Sunda, W.G. (2012) Feedback Interactions between Trace Metal Nutrients and Phytoplankton in the Ocean. *Front Microbiol.*, **3**: 204.

Suto, I. (2006) The explosive diversification of the diatom genus *Chaetoceros* across the Eocene/Oligocene and Oligocene/Miocene boundaries in the Norwegian Sea, *Marine Micropaleontology*, **58**(4): 259-269.

Svendrup, H.W. (1953) On conditions for the vernal blooming of phytoplankton. *J. Cons. Int. Explor. Mer*., **18**:287–295.

Taylor, B. L., & Zhulin, I. B. (1999). PAS Domains: Internal Sensors of Oxygen, Redox Potential, and Light, *Microbiology and Molecular Biology Reviews*, **63**(2): 479–506.

Tengs, T., Dahlberg, O.J., Shalchian-Tabrizi, K., Klaveness, D., Rudi, K., Delwiche, C.F. and Jakobsen, K.S. (2000) Phylogenetic analyses indicate that the 19'hexanoyloxy-fucoxanthin-containing dinoflagellates have tertiary plastids of haptophyte origin, *Mol. Biol. Evol.*, **17**: 718–729.

Terashima M., Petroutsos D., Hüdig M., Tolstygina I., Trompelt K., Gäbelein P., et al. (2012). Calcium-dependent regulation of cyclic photosynthetic electron transfer by a CAS, ANR1, and PGRL1 complex, Proc. Natl. Acad. Sci. U.S.A., **109**: 17717–17722.

Thamatrakoln, K., Korenovska, O., Niheu, A.K. and Bidle, K.D. (2012) Whole-genome expression analysis reveals a role for death-related genes in stress acclimation of the diatom ***Thalassiosira pseudonana***. *Enivron Microbiol.*, **14**: 67–81.

Thompson, P.A., Guo, M. and Harrison, P.J. (1992) Effects of variation in temperature I. On the biochemical composition of eight species of marine phytoplankton, *J. Phycol*., **28**: 481-488.

Tirichine, L. and Bowler, C. (2011) Decoding algal genomes: tracking back the history of photosynthetic life on Earth. *The Plant Journal*, **66**:45-57.

Toseland, A., Daines, S.J., Clark, J.R., Kirkham, A., Strauss, J., Uhlig, C. et al., (2013) The impact of temperature on marine phytoplankton resource allocation and metabolism, *Nature Climate Change*, **3**: 979-984.

Townsend, D.W., Cammen, L.M., Holligan, P.M., Campbell, D.E. and Pettigrew, N.R. (1994) Causes and consequences of variability in the timing of spring phytoplankton blooms, *Deep-Sea Res.* Pt. I, **41**:747–765.

Townsend, D.W., Keller, M.D., Sieracki, M.E. and Ackleson, S.G. (1992) Spring phytoplankton blooms in the absence of vertical water column stratification. *Nature*, **360**:59–62.

Turpin, H.D. (1991) Effects of inorganic N availability on algal photosynthesis and carbon metabolism, *J. Phycol.*, **27**: 14-20.

Valenzuela, J., Mazurie, A., Carlson, R.P., Gerlach, R., Cooksey, K.E., Peyton, B.M. and Fields, M.W. (2012) Potential role of multiple carbon fixation pathways during lipid accumulation in *Phaeodactylum tricornutum*, *Biotechnology for Biofuels*, **5**, 40.

Van Ruth, P.D., Qin, J.G. and Branford, A.J. (2012) Size dependent competition in centric diatoms as a function of nitrogen and silicon availability, *Open Journal of Marine Science*, **2**: 33-42.

Vaulot, D., Olson, R.J., Merke, S. and Chisholm, S.W. (1987) Cell-cycle response to nutrient starvation in two phytoplankton species, *Thalassiosira weisflogii* and *Hymenomonas carterae*, *Mar. Biol.*, **95**: 625-630.

Vavilin, D.V. and Vermaas, W.F.J. (2002), Regulation of the tetrapyrrole biosynthetic pathway leading to heme and chlorophyll in plants and cyanobacteria, *Physiologia Plantarum*, **115**: 9–24.

Veluchamy, A., Lin, X., Maumus, F., Rivarola, M., Bhavsar, J., Creasy, T. *et al.*, (2013) Insights into the role of DNA methylation in diatoms by genome-wide profiling in *Phaeodactylum tricornutum*, *Nature Communications*, **4**:2091.

Veluchamy, A., Rastogi, A., Lin, X., Lombard, B. Murik, O., Thomas, Y., Dingli, F. *et a.*, (2015) An integrative analysis of post-translational histone modifications in the marine diatom *Phaeodactylum tricornutum*, *Genome Biology*, **16**:102.

Villareal, T.A. (1994) Widespread occurrence of the Hemiaulus-cyanobacteria symbiosis in the southwest North Atlantic Ocean, Bull Mar Sci., **54**: 1–7.

Villareal, T.A., Brown, C.G., Brzezinski, M.A., Krause, J.W. and Wilson, C. (2012) Summer Diatom Blooms in the North Pacific Subtropical Gyre: 2008–2009, *PLoS* ONE, **7**(4): e33109.

Villareal, T.A., Joseph, I., Brzezinski, M., Lipschutz, F., and Altabet, M.A., (1999) Biological and chemical characterisation of the giant diatom *Ethmodiscus*

(Bacillariophyceae) in the central North Pacific gyre, *Journal of Phycology*, **35**: 896–902.

Villareal, T.A., Woods, S., Moore, J.K. and Culver-Rymsza, K. (1996) Vertical migration of *Rhizosolenia* mats and their significance to NO_3^- fluxes in the central North Pacific gyre, *J. Plankton Res.*, **18**:1103-1121.

Volk, T. and Hoffert, M.I. (1985) Ocean carbon pumps: analysis of relative strengths and efficiencies in ocean-driven atmospheric CO_2 changes. In Sundquist, E.T. and Broecker, W.S. (eds), *The Carbon Cycle and Atmospheric CO_2: Natural Variations Archean to Present.* American Geophysical Union, Washington, DC, pp. 99–110.

Vrieling, E.G., Sun, Q., Tian, M., Kooyman, P., Gieskes, W.W.C., van Santen, R. and Sommerdijk, N.A.J.M. (2007) Salinity-dependent diatom biosilicification implies an important role of exernal ionic strength, *Proceeding of the National Academy of Sience of USA*, **104**: 10441-10446.

Waite, A., Bienfang, P.K. and Harrison, P.J. (1992) Spring bloom sedimentation in subarctic ecosystem, II, Succession and sedimentation, *Mar. Biol.*, **114**: 131-138.

Walker, J.S., Keely, B.J., (2004) Distribution and significance of chlorophyll derivatives and oxidation products during the spring phytoplankton bloom in the Celtic Sea April 2002, *Organic Geochemistry*, **35**: 1289-1298.

Walsby, A.E. and Reynolds, C.S. (1980) Sinking and floating. In: Morris I (ed) (ed) The physiological ecology of phytoplankton. University rsity of California Press, Los Angeles, p 371-412.

Wang R, Guegler K, LaBrie ST, Crawford NM. 2000. Genomic analysis of a nutrient response in Arabidopsis reveals diverse expression patterns and novel metabolic and potential regulatory genes induced by nitrate, *Plant Cell*, **12**: 1491–509.

Wang, W., Vinocur, B., Shoseyov, O. and Altman, A (2004) Role of plant heat shock proteins and molecular chaperones in the abiotic stress response, *TRENDS in Plant Science*, **9**(5): 244–252.

Wells, M.L., Trainer, V.L., Smayda, T.J., Karlson, B.S.O., Trick, C.G. Kudela, R.M., et al. (2015) Harmful algal blooms and climate change: Learning from the past and present to forecast the future, *Harmful Algae*, **49**: 68–93.

Wichard, T., Gerecht, A., Boersma, M., Poulet, S.A., Wiltshire, K. and Pohnert, G. (2007) Lipid and fatty acid composition of diatoms revisited: rapid wound-activated change of food quality parameters influences herbivorous copepod reproductive success, *ChemBioChem*, **8**: 1146–1153.

Wiltshire, K.H. and Manly, B.F.J. (2004) The warming trend at Helgoland Roads, North Sea: phytoplankton response, *Helgoland Marine Research*, **58**(4): 269-273.

Worden, A.Z., Lee, J.H., Mock, T., Rouze, P., Simmons, M.P., Aerts, A.L. *et al.* (2009) Green evolution and dynamic adaptations revealed by genomes of the marine picoeukaryotes Micromonas, *Science*, **324**:268–272.

Wustman, B.A., Gretz, M.R. and Hoagland, K.D. (1997) Extracellular matrix assembly in diatoms (Bacillariophyceae) I. A model of adhesives based on chemical characterization and localization of polysaccharides from the marine diatom *Achanthes longipes* and other diatoms, *Plant Physiology*, **113**: 1059-1069.

Yan, W. and Hunt, L.A. (1999) An equation for modelling the temperature response of plants using only the cardinal temperatures, *Annals of Botany*, **84**: 607-614.

Yoon, H.S., Hackett, J., Ciniglia, C., Pinto, G. and Bhattacharya, D. (2004) A molecular timeline for the origin of photosynthetic eukaryotes, *Molecular Biology and Evolution*, **21**: 809–818.

Young, J. N., Heureux, A. M. C., Sharwood, R. E., Rickaby, R. E. M., Morel, F. M. M., & Whitney, S. M. (2016). Large variation in the Rubisco kinetics of diatoms reveals diversity among their carbon-concentrating mechanisms, *Journal of Experimental Botany*, **67**(11): 3445–3456.

Zaslavskaia, L.A., Lippmeier, J.C., Kroth, P.G., Grossman, A.R., and Apt, K.E. (2000) Transformation of the diatom *Phaeodactylum tricornutum* (Bacillariophyceae) with a variety of selectable marker and reporter genes, *J. Phycol.*, **36**: 379–386.

Zhang, Y., Liu, T., Meyer, C.A., Eeckhoute, J., Johnson, D.S., Bernstein, B.E., *et al.* (2008) Model-based analysis of ChIP-Seq (MACS), *Genome Biol.*, **9**:R137.

LIST OF APPENDICES

TpfcpnatASBIG1 (FB1AS)

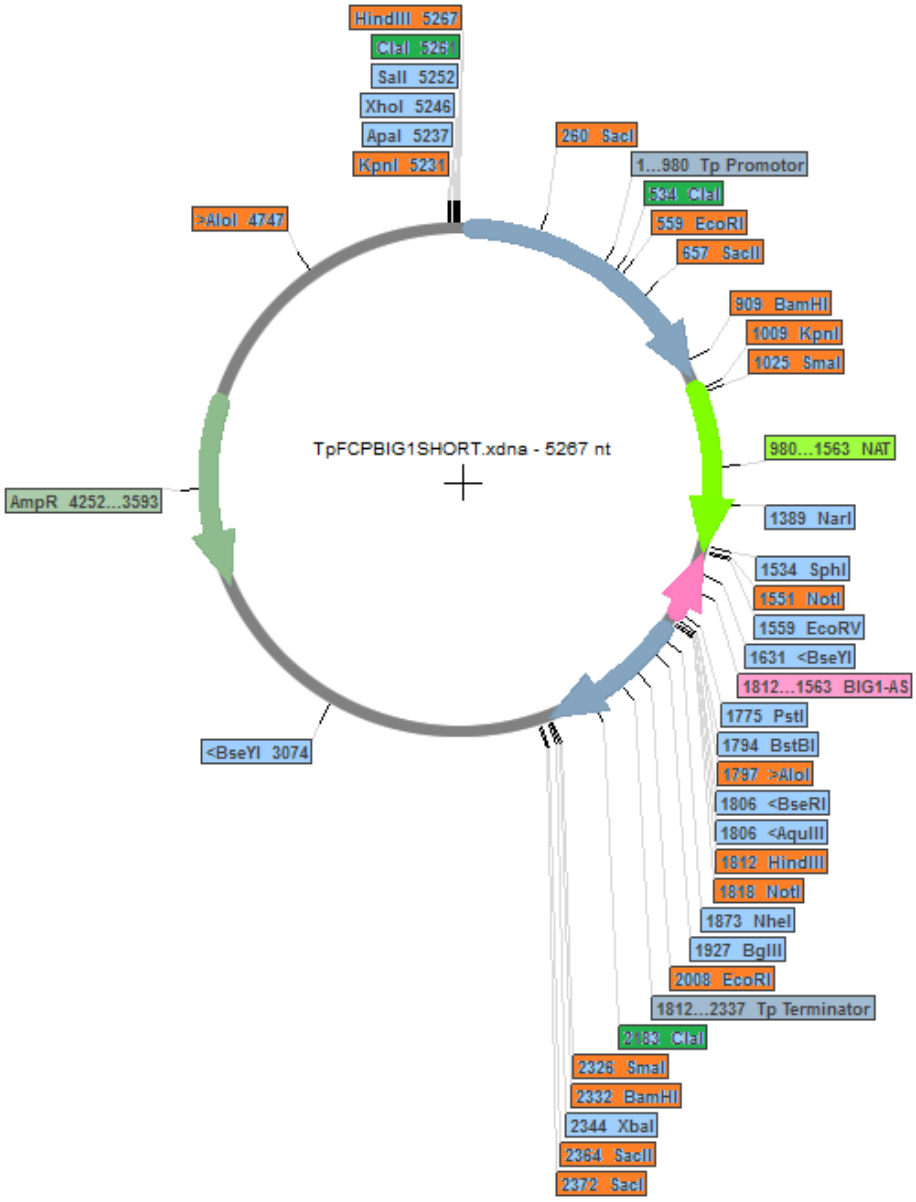

Appendix 1: *Restriction map of Tp FCP BIG Antisense (Short) Drawn with the freely available Serial cloner software* http://download.cnet.com/Serial-Cloner/3000-2054_4-10668328.html - *Courtesy of Amy Kirkham*

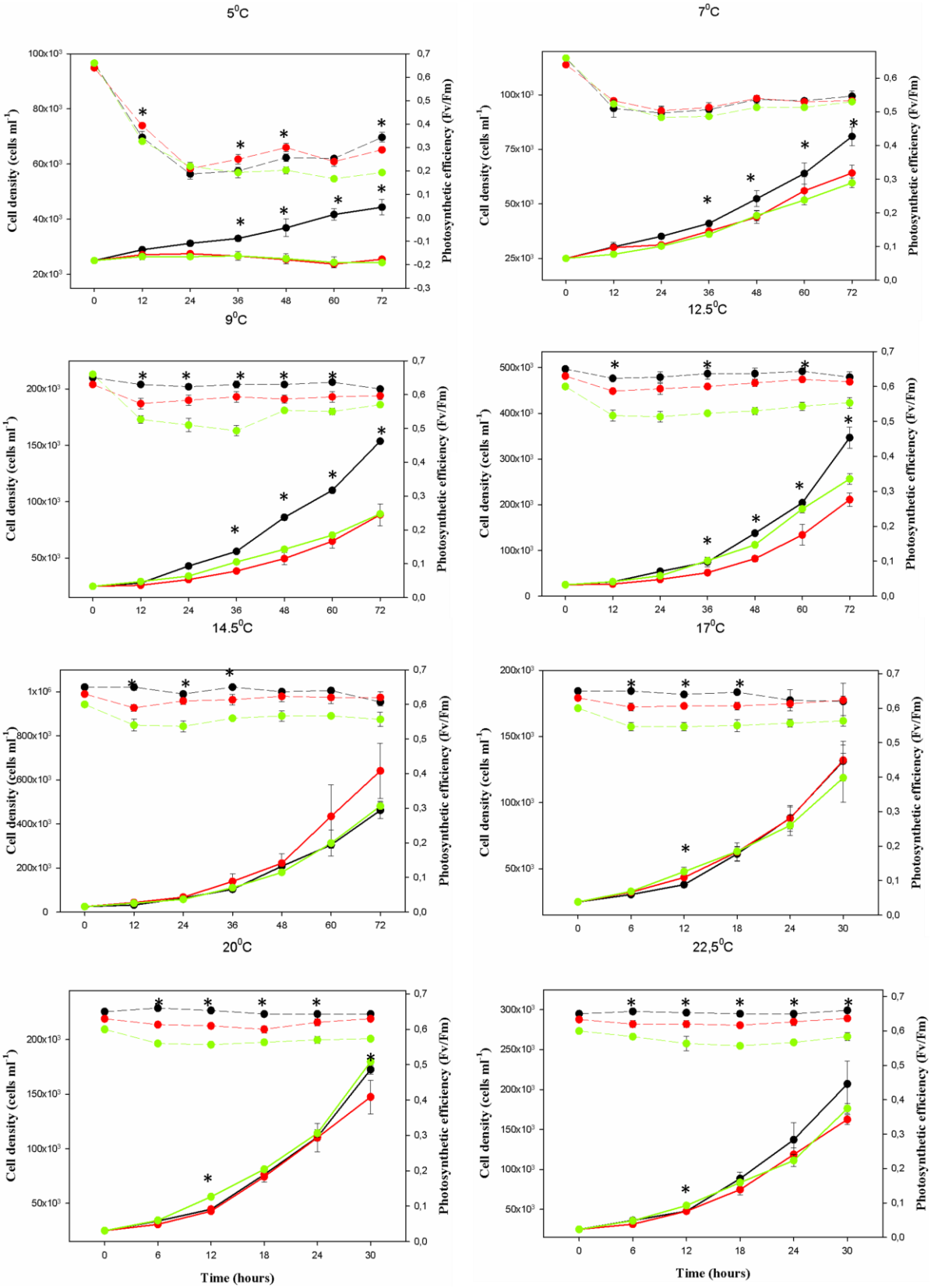
5°C
7°C
9°C
12.5°C
14.5°C
17°C
20°C
22,5°C
Cell density (cells ml-1)
Photosynthetic efficiency (Fv/Fm)
Time (hours)

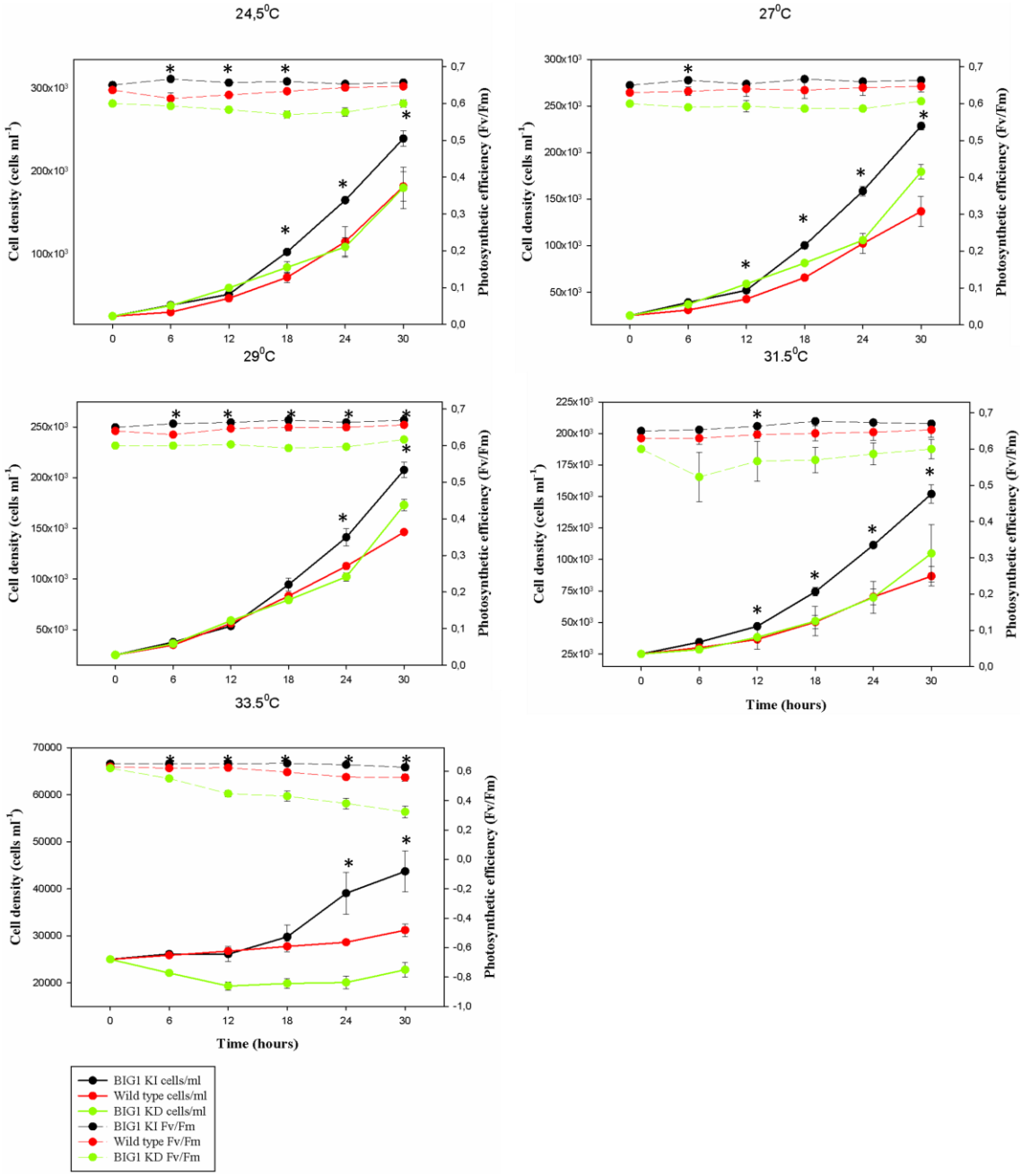

***Appendix 2**: Cell density and Fv/Fm recorded at mid exponential phase in temperature response over the temperature gradient of 5^0C – 33.5^0C*

***Appendix 3**: Averages of T.pseudonana cells/aggregates in response to temperature acclimation. Abbreviations as follows: overexpression of the BIG1 protein (BIG1 KI), knock-down of the BIG1 protein (BIG1 KD) and wild type (WT), standard errors were calculated from standard deviations (SD). The only possible aggregation tendency was associated to 31.5^{0}C and is highlighted in grey.*

Temperature	***Average of cells/aggregates***					
	BIG1 KI	***SD***	***WT***	***SD***	***BIG1 KD***	***SD***
5.0^{0}C	1.0691	0.0178	1.0629	0.0134	1.0832	0.0060
7.0^{0}C	1.1211	0.0389	1.0421	0.0061	1.0591	0.0076
9.0^{0}C	1.0608	0.0064	1.0389	0.0100	1.0590	0.0146
12.5^{0}C	1.0613	0.0091	1.0312	0.0030	1.0306	0.0030
14.5^{0}C	1.0750	0.0058	1.0354	0.0053	1.0301	0.0060
17.0^{0}C	1.0695	0.0155	1.0584	0.0339	1.0291	0.0049
20.0^{0}C	1.0500	0.0074	1.0219	0.0021	1.0399	0.0070
22.5^{0}C	1.0563	0.0056	1.0247	0.0033	1.0249	0.0028
24.5^{0}C	1.0683	0.0062	1.0354	0.0089	1.0339	0.0164
27.0^{0}C	1.0691	0.0116	1.0448	0.0041	1.0327	0.0075
29.0^{0}C	1.1362	0.0098	1.0754	0.0094	1.0369	0.0031
31.5^{0}C	1.2516	0.0217	1.1641	0.0227	1.0975	0.0141

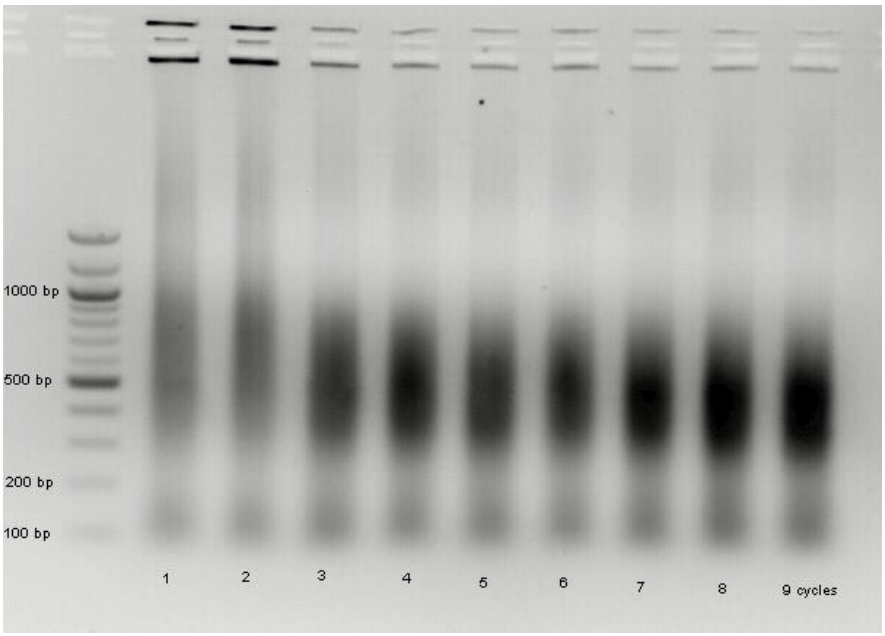

Appendix 4: *2% Agarose gel electrophoresis image of sonication efficiency control of DNA shearing, setting used 20 sec ON 3 min OFF*